Technische Universität München
Lehrstuhl für Steuerungs- und Regelungstechnik

Stable and User-Controlled Assistance of Human Motor Function

Heike Vallery

Vollständiger Abdruck der von der Fakultät für Elektrotechnik und Informationstechnik der Technischen Universität München zur Erlangung des akademischen Grades eines

Doktor-Ingenieurs (Dr.-Ing.)

genehmigten Dissertation.

Vorsitzender: Univ.-Prof. Dr.-Ing. Klaus Diepold

Prüfer der Dissertation:

1. Univ.-Prof. Dr.-Ing. (Univ. Tokio) Martin Buss

2. Univ.-Prof. Dr.-Ing. Dirk Abel,
Rheinisch-Westfälische Technische Hochschule Aachen

Die Dissertation wurde am 01.12.2008 bei der Technischen Universität München eingereicht und durch die Fakultät für Elektrotechnik und Informationstechnik am 29.06.2009 angenommen.

Foreword

The last four years were not only a very valuable experience, I also had a great time doing the research. This is especially due to the positive and stimulating environment I found both at the LSR in Munich and at the BW lab in Enschede.

First, I have to thank Prof. Dirk Abel from my "home university" Aachen for introducing me to my later supervisor, Prof. Martin Buss in Munich. Thank you, Martin, for providing me with excellent resources, open discussions, and all the freedom I needed. At the LSR, I found wonderful colleagues, and I enjoyed their pleasant company. Special thanks go to our loose LSR Biomedical group, Moritz Große-Wentrup, Tobias Göpel, Michael Bernhardt, and Thomas Pröll, who contributed to the project with continued discussions, ideas, and suggestions. My long-term office colleague Heide Brandtstädter not only helped improve my mathematical reasoning, I also have to thank her for conciliating words, and for organizing so many fun activities such as parties or "Memory" tournaments. Ulrich Unterhinninghofen, thank you for tirelessly solving my computer problems, for entertaining evenings, and for Brezn and Obatzten. Jan Wolff, your theoretical contribution, e.g. during passionate discussions on stability, was invaluable. In my opinion, your new job means a loss for academia! My statistical skills were significantly enhanced by Raphaela Groten, thank you for your support. Matthias Althoff, Matthias Rungger, and Marion Sobotka also contributed substantially, especially concerning stability questions. Thank you all for help and assistance, e.g. by revising papers, and for your valued friendship.

I started the project with little more than a fancy idea of future investigations. By and by, this evolved into more solid research, and important impulses came from my predecessor in the project, Dr. Thomas Fuhr, and two physicians: Dr. Jochen Quintern from Bad Aibling introduced me to the field of neurorehabilitation, and he continuously supported and influenced the project, making sure that obtained results would have practical relevance. Dr. Rainer Burgkart, Klinikum Rechts der Isar, is a man full of good ideas, for example he had the initial idea of controlling one leg via the other. Thank you for your enthusiastic contribution! I am looking forward to a continued collaboration.

During the starting phase, Dejan Popović and the summer school he organized in Montenegro affected me deeply, the event helped me acquire a more well-founded background, and I established relationships with other groups with similar aims. Montenegro was the place were I met Arno Stienen, one of the most efficient networkers I know, and a somewhat nice person, too ;) Thank you, Arno, for introducing me to the Twente group!

In Twente, I learned a lot in discussions with Dr. Herman van der Kooij and Prof. Frans van der Helm, thank you both for your continued support and advice, and for letting me contribute to the LOPES project. Nevertheless, I suspect that Herman only let me do all these experiments because he does not love the LOPES quite as much as its father, Jan Veneman, who certainly suffered during some barbaric experiments with his "kindje".

Thank you Jan, for your endurance and your help! Without the technical support of Gert-Jan Nevenzel, the experiments would never have been possible in the short time I spent in Twente. Thank you, Gert-Jan, for tireless replacement of overstrained Bowden cables, even repeatedly on weekends and at night. Ralf Ekkelenkamp, the ingenious chaotic control engineer, you were a pleasant partner in teaching the robot some behavior, thank you for this (and for supplying me with some nutrition in the lab). Last but not least, Edwin van Asseldonk, thorough co-author and wonderful colleague, thank you for gorgeous paper prose, clean Matlab code, and advice in all areas.

Special thanks go to all the students who worked in this project and who did a large deal of the work. Maximilian Neumaier, Adrian Lindner, Markus Rank, Pablo Lopez-Hidalgo, Andrea Bauer, Sjors Coenders, Cornelia Hartmann, and many others, your contribution is invaluable, and it was a pleasure to work with you. Furthermore, I would like to thank all subjects who took part in the often strenuous (LOPES) or painful (FES) studies.

Krauth + Timmermann (Medel GmbH, Hamburg) generously supplied the stimulator MOTIONSTIM8 for this work. Controlled by the open-source *Science Stim* protocol by Nils-Otto Negård and Thomas Schauer, the device was used for all FES experiments. The employed physiological gait trajectories were obtained from Carnegie Mellon University's public-domain motion capture database, mocap.cs.cmu.edu, which was created with funding from NSF EIA-0196217. To process the data, the *Mocap toolbox for MATLAB* was used, which was developed by N. D. Lawrence, University of Sheffield, UK.

During these years, the Studienstiftung des Deutschen Volkes was much more than my financial supporter. It helped me to concentrate also on things unrelated to my research (like foreign languages) and to meet other stipendiaries in stimulating discussions, e.g. at the "Doktorandentagungen". This organization and community I have perceived most positively, and I feel deeply indebted.

I deeply appreciate the contribution of my parents, who have always supported me. And, most important: Thank you, Michael, for sharing this time with me.

Munich, 2008. Heike Vallery

Contents

Notations

Abbreviations

AAN	Assist-as-Needed
BIBO	Bounded Input Bounded Output
BF	Biceps Femoris
BLUE	Best Linear Unbiased Estimator
CLME	Complementary Limb Motion Estimation
CNS	Central Nervous System
CoM	Center of Mass
DoF	Degree of Freedom
EMG	electromyography
FES	Functional Electrical Stimulation
Ga	Gastrocnemius (Lateralis)
LDI	Linear Differential Inclusion
LMI	Linear Matrix Inequality
MIMO	Multi Input Multi Output
NRBF	Normalized Radial Basis Functions
PCA	Principal Component Analysis
PID	Proportional-Integral-Derivative
RF	Rectus Femoris
PW	Pulse Width
PWM	Pulse Width Modulation
SEA	Series Elastic Actuator
SI	symmetry index
SISO	Single Input Single Output
TA	Tibialis Anterior
ZMP	Zero Moment Point

Scalars, Vectors, and Matrices

Scalars are denoted by upper and lower case letters in italic type. Vectors are denoted by lower case letters in boldface italic type, and a vector $\boldsymbol{x}$ is composed of elements x_i. Matrices are denoted by upper case letters in boldface type, and a matrix $\mathbf{M}$ is composed of elements m_{ij} (i-th row, j-th column).

x	scalar
$\boldsymbol{x}$	vector
$\mathbf{X}$	matrix

$f(\cdot)$	scalar function
$\boldsymbol{f}(\cdot)$	vector function
$\dot{\boldsymbol{x}}$, $\ddot{\boldsymbol{x}}$	equivalent to $\frac{\mathrm{d}}{\mathrm{d}t}\boldsymbol{x}$ and $\frac{\mathrm{d}^2}{\mathrm{d}t^2}\boldsymbol{x}$
$\mathbf{M}^T$	transposed of matrix $\mathbf{M}$
$\mathbf{M}^{-1}$	inverse of matrix $\mathbf{M}$
$\mathbf{M}^{\#}$	left pseudoinverse of matrix $\mathbf{M}$
$\mathbf{M}^*$	conjugate transposed of matrix $\mathbf{M}$
$\nabla_{\boldsymbol{x}} f$	Gradient of the scalar function f in direction of the vector $\boldsymbol{x}$

Subscripts and Superscripts

x_k	value of x at the k-th time instant
$\hat{x}$	estimate of x
$\bar{x}$	mean value of $x(t)$
x^*	optimal value of x
x_{ref}	reference trajectory for x
$\boldsymbol{x}_l$, $\boldsymbol{x}_r$	states $\boldsymbol{x}$ of left and right side
$\boldsymbol{x}_\varphi$	states $\boldsymbol{x}$ in joint space
$\boldsymbol{x}_x$	states $\boldsymbol{x}$ in Cartesian space

General

$\mathrm{Re}\{x\}$	real part of x
$\mathrm{Im}\{x\}$	imaginary part of x
j	imaginary unit, one solution of the quadratic equation $x^2 = -1$
$\mathbf{M}$	covariance matrix
$E(x)$	expected value of x
t	time
φ	joint angle
$\boldsymbol{\varphi}$	vector of joint angles
ω	angular velocity
τ	torque
F	force
J	moment of inertia
m	mass
g	gravity (9.81 m/s^2)
k	damping
c	stiffness

Optimization / Identification

C	cost function
L	Lagrange function
$\alpha_i, \beta_i, \gamma_j, r_j$	unknown coefficients
$\boldsymbol{\Theta}$	parameter vector

$\boldsymbol{h}(\cdot)$	vector of inequality constraints
$\boldsymbol{\mu}$	vector of Kuhn-Tucker multiplicators
$\mathbf{Q}$	weighting matrix
R^2	Coefficient of Determination

Control

$\boldsymbol{x}$	state vector
$\boldsymbol{u}$	control input
$\boldsymbol{y}$	output vector
$\mathbf{A}, \mathbf{B}, \mathbf{C}, \mathbf{D}$	system matrices in state space representation
$\mathbf{K}$	control gain matrix
w	process noise
v	measurement noise
s	complex Laplace variable
$G(s)$	transfer function
$G(j\omega)$	frequency response
T_t	dead time
T, T_d	time constants
ω_0	eigenfrequency
P	proportional gain
I	integral gain
D	derivative gain

Robotics

$\boldsymbol{\tau}$	vector of joint torques
$\boldsymbol{F}$	vector of forces in Cartesian space
$Z(s)$	impedance
$\mathbf{J}$	Jacobian matrix
$\mathbf{K}_\varphi$	stiffness matrix in joint space
$\mathbf{K}_x$	stiffness matrix in Cartesian space
$\mathbf{M}_\varphi$	mass matrix in joint space
$\mathbf{M}_x$	mass matrix in Cartesian space
$\boldsymbol{v}(\boldsymbol{\varphi}, \dot{\boldsymbol{\varphi}})$	Coriolis and centrifugal torques
$\boldsymbol{g}(\boldsymbol{\varphi})$	gravitational torques
K	Spring constant of a Series Elastic Actuator
$Z(s)$	impedance

Functional Electrical Stimulation

a	muscle activation level
f_r	recruitment curve
$G_a(s)$	activation dynamics

$f(\varphi_{\text{leg}})$	length dependency of muscle force
$g(\dot{\varphi}_{\text{leg}})$	velocity dependency of muscle force
$n_{\text{fes}}(t)$	influence of length, velocity, and fatigue on muscle force
$k_{\text{sat}}(t)$	influence of input saturation

Stability Analysis

V	Lyapunov function
Co	convex hull
p_i	uncertain parameter
Ω	matrix polytope

Abstract

This thesis addresses two main issues of devices that assist human movements: One is stability of the coupled human-robot system, the other is how to make the human the master of the device. Firstly, passive control of exoskeletons with Series Elastic Actuators (SEAs) is investigated. SEAs decouple motor inertia from the human by a spring, reducing undesired interaction forces as a prerequisite for making the human the master. An important result is that if passivity is desired, the SEA cannot guide the limbs with a higher stiffness than that of the spring. Besides passivity analysis, which does not require a model of the human, also model-based stability analysis of human-robot systems is presented, explicitly addressing nonlinearity, time-variability, input saturation, and uncertainty. The example is a Hybrid Neuroprosthesis, which combines an exoskeleton with electrical stimulation of the human muscles. Robustness and performance of different controllers is compared. Conservative over-approximation enables simple stability analysis of the complex structure, indicating that elastic coupling between human limbs and robot can cause instability. The required model of muscle recruitment dynamics is obtained via identification, using an inverted, anti-causal system description. Finally, a correlation-based method is proposed to estimate desired motion for impaired or missing human limbs by complementing residual body motion. This way, the assistive device is reduced to a mere tool for the human, who regains control of lost motor functions. All methods are evaluated in simulations and in practical experiments with healthy subjects.

Kurzfassung

Diese Arbeit untersucht zwei Hauptaspekte bei künstlicher Assistenz menschlicher Bewegungen: Zum einen Stabilität des gekoppelten Systems Mensch-Maschine, zum anderen Übertragung der Kontrolle über das Gerät auf den Menschen. Zunächst wird passive Regelung von Exoskeletten mit seriell-elastischen Aktuatoren (SEAs) untersucht. SEAs entkoppeln Motorträgheit vom Menschen durch eine Feder und reduzieren so unerwünschte Interaktionskräfte, eine Vorbedingung für Kontrolle durch den Menschen. Es zeigt sich, dass unter der Prämisse der Passivität der SEA die Gliedmaßen nur maximal mit der Steifigkeit der Feder führen kann. Neben Passivitätsanalyse, die ohne Modell des Menschen auskommt, wird auch eine modellbasierte Stabilitätsanalyse des Systems Mensch-Roboter präsentiert, die auf Nichtlinearitäten, Zeitvarianzen, Stellgrößenbeschränkungen und Unsicherheiten explizit eingeht. Als Beispiel wird eine Hybride Neuroprothese betrachtet, eine Kombination aus Exoskelett und elektrischer Stimulation der menschlichen Muskeln. Robustheit und Regelgüte verschiedener Regler wird verglichen, wobei konservative Überabschätzung eine einfache Stabilitätsanalyse der komplexen Struktur erlaubt und Risiken durch elastische Kopplung zwischen Roboter und Mensch aufzeigt. Das nötige Modell der Muskelaktivierungsdynamik wird mithilfe eines neuen Identifikationsverfahrens erstellt, das auf einer invertierten, antikausalen Systembeschreibung basiert. Schließlich wird eine korrelationsbasierte Methode zur Schätzung gewünschter Bewegungen beeinträchtigter oder fehlender menschlicher Gliedmaßen vorgestellt, die die Bewegung des übrigen Körpers vervollständigt. So wird das Assistenzgerät zu einem bloßen Werkzeug für den Menschen, der die Kontrolle über verlorene Motorik wiedererlangt. Alle Methoden werden in Simulationen und praktischen Experimenten mit gesunden Probanden evaluiert.

1 Introduction

1.1 Neural Impairment and Motor Rehabilitation

The human motor apparatus is controlled by a sophisticated interplay of various hierarchies in the Nervous System. The Nervous System consists of the *Central Nervous System* (CNS), incorporating spinal cord and brain, and of *peripheral* nerve pathways. Motor commands are encoded in sequences of electrical impulses, which travel via neuronal pathways to the muscles, and sensory information (afferent feedback) is sent back to the CNS.

A lesion to the nervous system, as for example due to stroke or spinal cord injury, can disrupt the generation of appropriate motor commands, and/or the signal transmission to and from the limbs. Stroke is a sudden brain lesion, which can either be due to an interruption of blood supply (*ischemic* stroke), or to bleeding into the brain (*hemorrhagic* stroke) [172]. The lack of oxygen causes the death of nerve cells and an abrupt loss of brain function. Another, less frequent lesion to the CNS is complete or incomplete Spinal Cord Injury (SCI). A frequent disability especially in stroke survivors is hemiparesis, which denominates the loss of sensorimotor functions on one half of the body. Hemiparesis can vary from one-sided weakness and numbness up to a complete paralysis, called hemiplegia.

Although the death of nerve cells is irreversible, the nervous system shows an astonishing capability of re-organizing itself, a phenomenon called plasticity [72]. Neuronal plasticity is a continuous process, which enables permanent adaptation to new challenges and the ability to acquire new skills. The size of the control region in the brain for a specific limb seems to be directly correlated with the use of this limb. For example, professional violinists have a significantly enlarged control area for their string digits compared to the bow hand [73]. Furthermore, new research has confirmed that besides neuronal reorganization, also neurogenesis (birth of new nerve cells) takes place, especially after severe lesions such as stroke [59]; and there are also indications for training-related plasticity at a spinal level [62]. However, when a patient does not use an impaired limb anymore but relies on compensatory movements in other limbs instead, CNS plasticity may even lead to further loss of function in the impaired limbs [7]. This phenomenon is called *learned disuse* [243].

Motor rehabilitation after a lesion to the CNS can exploit plasticity in a positive way, modulate cortical reorganization [168], and in some cases, even lead to a total recovery of the lost functions. A cue trigger for this neural reorganization seems to be *afferent* feedback [201], sensory information to the CNS. These signals are generated by muscle contractions and limb movement, and they can be triggered artificially using rehabilitation technology (Fig. 1.1): Depending on the type and level of the lesion, external stimulation can substitute motor commands in the nerves, it can provoke muscle contractions and thereby afferent feedback to the CNS. Nerves can be stimulated via electric or magnetic fields, and App. C contains a description of this principle. Here, the focus will be on electric

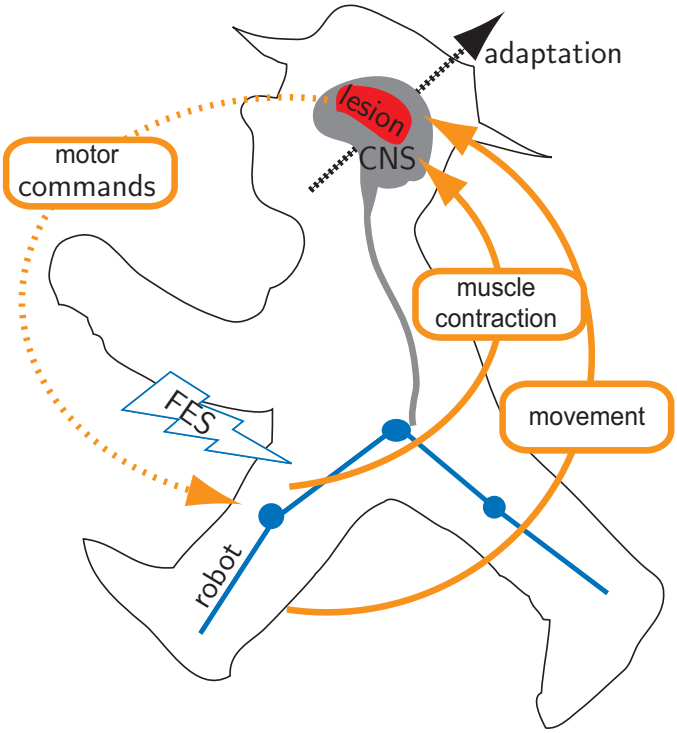

Figure 1.1: Plasticity of the Central Nervous System (CNS) is triggered by sensory feedback on muscle contraction and limb movement. This is facilitated by Functional Electrical Stimulation (FES) and robotic assistance, as the lesioned CNS fails to send sufficient motor commands.

stimulation, because this is easier to apply to moving limbs. For neurorehabilitation of upper extremities, Functional Electrical Stimulation (FES) has shown good results [191], and it can also be advantageous to apply electrical stimulation during walking [152]. FES has been shown to be superior to passive stretching exercises: [150] showed better hand function after cyclic neuromuscular electrical stimulation of hand and forearm. An extensive review of therapeutic applications of FES is given by Burridge and Ladouceur [42].

However, there seems to be a small time window in which rehabilitation is most beneficial, afterwards, in a chronic state, the chances of recovery decrease significantly [227]. Therefore, extensive training directly following a lesion to the nervous system is important. Such extensive training can greatly be facilitated by robotic rehabilitation technology. Robots can provide stability and ensure functional locomotion, thereby lowering the physical strain on physiotherapists.

The therapy effect depends on the specific intervention paradigm. Whenever a human subject tries to acquire new movement skills, active participation of the subject is a key to efficient learning, and unnecessary assistance is counterproductive. Recent studies on human motor learning revealed that making errors is an important driving force of learning a new task, because the required mental task representation is built in an error-driven adaptive process [218, 246]. Departing from this finding, Emken and Reinkensmeyer [75] hypothesized that *augmentation* of the errors of a subject can accelerate the adaptive process and lead to even faster learning, and they were indeed able to show this effect (though it is small) in healthy subjects in experiments with robotically applied force fields

during treadmill stepping. A recent study [264] compared various force fields in terms of the motor adaptation they provoke: Subjects are exposed to visuomotor rotations, and they have to learn to perform a reaching task. While doing this, they are either passively moved, guided along the correct path (soft or hard), left to move unhindered, or subjected to error-augmenting forces. Results show that active and error-augmented group adapt to the visuomotor rotation much better than the other groups, though with no significant differences between active and error-augmented group. A conceptual framework that explains basic motor learning mechanisms is the *challenge point* idea [95]. This theory sees the amount and interpretability of information that can be gained during a motor task as the driving motor for learning. As the amount of available information depends on task difficulty, and the interpretability of information depends on the skill level of the subject, it is hypothesized that task difficulty needs to increase with skill in order to train at the point of optimal learning. This would explain why too much assistance is counterproductive.

In systematic studies with patients, many findings on motor learning of healthy subjects showed to transfer also to neurorehabilitation. Active patient participation is essential for successful rehabilitation [44, 82, 110, 138], and encouragement therefore remains the most important therapeutic means. An extreme example is *Constraint Induced Movement Therapy* (CIMT) [243], which shows remarkable improvements by simple immobilization of the patient's sound arm, such that he has to use the paretic one. Analog observations have been made in FES therapy: The combination of FES and voluntary activity to Functional Electrical Therapy (FET) also showed to be more efficient than FES alone [227]. Burridge and Ladouceur [42] also stress the importance of a volitional component during therapy and use the metaphor of a "catalyst" to describe the effect of FES. Patton has also shown the benefits of error augmentation during robot-assisted rehabilitation compared to guidance along the correct path [176]. In conventional manual physiotherapy, there are also methods that increase task difficulty instead of making it easier. For example, "Proprioceptive Neurofacilitation (PNF)" [273] includes resisting instead of assisting a patient's motion. It has been shown that such a challenging exercise is beneficial after neurologic injury [276].

1.2 Technology to Assist Human Movement

In a stroke rehabilitation scenario with robotic assistance and Functional Electrical Stimulation, as motivated in the previous section, various control aspects need to be considered. Fig. 1.2 shows a hierarchical control concept with four main sub-tasks for such a system: Low-level control aspects are the control of each individual actuator, i.e. the robot and the patient's muscles. In addition, both actuators need to be coordinated in a cooperative manner. A top level defines the reference for the assistive system, in close interaction with the patient. The following sections provide a short overview of the State of the Art with respect to these four sub-tasks.

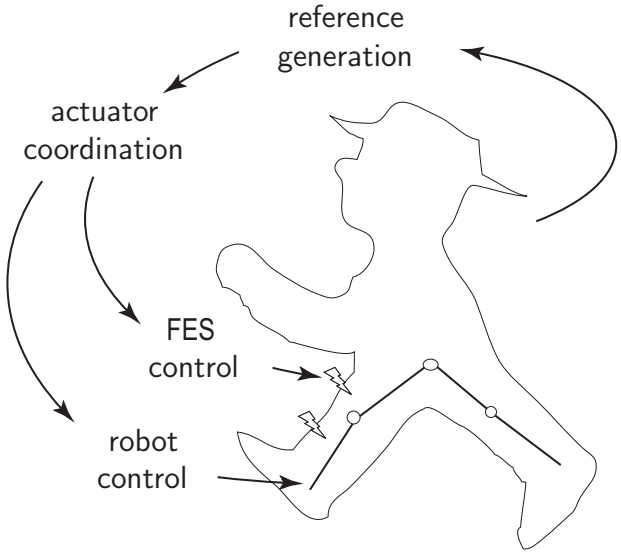

Figure 1.2: Investigated control aspects of assistive technology for gait rehabilitation.

1.2.1 Rehabilitation Robots

Robots that assist human subjects to perform movements represent a special class of *haptic interfaces*. A haptic interface is a robotic manipulator in contact with human limbs (e.g. the hand), which provides a *kinesthetic* (sensed by muscle force sensors) or *tactile* (sensed by skin sensors) impression of a virtual or *telepresent* (remote) environment. Haptic interfaces are not limited to therapeutic applications for motor-impaired patients. They are also used to enhance or train motor capabilities in healthy subjects, such as a knee simulator for orthopedic education [203] or a bone drilling simulator for surgeons [78]. Independent of the application, there are many common issues in haptic devices, such that rehabilitation robot technology can build on a broad basis of experience with physical human-robot interaction.

Hardware Concepts

To categorize rehabilitation robots, one division can be made according to whether the robot is intended for upper or for lower extremities. An early overview of rehabilitation robots for arms and legs is given in [102]. For the arms, there exists a large variety of assistive robots, e.g. [46,109,167,235]. These devices are mainly intended for rehabilitation. Due to fundamental differences between arms and legs (e.g. postural stability during gait, higher forces, almost periodic versus discrete movements, etc.), the scope of this thesis is narrowed down to the lower extremities.

An alternative categorization can be made according to the kinematic concept, which can either be an end-effector-based robot, or a so-called *exoskeleton*. An exoskeleton is an actuated orthosis that kinematically resembles the human Degrees of Freedom (DoFs), and which is attached externally to the limbs. This is the most frequent realization for a gait rehabilitation robot. In contrast, in an end-effector-based concept, the robot is only in contact with the human at a single interaction point. Such a concept for the lower extremities

is e.g. represented by the mechanized gait trainer [104, 277]. This robot uses footplates, which are operated by a doubled crank and rocker gear system, and it generates foot trajectories that emulate normal walking. Its advanced version, the HapticWalker [219], allows almost arbitrary foot trajectories, such that e.g. stair climbing can be emulated.

A third categorization can be made according to the portability of the device. On the one hand, there are lightweight, low-power devices that the user can carry around and obtain functional assistance in everyday life. The RoboKnee [196] and the active knee orthosis presented in [171] assist only the knee during locomotion, and the Human Muscle Enhancer [157] provides assistive torques to the whole leg for partial weight support. The HAL (Hybrid Assistive Limb) system [130] can compensate the lack of muscle strength by a 2-DOF exoskeleton and a force-augmenting control. This is done via electromyographic (EMG) measurement of muscle activity. An EMG-controlled actuated knee orthosis has also been proposed by Fleischer [83]. The BLEEX (Berkeley Lower Extremity EXoskeleton) [52], and the exoskeleton developed by Sarcos Incorporated in Utah, USA, can provide super-human forces to the human body, and they are intended for military applications. An interesting development is a swimming exoskeleton for underwater assistance [169]. The mentioned devices are wearable and lightweight, and thus they are interesting for healthy and disabled alike. From pioneering work of Vukobratović in Belgrade [274] to the ReWalk currently developed by Argo Medical Technologies in Israel, a major goal of portable devices remains re-enabling spinal cord-injured users to walk. Another focus of newly developed active orthoses, especially in Korea and Japan, is to assist the elderly (see e.g. [136]). A recently presented assistive device by Honda, Japan, resembles a bike saddle with legs, and it enables variable body weight support during walking. A comprehensive review of portable lower-extremity exoskeletons is given in [66].

On the other hand, there are non-portable gait trainers, which are mainly intended for time-limited use during rehabilitation. These devices are often stationary and combined with treadmills. The first commercially available gait training robot was the Lokomat [55], which has already become a standard tool for gait therapy in many clinics. It allows patients with strong lesions to walk in a very early stage of therapy, as it incorporates a suspension system and does not require balance nor the ability to stand freely. However, the Lokomat has only two Degrees of Freedom per leg, constraining lateral motion of the pelvis. Today, maximum freedom for the human is increasingly recognized as an important feature. This is realized firstly by compliant actuation, like in PAM (Pelvic Assist Manipulator) and POGO (Pneumatically Operated Gait Orthosis) presented in [13], in the LOPES (LOwer extremity Powered ExoSkeleton) [269], or in the pneumatic exoskeleton presented in [27]. Secondly, the human Degrees of Freedom are left unconstrained, either by a high number of DoFs in the robot, like in the LOPES, or by minimizing contact between human and robot, as in the overground walking apparatus KineAssist [180] and WalkTrainer [35]. The LOPES is a treadmill-based stationary exoskeleton similar to the Lokomat, but in contrast to that device, it allows also lateral pelvis translation and hip ab-/adduction. There are also robots that are not portable, but still enable overground gait training: The KineAssist [180] and the WalkTrainer [35] are mobile overground walking devices with a body weight support system that can apply guiding forces at the hip. The ALEX (Active Leg EXoskeleton) [19] similarly allows overground walking, and it also includes an

exoskeleton for the legs. The Zero-G [166] is a simplistic actuated body weight support system that runs on rails on the ceiling.

This list is not exhaustive, as the number of assistive robots for the lower extremities has been growing almost exponentially over the last years.

Control of Rehabilitation Robots

Motivated by the findings above on how important active patient participation is for motor learning and rehabilitation, control strategies for rehabilitation robots have changed fundamentally in recent years: Whereas the first generation devices were optimized to stiffly guide the subject's limbs, second-generation devices aim at concepts like *Assist-as-Needed* (AAN) [74]. This type of strategy determines the level of assistance required by the subject in order to perform a certain task, and the device provides exactly this needed amount of assistance. AAN means that the device only helps when it is crucial for task execution, and whenever the subject can move autonomously, the device should be maximally *transparent*, implying that the subject should hardly feel the robot.

To enable AAN, a cooperative assistive device must be able to guide the human limbs with a varying amount of stiffness or *impedance*. For a haptic interface, this implies that assistance must range from stiff guidance to minimal interaction forces between robot and human. These requirements can be translated to stiff *position control* of the device on the one hand, and *zero-torque control* on the other hand. Whereas position control enforces tracking of a trajectory despite any interaction forces by the human, zero-torque control aims for transparent behavior. High transparency depends on good force tracking capabilities, which implies that the robot should be a good force source.

There is a trade-off to be considered in the hardware design, making the device more suitable either for stiff guidance or for zero-torque tasks. This trade-off lies mainly in the choice of the actuation principle: A robot optimized for stiff position control will be equipped with stiff actuators, like the Lokomat gait rehabilitation robot [55]. It is possible to render stiff robots somewhat compliant by control using concepts based on *impedance control* or *admittance control* (see e.g. [40, 45, 108, 174, 222, 251]). Impedance control has therefore been implemented on the Lokomat [205]. However, a stiff robot's actuator inertia cannot be fully masked by any causal controller [53], and this inertia can lead to large undesired interaction forces between human and robot during dynamic movements. A relatively new actuator design with an elastic element between drive and user has been shown to improve transparency. This concept was first introduced by Pratt and termed *Series Elastic Actuator* (SEA) [194]. Excellent force tracking and inherent safety are the two major reasons why compliant actuation is more and more incorporated in rehabilitation robots, like linear springs in the actuation of LOPES [269] or pneumatic actuators in POGO [13]. Although such a robot is not optimal anymore for stiff trajectory tracking, its force tracking capabilities enable high transparency and make it more suitable for direct interaction with humans.

1.2.2 Functional Electrical Stimulation

Benefits

Motor neuroprostheses based on Functional Electrical Stimulation (FES), frequently also termed Functional Nerve Stimulation (FNS), are applied successfully today in many areas. For example, neuroprostheses control control bladder function for SCI patients [127], or they treat the so-called drop foot in stroke patients. Such a restoration of function is an important application area of FES. It has been shown that motor neuroprostheses using *transcutaneous* (surface) stimulation for the lower extremities can allow the realization of functional gait for paraplegic patients [86, 88], and even stair ascending and descending [89]. However, due to rapid fatigue, high complexity, and limited controllability, these applications have rarely gone beyond laboratory experiments. In contrast, more simple stimulation devices have become common, e.g. stimulators that permanently correct the frequent impairment of foot drop. A review of foot-drop stimulators can be found in [147]. For such long-term applications, it is in some cases justified to use implantable stimulators instead of transcutaneous stimulators, because they provide more selective control of muscle activation. For example, [145] presented an implantable system for foot drop, which has been found to be a feasible alternative to surface stimulation by [275].

Besides restoration of function, FES has also other effects and purposes, for example a training effect. Muscle training is important in the case of paralysis, because atrophied muscles can lead also to secondary problems with the motor apparatus, e.g. with bones. With the training effect in focus, paraplegic cycling [117, 241] is much more convenient compared to the physically straining gait training. Therefore, it is a popular application of FES for paralyzed users, who experience a certain mobility using their own muscles again. Furthermore, it allows more simple control structures due to the reduced number of Degrees of Freedom. There are other beneficial effects of FES, e.g. it was reported to reduce tonic spasticity [232].

Most important in the context of this thesis, however, is the indirect effect of FES: It stimulates efferent pathways and activates muscle groups or reflexes. Thus, by increasing sensory input to the CNS, FES aims to trigger neural plasticity and to restore the patient's own neural control of the muscles. This importance of FES as a therapeutic means in neurorehabilitation has already been outlined in Sec.1.1.

Control of Functional Electrical Stimulation

Control of electrically stimulated muscles has been investigated for decades (e.g. [271,272]) and applied for neuroprostheses. However, artificial muscle activation is still a challenging task for control design due to numerous reasons: Firstly, electrically stimulated muscles are not recruited in a physiological manner, which leads to substantially increased fatigue. Secondly, muscle response to stimulation is highly nonlinear and exhibits time delays (see App. C). Thirdly, surface stimulation cannot offer sufficient selectivity, which means that motor units cannot be targeted precisely enough. This results in suboptimal force generation and a high uncertainty. One of the main sources of variability has been identified

by [250] as being related to the movement of different tissues between the electrodes and the nerve.

In order to reduce the influence of fatigue, different stimulation pattern shapes have been investigated: Lower frequency reduces fatigue [230], although this competes with the desire for maximum output power, which increases with frequency (with the optimum at 50 Hz) [79]. Furthermore, other shapes have been investigated apart from the conventional single pulse (with a complementing pulse with opposite sign, to prevent accumulation of charge in the tissue) followed by a pause: [26] showed that n-lets (e.g. doublets or triplets) can postpone the onset of fatigue, and this result was confirmed both for healthy [128] and for paralyzed muscle [85].

Delays in the system can be addressed by using feedforward muscle control with pre-calculated patterns. Thereby, principles of optimality can be utilized as in [267]. To deal with nonlinearities, [268] presented a study that compared a linear PID controller with and without a nonlinear compensator to compensate angle-torque and velocity-torque relationship in a cat hind limb. However, the results showed that the combination of the two is only slightly better than the PID alone. This indicates that the main task is to deal with the uncertainty of the muscle behavior.

The high uncertainty and time-variance of the muscle behavior motivated extensive investigations on closed-loop control of FES, e.g. by Hunt and colleagues [115]. Linear closed-loop control of muscle recruitment does still not suffice to make the muscles a reliable means of actuation, due to excessive time-variance, nonlinearities and delays in the system [215]. Therefore, diverse nonlinear and adaptive control methods have been suggested. To deal with time-varying behavior, adaptive cycle-to-cycle control has been investigated by [86]. Riess and Abbas [206] developed adaptive controllers based on artificial neural networks. They showed that the controller can adapt on-line to fatigue [207]. A general possibility to deal with time-varying gains is to use gain scheduling, i.e. to update the controller parameters to follow the time-varying gains [31]. The drawback of this method is that the gains need to be known. Being a popular control method for uncertain systems, Sliding Mode control has frequently been applied to control FES, both in theoretic and practical investigations. For example, [122] used the Lokomat (in zero-torque mode) to provide a testbed for FES with a Sliding Mode controller. High-order Sliding Mode appeared to be less sensitive to disturbances for this application than predictive control in simulation studies [158]. Finally, uncertainty can be reduced in part by better targeting of the specific muscle groups. With surface electrodes, such better selectivity can be obtained by making the electrode shape adaptive, i.e. by using a freely configurable matrix or multi-field electrode array [193].

Most of the studies on FES control have been performed on able-bodied subjects. In neurologically impaired patients, the limitations are even more severe: Sensory-motor mechanisms are modified and the muscles do not respond in the same way as the muscles would in able-bodied humans. Furthermore, modified reflexes produce major problems since stimulation triggers unwanted responses. Especially in this context, reliable tracking with artificial muscle stimulation alone remains a challenging task. Therefore, FES is difficult to apply as the only therapeutic means during gait training.

1.2.3 Hybrid Neuroprostheses

When FES is combined with a robot, the advantages of both methods can be combined: The robot assures stability, FES maximizes afferent input to the CNS, which is relevant for rehabilitation, trains the muscles, and lowers power requirements of the robot. For gait rehabilitation, it has already been shown that the restoration of motor control is supported better by a combinative therapy involving a robot and FES than by mere external guidance by the robot [43]. When exoskeleton and FES are combined, a *hybrid* structure results. Here, the attribute "hybrid" refers to a parallel usage of two redundant actuators: One actuator is represented by the patient's muscle, the other is the robot, which can generate additional joint moments.

The hybrid motor neural prosthesis for the application in paraplegic patients was introduced in the seventies by Tomović [188,248] and little later by Andrews [11] and colleagues. Solomonow and colleagues also investigated the application of FES with unpowered walking orthoses for paraplegics [107]. Popović et al. developed powered walking orthoses and introduced the concept of hybrid control [186, 187]. One important finding from these studies is that a powered orthosis for use in paraplegics has to be adaptive and lightweight and that in most cases it will not be accepted by patients.

New developments focus less on functional restoration of gait, but on rehabilitation and muscle training, like the MotionMaker [154] or projects for paraplegic cycling [117, 241]. These vehicles often dispose of a motor as a second actuator, which improves both exercise quality and range of operation. Thus, they also represent hybrid, or redundantly actuated systems. For therapeutic use in arm rehabilitation, Popović today recommends again the application of a Hybrid Assistive System (HAS) [190]. There, he suggests a serial combination, where the exoskeleton guides the arm, and FES actuates the fingers.

1.2.4 Intuitive Interfacing

As outlined in Sec. 1.1, active patient participation is essential for successful rehabilitation. Therefore, the robot should not enforce given motions on the patients, but it should be cooperative and allow the patients to take part as much as possible. Various concepts have been introduced that allow human users to intuitively control robotic manipulators, and the term *shared control* is frequently used in this context. The aim is often to combine the advantages of robotic manipulators (precise execution) and human capabilities, like for example in the development of microsurgical devices that enable tremor-free microscopic manipulation [244].

A frequent concept in shared control is to classify the human's intended motion, followed by assistance in this specific manipulation task (see e.g. [1] for an overview). With low-level tasks, like grasping and holding objects, assigned to the robot, the human user can concentrate on high-level control tasks like using the grasped object as a tool [93]. It has been shown that shared control of the robotic manipulator can even improve the perception of *presence* in a remote, telepresent environment [252]. Similar concepts have been used to estimate the intention of a wheelchair user [64]. However, such a strategy assumes that the task can be divided hierarchically: A discrete level of motion primitives (e.g. movements

to different targets) supersedes a continuous domain of corresponding trajectories (e.g. straight lines to these targets). The robot's task is to disburden the human from the low-level motions with an arbitrary degree of assistance. However, there are two important limitations: Firstly, success depends on a sufficiently large space of motion primitives, and on a correct classification of the motion. Secondly, the subdivision into high-level and low-level tasks, as well as the degree to which the human should participate is often not that clear. For example, in a rehabilitation scenario, the focus is on training of the continuous motion itself, not on "disburdening" the human.

Shared control is often also based on the principle of *Virtual Fixtures* introduced by Rosenberg [212], which provide physical constraints to facilitate task execution (like a ruler for moving in a straight line). Similar concepts have been suggested to provide a virtual "tunnel" or path for joint angles during motion training. For example, the strategy of *Path Control* [67, 254] supervises correct execution of a gait trajectory during robotic gait rehabilitation only in terms of the spatial course of joint angles, and the timing of the motion is left free to the patient.

An intuitive approach to make the robot a simple tool for the user is to augment any motion the user might perform, which can be done using positive feedback as in the BLEEX [131] and by inverse dynamics, as suggested for a patient-controlled neuroprosthesis [204]. For the control of human limbs with at least partially preserved neuronal activity, it is also possible to directly use the electric motor commands sent to the human muscles, which can be measured by *electromyography*. This has e.g. been suggested by [83] for the control of an exoskeleton. Similar approaches have been used for a long time for so-called *myoelectric* prostheses, especially to restore arm and hand function [139]. EMG-based estimation of the user's intention has also been combined with FES; pioneering work was done by Hansen [266]. However, there are several difficulties that arise during simultaneous EMG and FES, which require sophisticated signal detection and filtering, as e.g. used in the EMG-controlled neuroprostheses proposed in [217] or [132].

Major difficulties arise when there is hardly any coordinated activity in the limbs to be assisted. Then, the described strategies, which augment human motion, will fail. However, there are still possibilities to estimate the intended movement for disabled limbs: The remaining limbs of the body, as well as contact with the environment can still be observed and used for control. A selection of motion primitives can be performed by a manual switch-based interface, as e.g. in the neuroprosthetic system proposed by Fuhr [88], or by an intention estimation similar to the hybrid discrete-continuous concepts mentioned above. For example, Azevedo and Héliot [15] deduced the intention of a paraplegic user to stand up from his thorax acceleration. The leg prosthesis C-Leg (Otto Bock AG, Duderstadt), detects the current gait phase and adapts damping properties of the controlled knee joint appropriately. These are all rather discrete, high-level interfaces, because transferring full control of movement (possibly of multiple joints) in the continuous domain to the user poses high demands on the interface, otherwise it will put a burden on the subject's cognitive functions. For some special cases, where motions are symmetric, a mirror-control can be used. This is e.g. done in rehabilitation of *hemiparetic* (having a half-sided partial paralysis) patients, who can use their "good" arm to generate reference trajectories for their paretic arm, such that the motion can then be assisted by a robot [103]. However,

for general assistive systems, mirror control does not suffice, and more generic interfacing methods need to be found, while still not augmenting the cognitive burden for the user.

1.3 Stability Considerations in the Control of Biomechanical Systems

Whenever human limbs are part of a control loop, safety is one of the most important issues. Absolute safety can never be guaranteed during direct contact of a technological device with a human user, but should nevertheless be striven for. Various hazards need to be considered, and redundant measures should be taken to minimize the chance of injury. The general term "safety" subsumes a multitude of requirements. For example, the range of motion in the human joints should not be exceeded, malfunctioning of a robotic device should not lead to electric shocks to the patient, etc.. A particularly important facet of safety is stability. This term is still ambiguous, and various aspects of stability are relevant in an assistive device, especially for gait therapy.

For a device that assists walking, postural stability is an essential requirement. This means that the subject's balance must be maintained, such that he cannot stumble and fall. For knee exoprostheses, stability has been defined as "the avoidance of sudden or uncontrolled flexion" during stance phase [189]. For postural stability, methods from biped robots can be applied, like supervision of the so-called *Zero Moment Point* (ZMP). In analogy to walking robots, it might also be desirable to assure global stability, i.e. a so-called *limit cycle* behavior with a stably repeating gait pattern. Such a global stability analysis of periodic trajectories is generally done via Poincaré maps. An exemplary application of ZMP control and Poincaré maps can be found in [229].

When a robot is in physical interaction with a human, stability should comprise local asymptotic stability or BIBO (Bounded Input Bounded Output) stability. A frequent example definition of local stability is that the interaction forces between robot and human or the energy exchanged must be bounded. Harwin [97] points out that in all assistive robots for "prosthetics, aids for daily living and physiotherapy [...] there is the potential for the interaction to be non-passive with a resulting potential for the human/machine/environment combination to become unstable".

In the specific context of biomechanical systems, there is the special challenge of high uncertainties within the loop, generated by unpredictable voluntary human behavior and still deficient knowledge of the exact biomechanical properties. For any practical system, it will be impossible to model all factors. Thus, a high degree of uncertainty in the control loop has to be tolerated, and there is hardly any "nominal" operating point like in a deterministic machine. Instead, the system must be robust, i.e. stable for a large uncertain manifold. Generally, there are two fundamentally different approaches to prove stability of coupled systems (like a robot and a human), which will be outlined in the following.

The first approach is to model the entire system with human biomechanics and robot, to quantify uncertainties, and to design a controller that leads to stable behavior for the entire

uncertain manifold. However, there is an almost infinite number of influencing factors in the human biomechanical system. Therefore, simplified models are commonly used for the compound of assistive device and human, controllers are designed for this nominal behavior, and it is not investigated which repercussions the initial simplifications have on stability. One example is the common simplifying assumption of rigid human-robot contact. Although this is incorrect due to multiple elastiticies in the coupling and in the human tissue, it is generally justified by the fact that a reliable quantification of the time-varying elasticity between robot and bone is very difficult. Although discrepancies between the predicted outcome of rigid models and actual behavior of actuated orthoses have been documented by various groups [8,83,184], repercussions of the simplifications during control design in terms of stability have not been analyzed systematically. Such an analysis can be done by formulating the system as having time-varying uncertain parameters and applying the concept of Lyapunov [146]. Using so-called common or piecewise Lyapunov functions, conditions for the stability of systems with parameters that are variable but confined in given polytopes can be derived [4, 9, 36, 124, 283]. As far as relevant for the investigations in this thesis, this literature will be reviewed in Chap.4, more specifically in Sec. 4.4.

The second approach is to separate human biomechanics and robot, and to design a controller for the robot that ensures *passivity* [54]. A passive system is stable when coupled to any other passive system. Therefore, this approach does not need an explicit model of the human, and it does not rely on the simplifying assumption of rigid coupling. Instead, it suffices to assume the abstract property that the human behaves passively, too. This method has several drawbacks: The assumption that the human behaves passively is not valid when e.g. the limbs are spastic. Furthermore, the concept can only be used when a clear cut can be made between biomechanics and device; for example, it cannot be easily transferred to closed-loop control of neuroprostheses. However, compared to an explicit model of both robot and human, passivity analysis of only the robot is attractive due to its simplicity, and because it is a conservative approach. This method has been applied to control of rigid robots [53], and also to early control concepts for compliantly actuated robots [194]. However, more efficient later control strategies for compliant robots have not been analyzed with respect to stability, which means that theoretical limitations of these robots in terms of robustly achievable performance are still not known.

1.4 Contribution and Outline

This thesis investigates suitable control strategies for rehabilitation robots, FES, and combinations in form of Hybrid Neuroprostheses. Several methods are proposed to match the derived requirements of stable and user-controlled assistance from different points of view. This thesis is organized according to the hierarchic control concept in Fig. 1.2, and each of the following chapters is dedicated to one of the four aspects. The derived methods can also be used on a stand-alone basis.

First, Chap. 2 investigates haptic interfaces with compliant actuation, a hardware concept that is increasingly used in rehabilitation robotics. To allow variable assistance tailored to the patient's individual needs, the aim is to maximize both achievable transparency and achievable stiffness. The main focus here is on stable human-robot interaction. The

control approach is based on impedance control, and it proceeds from the inside to the outside: First, the inner force controller is designed, with the aim to minimize undesired interaction in zero-torque control (i.e. make the device transparent), and to achieve good force tracking properties. Then, the outer impedance loop is closed, in order to investigate maximum achievable stiffness. Stability in interaction with a human user is investigated by the concept of passivity, which means that no explicit model needs to be assumed, neither of the human biomechanics, nor of the human-exoskeleton coupling. As a contribution to the field of compliant robots, the passivity analysis delivers both practical constraints for parameter tuning, as well as theoretical insights into performance limitations of SEAs. The most prominent result is that the rendered stiffness cannot be increased arbitrarily if passivity is desired; instead, it is limited by the intrinsic compliance of the elastic element. In practical experiments with the LOPES robot, the excellent force tracking capabilities are validated, and theoretical predictions of performance limitations are compared to practical results.

Chap. 3 addresses modeling issues for the control of Functional Electrical Stimulation. To obtain a biomechanical model and to quantify associated uncertainties for an individual human subject, identification is necessary. The biomechanical model can be split into two parts: One part contains the mechanical properties of the leg and exoskeleton, like inertia, mass, and elastic joint moments. This can be robustly done using state-of-the-art identification methods, and the procedure is explained in App. E. The second part, muscle response to Functional Electrical Stimulation, is difficult to identify due to a high number of unknown influencing factors. Under isometric conditions (constant muscle length), muscle response to FES is commonly described by a Hammerstein model. Hammerstein models consist of a nonlinear recruitment curve in series with linear activation dynamics. To identify these dynamics, mainly forward approaches are used. The advantage, provided that the nonlinearity and the dynamics are linear in the parameters, is that a simple least-squares solution can be found. However, for model-based control with input-output linearization, the inverse nonlinearity is needed, and the identified nonlinearity is not necessarily invertible. Furthermore, muscle recruitment is generally of saturation characteristic, complicating a linear parameterization with a low number of parameters. Here, a reverse identification is performed, changing the structure to Wiener type. The number of parameters can be very low, exploiting the fact that an inverted saturation characteristic is approximated well by a simple third-order polynomial. The algorithm is evaluated in practical experiments with quadriceps and hamstrings muscles of healthy human subjects.

Chap. 4 is concerned with the coordination of the two actuators, a robot and the patient's muscles. Based on the obtained biomechanical model, four different controllers are designed for the redundantly actuated system. These controllers aim at a varying task distribution for the two actuators. The concepts range from shared, pari passu control over a master-slave concept to a concept where the motor is solely responsible for tracking, and the muscles are simply incorporated in a feedforward manner. In the course of this work, a detailed model of the system has been identified, incorporating numerous parameters; however, such a procedure is almost impossible in a practical environment. There, simplified models will have to be used and controllers must be robust. To investigate the repercussions of such model simplifications during the design process, all controllers are designed based on a simplified behavior. The major simplification is the common assump-

tion of rigid coupling between robot and human. Furthermore, parameters are assumed to be constant. The stability analysis is then performed based on the full model with non-rigid coupling, as well as on the identified model uncertainty. Theoretical predictions of the stability analysis are compared to practical results obtained with healthy subjects, and performance and robustness of the various control concepts are evaluated.

In Chap. 5, the aim is to investigate intuitive interfaces that allow subjects with partial paralysis (or amputation) to regain control of their limbs via an assistive device. The example system is again the lower extremity exoskeleton LOPES. The challenge is to maximize information transfer about the intended movement from the human to the device, without a heavy cognitive burden on the human. The contribution of this work is a new method to estimate intention based on *synergies* between different limbs. Healthy human motion is controlled via a sophisticated hierarchical network with multiple inter-dependencies. These inter-dependencies can be used to retrieve information about the intended motion of the whole body by observation of only a limited number of joints. With this information, it is possible to complement the motion also for limbs that can no longer be controlled by the human. This approach is named *Complementary Limb Motion Estimation* (CLME). Groups that might profit from this method are patients with complete or incomplete loss of function in parts of their body, which are e.g. stroke patients, patients with incomplete Spinal Cord Injury, and amputees. The example application used for evaluation is a lower-leg exoskeleton, and a half-sided impairment of the patient. The method is implemented on the LOPES gait rehabilitation robot and evaluated with healthy subjects in two experiments: In a first study, subjects walk only with one leg, while the robot's other leg acts as a fake prosthesis, to simulate complete loss of function in one leg. In a second study, subjects walk with both their own legs to assess the interference with self-determined, normal walking. Walking with zero-torque control is thereby chosen as the baseline of minimum achievable interference. Evaluation criteria are joint power introduced by the robot, as well as changes in muscle activity (measured by *electromyography*, EMG) and kinematic distortions compared to the zero-torque case.

2 Biomechanics in a Black Box: Passivity-Based Control of a Compliant Assistive Robot

2.1 Introduction and State of the Art

For the control of haptic manipulators, which interact with a human being, safety concerns are among the most important issues during the design process. Stability of the manipulator, however, does not suffice. The manipulator and the human, being in direct contact, become a coupled system. Coupled systems may become unstable, even if all their components are stable. The main problem is that the control strategies of the human are far from known, complicating the design process of the manipulator. A conservative procedure is to design the manipulator in such a way that the range of stable couplings with different environments is as large as possible. For the family of passive systems, general statements about coupled stability can be made: It can be shown that passive systems coupled in feedback or in parallel manner again yield a passive system. Therefore, it is commonly assumed that the human being acts as a passive system, resulting in the requirement that the controlled manipulator needs to be passive. The design of passive control for stiff actuators has been investigated for a long time. In recent years, however, compliant actuation of robots is becoming more and more common, because it allows the realization of highly interactive haptic interfaces with low undesired interaction forces. As these compliant mechanisms still represent a young actuation principle for haptic manipulators, little investigations have been performed concerning stability or passivity. This chapter investigates compliant actuators under the aspect of passivity. From this analysis, limitations in achievable performance are derived, mainly concerning achievable stiffness and bandwidth.

2.1.1 The Series Elastic Actuator (SEA)

For haptic interfaces, a variety of actuation principles is possible, e.g. as surveyed in [112] or [286]. After the introduction of a compliant actuation principle termed *Series Elastic Actuator* (SEA) by Pratt [194], a large number of actuators with series elastic elements has been presented. Before, compliance had always been considered a disturbing component and was treated as such [18]. Various robots with SEAs were developed by MIT groups [210, 249], Sensinger and Weir [224–226], or Wyeth [282]. A translatory SEA version has been proposed in form of the *robotic tendon* by Sugar [237]. SEAs are used for various applications, e.g. for walking robots [96], for prosthetic and orthotic leg systems [101], or for force-sensing robot arms [134]. Similar principles have also been investigated, such as e.g. the SDA (Series Damper Actuator) [50], or a compliance in parallel with the actuator [98, 238]. In recent years, there is also a growing number of compliant robots with mechanically

adjustable stiffness, for example a version of the robotic tendon that varies the number of active spring coils [111], the MACCEPA [96], or the Variable Stiffness Mechanism [100]. The investigations of this chapter are limited to SEAs with linear stiffness as the basic concept.

The principle of a rotary SEA is schematically illustrated in Fig. 2.1, and the idea can easily be transferred to the linear case[1]. The load is coupled to the drive via a compliant element, in this case a spring with linear characteristic.A relative displacement of load and actuator provokes a spring torque τ_L, making the spring length a direct measure of the interaction torque.

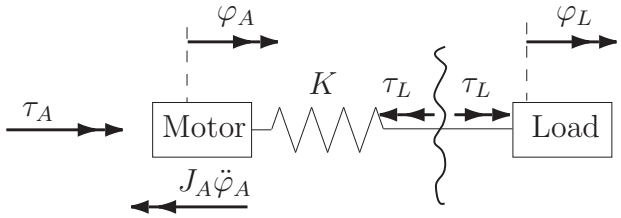

Figure 2.1: Series Elastic Actuator. The drive is connected to the load via a compliant element (here a torsion spring with constant K). Drive inertia is J_A, the motor torque is τ_A. The spring torque τ_L acting on the load is proportional to the difference between motor angle φ_A and joint angle φ_L.

2.1.2 Advantages and Limitations of a SEA

Although an elastic concept does have several drawbacks, such as limited bandwith [76], it has its advantages in the extremely low realizable impedance. As the force-elongation relationship of the elastic element is known, the elongation can be used for a very cheap force sensor. Furthermore, in contrast to stiff actuators, where actuator saturation leads to high torques at high load accelerations (such as the onset of a movement), a Series Elastic Actuator takes on the low natural impedance of the elasticity at high frequencies.

Table 2.1 lists advantages and drawbacks of Series Elastic Actuation. One important advantage is that it allows treating the force control loop as a position control, because the spring length can be considered proportional to the force output. It has been demonstrated that a higher compliance in the force control loop allows for higher control gains [209]. This way, better force tracking performance can be achieved.

PROS	CONS
Decoupled Actuator Inertia	Limited Stiffness
Reduction of Friction Effects	Limited Bandwidth
Inherent Safety and Impact Resistance	Extra Mechanical Element
Energy Storage	High Power Requirements

Table 2.1: Advantages and Disadvantages of Series Elastic Actuation

[1]Figures in this chapter are re-printed, with permission, from [259], ©[2007] IEEE / [262], ©[2008] IEEE.

Another important advantage of a SEA is that the spring decouples motor inertia from the exoskeleton. This reduces the reflected mass of the device, which is crucial to lower undesired interaction torques, especially at high frequencies. A compliantly actuated robot will give way at impact. This is advantageous in terms of safety issues and actuator impact resistance, as well as for realistic experience and training efficacy during impact-type events.

The SEA thus gains easier and robust force control without depending on expensive (high speed, high precision) mechatronics components, yet there is a price to pay in terms of bandwidth and achievable stiffness. This will be outlined in a theoretical and practical evaluation of impedance control performance.

The properties mentioned above make the SEA highly attractive for rehabilitation robots: During rehabilitation, active participation of stroke survivors is required since it promotes neural recovery [44, 110]. New developments in the field therefore focus on interactive control algorithms to assist the subjects only when it is needed, so that the patients are challenged to walk themselves and not to rely on the robot.

2.1.3 Control Strategies for the SEA

Force and impedance control of Series Elastic Actuators are generally kept very simple and linear. The common approach is to design an inner force control loop with the aim to make the spring torque τ_L track a desired spring torque $\tau_{L,\mathrm{ref}}$. An outer impedance loop can then be used to generate a force depending on the current load position, for example to guide the user along a reference position trajectory with a certain stiffness.

The controller suggested by Pratt [194] is a simple PID (Proportional-Integral-Derivative) torque controller with some feedback terms added to it. In transfer function notation, this gives the control law:

$$\tau_A(s) = \tau_{L,\mathrm{ref}}(s) + G_{\mathrm{PID}}(s)[\tau_{L,\mathrm{ref}}(s) - \tau_L(s)] + \frac{J_A}{K} s^2 \tau_{L,\mathrm{ref}}(s) + k_b J_A s^2 \varphi_L(s), \tag{2.1}$$

with

$$G_{\mathrm{PID}}(s) = P + \frac{Ds}{Ts+1} + \frac{I}{s}. \tag{2.2}$$

If there is no sensor for the acceleration $\ddot{\varphi}$, then the last term cannot be implemented, because it can easily be shown that filtered differentation will derogate passivity for any value of k_b. Therefore, this feedforward term is neglected from here on. Furthermore, the system will not be passive for any value of $I > 0$, such that [194] decided to replace the integrator term by a first order lowpass, which, however, does not counteract static errors. Later, the group proposed driving the motor by a voltage source for the robot Troody [195], this way closing an inner loop for the motor velocity, which is in their case measured via Hall sensors. Wyeth [282] also suggested using a cascaded control loop with Proportional-Integral (PI) controllers, but encoder-based. Sugar suggested control concepts for the *Robotic Tendon* [237], which can be regarded as a translatory SEA version. Moreover, his control concepts (*nut control* and *equilibrium controlled stiffness*) are also very similar: The inner loop is a PD position control of the motor position, which is mathematically equivalent to a PI motor velocity control. Around this inner position controller, Sugar

closes a loop that calculates the reference motor position linearly depending on the desired force and the actual spring length, which amounts to a derivative controller in the outer loop of a velocity-based control. Therefore, the mechanical concept and control for the robotic tendon is equivalent to the cascaded schemes proposed later by Pratt and Wyeth for the SEA, only with the outer controller relying on D action instead of PI action.

Pratt also presented another control scheme [195], which couples outer impedance loop and inner force control loop. Besides a desired offset torque, the outer impedance loop commands virtual stiffness and damping to the inner loop, such that a structure-varying system results. Stability and passivity issues of such time variant systems are tedious. Furthermore, this scheme seems not suitable for impedances close to zero, because nonzero virtual elasticity and damping parameters have to be given. Therefore, this control scheme is not considered here, and the analysis is limited to the cascaded schemes.

In contrast to stability of undesired elasticity [91], stability of SEAs has only rarely been investigated. Except for the investigations in [194], which concern earlier, suboptimal control attempts, there is no systematic analysis of coupled stability of humans in interaction with SEAs. Passivity properties of newer control concepts, which are based on cascaded force control, have not been investigated yet.

2.1.4 Contribution and Outline of this Chapter

This chapter investigates and illustrates the trade-off introduced by the use of compliant actuation in light of stability and passivity. First, the state-of-the-art force control schemes for Series Elastic Actuators are investigated. By using a PID controller for the outer force control loop and an inner velocity loop, all control concepts can be generalized, and each concept represents a special case with varying parameters set to zero. The properties derived in this chapter are thus valid both for the SEA and the robotic tendon. As a result of the comparison, cascaded control with inner velocity loop is chosen and passivity-ensuring boundaries for controller parameters are calculated. The presented control design process is straightforward and allows proceeding from the inside to the outside.

Around the force control loop, an impedance control loop is closed. For this complete scheme, passivity is analyzed again. The stability analysis provides an interesting new result: If the rendered stiffness of an elastically actuated joint is increased beyond the intrinsic stiffness of the elastic element, stability of the coupled system human-robot cannot be guaranteed, at least not in the conservative terms of passivity. Furthermore, the compliance severely limits bandwidth, and the reflected mass of the exoskeleton further limits the effectiveness of impedance control to low frequencies.

Using the gait rehabilitation robot LOPES of the university of Twente [269] as a testbed, experimental results are presented to compare theoretical predictions with practice. Following the description of force control and impedance control of the LOPES, the advantages and limitations of SEAs will be illustrated. In this treadmill-based exoskeleton, the torques are transmitted from synchronous motors via Bowden cables and springs to the joints. Higher gains allow the realization of proper feedback controlled torque actuators for LOPES despite substantial adverse effects of high friction and stick-slip in the Bowden

cables, as well as play in the transmission. In LOPES, reduction of mass is achieved by two complementary features of the actuation: Firstly, using the concept of Series Elastic Actuators, drive inertia is decoupled from the load side. Secondly, the drive units are also locally detached from the exoskeleton by the use of Bowden cables. More information on the LOPES is given in App. A. The low realizable impedance of the LOPES robot will be demonstrated in practical experiments.

2.2 Force Control

The task of the inner force control loop is to make the spring torque τ_L track the desired spring torque $\tau_{L,\mathrm{ref}}$. The goal is to reach a relationship as close as possible to $\tau_L = \tau_{L,\mathrm{ref}}$, which would also allow for an ideal realization of zero impedance. An important constraint is the conservation of stability and passivity aspects, which leads to certain boundaries for the control parameters.

2.2.1 Generalization of Existing Strategies

First, the SEA is modeled as a plant to be controlled. The differential equation for the system in Fig. 2.1 is

$$J_A\ddot{\varphi}_A = \tau_A - \tau_L = \tau_A - K(\varphi_A - \varphi_L), \tag{2.3}$$

with φ_L and φ_A denoting load and motor angles, respectively, J_A the motor moment of inertia, τ_A the motor torque and K the torsion spring constant. Fig. 2.2 displays the block chart. Seen from the motor, the uncontrolled system ($\tau_A = 0$) has the input $-\varphi_L$ (load

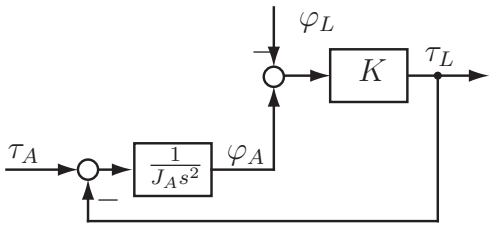

Figure 2.2: Block chart of the plant, i.e. the uncontrolled SEA. Motor dynamics are represented by the inertia J_A. The spring torque depends on motor angle φ_A and joint angle φ_L, the spring constant is K.

displacement that provokes spring compression), and the output τ_L (the spring torque that counteracts compression). Thus, the position-torque transfer function $G_p(s)$ of the uncontrolled plant is:

$$G_p(s) = \frac{\tau_L(s)}{-\varphi_L(s)} = \frac{J_A K s^2}{J_A s^2 + K}. \tag{2.4}$$

Now, the control strategies mentioned above are subsumed in a generalized control, as displayed in Fig. 2.3. In order to keep the notation simple, the dependency on s in transfer

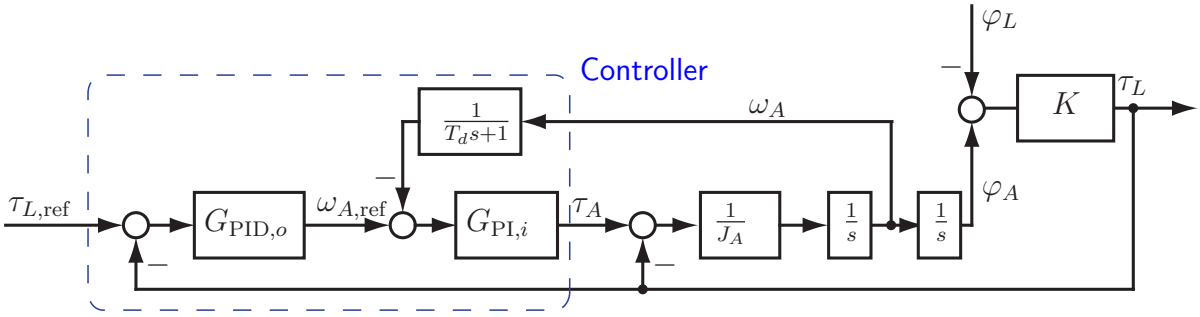

Figure 2.3: Generalized cascaded torque controller. An inner PI velocity loop controls motor velocity ω_A. A first-order lowpass represents delay caused by numerical differentiation of the motor angle. The reference velocity is calculated by an outer PID controller for spring torque τ_L.

function notation will not be indicated explicitly anymore in the following. With the inner and outer controllers

$$G_{\mathrm{PI},i} = P_i + \frac{I_i}{s}, \quad G_{\mathrm{PID},o} = P_o + \frac{I_o}{s} + \frac{D_o s}{Ts+1}, \tag{2.5}$$

the reference velocity $\omega_{A,\mathrm{ref}}$ is given in dependence of the torque error:

$$\omega_{A,\mathrm{ref}} = G_{\mathrm{PID},o}(\tau_{L,\mathrm{ref}} - \tau_L), \tag{2.6}$$

and the general control law can be written as:

$$\tau_A = G_{\mathrm{PI},i}[\omega_{A,\mathrm{ref}} - \frac{\omega_A}{T_d s+1}] = G_{\mathrm{PI},i}[G_{\mathrm{PID},o}(\tau_{L,\mathrm{ref}} - \tau_L) - \varphi_A \frac{s}{T_d s+1}]. \tag{2.7}$$

In any setup similar to LOPES, where the motor encoder signal is less noisy than the potentiometer for spring length measurement, the necessary time constant T of the spring torque differentiation filter will be larger than the necessary time constant T_d for the motor angle differentiation filter. If the inner velocity loop is already closed in the PWM with Hall-based velocity sensors instead of filtered differentation of the encoder signal, the inner phase delay vanishes, $T_d \approx 0$.

In contrast to the single-loop force control mentioned above, this cascaded scheme can ensure passivity while still counteracting static errors via integrators, if some boundaries on the parameters are obeyed. This will be outlined in the following.

For haptic systems, the impedance $Z(s)$ is generally defined as the transfer function from input velocity to opposing torque. This definition allows to assess stability in terms of passivity. First, the autonomous case is considered where $\tau_{L,\mathrm{ref}} = 0$, which is equivalent to zero desired impedance. Using the notation of Fig. 2.3, $Z(s)$ equals:

$$Z(s) = \frac{\tau_L}{-\varphi_L s}. \tag{2.8}$$

This results in:

$$Z(s) = \frac{K(P_i s + I_i + J_A T_d s^3 + J_A s^2)s(Ts+1)}{\sum_{i=0}^{6} d_i s^i} \tag{2.9}$$

with

$$\begin{aligned}
d_6 &= J_A T_d T \\
d_5 &= J_A (T_d + T) \\
d_4 &= K(P_o P_i + 1) T_d T + K D_o P_i T_d + J_A \\
&\quad + T P_i \\
d_3 &= P_i + T I_i + K[(I_o P_i + P_o I_i) T_d T \\
&\quad + (P_o P_i + 1)(T_d + T) + D_o P_i + D_o I_i T_d] \\
d_2 &= I_i + K[(I_o P_i + I_i P_o)(T_d + T) \\
&\quad + P_o P_i + D_o I_i + 1 + I_o I_i T T_d] \\
d_1 &= K[I_i I_o (T + T_d) + I_o P_i + I_i P_o] \\
d_0 &= K I_o I_i.
\end{aligned}$$

2.2.2 Stable and Passive Force Control

Now, passivity conditions for the force control of Fig. 2.3 will be investigated, resulting in bounds for the control gains.

Passivity is ensured if the impedance (2.8) is positive real [54]. Necessary and sufficient conditions for this are:

- $Z(s)$ must be stable,
- the real part of $Z(j\omega)$ must be nonnegative for all ω for which $j\omega$ is not a pole of $Z(s)$.

First, the real part of $Z(j\omega)$ is calculated, which gives:

$$\mathrm{Re}\{Z(j\omega)\} = r(a\omega^8 + b\omega^6 + c\omega^4 + d\omega^2), \tag{2.10}$$

with

$$\begin{aligned}
a &= K^2 J_A T_d^2 [D_o(P_i - T I_i) \\
&\quad - T^2(I_o P_i + P_o I_i)] \\
b &= K^2 [D_o[(P_i - I_i T) J_A + (T - T_d) P_i^2] \\
&\quad + T^2[(P_i - I_i T_d) + P_i^2 (I_o T_d + P_o)] \\
&\quad - J_A (T^2 + T_d^2)(I_o P_i + P_o I_i)] \\
c &= K^2 [I_i^2 (D_o (T - T_d) + T^2 (P_o + I_o T_d)) \\
&\quad + P_i^2 (I_o T_d + P_o) - J_A (I_i P_o + P_i I_o) \\
&\quad + P_i - I_i T_d] \\
d &= K^2 I_i^2 (I_o T_d + P_o) \\
r &> 0
\end{aligned}$$

Equation (2.10) is nonnegative for all $\omega \neq 0$, if all coefficients a, b, c, d are nonnegative. During controller design, these inequalities have to be checked. First, the case of encoder-based

velocity control is considered, which implies a nonzero phase delay in the differentiation with $T_d \neq 0$. Then, in order to ensure positiveness of coefficient a, there are only two options: Either the integrators cannot be used, or an outer D_o has to be implemented. However, the latter is undesirable in most cases, because it requires numerical differentiation of two possibly noisy signals: the torque sensor signal, and the reference signal, which generally originates from an outer impedance controller. Therefore, T_d should be as small as possible, ideally it should completely be removed by using a motor velocity sensor. However, this is a conservative, theoretical case. In a technical realization, there is always damping present, e.g. due to friction. Viscous friction v, which can be modeled by replacing the term $(J_A s^2)$ by $(J_A s^2 + vs)$, also allows to implement nonzero values for both integrator gains I. However, for the Bowden cables used, friction is hard to quantify due to the complex and highly time variant behaviour.

For easy tuning of both controllers separately, a possible set of simple rules that ensures obedience of passivity requirements is (assuming $T_d < T$):

$$\begin{aligned} & P_i > J_A \\ \wedge \quad & I_i < 0.5 P_i \\ \wedge \quad & I_o < 0.5 P_o \\ \wedge \quad & D_o > 4T^2 P_o. \end{aligned} \tag{2.11}$$

By checking the Hurwitz determinants, it can be shown that the conditions above also ensure asymptotic stability. If $T_d = 0$, the inequalities generated from (2.10) become very simple and D_o may be omitted. However, the first 3 rules should still be followed.

2.3 Impedance Control

Fig. 2.4 shows the force control of the SEA with $T_d = 0$ embedded in a Single Input Single Output (SISO) impedance control loop. The outer impedance controller sets the desired impedance, whereby only the case of a rendered stiffness P is considered. The analysis of

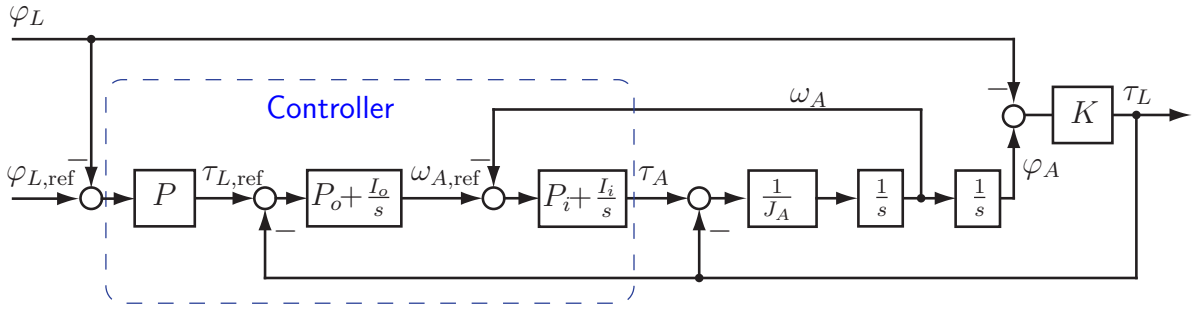

Figure 2.4: Impedance control. Around the cascaded torque controller, an impedance control loop is closed on the joint angle φ_L. Here, it displays a virtual stiffness P.

impedance control with the SEA will first illustrate the well-known drawback of bandwidth limitations in a compliant actuator [76]. Then, a new result will be presented: The fact that the rendered stiffness of the device cannot be increased beyond the stiffness of the

elastic element, if passivity is to be maintained. The analysis concludes with the influence of these limitations, as well as the influence of uncompensated exoskeleton mass, on the performance of impedance control in Cartesian space.

2.3.1 Bandwidth Limitations

Bandwidth limitations will be illustrated on the example of the LOPES actuators, first for the SEA alone and then for the more realistic case, in which there is an extra endeffector mass (an exoskeleton) between the patient and the elastic element.

Bandwidth of the SEA with Massless Endeffector

The impedance $Z(s)$ is now calculated again according to (2.8). With the simplified model of Fig. 2.1, which neglects friction and elasticity of the Bowden cables, and with the parameters given in Fig. 2.4, the impedance transfer function is:

$$Z(s) \quad = \frac{K(J_A s^4+P_i s^3+(P_i P_o P+I_i)s^2+\psi P s+I_i I_o P)}{(J_A s^4+P_i s^3+(P_i P_o K+K+I_i)s^2+\psi K s+I_i I_o K)s}, \tag{2.12}$$

with $\psi = (I_i P_o + I_o P_i)$.

Replacing the complex variable s in (2.12) by $j\omega$, the frequency response $Z(j\omega)$ is obtained:

$$Z(j\omega) \quad = \frac{K(J_A(j\omega)^4+P_i(j\omega)^3+(P_i P_o P+I_i)(j\omega)^2+\psi P(j\omega)+I_i I_o P)}{(J_A(j\omega)^4+P_i(j\omega)^3+(P_i P_o K+K+I_i)(j\omega)^2+\psi K(j\omega)+I_i I_o K)(j\omega)}, \tag{2.13}$$

A look at asymptotic behavior of $Z(j\omega)$ is useful for an intuitive understanding of the SEA behavior: For low frequencies ($\omega \to 0$) and nonzero integrators, the programmed impedance can be achieved, which is that of a virtual spring with stiffness P:

$$\lim_{\omega \to 0} Z(j\omega) = \frac{P}{j\omega}. \tag{2.14}$$

For high frequencies ($\omega \to \infty$), however, the impedance of the haptic display will approach the impedance of the SEA's mechanical spring with stiffness K:

$$\lim_{\omega \to \infty} Z(j\omega) = \frac{K}{j\omega}. \tag{2.15}$$

The integrators only show considerable influence for low frequencies; thus bandwidth analysis can be simplified by considering only the case where both integrator gains are zero. This makes major effects more obvious as it reduces (2.12) to

$$Z(j\omega)|_{I_i=I_o=0} = K\frac{J_A(j\omega)^2 + P_i j\omega + P_i P_o P}{(J_A(j\omega)^2 + P_i j\omega + P_i P_o K + K)j\omega}. \tag{2.16}$$

The actually displayed stiffness value K_{disp} at low frequencies deviates from the value of P if no integrators are employed:

$$K_{\text{disp}} = \lim_{\omega \to 0} j\omega Z(j\omega)|_{I_i=I_o=0} = \frac{P P_o P_i}{1 + P_o P_i}, \tag{2.17}$$

and a desired stiffness K_{ref} must be mapped to a higher P.

Fig. 2.5(a) illustrates bandwidth limitations: For low frequencies, the desired impedance is successfully rendered, whereas for frequencies above the bandwidth, the system behaves like the (stiffer) mechanical spring. For frequencies in between, the behavior approaches a spring-damper, the damping parameter of which only depends on the control parameters P_i and P_o. A look at the intersection of asymptotes of damper and rendered spring in Fig. 2.5(a) shows that the bandwidth, i.e. the maximum frequency until which rendering of the pure desired stiffness is possible, is bounded by $\omega = PP_o$. This implies that the control gain P_o can be used to increase bandwidth. A high value of P_o, however, lowers the damping characteristics of $Z(s)$ which can easily be seen in (2.16). To counteract this, the motor velocity loop gain value P_i needs to be increased as well. Practical considerations such as motor saturation, however, put bounds on the realizable gains.

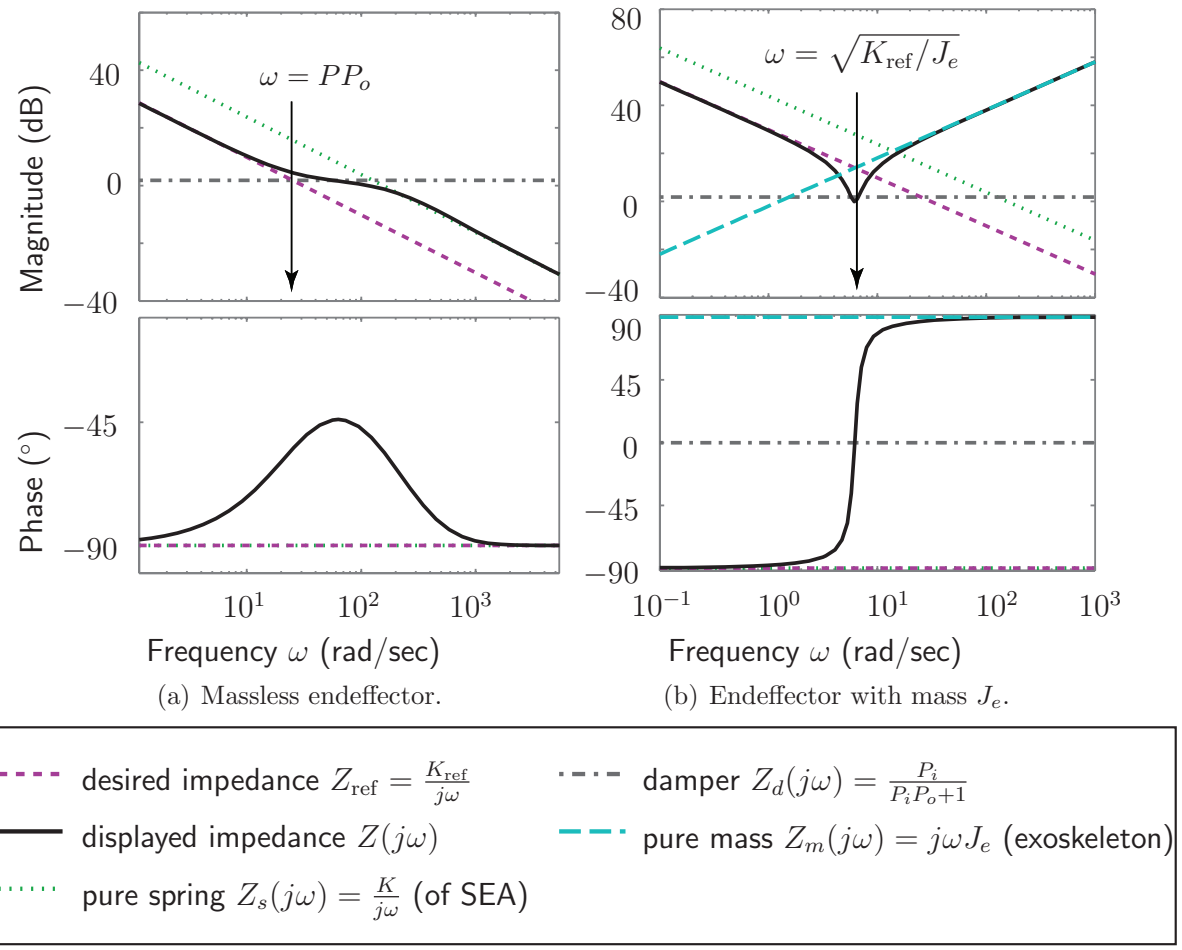

(a) Massless endeffector. (b) Endeffector with mass J_e.

Figure 2.5: Bandwidth limitations. (a) Massless endeffector: At high frequencies, the displayed impedance matches the spring stiffness. Bandwidth depends on the torque control gain P_o. (b) Additional mass at the load side (e.g. an exoskeleton) further limits bandwidth.

Influence of Exoskeleton Mass on Bandwidth

In a realistic rehabilitation robot, there will always be some mass between the actuator and the patient, generally connection elements like an exoskeleton. The exoskeleton LOPES is constituted of several coupled segments, such that a Multi Input Multi Output (MIMO) system results. For schematic purposes, i.e. to illustrate the general influence of this extra mass on bandwidth, only the simplified case is considered where a rigid body with inertia J_e is introduced on the load side of the SEA model of Fig. 2.1, which could be interpreted as a 1-DoF exoskeleton. This extra mass augments the impedance transfer function (2.12) by the extra summand $J_e s$. The system will no longer behave like a spring at high frequencies, its behavior will then be dominated by the added mass, as displayed in Fig. 2.5(b). Depending on its value, such an additional mass can also lower the bandwidth even further: Another upper bound for the bandwidth is indicated at the intersection of the asymptotes in Fig. 2.5(b), with a value of $\omega = \sqrt{K_{\text{disp}}/J_e}$.

2.3.2 Stiffness Limitations due to Passivity Concerns

Now, passivity conditions for the impedance control of Fig. 2.4 will be investigated with similar methods as in section 2.2.2, resulting in bounds for the control gains (with integrators).

First, we look again at the stability condition for the impedance (2.12). As the system poles are independent of the impedance parameters, stability only depends on the inner force control loop. Checking the Hurwitz determinants gives a necessary and sufficient condition:

$$P_i P_o I_i^2 + K P_i (1 + P_o P_i)\psi - K J_A \psi^2 > 0. \tag{2.18}$$

This can e.g. conservatively be achieved by following the simple rules in [259], which is to select a velocity loop gain higher than the motor inertia, and constraining both integrator gains to half of the respective proportional gain values.

Here, $Z(j\omega)$ is a fraction of the form

$$Z(j\omega) = A(j\omega)/B(j\omega). \tag{2.19}$$

For passivity, the real part of $Z(j\omega)$ has to be nonnegative for all $\omega \in (-\infty, \infty)$ that are not roots of the denominator B. For nonzero denominator B, the real part of the complex fraction can only be nonnegative if the function $R(\omega)$ with

$$R(\omega) = \text{Re}\{A\}\text{Re}\{B\} + \text{Im}\{A\}\text{Im}\{B\} = \sum_{i=1}^{8} d_i \omega^i \tag{2.20}$$

is nonnegative for all $\omega \in (-\infty, \infty)$. All coefficients d_i of the polynomial in ω are zero, except for d_4 and d_6:

$$\begin{aligned} d_6 &= K[(P_i^2 P_o - \psi J_A)(K - P) + P_i K] \\ d_4 &= K[I_i^2 P_o (K - P) - \psi K P]. \end{aligned}$$

The requirement that both coefficients have to be nonnegative bounds the achievable stiffness: With positive integrator gains, the coefficient d_4 is only nonnegative for

$$P \leq K \frac{I_i^2 P_o}{I_i^2 P_o + \psi K} < K. \tag{2.21}$$

With zero integrator gains, (2.20) simplifies to

$$R(\omega) = \omega^6 K(-P_i^2 P_o P + P_i^2 P_o K + P_i K) \geq 0. \tag{2.22}$$

The controller gain P may thus exceed the value of K. However, without integrators, the stiffness displayed at low frequencies deviates from the value of P, as given in (2.17), and the actually displayed stiffness K_{disp} equals K for the maximum value of P allowed in (2.22). This implies that:

The Series Elastic Actuator cannot display a higher pure stiffness than the spring stiffness, if passivity is desired.

It is important to note that the real part of the impedance and thus passivity is independent of the presence of additional endeffector mass J_e, because this simply adds the imaginary term $j\omega J_e$ to the frequency response.

Fig. 2.5(a) and Fig. 2.5(b) feature a desired stiffness lower than the allowed value. The phase never leaves the range of +90° to -90°, which is equivalent to a positive real part, thus the system is passive. In constrast, Fig. 2.6 illustrates the case of an excessive desired stiffness: The phase falls below -90°. This implies that the haptic display is not passive, and the coupled system will only be stable with a certain number of environments, for example with a pure spring (a differentiator, which shifts the phase up). However, coupled to a pure mass (an integrator), the open loop frequency response will invariably have a phase below -180° for all frequencies, and thus the closed loop system is unstable.

2.3.3 Limitations in Cartesian Space

One of the control approaches implemented on the LOPES robot is Virtual Model Control (VMC) [71, 263]. VMC attempts to separately modify selected gait characteristics using virtual passive components such as springs and dampers. These elements are mainly implemented in Cartesian space, e.g. to intuitively modify step height or step length. As indicated in the preceding section, both the bandwidth and the maximum value of the rendered stiffness are constrained in joint space due to the compliant actuator. Further performance limitations originate from undesired interaction forces due to exoskeleton inertia. The influence of these effects on the achievable stiffness and bandwidth in Cartesian space has been analyzed in [262] by the coauthor Herman van der Kooij, and this analysis is given in App. B.

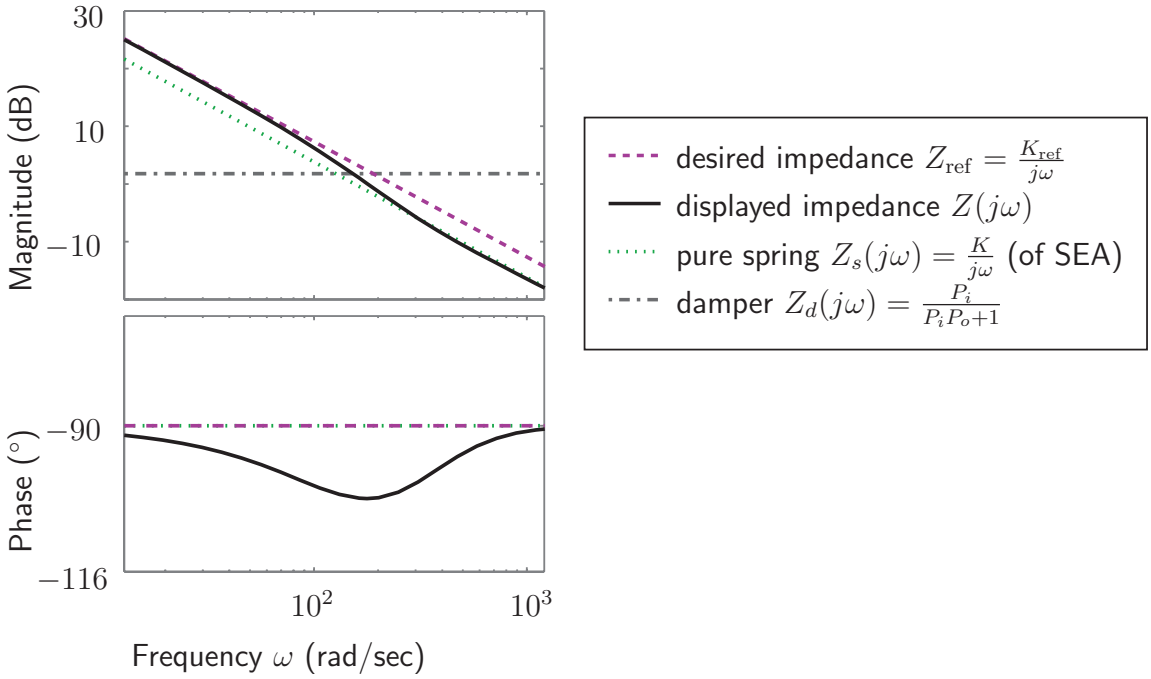

Figure 2.6: Impedance control with too high desired stiffness (exceeding the natural spring stiffness): The phase has values below -90°, thus the system is not passive.

2.4 Practical Evaluation

2.4.1 Force Control Performance

For the practical implementation, we use an inner velocity loop in the PWM to control a brushless synchronous motor. The SEA is controlled via MATLAB/Simulink xpc, the sampling frequency is 1000 Hz. For the force controller, we chose control parameters $P_o = 0.8$ (rad/s)/Nm and $P_i = 5$ Nm/(rad/s), with the integrator gains at 1/3 of the respective proportional gains. The joint is restrained manually in the experiments. In Fig. 2.7, the tracking performance for different frequencies is illustrated. The time plot illustrates the influence of friction, which is compensated well. Frequency analysis of the input-output data shows a bandwidth of 16 Hz, with a phase lag of 112° at this cutoff frequency. However, motor saturation prohibits amplitudes larger than 5 Nm at this frequency. The analysis is performed using system identification methods (Matlab procedure: pem). The theoretic response for comparison also includes a measured average viscous friction of 4 Nm/(rad/s). In order to illustrate the zero-torque behavior, the joint was moved manually at different frequencies. The resulting interaction torques are displayed in Fig. 2.8. At the onset of a motion, peak torques can be noticed, probably due to backlash and stick-slip. However, these are hardly perceivable in practice, and maximum torques are very low, ranging around 5 Nm.

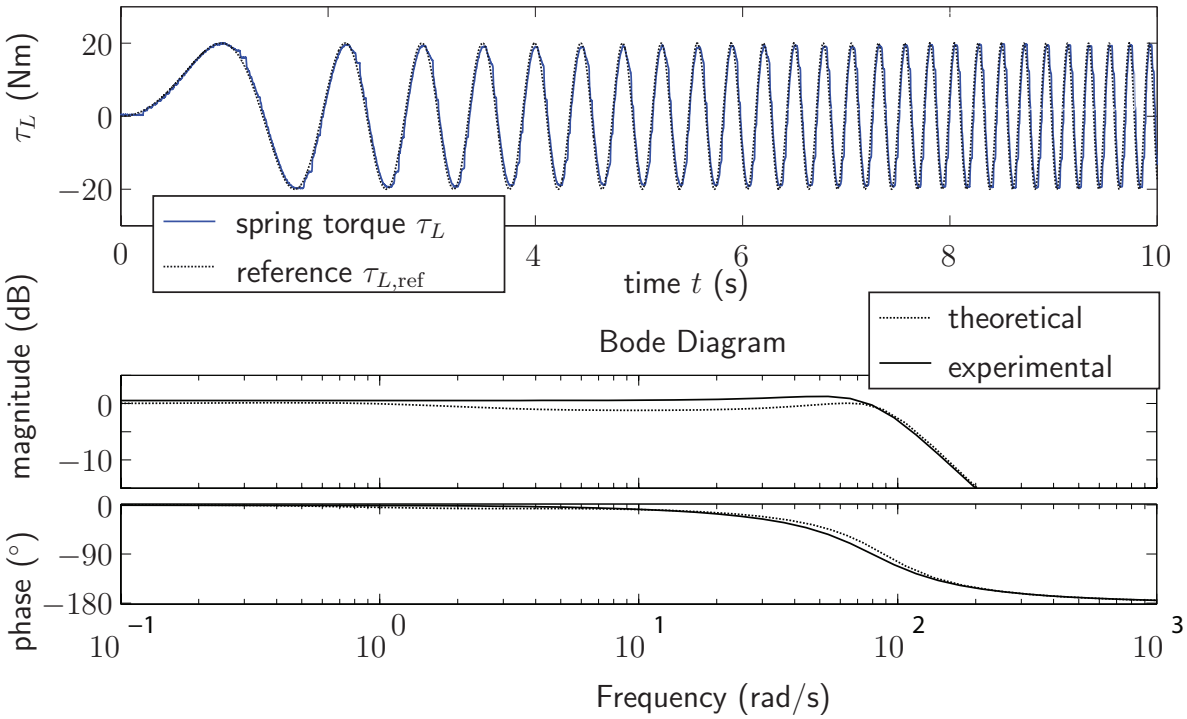

Figure 2.7: Force tracking performance of the Controlled SEA, assessed via a sine sweep. Above, an excerpt of the time response is plotted, with frequencies ranging from 0 to 6 Hz. Below, the bode plot illustrates magnitude and phase of the experimental and the theoretically expected frequency response.

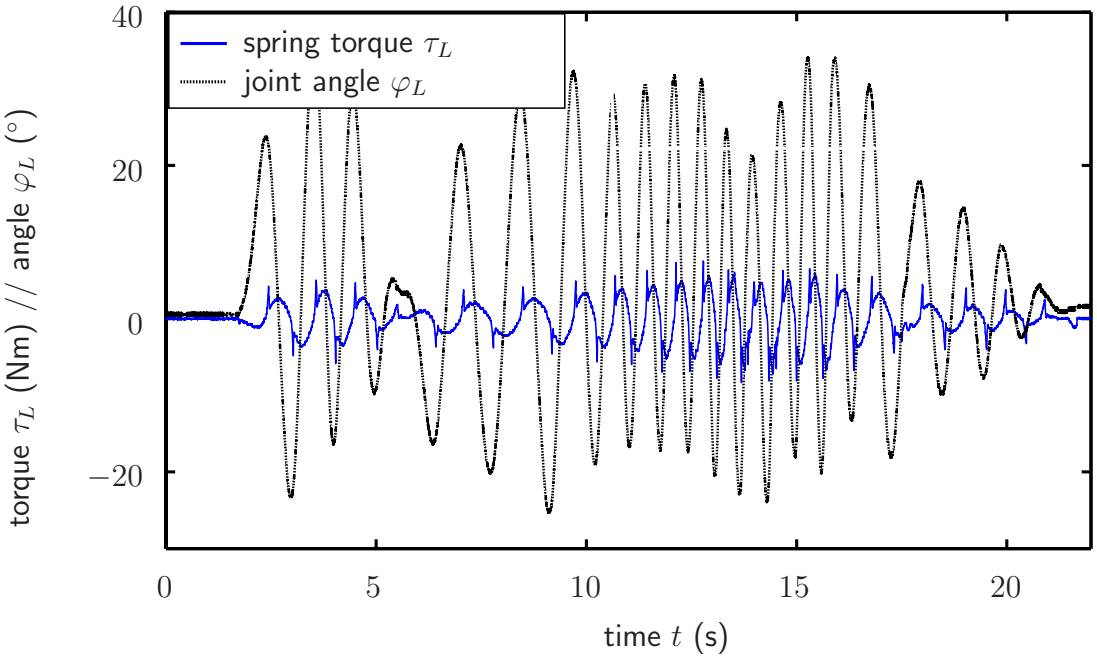

Figure 2.8: User-induced joint movement and resulting interaction torque in zero-torque mode of the controlled SEA.

2.4.2 Impedance Control Performance

To evaluate limitations of renderable stiffness, two different experiments have been conducted: Firstly, an evaluation of maximum achievable impedance with the "empty" exoskeleton, and an evaluation of maximum achievable stiffness with a human subject. As representative values of achievable impedance during walking, the results of Virtual Model Control (VMC) [71, 263] with the LOPES robot are used. The goal of VMC is to modify selected gait characteristics while leaving others unaffected. Virtual passive components such as springs and dampers can be chosen intuitively, such that a therapist-friendly training is achieved. In the experiments, the employed elements influence step height and step length.

For control of an individual joint of the exoskeleton alone (without human subject), the maximum achievable stiffness before undesired oscillations occurred is almost exactly equal to the spring stiffness ($\pm 10\%$, depending on gain variations in the torque control loop), as predicted by the theoretical analysis.

In contrast, the maximum achievable Cartesian stiffness in practical experiments with healthy subjects walking under the influence of Virtual Model Control (VMC) resulted to be 1500 N/m in vertical direction (step height control), and 700 N/m in horizontal direction (step length control), which is considerably higher than the theoretic worst-case bound: Following the derivation in App.B, more specifically (B.1), the Cartesian stiffness should be limited to 200 N/m in horizontal direction, and to 355 N/m in vertical direction, given the joint angles occurring in the experiment.

The reflected mass of the exoskeleton constrains the achievable bandwidth, as illustrated in section 2.3.1 for the SISO case: The limit is given by the square root of the desired stiffness of the virtual component divided by the reflected exoskeleton mass. Below this frequency, the virtual spring is felt, whereas above, the reflected device mass is felt. In case the reflected mass is minimal (0.95 kg), this frequency is 4.3 and 6.3 Hz for the stiffnesses of 700 and 1500 N/m, respectively. For a desired stiffness of 700 N/m and using a worst case approach, it reduces to 2.14, 1.93, 1.21, and 0.44 Hz for 90^o, 60^o, 30^o, and 10^o knee flexion, respectively.

Despite these heavy bandwidth limitations, the combination of the mechanical design of LOPES and Virtual Model Control (VMC) was well able to modify step height and step length of healthy subjects [263]. Each of the two parameters could be lengthened or shortened by VMC, simply by scaling the reference path. The change in each specific gait parameter left other parts of the gait cycle almost unaffected, and the modification was not perceived awkward until it got excessively large. In experiments with varying stiffness we found that subjects perceived stiffer controllers as less comfortable; they preferred more compliant virtual springs. Adjustment of the reference parameters beyond the desired value in combination with a softer controller (equivalent to additional feedforward torques, which is not unique to VMC) also achieved the desired modification and was perceived as more comfortable than a stiff control. However, the step length was not exactly modified by the desired 20% due to the compliant interface. The experiments are described in detail in [70].

2.5 Discussion

A comparison of theoretically predicted stability limitations in Sec. B.1 and experimental outcome in Sec. 2.4.2 shows good agreement for joint-space control with constant stiffness and without human subject. However, it also shows that the Cartesian stiffness used with healthy subjects walking in LOPES can be higher than the theoretically derived worst case bound. The fact that this higher stiffness is rendered without stability problems can be explained by several factors: Firstly, the "worst case" in terms of kinematic configuration hardly occurred in the practical experiments, or at least the system never remained in this state for long, such that instable effects might have been transient. Secondly, passivity is a conservative means of ensuring stability of coupled systems, and a less conservative, explicit MIMO stability analysis could replace it (requiring the exoskeleton, the patient's impedance, the compliant coupling between human and exoskeleton, and the environment to be modeled reliably, which is difficult). A contraindication of this second reasons is that without human subject, theoretical and practical results coincided well. Therefore, a probable reason is that the healthy subjects did not behave like pure masses, the "worst environment" of section 2.3.2, but formed stabilizing elements in the control loop. This positive contribution might stem from intrinsic and neuronally coordinated stiffness and damping, and it is e.g. exploited for the control of robots that are intentionally not passive, like the BLEEX [131]. Although it seemed possible to render higher stiffness for healthy subjects than theoretically derived, it might not be advisable to rely on this effect when working with patients. Instead, the stiffness of the SEA was increased by a factor of 2.5 in reaction to the experimental outcome. Equipped with these stiffer springs, LOPES can operate with sufficiently stiff VMC, and still remain within the conservative limits resulting of the passivity analysis. Generally, there is a trade-off between achievable stiffness on the one hand, and low undesired interaction torques on the other. One possibility would be to use an adaptive compliance, as e.g. suggested by [111], to meet the individual patient's needs.

2.6 Conclusion

This chapter explored performance limitations of impedance-controlled Series Elastic Actuators under the premise of passivity. The passivity analysis follows control design from the inside to the outside, beginning with the internal force control loop.

First, a systematic analysis of existing approaches to force control of Series Elastic Actuators is presented. The resulting recommended control is based on cascaded PI controllers with an inner motor velocity loop. Using passivity analysis, simple boundaries for the control parameters are calculated. The advantages of the scheme are the the possibility to include integral action without jeopardizing passivity. Both theoretically and in practical experiments, the effectiveness of a fast inner velocity loop for good force tracking and low realizable impedances has been shown.

Based on an outer impedance control loop, benefits and limitations of compliant actuation for rehabilitation robots on the example of the LOPES are discussed, focusing on the

limitations. After illustrating bandwidth limitations, a new result is derived: If stability in terms of passivity of the haptic device is desired, the renderable stiffness is bounded by the stiffness of the SEA's elastic component.

Practical experiments demonstrate the good performance of the force control scheme in terms of low undesired interaction torques. Furthermore, experimental studies with healthy subjects walking in LOPES also demonstrate the theoretically derived limitations of SEAs: Desired gait modifications were not tracked exactly, because the subjects were able to deviate from the prescribed pattern even in the stiffest possible configuration. However, rendered stiffnesses with healthy subjects walking in the robot can be higher than those predicted by theory, and also higher than renderable stiffness in the empty robot. The discrepancy between theoretical bounds and rendered stiffness indicates that healthy subjects might represent a stabilizing component of the coupled system. This could be different for patients. In light of the theoretical stability analysis and with the focus on patients, the LOPES actuation has been slightly modified after these experiments: The robot is equipped with stiffer springs in order to obtain sufficient stiffness and to ensure stability without relying on stabilizing effects of the human.

For this specific application, the disadvantages of compliant actuation can thus be tolerated or dealt with, and they are small compared to the advantages: Given that a rehabilitation robot, in the first place, is supposed to imitate therapist action, limitations of bandwidth and stiffness do not pose severe problems. In contrast, safety and backdrivability are highly relevant, and they can be ensured more easily with a compliant actuator.

3 Identification of Muscle Response to Functional Electrical Stimulation

3.1 Introduction and State of the Art

As muscle activity is triggered by electrical signals transmitted by the nerves, deficient motor control can be assisted using an external electrical field. Such assistance is called Functional Electrical Stimulation (FES). To allow model-based control of these artificially induced contractions, this chapter deals with robust identification of muscle response to FES. The analysis is limited to the *isometric* case (constant muscle length), where the response is generally described by a Hammerstein model in the literature. Here, a reverse identification is performed, changing the structure to Wiener type. The algorithm is compared to forward nonlinear and linear identification in practical experiments.

3.1.1 Modeling and Identification of FES

In FES, the correlation between stimulation parameters and muscle force is strongly nonlinear and time-variant. The generated joint torque depends on spatial and temporal muscle fiber recruitment, on muscle length, and on the velocity of contraction.

There is a considerable amount of different muscle models, some of which are rich in physiological detail and have many parameters; for example, [99] describes muscle activity using a set of differential equations. A survey on muscle models with varying complexity can be found in [280]. However, mainly simple models have been used in clinical practice, most are based on the models developed by Hill [106]. A very popular one is given by Veltink et al. [268], which describes the muscle by a simplified nonlinear model in terms of the easily measurable quantities joint angle and velocity instead of muscle length and contraction velocity. This model is described in detail and with the physiological background in App. C. In this model, the recruitment dynamics are modeled by a static nonlinearity (the *recruitment curve*) followed by a linear transfer function, which is a Hammerstein structure. Joint angle and angular velocity also influence the generated joint torque.

It needs to be mentioned that a linear representation of the activation dynamics can only provide a very crude approximation. For example, an important property of muscle behavior is that muscles take longer to turn off than to turn on [278]. Furthermore, hysteresis effects have been observed [137], and the concept of superposition does not hold for muscle recruitment [41,175,233,284]. According to [178], the largest deviations from the linear assumption are transient and appear at the onset of recruitment and derecruitment. However, it is common practice to use a linear transfer function to model the dynamics of muscle recruitment and derecruitment together, and Veltink's model was reported to have

an accuracy of 85 to 90% when tested on a cat hind limb, whereby recruitment, angle, and angular velocity were varied simultaneously, independently, and in a pseudorandom manner [268].

The most frequent procedure to identify the model's parameters is to identify recruitment dynamics in an *isometric* (constant muscle length) setup, and to determine the nonlinear dependencies on muscle length and contraction velocity in a separate setup, e.g. with the widely used commercial product Kin Com (IsoKinetic International, USA) for *isokinetic* (constant force) identification.

To reduce the time needed for identification, both activation dynamics and nonlinear dependency on muscle length and contraction velocity can be quantified simultaneously under non-isometric conditions, provided that the biomechanical properties of the leg (mass, inertia, etc.) are known. A feasible strategy is then to adapt the muscle model parameters using the (measurable) error in joint position instead of the (unmeasurable) error in produced muscle force. The joint position error follows from the muscle torque error, which is filtered by the known transfer function of the limb dynamics. In case this error transfer function is asymptotically stable (or can be transformed using suitable observer techniques [221] to fulfill this criterion), convergence of the adaptation is guaranteed [163]. This method has successfully been employed for non-isometric identification during magnetic stimulation of the biceps brachii by Bernhardt [24]. Schauer et al. also proposed a procedure for non-isometric identification of the quadriceps and hamstrings [216]. The investigations here are limited to isometric identification only.

For the identification of Hammerstein models, there exists a large variety of identification methods. For example, iterative correlation analysis has been suggested, orthonormal basis functions [61, 92], and discrete-time Volterra models (DVMs) [151]. DVMs are a special class of feedforward artificial neural networks with polynomial activation functions and have been found suitable in the context of muscle recruitment dynamics [12]. Another method is the so-called small signal identification [17]. Furthermore, identification in the frequency domain is popular [182].

Frequently, muscle identification approaches employ iterative computation. A recent systematic study concerning the efficacy of iteratively identified Hammerstein models to describe muscle behavior at different frequencies has been conducted by Chou at MIT [51] on leopard frog (*Rana pipiens*) plantaris longus muscles. For low stimulation frequencies, a high success in convergence and good estimation performance was obtained. However, success rate and error degraded with frequencies above 40 Hz. Bai suggested a method to separate nonlinearity and dynamics of Hammerstein models [16], which ensures convergence. Based on this concept, a reverse identification of models for heart rate has been suggested [236]. However, Bai's method requires specially shaped input signals, pseudorandom binary sequences (PRBS), and it thus depends on calibration and identification routines prior to any actually functional control. In order to deal with more general experimental data, for example gathered during FES therapy, nonlinearity and dynamics still need to be identified in conjunction. In the context of the work presented here, preliminary attempts with various iterative identification methods have also been made to identify hamstrings and quadriceps of healthy subjects [197, 198]. There, a two-step identification strategy following the Narendra-Gallmann algorithm [164], which reduces the number of it-

eratively determined parameters, showed considerably improved robustness [170] compared to the simple Prediction Error Method with gradient descent of all parameters. However, the convergence was still not satisfying.

To avoid local minima and to increase robustness, two strategies are possible: One is to reduce the number of model parameters, and the other is to resort to non-iterative identification based on analytical solutions. Analytical solutions are readily found for a model that is linear in its parameters. However, an accurate description of the nonlinear recruitment curve that linearly depends on a low number of parameters is difficult, as the curve is of saturation type. Such curves are e.g. not well represented by polynomials, which would be the simplest basis functions. The difficulty of finding such simple models may be one reason why only few attempts have been made to identify Hammerstein models based on analytical solutions, e.g. by [47].

3.1.2 Contribution and Outline of this Chapter

In this chapter, an anti-causal or reverse identification method for Hammerstein models is employed, as presented at [260]. The system order is reversed, such that a linear anti-causal transfer function is followed by the inverted recruitment curve. Such an inverted muscle recruitment curve resembles a polynomial of third order, which can be exploited to describe it in a linear fashion using a very low number of parameters. This allows analytical optimization, such that finding the global minimum is guaranteed. The main advantage of the anti-causal approach is that the identified recruitment curve can be used directly to transform the stimulation input, in order to obtain an input-output linearized system. In contrast, a forward-identified nonlinearity is not necessarily invertible and may need further processing to be used for this purpose.

The reverse algorithm is tested in a practical setup on hamstrings and quadriceps muscles of two healthy subjects, and it is compared to forward identification with various basis functions, and to purely linear identification.

3.2 Muscle Model for Isometric Contractions

Muscle response to FES is modeled by a Hammerstein model, which consists of a static nonlinearity followed by a linear transfer function, as displayed in Fig. 3.1.

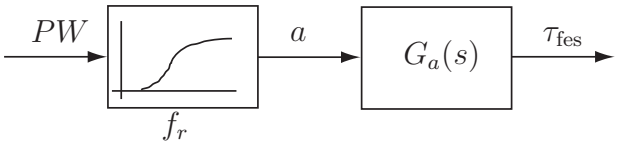

Figure 3.1: The stimulated muscle with stimulation pulse width PW as input and the effective torque τ_{fes} on the joint as output can be modeled as a Hammerstein Model: A static nonlinearity f_r is followed by a linear transfer function $G_a(s)$.

The pulse width PW of the FES signal is the input to a system with a static nonlinearity f_r (the *recruitment curve*) in series with a linear dynamic model (the *activation dynamics*), represented by the transfer function $G_a(s)$. The output of the nonlinearity is termed *activation level* a. In the isometric case, the output of the transfer function is the torque τ_{fes} acting on the joint.

The transfer function $G_a(s)$ is a critically damped second-order system with eigenfrequency ω_0:

$$G_a(s) = \frac{\tau_{\text{fes}}(s)}{a(s)} = \frac{\omega_0^2}{s^2 + 2\omega_0 s + \omega_0^2}\, e^{-sT_t} \quad . \tag{3.1}$$

The dead time T_t in this model is due to signal transport in the nerve pathways. Its value is about 25 ms [185]. Further details and background of the model can be found in App. C.

3.3 Nonlinear Identification

For identification, the linear dynamics in (3.1) are expressed in a more general time-continuous representation[1]:

$$y(t + T_t) = -\sum_{i=1}^{n} \alpha_i y^{(i)}(t + T_t) + a(t), \tag{3.2}$$

with the superscript $^{(i)}$ denoting the i-th time derivative. Here, the output y is the torque τ_{fes}, the input u is the pulse width PW, and a is the activation level. The dead time T_t is assumed to be known.

3.3.1 Forward Identification

The conventional, intuitive approach to fit the model to measured data is forward identification, modeling the nonlinearity by a sum of several basis functions:

$$a(t) = f_r(u(t)) = \sum_{j=0}^{m-1} \gamma_j\, f_j(u(t)). \tag{3.3}$$

The estimated output $\hat{y}$ then follows from the input u and the output time derivatives depending on the parameters α_i in (3.2) and γ_j in (3.3), and the formulation is linear in these parameters. This allows easy calculation of globally optimal parameter estimates (subsumed in the vectors $\boldsymbol{\alpha}$ and $\boldsymbol{\gamma}$) using N data points at time steps t_k with the cost function:

$$C(\boldsymbol{\alpha}, \boldsymbol{\gamma}) = \frac{1}{N} \sum_{k=1}^{N} q_k \epsilon^2(t_k, \boldsymbol{\alpha}, \boldsymbol{\gamma}) \tag{3.4}$$

[1] A yet more general approach would be to allow dynamics that include also zeros and not only poles. A possible procedure then would be to treat the system as a multi-input single-output system, where each derivative of u is a separate input. This has been proposed and evaluated by [47] for Hammerstein models.

with

$$\epsilon(t, \boldsymbol{\alpha}, \boldsymbol{\gamma}) = y(t + T_t) - \hat{y}(t + T_t) \tag{3.5}$$

and weighting factors q_k.

It is possible to identify the parameters of the dynamics and of the nonlinearity together using Least Squares. However, in the present application, additional knowledge can be used, being that the activation dynamics are critically damped, as described in (3.1). Therefore, the parameters of the dynamics depend nonlinearly on the muscle's eigenfrequency ω_0:

$$\boldsymbol{\alpha} = \begin{pmatrix} \frac{2}{\omega_0} & \frac{1}{\omega_0^2} \end{pmatrix}^T. \tag{3.6}$$

With this constraint, the problem is not of Linear Least Squares form anymore. However, the solution is still simple: Using Separable Least Squares, the optimal parameters γ_j can be expressed as functions of the parameter ω_0, and the remaining one-dimensional problem can be solved for ω_0.

The choice of basis functions f_i usually depends on *a priori* knowledge about the nonlinearity. Popular choices in the context of saturation characteristics are polynomials, radial basis functions (RBFs), and superpositions of arctan or tanh-functions.

A major disadvantage is that the resulting forward nonlinearity is not necessarily invertible. However, the inverse recruitment function is often needed for transformation of the input, to cancel recruitment nonlinearity and to obtain a linear control system. Therefore, an additional post-processing of the nonlinearity may be required to make it invertible, and the resulting processed function is not optimal anymore.

3.3.2 Reverse Identification

Due to the these limitations of the forward model in the context of saturation-type nonlinearities, a different approach is used here: The system order is reversed, making the inverse dynamics the first, and the inverse nonlinearity the second part. The torque is then system input, and the stimulation is system output, which produces a system of Wiener type. From this theoretical point of view, the dynamics become anti-causal.

There are two advantages of this approach: One is that the inverse function can directly be used for input-output linearization, and the other is that an inverted saturation is easily represented by a simple third-order polynomial, reducing the number of necessary basis functions without requiring previous knowledge on the recruitment curve.

Like the forward identification, the linear dynamics are described as in (3.2), but now an estimate for the activation level is obtained from the muscle torque using backward calculation:

$$\hat{a}(t) = y(t + T_t) + \sum_{i=1}^{n} \alpha_i y^{(i)}(t + T_t). \tag{3.7}$$

The nonlinearity is also modeled inversely, such that an estimate for the input u is given in dependence of the estimated activation level $\hat{a}$, and thus as a function of the output y:

$$\hat{u}(t) = f_r^{-1}(\hat{a}(t)) = \sum_{j=0}^{m-1} r_j g_j(\hat{a}(t)). \tag{3.8}$$

The parameters α_i and r_j describing nonlinearity and dynamics are subsumed in the vectors $\boldsymbol{\alpha}$ and $\boldsymbol{r}$. The cost function is analogous to the one in (3.4), but in contrast to the forward identification, the error values are now defined depending on the input u:

$$\epsilon(t, \boldsymbol{\alpha}, \boldsymbol{r}) = u(t) - \hat{u}(t). \tag{3.9}$$

The choice of basis functions is easy, because the inverse recruitment curve is approximated well by an (odd) polynomial of low order. This is due to the fact that the function values go to infinity for large input values, like in polynomials. In this work, the inverse relationship between input u (pulse width PW) and activation level a is approximated by a third-order polynomial, in order to keep the number of parameters as low as possible:

$$\hat{u}(t) = r_3\, a^3(t) + r_2\, a^2(t) + r_1\, a(t) + r_0 \tag{3.10}$$

The simultaneous iteration of all unknown parameters in $\boldsymbol{\alpha}$ and $\boldsymbol{r}$ can be avoided by a Separable-Least-Squares approach, which is basically analogous to the forward identification algorithm. However, in contrast to the unconstrained optimization performed there for the parameters $\boldsymbol{\gamma}$, the optimization for the parameters $\boldsymbol{r}$ of the inverse nonlinearity is constrained, in order to obtain an invertible solution. To enable inversion, the function $f_r^{-1}(a)$ in (3.8) needs to be monotonically increasing or decreasing. For muscle recruitment curves, only increasing functions are plausible. Requiring the function's derivative to be positive for all values of a and using the parameterization in (3.10) leads to the following inequality constraints for the coefficients r_i:

$$r_3 \geq 0 \quad \wedge \quad r_2^2 - 3 r_3 r_1 \leq 0. \tag{3.11}$$

These constraints define a convex set $\mathbf{X}$ for the entries of $\boldsymbol{r}$ (see proof in App. D.1). As the error function is quadratic and thus convex as well, the resulting internal optimization problem in $\boldsymbol{r}$ is convex and therefore easy to solve for the global minimum $\boldsymbol{r}^*$ for a given $\boldsymbol{\alpha}$. The analytical solution is given in App. D.2.

Replacing the estimate of $\boldsymbol{r}$ in the cost function (3.4), with (3.9) and (3.10), only an optimization problem in $\boldsymbol{\alpha}$ remains. Additional knowledge of the critical damping of the system allows to replace the entries of $\boldsymbol{\alpha}$ by functions of ω_0, as given in (3.6), so that again a one-dimensional optimization problem in the variable ω_0 results.

This approach provides an injective function with a as input, as needed for compensation of the recruitment curve.

Remark: For identification in the continuous domain, good estimates of $\dot{y}$ and $\ddot{y}$ need to be provided. Here, the estimates are obtained by local polynomial approximation of the output y, which has recently been proven to be optimal in the presence of noise [149]. To avoid the usage of time derivatives, a discrete-time algorithm could be used alternatively.

3.4 Evaluation and Results

3.4.1 Experimental Protocol and Data Analysis

The reverse algorithm based on a polynomial of third degree for the inverse nonlinearity is now used to identify muscle behavior, and the results are compared to linear and nonlinear forward identification. For the nonlinear forward identification, three different models of the nonlinearity are employed: A polynomial approach, normalized radial basis functions (NRBFs) of Gaussian form, and a superposition of tanh functions.

An isometric test setup for force measurement was designed, which couples the ankle to a 6-DOF force sensor using a custom-made orthopedic cuff and a pre-stressed cable. The apparatus is displayed in Fig. 3.2. With this setup, a quite rigid connection can be

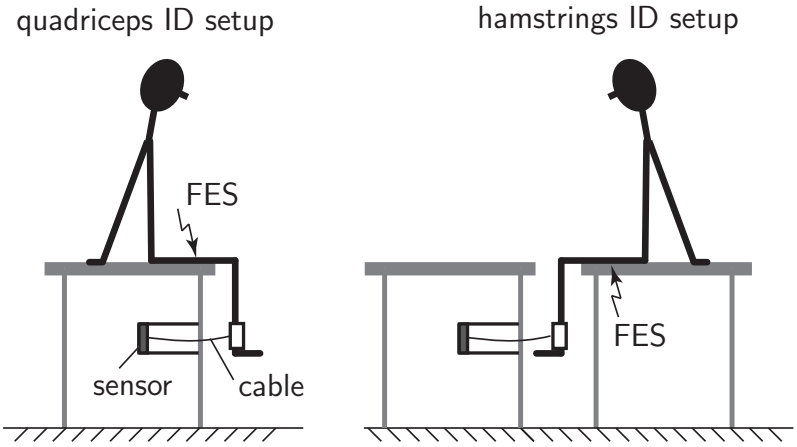

Figure 3.2: Torque response of quadriceps (left) and hamstrings (right) to Functional Electrical Stimulation is measured using a force sensor connected to the ankle via a pre-stressed cable and a custom-made orthopedic cuff. The tables do not move.

realized at the ankle joint with its predominantly bony structure. Quadriceps group and hamstrings, respectively, are stimulated transcutaneously using the commercially available stimulator MOTIONSTIM8 from Krauth+Timmermann (Hamburg), which is accessed via a freely available Matlab/Simulink protocol using RTAI Linux RealTime communication. Biphasic pulses are applied with a frequency of 40 Hz. The pulse width is varied in order to change stimulation intensity. The current is adjusted so that the stimulator's maximum pulse width (500 μs) can be applied without exceeding the subject's pain limit.

The excitation signal, i.e. the pulse width trajectory, contains a succession of two different signals (with two seconds pause in between): A trapezoidal trajectory, and a step followed by a sine sweep. The composite signal is applied to the muscles 2 times in a row, and then a pause of about 3 minutes follows, to avoid fatigue. This procedure is repeated 3 times, such that each of the two excitation signals is applied 6 times. The muscle torque response of these six trials is measured using the force sensor attached to the ankle via the cuff and a steel cable. For identification, the mean torque responses of the six trials is used. These two different signals allow identification and testing with qualitatively different data: The

identification is done based on the dynamic sweep excitation, and the model is evaluated using the quasi-static slow ramp up-ramp down signal.

For identification, the following five algorithms and models of the nonlinearity are used:

1. Linear identification, LIN
2. Inverse identification, polynomial of third order, INV
3. Forward identification, superposition of four tanh functions, F-t
4. Forward identification, polynomial of third order, F-p
5. Forward identification, superposition of four Normalized Radial Basis Functions, F-r

All nonlinear algorithms use four parameters to describe the nonlinearity, and only one parameter (ω_0) to describe the dynamics. This is done to make the approaches comparable. All solutions are found analytically and not iteratively, to ensure global optimality. Furthermore, the error weighting matrix $\mathbf{Q}$ is the identity matrix.

To compare the different approaches, the identified models are simulated in a forward manner. For the inverse identification, this requires prior inversion to obtain the forward model. To quantify *goodness of fit*, the Coefficient of Determination is used. This commonly used measure is defined according to [80]:

$$R^2 = 1 - \frac{\sum_{i=1}^{N}(y_i - \hat{y}_i)^2}{\sum_{i=1}^{N}(y_i - \bar{y})^2}. \tag{3.12}$$

with y_i, $i = 1, ..., N$ being the output torque to be approximated, and $\hat{y}_i$ being the corresponding model estimates. Thus, R^2 is related to the variance in the data y that cannot be explained by the model (unexplained variance). A flawless model ($\hat{y}_i = y_i \forall i \in \{1, ..., N\}$) yields a value of $R^2 = 1$.

It should be noted that this performance measure biases the results slightly in favor of the forward identification, because for that algorithm, the cost is defined in the output domain both for identification and for evaluation. The reverse algorithm defines the cost based on the input.

3.4.2 Results

Two healthy subjects (24 and 27, one male, one female) took part in the evaluation. Fig. 3.3 shows the Coefficient of Determination R^2 achieved by the five approaches for hamstrings and quadriceps. The R^2 value is high for most trials. However, for one subject and one muscle, the models hardly explain the behavior. An advantage of one the various nonlinear identification methods against each other or compared to linear identification cannot be deduced from these results. The ramp response time courses are plotted in Fig. 3.4 to analyze this behavior in more detail.

Furthermore, the maximum muscle torque during slow ramp stimulation is much higher than the maximum torque observed during sine-sweep stimulation, although the maximum ramp pulse width is only at 80% of the sine amplitude.

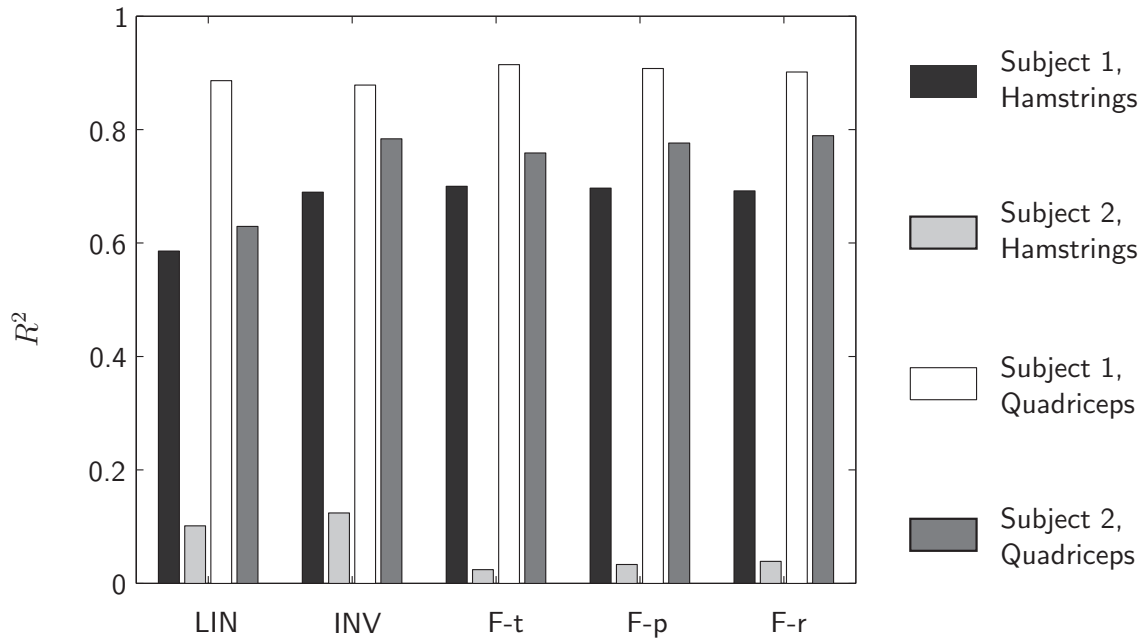

Figure 3.3: Coefficient of Determination of the models that have been identified using a sine sweep, when excited by a trapezoidal stimulation signal.

3.5 Discussion

The ramp response shows that the identified nonlinearities of the forward algorithms are almost indistinguishable, such that the choice of basis functions for the nonlinearity does not seem to play an important role concerning modeling performance. The identification direction does not make a large difference in performance either.

Furthermore, Fig. 3.4 shows heavy, non-Gaussian modeling uncertainty: Firstly, there are indications that muscle dynamics are not sufficiently described by a single transfer function in combination with a nonlinearity. In fact, the response looks like the superposition of two responses, i.e. at a certain threshold, a second muscle group seems to be superimposed.

The simple model thus cannot capture the dominant effects reliably, such that the resulting uncertainty in torque generation can indeed be very large (more than factor 2).

Secondly, the figure shows the high degree of inter-trial variability present in the data (indicated by the shaded standard deviation), even when excited with identical input signals. This variability does not exhibit a systematic variation, e.g. a decline due to fatigue.

Deficiencies of the setup may have caused some of these effects. For example, as the subject is sitting on the hamstrings, and muscle contractions under these circumstances can cause shear forces and displacement of the electrodes. This may be one explanation why the hamstring identification worked less well. However, the aim was not to develop ideal laboratory conditions, but to find identification algorithms that work robustly under practical circumstances.

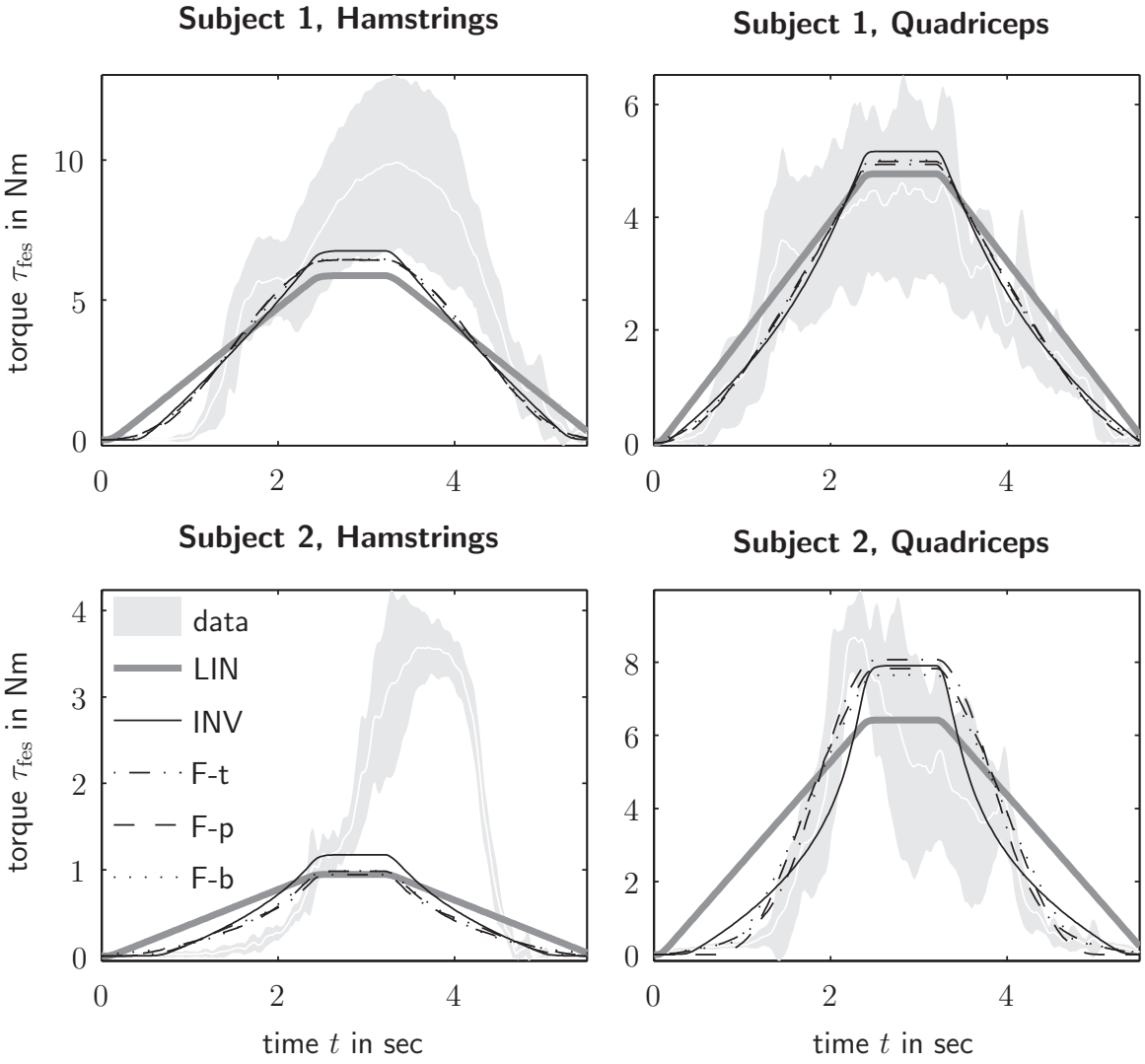

Figure 3.4: Measured and predicted muscle torque in response to stimulation with a pulse width of slow trapezoidal time course, with mean and standard deviation over six trials. The models have been identified using a different excitation signal, a sine sweep.

With the given data, the nonlinear models do not show many advantages compared to the linear one. This may partly be due to the fact that in the experiments, stimulation levels were below the saturation limits, where the recruitment nonlinearity does not exhibit extensive plateaus and is still well approximated by a linear function. Further experiments with higher stimulation levels could not be conducted because they would have exceeded the pain limit for the healthy subjects in this study.

The main reason might be that the Hammerstein model itself does not capture the dominant effects satisfactorily, such that the large uncertainties render the differences between identification methods marginal. A source of large uncertainty is the large skin and tissue displacement that is observed during stimulation. Unpredictable fluctuations within the tissue can be observed visually, such that varying motor units or even different muscle groups are activated. This is congruent with the literature: Trnkoczy [250] identified the unpredictable tissue displacement between electrodes and stimulated nerve as one of the

main sources of torque variability, and he even postulated that closed-loop control of such a variable actuator could not be efficient enough for an orthosis, whether controlled via surface or implanted stimulation systems. Investigations of Hunt et al. [116] also indicate that Hammerstein models do not accurately represent isometric muscle contractions.

3.6 Conclusion

This chapter focused on robust identification of Hammerstein models for Functional Electrical Stimulation. An analytical anti-causal identification has been performed. This reverse algorithm is especially suitable if the nonlinearity has a saturation characteristic: It exploits the fact that an inverse saturation curve resembles a third-order polynomial, such that it can be described by a simple model that depends linearly on a low number of parameters. Furthermore, the algorithm outputs the inverse nonlinearity, which is needed commonly for compensation of the nonlinearity during control.

The proposed algorithm has been tested in a practical setup and compared to forward nonlinear and linear identification. The results show that both forward and reverse nonlinear models do not fit the observed dynamics much better than a simple linear model, although the global parameter optimum is found in each case using analytical optimization. This indicates that the Hammerstein model does not predict muscle recruitment reliably enough to allow generalization from the dynamic training excitation to the quasi-static evaluation excitation, which makes it difficult for the more detailed models to outperform simple ones. Thus, it is doubtable whether the effort of such complex identification approaches is justified in a practical setup e.g. in a clinical environment, where uncertainties are dominant.

4 Model-Based Control of a Hybrid Robotic/Biomechanical System

4.1 Introduction and State of the Art

Functional Electrical Stimulation (FES) is a state-of-the-art therapeutic tool in clinical practice. Besides restoration of muscle function, it also induces a training effect and promotes neural rehabilitation. However, artificially recruited muscles do not represent reliable actuators due to adverse properties such as time-variance and uncertainties, as outlined in the preceding chapter and in Sec. 1.2.2. To remedy this issue, FES can be complemented by a robotic exoskeleton. Such a *Hybrid Neuroprosthesis* combines the advantages of the two systems, which are therapeutic benefit and reliable motion execution, as motivated in Sec. 1.2.3. Main questions to be investigated in this chapter concern modeling of the redundantly actuated system, cooperative control of the actuators, and analysis of robustness to heavy uncertainties.

4.1.1 Control of Redundantly Actuated Systems

With a complementary exoskeleton, many disadvantages of FES can be overcome. Correct task execution can be ensured by the reliable motors, such that the heavy uncertainties of the biomechanical system are less grave.

Although a large amount of research has been done in the field of closed-loop FES control on its own, there is a lack of systematic investigations which concepts are most efficient in combining the two actuators, and which are most robust given the heavy uncertainties of the biomechanical part of the system. In the realizations of Hybrid Neuroprostheses, control is frequently rule-based, such as in [11] or in [186, 187]. For such an approach, however, extensive expert knowledge has to be integrated, and stability analysis is difficult. Automated design methods have been suggested for paraplegic cycling, e.g. in [117]: First, the controller for the additional motor is designed with inactive muscles (via pole placement), based on an identification of the leg's passive dynamical properties. Then, the motor is used to generate motion, and the muscle's power output is identified in response to pulse width. Finally, pole placement is used again for closed-loop FES power control, and muscle power can then controlled. Disturbance rejection properties are quantified in practical experiments, but stability is not analyzed theoretically. In the MotionMaker [154], which is intended for training, muscles and motors do not cooperate, instead they work against each other, and the motors are used to generate resistance for the muscles, which are controlled to generate a desired force.

There are many other examples of systems where the number of actuators exceeds the number of Degrees of Freedom, such that there are various control strategies that might also be applicable for Hybrid Neuroprostheses. For example, missiles have multiple actuators to control direction: Their fins are "cheap" actuators, but they have the problem of saturations. The additional reaction jets are expensive, yet do not suffer from saturation. To exploit both actuators optimally, actuator blending has been suggested by [58, 153]. Another example are CPUs, which allow distributed computation. Power Plants are yet another example, where low-potent actuators with fast, and high-potent actuators with slow dynamics are coordinated in order to react dynamically to varying demands. For valves, which cover only part of the range, so-called "split-range" concepts are employed. Load sharing is not necessarily done using software methods, it can sometimes also be performed mechanically, as in power-split transmissions that variably coordinate electrical motors and combustion engines.

A popular concept to combine two actuators is the master-slave concept, as used e.g. for inverters and converters. Another popular control concept to combine two actuators is the so-called Macro/Mini concept, where one serves the base demand, and the other actuator can cope with high-frequent tasks. It has e.g. been used to combine a compliant and a stiff actuator [161], and it has already been applied in a setup similar to the one here: Artificial air muscles combined with a stiff actuator [214].

A frequent observation in redundant systems is that several actuators do not necessarily cooperate well. For example, in dual-actuator hard disk drives, vibrations may occur due to their interaction. Therefore, a feedforward decoupling control has been suggested by [285].

The Hybrid Neuroprosthesis does exhibit some similarities to the afore mentioned systems: One actuator has slower dynamics and saturations, but is supposed to participate as much as possible (which corresponds to a less capable, but "cheap" actuator). However, the application differs also from the other examples: In contrast to most other examples, there are additional considerable uncertainties in the slow actuator, which also need to be compensated by the fast one. Another major difference lies in the fact that Functional Electrical Stimulation (in a therapeutic environment) is mainly used to generate proprioceptive feedback. Studies with Functional Electrical Stimulation stress the importance of proprioceptive feedback, as well as functional movements. This implies that the torque produced by the muscles, which is sensed via proprioceptive feedback, should be congruent with the generated motion. Therefore, the concept has to consider this in a therapeutic application, and the load cannot be distributed arbitrarily between the actuators. Concepts such as the Macro/Mini might be functionally beneficial, yet their therapeutic outcome would be doubtful.

4.1.2 Contribution and Outline of this Chapter

In this chapter, general control aspects of Hybrid Neuroprostheses are studied exemplarily in a single-joint study conducted with healthy subjects: A motor-driven orthosis, in addition to the stimulated muscles, exerts a torque on the knee of a sitting subject (Fig. 4.1).

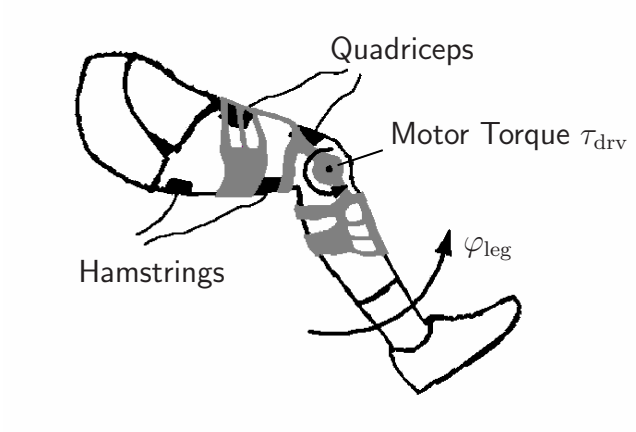

Figure 4.1: Motor-driven orthosis and electrically stimulated muscles (quadriceps and hamstrings) to control the knee joint angle φ_{leg}.

Main foci are on modeling and stability analysis of systems that exhibit time-variability, parameter uncertainty, and nonlinearities. Especially for the unreliable muscles, parameter identification is a considerable challenge and motivated the development of robust identification methods, as described in the preceding chapter. The present application of a Hybrid Neuroprosthesis is used as a prototypical biomechanical example system to illustrate that time-variability, parameter uncertainty, and nonlinearities can frequently be modeled as structure-variability in a simple polytopic description, such that they can all be assessed the same way (if a certain amount of conservatism is tolerated) during stability analysis using state-of-the art control theoretic methods. Based on the obtained models for the Hybrid Neuroprosthesis, different control strategies are investigated to coordinate the redundant actuators. Some of the above mentioned control concepts are used and modified to suit the demands of the Hybrid Neuroprosthesis. Four approaches are compared, whereby the baseline is represented by a MIMO controller with full state feedback, which is designed based on optimal feedback control. Both stability properties and performance of the controlled systems are evaluated, with a special focus on the individual influence of the various uncertainties.

4.2 Biomechanical Modeling

For reliable control design and stability analysis, knowledge of the plant and the residual modeling uncertainty plays a vital role. Numerous models of the human body can be found in the literature, which vary widely in their degree of detail. Especially the actuators of the human body, i.e. the muscles, and their complex functioning, have motivated extensive investigations. However, it is hardly feasible to model all inter-dependencies and measure all influencing variables in a practical environment. Therefore, always a compromise has to be found between modeling complexity and tolerable uncertainty.

4.2.1 Sources of Variability

The problems that arise in FES control are common for biomechanical control applications, which frequently face a large number of time variabilities and uncertainties of different types. For example, when black-box models are used and identified, structural uncertainties are introduced by unknown system order. Another example are unmodeled nonlinearities, such as input saturations. Parametric uncertainties are large when model parameters are empirical and not sufficiently tailored to the individual patient. Time variability is e.g. introduced by muscle fatigue in artificially recruited muscles.

More generally, the following frequent sources of state- or input-dependent uncertainty and time-variability in biomechanical applications can be identified.

1. Linearized system descriptions that deviate from the true, nonlinear behavior
2. Time-dependent plant parameter variations
3. Input saturation
4. Varying controller gains, e.g. in adaptive control
5. Unmodeled plant dynamics

Using the example of a Hybrid Neuroprosthesis, the above mentioned sources of uncertainty will now be specified exemplarily.

Concerning the first type of variability, (which is only an ostensible variability due to a linearized system representation), there are the nonlinearities in leg and muscle. The simplified muscle model to be used in the following does not include the considerable dependency of muscle torque and joint angle and velocity, which is both intrinsic and reflexive. Furthermore, the nonlinearities of elastic joint moments in the leg are replaced by linear functions during control design.

Of the second kind, there is e.g. the influence of fatigue or varying temperature on muscle force generation. In Functional Electrical Stimulation, muscles are subject to heavily accelerated fatigue.

Input saturations also mainly concern the muscle, if the assistive robot is dimensioned appropriately. In transcutaneous electrical stimulation, the muscle torque is severely limited compared to healthy muscle activity.

The fourth source of variability is the only variability that is deliberately introduced by the designer: The control strategies might involve an adaptive component. In the exemplary strategies to be presented, such an adaptive component is integrated by a varying amount of desired muscle participation.

The compliant coupling between leg and orthosis is an important factor, yet nonlinear and difficult to quantify or supervise. Therefore, it is neglected during control design, yet needs to be considered during stability analysis. Further unmodeled dynamics could be spasms or correlated voluntary activity that might be provoked by stimulation.

4.2.2 Objective: Affine System Representation

A popular modeling assumption in the context of stability analysis for uncertain, time-varying systems is that the uncertainty can be expressed in the form of time-varying parameters that affect the state space matrix in an affine manner. To make these powerful tools applicable for stability analysis, the aim of the following sections is to use state-of-the-art muscle and leg models to represent the Hybrid Neuroprosthesis as a structure-varying system that is linear in uncertain, time-varying parameters p_i. In other words, a representation of the form

$$\dot{\boldsymbol{x}} = \mathbf{A}(t)\boldsymbol{x} \tag{4.1}$$

$$\mathbf{A}(t) = \mathbf{A}_0 + \sum_{i=1}^{n} p_i(t)\mathbf{A}_i \tag{4.2}$$

is to be found, with constant matrices $\mathbf{A}_i, i = 0, ..., n$.

This representation is obtained in a modular manner: First, the integrands of the biomechatronic system are modeled separately, i.e. the leg, the muscles, and the coupling between leg and exoskeleton. Then, the three components are combined to a complete system description.

4.2.3 Leg Model

The human knee and shank are modeled as a simple pendulum as displayed in Fig. 4.2, and the degree of freedom of the ankle joint is neglected. Biomechanical parameters that are assumed to be constant are the mass m_{leg} of the limb, the distance l_s between joint and center of mass of the shank, and its inertia J_{leg}. Time-varying parameters are subsumed in the nonlinear function $\mathcal{N}_p(\varphi_{\text{leg}}, \dot{\varphi}_{\text{leg}})$, which contains the (nonlinear) passive elastic joint moments [69] and damping.

The dynamics of the leg in dependence of the joint torque τ_{leg} are described by the differential equation

$$J_{\text{leg}}\ddot{\varphi}_{\text{leg}} + m_{\text{leg}}gl_s \sin\varphi_{\text{leg}} + \mathcal{N}_p(\varphi_{\text{leg}}, \dot{\varphi}_{\text{leg}}) = \tau_{\text{leg}}. \tag{4.3}$$

With appropriate coordinate transformation of φ_{leg} and the definition of a generalized joint impedance described by the variable parameters $c_{\text{leg}}(\varphi_{\text{leg}}, \dot{\varphi}_{\text{leg}})$ for elasticity and $k_{\text{leg}}(\varphi_{\text{leg}}, \dot{\varphi}_{\text{leg}})$ for damping, the dynamics are rewritten as

$$J_{\text{leg}}\ddot{\varphi}_{\text{leg}} + c_{\text{leg}}(\varphi_{\text{leg}}, \dot{\varphi}_{\text{leg}})\varphi_{\text{leg}} + k_{\text{leg}}(\varphi_{\text{leg}}, \dot{\varphi}_{\text{leg}})\dot{\varphi}_{\text{leg}} = \tau_{\text{leg}}. \tag{4.4}$$

A state-space representation with the state vector

$$\boldsymbol{x}_{\text{leg}}^T = \begin{pmatrix} \varphi_{\text{leg}} & \dot{\varphi}_{\text{leg}} \end{pmatrix}, \tag{4.5}$$

and input $u_{\text{leg}} = \tau_{\text{leg}}$ is given by

$$\dot{\boldsymbol{x}}_{\text{leg}} = \mathbf{A}_{\text{leg}}(\boldsymbol{x}_{\text{leg}})\boldsymbol{x}_{\text{leg}} + \mathbf{b}_{\text{leg}}\tau_{\text{leg}} \tag{4.6}$$

$$\varphi_{\text{leg}} = \boldsymbol{c}_{\text{leg}}^T\boldsymbol{x}_{\text{leg}}. \tag{4.7}$$

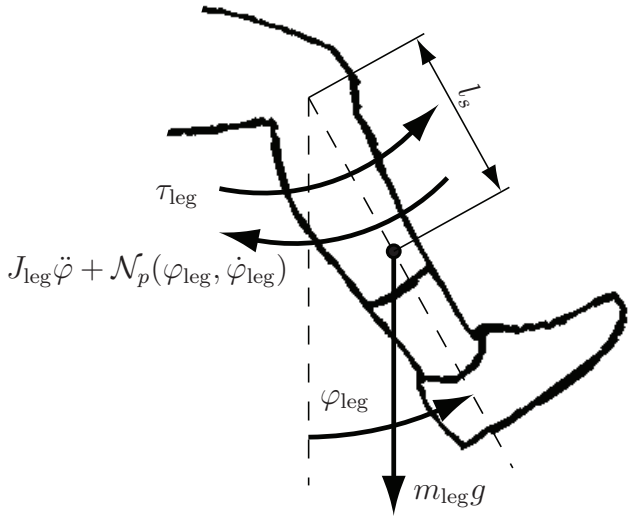

Figure 4.2: The shank is modelled as a simple pendulum with inertia J_{leg}, mass m_{leg}, and nonlinear damping and elasticity $\mathcal{N}_p(\varphi_{\text{leg}}, \dot{\varphi}_{\text{leg}})$. The location of the Center of Mass is defined by l_s. A torque τ_{leg} acts on the shank (which is produced by muscles and exoskeleton), and the leg's motion is described by the angle φ_{leg}

The matrices are

$$\mathbf{A}_{\text{leg}}(\boldsymbol{x}_{\text{leg}}) = \begin{pmatrix} 0 & 1 \\ -\frac{c_{\text{leg}}(\boldsymbol{x}_{\text{leg}})}{J_{\text{leg}}} & -\frac{k_{\text{leg}}(\boldsymbol{x}_{\text{leg}})}{J_{\text{leg}}} \end{pmatrix}, \quad \boldsymbol{b}_{\text{leg}} = \begin{pmatrix} 0 \\ \frac{1}{J_{\text{leg}}} \end{pmatrix}, \quad \boldsymbol{c}_{\text{leg}}^T = \begin{pmatrix} 1 & 0 \end{pmatrix}. \tag{4.8}$$

Parameterization of the leg model is achieved via identification with state-of-the-art nonlinear identification algorithms. The procedure is described in App. E.

4.2.4 Muscle Model

In FES, the correlation between stimulation parameters and exerted torque by muscle contraction is strongly nonlinear and time-variant. The torque depends on the spatial and temporal recruitment of muscle fibers, on the muscle length, and on the velocity of contraction.

As has been mentioned in the previous chapter, a large number of muscle models are available in the literature [280]. Here, the scope is limited to the popular model in [268], which is based on works of Hill [106]. There, the muscle torque is calculated in dependence of joint angle and velocity rather than muscle length and contraction velocity. The effects of the varying moment arm of the muscle are thus included implicitly.

This muscle model is illustrated in Fig. 4.3: The pulse width PW of the stimulation signal is the input to a system with a static nonlinearity f_r (the *recruitment curve*) in series with a linear dynamic model (the *activation dynamics*), represented by the transfer function $G_a(s)$. In analogy to Chap. 3, this transfer function is a critically damped second-order system with eigenfrequency ω_0:

$$G_a(s) = \frac{\tau_{\text{fes}}(s)}{a(s)} = \frac{\omega_0^2}{s^2 + 2\omega_0 s + \omega_0^2}\, e^{-sT_t} \quad . \tag{4.9}$$

The dead time T_t in this model accounts for signal transport in the nerve pathways. Its value is about 25 ms [185]. The output of the nonlinearity is termed *activation level* a. This output is multiplied by nonlinear terms depending on joint angle and angular velocity, and then yields the muscle torque τ_{fes} acting on the joint.

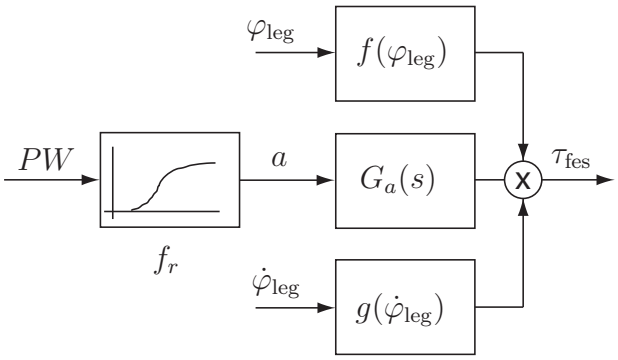

Figure 4.3: Torque response τ_{fes} to FES is modeled with a nonlinear recruitment curve f_r that relates pulse width PW and activation level a, followed by a linear transfer function $G_a(s)$, and a multiplicative dependency on joint angle and angular velocity (modified from [185]).

This model is very much simplified, and it cannot explain measurable effects such as hysteresis [143] and dependence of the muscle response on history of stimulation and movement. However, according to [268], the model proved to be accurate to 85 to 90% when tested on a cat hind limb, whereby recruitment, angle, and angular velocity were varied simultaneously, independently, and in a pseudorandom manner. In App. C, the biological background and typical characteristics of the different parts of the model (activation dynamics, force-length and force-velocity feedback) are explained.

Although the physiological processes are described in a highly simplified macroscopic manner, the muscle model is still complex and nonlinear, and there is also time variance to be considered due to fatigue. The usual approach for its parameterization includes several measurements on the subject in *isokinetic* (constant muscle force) and *isometric* (constant length) test setups. Isometric identification has been described in Chap. 3. To complement the contraction dynamics under non-isometric conditions, the nonlinear dependencies on muscle length and contraction velocity can be quantified in a separate setup, e.g. with the widely used commercial product *Kin Com* (IsoKinetic International, USA) for isokinetic measurement.

Here, a different approach is taken: The description is simplified even further, but all unmodeled effects are implicitly considered and described as uncertainties. This reduces the time and effort needed to adapt the model to a specific human subject, and it also leads

to a conservative system description for robust controller design. To simplify the model, the explicit dependencies on muscle length and contraction velocity are not identified. Instead, the nonlinear dependency on angle and angular velocity is accounted for by unknown, time-varying, bounded functions of time. It will now be shown that these uncertain nonlinear functions, as well as input saturations, imperfect modeling of the recruitment curve, and fatigue effects can be treated in a very similar fashion, such that all these influences can be included in form of time-varying factors in an affine description according to Sec. 4.2.2.

First, the static nonlinearity of the Hammerstein muscle model is compensated by using its inverse to transform the input, the stimulation pulse width. This cancellation is only valid for the region where the recruitment curve is invertible, i.e. as long as the desired torque stays below the maximum realizable torque. Above the maximum achievable muscle torque $\tau_{f,max}$ given by the saturation value of the recruitment characteristic, the controller output needs to be saturated. Using the control signal $\tilde{u}_{\text{fes}}$ as a virtual input for the input-output linearized muscle model, the nonlinear transformation is written as:

$$PW(t) = \begin{cases} f_r^{-1}(\tilde{u}_{\text{fes}}(t)) & \text{for} \quad \tilde{u}_{\text{fes}}(t) \in [0, \tau_{f,max}] \\ f_r^{-1}(\tau_{f,max}) & \text{for} \quad \tilde{u}_{\text{fes}}(t) > \tau_{f,max}, \end{cases} \tag{4.10}$$

such that

$$a(t) = \begin{cases} \tilde{u}_{\text{fes}}(t) & \text{for} \quad \tilde{u}_{\text{fes}}(t) \in [0, \tau_{f,max}] \\ \tau_{f,max} < \tilde{u}_{\text{fes}}(t) & \text{for} \quad \tilde{u}_{\text{fes}}(t) > \tau_{f,max}. \end{cases} \tag{4.11}$$

To obtain the desired affine system representation, a polytopic description of $a(t)$ is used, which does not require knowing the exact course of $\tilde{u}_{\text{fes}}(t)$. Introducing the saturation factor k_{sat}, the reduction of $a(t)$ due to saturation can then be written more generally:

$$a(t) = k_{\text{sat}}(t)\tilde{u}_{\text{fes}}(t)\,, \quad k_{\text{sat}}(t) \in [0, 1] \quad \forall t. \tag{4.12}$$

This description conservatively overbounds imperfect cancellation of the recruitment curve, at least as long as the erroneously modeled nonlinearity consistently *over*-estimates the achievable muscle torque.

The force-velocity and force-length relationships are now subsumed in the single factor

$$n_{\text{fes}}(t) := g(\dot{\varphi}_{\text{leg}})\, f(\varphi_{\text{leg}}), \tag{4.13}$$

which is also simply handled as an unknown, yet bounded function of time in the following: Using physiological knowledge, as presented in App. C, and identification results of the preceding chapter, the boundaries are chosen as

$$n_{\text{fes}}(t) \in [0, 2]. \tag{4.14}$$

Muscle fatigue mainly influences the static gain of the muscle response [160]. Being a slow process, this reduction can be interpreted as a reduction of torque, expressible by a reduced value of n_{fes}, or as a further input saturation, thus decreasing the value of k_{sat}. In the following, it is interpreted as a reduction of n_{fes}.

Taking the antagonistic muscle pair of hamstrings and quadriceps, positive and negative torques on the joint can be realized. The muscle behavior can then be represented in state-space form with state vector

$$\boldsymbol{x}_{\text{fes}}^T = \begin{pmatrix} \tau_{\text{fes}} & \dot{\tau}_{\text{fes}} \end{pmatrix}, \tag{4.15}$$

and output $y_{\text{fes}} = \tau_{\text{fes}}$ by transformation of the previously given transfer-function representation (4.9):

$$\dot{\boldsymbol{x}}_{\text{fes}} = \mathbf{A}_{\text{fes}}\boldsymbol{x}_{\text{fes}} + \boldsymbol{b}_{\text{fes}}\tilde{u}_{\text{fes}}(t - T_t) \tag{4.16}$$

$$\tau_{\text{fes}} = \boldsymbol{c}_{\text{fes}}^T(t)\boldsymbol{x}_{\text{fes}}, \tag{4.17}$$

with matrices

$$\mathbf{A}_{\text{fes}} = \begin{pmatrix} 0 & 1 \\ -\omega_0^2 & -2\,\omega_0 \end{pmatrix}, \quad \boldsymbol{b}_{\text{fes}} = \begin{pmatrix} 0 \\ k_{\text{sat}}\omega_0^2 \end{pmatrix}, \quad \boldsymbol{c}_{\text{fes}}(t)^T = \begin{pmatrix} n_{\text{fes}}(t) & 0 \end{pmatrix}. \tag{4.18}$$

Robust identification methods for the muscle model's parameters have been described in Chap. 3.

4.2.5 Compliant Coupling between Limbs and Exoskeleton

Although commonly neglected, the compliance in the coupling between leg and exoskeleton has an important influence on performance and stability of the controlled system, as will be outlined later. This influence grows with the extent the muscles get involved. As a basis for later theoretical investigations, a simplified model of the compliant coupling is provided here, which augments the system dynamics by two additional states.

Fig. 4.4 displays the elastic coupling between the orthosis and the leg. The torque τ_{exo}

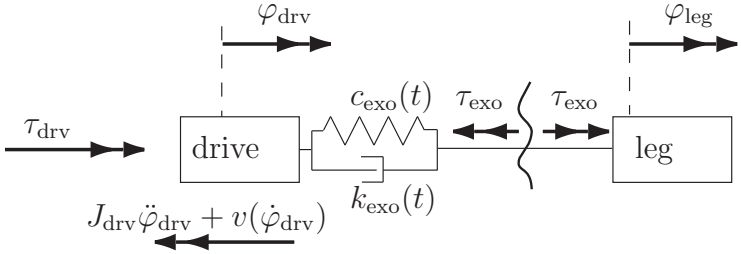

Figure 4.4: Compliant coupling between orthosis and leg: The drive produces a torque τ_{drv}, which acts on the drive unit with inertia J_{drv} and friction v depending on the angular velocity $\dot{\varphi}_{\text{drv}}$ of the drive. The torque τ_{exo} is transmitted to the leg via a compliant coupling, described by a varying stiffness $c_{\text{exo}}(t)$ and damping $k_{\text{exo}}(t)$.

introduced into the leg by the exoskeleton is

$$\tau_{\text{exo}} = c_{\text{exo}}(t)(\varphi_{\text{drv}} - \varphi_{\text{leg}}) + k_{\text{exo}}(t)(\dot{\varphi}_{\text{drv}} - \dot{\varphi}_{\text{leg}}) \tag{4.19}$$

with $c_{\text{exo}}(t)$ and $k_{\text{exo}}(t)$ denoting the variable stiffness and damping of the entire transmission between orthosis and bone, thus comprising the connecting elements themselves (orthosis and straps), as well as impedance of muscles and tissue during compression. The angle φ_{drv} and velocity $\dot{\varphi}_{\text{drv}}$ are the states of the drive unit.

The drive torque τ_{drv} and the load torque τ_{exo} act on the drive unit with inertia J_{drv} (the orthosis has negligible mass and inertia) and friction $v(\dot{\varphi}_{\text{drv}})$:

$$\tau_{\text{drv}} - \tau_{\text{exo}} = J_{\text{drv}}\ddot{\varphi}_{\text{drv}} + v(\dot{\varphi}_{\text{drv}}). \tag{4.20}$$

These two equations can be used to derive a state-space model for the exoskeleton dynamics. With the state variables of the exoskeleton selected as the angle φ_{drv} and velocity $\dot{\varphi}_{\text{drv}}$ of the drive unit:

$$\boldsymbol{x}_{\text{exo}}^T = \begin{pmatrix} \varphi_{\text{drv}} & \dot{\varphi}_{\text{drv}} \end{pmatrix}, \tag{4.21}$$

input τ_{drv} and output τ_{exo}, the model can be written as:

$$\begin{aligned} \begin{pmatrix} \dot{\varphi}_{\text{drv}} \\ \ddot{\varphi}_{\text{drv}} \end{pmatrix} &= \begin{pmatrix} 0 & 1 \\ -\frac{c_{\text{exo}}}{J_{\text{drv}}} & -\frac{k_{\text{exo}}+v}{J_{\text{drv}}} \end{pmatrix} \begin{pmatrix} \varphi_{\text{drv}} \\ \dot{\varphi}_{\text{drv}} \end{pmatrix} + \begin{pmatrix} 0 & 0 \\ \frac{c_{\text{exo}}}{J_{\text{drv}}} & \frac{k_{\text{exo}}}{J_{\text{drv}}} \end{pmatrix} \begin{pmatrix} \varphi_{\text{leg}} \\ \dot{\varphi}_{\text{leg}} \end{pmatrix} + \begin{pmatrix} 0 \\ \frac{1}{J_{\text{drv}}} \end{pmatrix} \tau_{\text{drv}} \\ \tau_{\text{exo}} &= \begin{pmatrix} c_{\text{exo}} & k_{\text{exo}} \end{pmatrix} \begin{pmatrix} \varphi_{\text{drv}} \\ \dot{\varphi}_{\text{drv}} \end{pmatrix} + \begin{pmatrix} -c_{\text{exo}} & -k_{\text{exo}} \end{pmatrix} \begin{pmatrix} \varphi_{\text{leg}} \\ \dot{\varphi}_{\text{leg}} \end{pmatrix}, \end{aligned} \tag{4.22}$$

or rewritten in short notation, considering the variability of c_{exo} and k_{exo}:

$$\dot{\boldsymbol{x}}_{\text{exo}} = \mathbf{A}_{\text{exo}}(t)\boldsymbol{x}_{\text{exo}} + \mathbf{B}_{\text{exo}}(t)\boldsymbol{x}_{\text{leg}} + \boldsymbol{b}_{\text{drv}}\tau_{\text{drv}} \tag{4.23}$$

$$\tau_{\text{exo}} = \boldsymbol{c}_{\text{exo}}(t)^T\boldsymbol{x}_{\text{exo}} + \boldsymbol{d}_{\text{exo}}(t)^T\boldsymbol{x}_{\text{leg}}. \tag{4.24}$$

To parameterize the model, the stiffness c_{exo} is quantified using a simple test setup: The leg is immobilized (by placing the foot on the ground) and a slow sinusoidal feedforward torque is applied to the motor. Afterward, encoder angle and motor torque are used to quantify the impedance of the coupling as a function of direction and magnitude of the transmitted torque.

4.2.6 Complete Model

The joint torque τ_{leg} acting on the leg is a superposition of the torque τ_{exo} transmitted by the orthosis and the muscle torque τ_{fes}, as indicated in Fig. 4.5:

$$\tau_{\text{leg}} = \tau_{\text{exo}} + \tau_{\text{fes}}. \tag{4.25}$$

Subsuming the models of leg, muscles, and compliant coupling of the previous sections, a state space representation of the redundant system can now be written as:

$$\dot{\boldsymbol{x}} = \mathbf{A}(t)\boldsymbol{x} + \mathbf{B}(t)\boldsymbol{u} \tag{4.26}$$

$$y = \boldsymbol{c}^T\boldsymbol{x} \tag{4.27}$$

with

$$\mathbf{A}(t) = \begin{pmatrix} \mathbf{A}_{\text{fes}} & \mathbf{0} & \mathbf{0} \\ \mathbf{0} & \mathbf{A}_{\text{exo}} & \mathbf{B}_{el} \\ \boldsymbol{b}_{\text{leg}}\boldsymbol{c}_{\text{fes}}^T & \boldsymbol{b}_{\text{leg}}\boldsymbol{c}_{\text{exo}}^T & \mathbf{A}_{\text{leg}} + \boldsymbol{b}_{\text{leg}}\boldsymbol{d}_{el}^T \end{pmatrix} \tag{4.28}$$

$$\mathbf{B}(t) = \begin{pmatrix} \boldsymbol{b}_{\text{fes}} & \mathbf{0} \\ \mathbf{0} & \boldsymbol{b}_{\text{drv}} \\ \mathbf{0} & \mathbf{0} \end{pmatrix}, \quad \boldsymbol{c}^T = \begin{pmatrix} 0 & 0 & 1 & 0 & 0 & 0 \end{pmatrix} \tag{4.29}$$

$$\boldsymbol{x} = \begin{pmatrix} \boldsymbol{x}_{\text{fes}} \\ \boldsymbol{x}_{\text{exo}} \\ \boldsymbol{x}_{\text{leg}} \end{pmatrix}, \quad y = \varphi_{\text{drv}}, \quad \boldsymbol{u} = \begin{pmatrix} \tilde{u}_{\text{fes}}(t - T_t) \\ \tau_{\text{drv}} \end{pmatrix}. \tag{4.30}$$

4

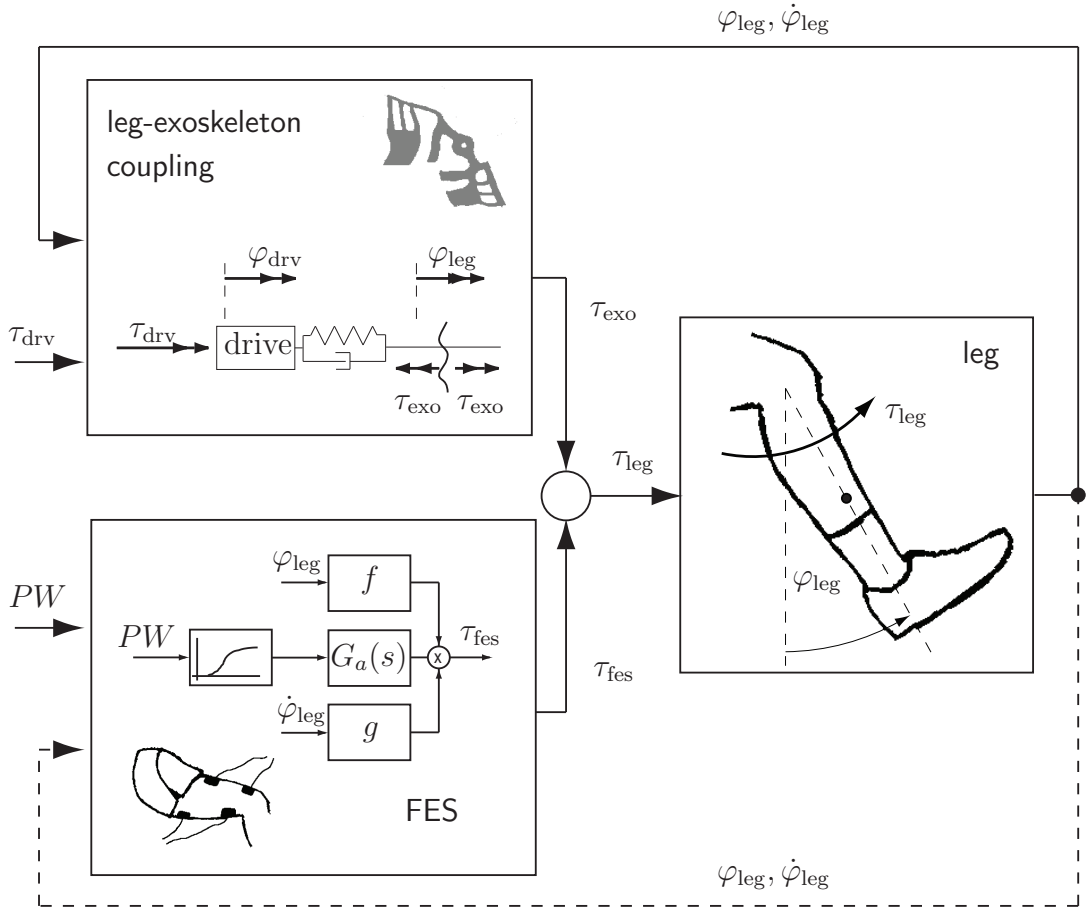

Figure 4.5: The three modular descriptions are combined to a complete model: Both muscles and exoskeleton exert a torque on the leg, which is modelled as a simple pendulum. Feedback of leg angle and angular velocity is explicitly modelled for the compliant coupling, and it is implicitly included in the muscle model.

This is the description of a structure-varying system, although the time-dependency of the individual matrices and vectors in $\mathbf{A}(t)$ has not been explicitly indicated here to improve readability. The motor angle φ_{drv} is the only measurable output, it is measured by the motor encoder signal. In App. F, the explicit entries of the matrices are given.

The system matrix is linear in the uncertain, time-varying parameters p_i of leg, muscle, and exoskeleton-leg coupling, i.e. in c_{leg}, k_{leg}, n_{fes}, c_{exo}, and k_{exo}, and can thus be written in the required affine notation of (4.2). A noticeable characteristic of the system matrix $\mathbf{A}(t)$ is that the parameters c_{leg} and k_{leg} only appear in sum with the coupling parameters c_{exo} and k_{exo}.

4.3 Control of the Hybrid Neuroprosthesis

This section deals with the control of the Hybrid Neuroprosthesis. Thereby, four different control approaches are presented, which exploit the redundancy of the actuators to a

varying extent. Control and observer design are based on a simplified model with nominal, constant parameters.

4.3.1 Model Simplifications during Control Design

The Hybrid Neuroprosthesis represents a highly nonlinear system. Simplifying the descriptions of the previous sections, control design is based on a linear model with constant parameters. The uncertain function $n_{\text{fes}}(t)$ of (4.14) in the muscle model is set to unity, such that the muscle force is calculated directly as a function of the activation level a. This simplification is acceptable for short-time isometric contractions or at least for slow motions with small range, otherwise it will lead to errors. These errors appear as uncertainties during observer design and in the stability analysis. The nonlinearities of gravitational components and elastic joint moments of the leg are not compensated, as the superposition of both is already well represented by its linearization, at least for the knee angle range used in the practical experiments (see App. E). Furthermore, the coupling between exoskeleton and human bone is assumed to be rigid. This assumption is incorrect, because the value of coupling stiffness varies strongly. However, this assumption is commonly made, and it can be justified by the argument that coupling stiffness can hardly be measured nor adapted robustly during the experiments. The repercussions of this grave simplification will be investigated later during a stability analysis.

In the consequent simplified system representation for controller design, the parameters thus equal the following nominal values:

$$
\begin{aligned}
c_{\text{leg}}(t) &= \bar{c}_{\text{leg}} = const. && (4.31)\\
k_{\text{leg}}(t) &= \bar{k}_{\text{leg}} = const. && (4.32)\\
n_{\text{fes}}(t) &= 1 = const. && (4.33)\\
k_{\text{sat}}(t) &= 1 = const. && (4.34)\\
c_{\text{exo}}(t) &\rightarrow \infty && (4.35)\\
k_{\text{exo}}(t) &\rightarrow \infty && (4.36)
\end{aligned}
$$

Inputs to the combined system are the virtual input $u_1 = \tilde{u}_{\text{fes}}(t - T_t)$ for the muscle, and the motor torque $u_2 = \tau_{\text{drv}}$ of the motor; output is the knee joint angle $y = \varphi_{\text{leg}}$. With rigid coupling, angles and velocities of the drive unit and of the leg are identical:

$$\boldsymbol{x}_{\text{exo}} = \boldsymbol{x}_{\text{leg}}. \tag{4.37}$$

The simplified state space representation of the complete system with rigid coupling is:

$$
\begin{aligned}
\dot{\boldsymbol{x}}_{\text{rig}} &= \mathbf{A}_{\text{rig}}\,\boldsymbol{x}_{\text{rig}} + \mathbf{B}_{\text{rig}}\,\boldsymbol{u} && (4.38)\\
y &= \boldsymbol{c}_{\text{rig}}^{T}\,\boldsymbol{x}_{\text{rig}}. && (4.39)
\end{aligned}
$$

$$\text{with} \quad \boldsymbol{x}_{\text{rig}} = \begin{pmatrix} \boldsymbol{x}_{\text{fes}} \\ \boldsymbol{x}_{\text{leg}} \end{pmatrix}, \quad \boldsymbol{u} = \begin{pmatrix} \tilde{u}_{\text{fes}}(t - T_t) \\ \tau_{\text{drv}} \end{pmatrix}, \quad y = \varphi_{\text{leg}} = \varphi_{\text{drv}}. \tag{4.40}$$

The system matrix $\mathbf{A}_{\text{rig}}$, the input matrix $\mathbf{B}_{\text{rig}}$, and the output vector $\boldsymbol{c}_{\text{rig}}^T$ are composed as follows (compare the full state space representation of (4.26)):

$$\mathbf{A}_{\text{rig}} = \begin{bmatrix} \mathbf{A}_{\text{fes}} & \mathbf{0} \\ \boldsymbol{b}_{\text{leg+drv}}\boldsymbol{c}_{\text{fes}}^T & \mathbf{A}_{\text{leg+drv}} \end{bmatrix}, \qquad \mathbf{B}_{\text{rig}} = \begin{bmatrix} \boldsymbol{b}_{\text{fes}} & \mathbf{0} \\ \mathbf{0} & \boldsymbol{b}_{\text{leg+drv}} \end{bmatrix}, \qquad \boldsymbol{c}_{\text{rig}}^T = \begin{pmatrix} \mathbf{0} & \boldsymbol{c}_{\text{leg}}^T \end{pmatrix}. \quad (4.41)$$

The index leg + drv indicates that instead of the moment of inertia J_{leg} only, the combination $J_{\text{leg}} + J_{\text{drv}}$ is used within the respective leg model matrices.

4.3.2 Observer-Predictor

For a full state-feedback controller, all states need to be provided. To obtain an estimate of the muscle torque, the simple model of Sec. 4.3.1 is used to design an observer-predictor of the muscle states using the standard procedure of a Kalman Filter in combination with a least mean-squares predictor [135].

It is assumed that model uncertainties of each of the two model parts (muscles and leg) in (4.38-4.39) can be modeled as a combination of process noise $\boldsymbol{w}$ and measurement noise v:

$$\dot{\boldsymbol{x}}_{\text{rig}} = \mathbf{A}_{\text{rig}}\,\boldsymbol{x}_{\text{rig}} + \mathbf{B}_{\text{rig}}\,\boldsymbol{u} + \boldsymbol{w}, \quad \boldsymbol{w}^T = (\boldsymbol{w}_{\text{fes}}^T \quad \boldsymbol{w}_{\text{leg}}^T) \quad (4.42)$$

$$y = \boldsymbol{c}_{\text{rig}}^T\,\boldsymbol{x}_{\text{rig}} + v \quad (4.43)$$

The values $\boldsymbol{w}_{\text{fes}}$ and $\boldsymbol{w}_{\text{leg}}$ denote the process noise of muscle and leg, respectively, whereby $\boldsymbol{w}_{\text{fes}}$ contains both voluntary activity of the subject, as well as spasticity or model uncertainties. The process noise $\boldsymbol{w}_{\text{leg}}$ represents uncertainties of the ideally modeled motor, modeling uncertainties of the leg, as well as also not stimulation-related muscle activity. Measurement noise v mainly results from elasticity in the orthosis, as well as in the leg tissue. During identification, both systems are separately analyzed regarding their parameters and uncertainties. Therefore, also a measurement noise v_{fes} of the muscle torque is determined, which disturbs the muscle model output, but this is assigned to the force sensor and therefore neglected in the overall observer design.

During this design of the Kalman filter, several important assumptions required for the Kalman Filter to be stochastically optimal are violated: The errors of the leg model are mainly caused by elasticities, which represent additional dynamics and not Gaussian noise. The simple model has only two states, reducing the system order by two. Furthermore, during the experiments, the muscles are no longer recruited in an isometric manner, adding further (state-correlated) error sources that are not considered during observer design. Although the Kalman filter provides a good approximation also when noise is not Gaussian and dynamics are nonlinear [60], it must be noted that the observed muscle torque can only provide a rough approximation of the true value. Furthermore, the predictor requires the time delay to be known well, otherwise it can lead to unstable behavior.

One possibility to quantify the noise levels of leg and muscles is to use an innovation sequence approach [33]. However, the noise covariance matrix entries could not be quantified with this approach because the algorithm did not converge. Therefore, process noise is calculated by reverse calculation of the states and inputs under the assumption that measurement noise can be removed (via phaseless filtering based on local polynomial approximation of the measured variable). This is possible because both leg and muscle models

are *flat*. Flatness means that there is an output y such that the states and inputs can all be expressed as functions of derivatives of y [84]. Here, the *flat* output y is the torque τ_{fes} for the muscle model, and the leg angle φ_{leg} for the leg model (including drive inertia as well, due to the assumption of rigid coupling).

The observer theoretically produces the best possible estimate under consideration of the comparably low uncertainties of the leg model and the high uncertainties of the muscle model. However, the leg model is so much more reliable compared to the muscle model (compare Chap. 3 and App. E) that the observer feedback matrix has to be saturated to avoid numerical problems. Therefore, almost a Sliding Mode input observer results, mainly calculating backwards from the leg model.

4.3.3 Controllers

The muscle model presented in Sec. 4.2.4 is extremely simplified and subject to considerable uncertainties. Due to this reason, the muscle controller is most probably not suitable for good tracking of the reference trajectory. However, using the motor as a second, highly reliable actuator, tracking is assured. The purpose of muscle activation is then primarily reduced to the generation of proprioceptive feedback, the provocation of voluntary activity, and a training effect. In other words, it is desired that the muscle activation is correlated with the motion produced in order to produce suitable proprioceptive feedback, but high control performance is traded in for low calibration effort.

Four different approaches will be presented and compared: A Linear Quadratic Gaussian controller, a blending strategy with variable torque distribution, a master-slave concept, and a simple feedforward approach for the muscles combined with closed-loop control for the motor. The four approaches are shown schematically in Fig. 4.6.

In all controllers, there is a *recruitment factor* $r(t)$. This factor is constrained in the interval $[0, 1]$, and it represents a possible control gain variation for muscle recruitment. This includes the possibility to switch muscles on or off, or to recruit them more or less according to the current situation. This more general factor can also take over the role of the unavoidable saturation factor k_{sat} of (4.12), if the muscle input signal is constrained appropriately:

$$\left(r(t) \leq \left| \frac{M_{f,max}}{\tilde{u}_{\text{fes}}} \right| \wedge 0 \leq r(t) \leq 1 \right) \forall t \quad \Rightarrow k_{\text{sat}} = \text{const.} = 1 \quad . \tag{4.44}$$

The blending controller makes explicit use of this time-variable recruitment factor, in order to tune the muscle participation freely and shift load variably from one actuator to the other. The LQG controller is designed for the time-invariant case, and the recruitment factor represents an unavoidable disturbance. Both the Master-Slave concept and the muscle feedforward controller are designed to tolerate this unavoidable saturation, as well as other disturbances in the muscle model subsumed in n_{fes} in (4.13), and motor participation is increased or reduced based on the observed currently active muscle torque.

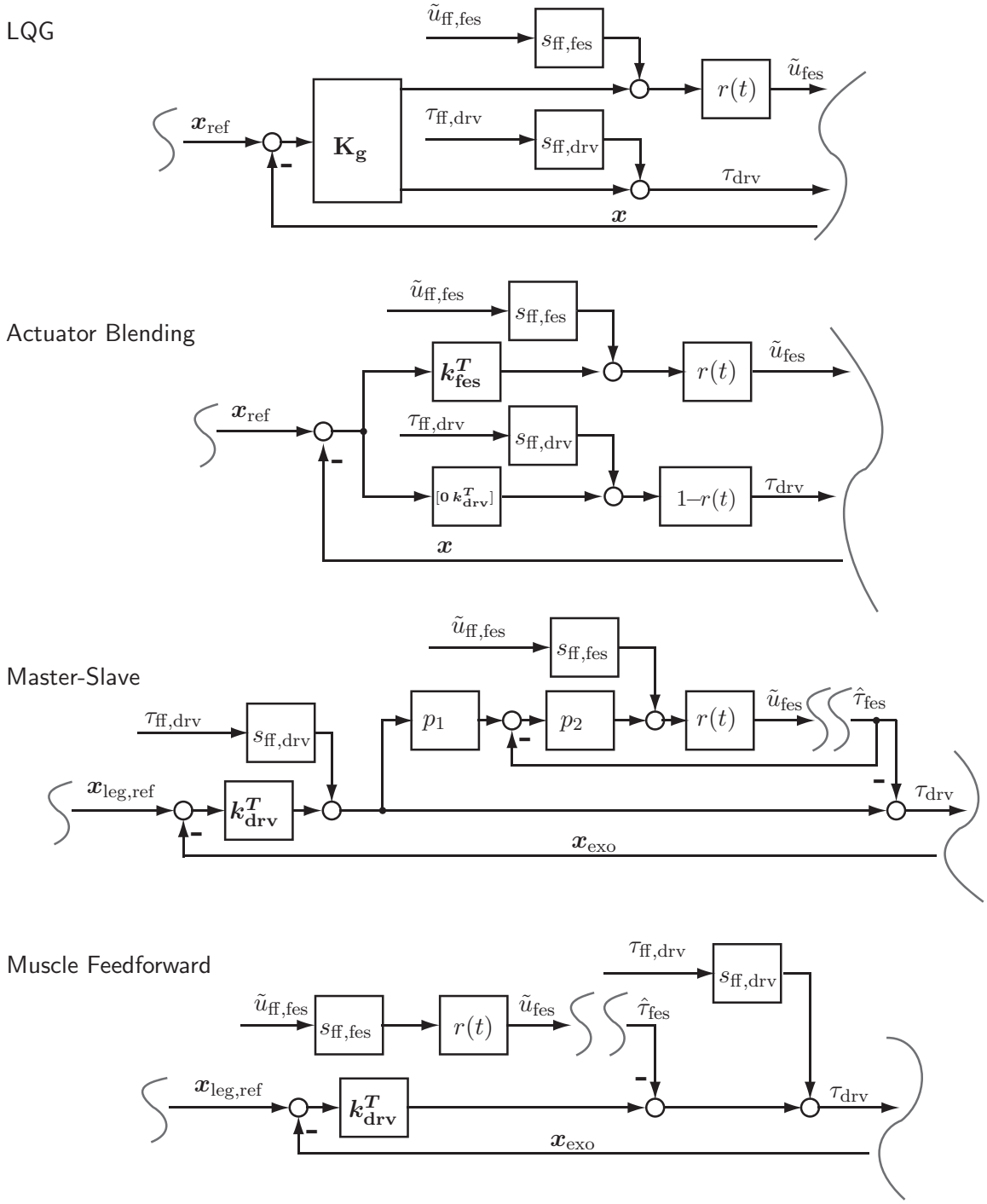

Figure 4.6: Block diagrams of the four controllers. Feedforward inputs (with index ff) for muscles and motors are designed for the single-actuator case, and the distribution of desired torque between the actuators is realized via factors s_{ff}. Time-variable control gains are represented by a scalar factor $r(t)$.

LQG controller

The first controller is designed via conventional linear quadratic dynamic optimization, and it provides a baseline of maximum performance for the other controllers. The functional to be optimized during the control design combines criteria of tracking performance and energy consumption. By using a weighting matrix with different weights for energy consumption of the actuators, muscle recruitment in comparison to exoskeleton power generation can be adapted to the patient. The disadvantage of this full state feedback is that also for control of the motor, it relies on the leg model, which is only accurate in a theoretical environment of a freely swinging shank. For practical purposes, e.g. during gait, it is rarely possible to provide a full model of the legs, especially during stance phase. This controller is not designed to exploit fluctuations of the recruitment factor r, as the motor gain does not vary with varying muscle participation.

Actuator Blending

This control scheme is directly developed to account for adaptive muscle recruitment and adaptive motor assistance. Each controller is designed independently as if it was the only one. Then, the recruitment factor $r(t)$ is used to blend variably between these controllers. In the extremes, either only motor or only muscle are used. The motor controller is fully independent of observed muscles states and thus of the patient model.

Master-Slave

The third control concept is designed to deal with uncertain muscle response to stimulation: The motor controller is designed in a way that it is solely responsible for tracking. The muscles receive a fraction of the motor torque and are controlled to track this torque in a separate loop. The parameters p_1 and p_2 are thereby used to tune the muscle control loop manually. A compensation of the observed muscle torque can be performed if available (e.g. during swing phase, when a more reliable leg model is assumed). The motor then only provides the residual torque that is not (yet) exerted by the muscles. Theoretically, the muscle's slow dynamics are compensated fully and the system behaves as if controlled by the motor alone. This scheme can also be interpreted in a different way: The muscles are a disturbance to the motor controller, but an observable and thus compensable one. Although this is probably not fully achieved in a practical surrounding due to the muscle uncertainties and the inexact observer, increased robustness of this approach is expected in comparison to the preceding two strategies. This controller can deal with varying muscle recruitment as represented by $r(t)$, because the motor constantly reacts on the actually active (observed) muscle torque.

Feedback Motor Control and Feedforward Muscle Control

The last control approach almost completely absolves the muscles from the tracking task. They are recruited in a feedforward manner with pre-specified patterns. The motor, which

is in feedback control, is responsible for tracking. This way, the muscles are mainly recruited for proprioceptive feedback. Like in Master-Slave control, a compensation can be performed if a reliable muscle torque estimate is available, and fluctuations of the recruitment factor $r(t)$ are therefore dealt with. From this concept, maximum robustness is expected.

Flatness-based Feedforward Components

Assuming rigid coupling of exoskeleton and leg, the compound is a flat system, and the flat output is measurable. Flatness has already been used for noise quantification during observer design in Sec. 4.3.2: It means that with a finite number of derivatives of the output y (the angle φ_{leg}), the input u (the necessary joint torque τ_{leg} to move leg and drives), can be reconstructed. The muscles are also a flat system, i.e. with known torque τ_{fes}, the pulse width can be reconstructed (at least for torques below the maximum achievable value). For each of the two actuators, feedforward input signals u_{ff} can thus be calculated that would be needed if the respective actuator was solely active. Then, the torque is distributed a priori via the factors s_{ff} to the two actuators. All controllers except for the LQG controller intrinsically resolve the problem of redundancy also in the feedforward components, but the factors s_{ff} are included in every scheme in order to achieve a uniform description.

4.3.4 State-Space Description of the Controlled System

In a practical environment, it might be convenient or necessary to be able to switch the muscles off abruptly, to saturate the muscle torque, or to blend the muscles in or out arbitrarily. This possibility has been prepared by the scalar recruitment factor $r(t)$ in each controller.

To enable more general stability analysis of all controllers in the same fashion, each one can be represented in the autonomous case by a time-varying state feedback matrix $\mathbf{K}(t)$ with

$$\boldsymbol{u} = -\mathbf{K}(t)\boldsymbol{x}, \tag{4.45}$$

whereby the variability is given by a convex combination of two matrices $\mathbf{K}_1$ and $\mathbf{K}_2$:

$$\mathbf{K}(t) = r\mathbf{K}_1 + (1 - r(t))\mathbf{K}_2, \quad r(t) \in [0, 1]. \tag{4.46}$$

With such a variable control strategy introduced in the original, not simplified system equation (4.26), the controlled system matrix is

$$\mathbf{A}_c(t) = \mathbf{A}(t) - \mathbf{B}\mathbf{K}_2 + r(t)\mathbf{B}(\mathbf{K}_2 - \mathbf{K}_1), \quad r \in [0, 1]. \tag{4.47}$$

This description also includes the special case of hard switching, e.g. if $r(t)$ is only piecewise continuous, which amounts to a hybrid system[1].

Interpreting the recruitment factor $r(t)$ as yet another time-varying parameter, the augmented description is still of the required affine form of (4.2).

[1] Deviating from the prior definition, the attribute "hybrid" is used in its control-theoretic connotation as a combination of discrete and continuous dynamics.

4.4 Analysis of Robustness

In the preceding sections of modeling and control, the system matrix of the controlled Hybrid Neuroprosthesis has been prepared in (4.26) and (4.47) in a way that it is linear in the parameters p_i and can be represented by:

$$\mathbf{A}_c = \mathbf{A}_0 + \sum_{i=1}^{n} p_i \mathbf{A}_i, \tag{4.48}$$

with appropriate constant matrices $\mathbf{A}_0$ and $\mathbf{A}_i$.

This describes an uncertain time-varying linear system, also termed Linear Differential Inclusion (LDI).

The predominant goal of the following analysis is to look at the importance of the various uncertainties in terms of their influence on system stability in different control architectures. This is done by observation of the stability margins during augmentation of the parameter intervals. The observed sensitivity then provides guidelines for the relevance of the individual uncertain parameters. In other words, the analysis aims to provide answers to the questions: Which variability is most hazardous for stability? And which control architecture is most tolerant in this context?

4.4.1 Tools to Analyze Stability of Uncertain Systems

To enable analysis of uncertain systems, a frequent assumption is that the uncertain parameters p_i in (4.48) are confined in a polytope. Another frequent simplification is to over-approximate the polytope by the convex hull (which is largest if the parameters vary independently). Both for constant and for time-varying uncertain parameters, well-founded tools to investigate stability are available, which will briefly be summarized in the following.

Time-Invariant Uncertain Parameters

If the system (4.48) is *time-invariant*, i.e. the p_i have uncertain, yet constant values (or if they vary slowly with time and assume quasi-static values) within the interval $[p_{i,min}, p_{i,max}]$, Kharitonov's theorem [21, 133] can be used to analyze stability. This is done by considering the set of all possible Hurwitz polynomials, i.e. a so-called *interval polynomial*, where the coefficients are not known exactly, but the intervals they are in, are known. However, this procedure is conservative, as it neglects possible correlations of the coefficients. Bartlett, Hollot and Lin [20] removed some of the conservatism by focusing on polynomial families which are polytopic in coefficient space. Their *edge theorem* states that in order to show that a Hurwitz polynomial is stable for any values of the coefficients within the allowed polytope, it suffices to check stability for the parameters on the edges of this polytope (The vertices are not sufficient in the general case).

Later, stability of uncertain systems has also been investigated in the state space domain. To prove stability of matrices that depend linearly on parameters that are bounded within polytopes (so-called *matrix polytopes*), necessary and sufficient conditions have been derived. For the special case of a hypercube, [34] used a Lyapunov function that depends polynomially on the uncertain parameters and found necessary and sufficient Linear Matrix Inequality (LMI) conditions. This result was later extended to the general case by [48], who introduced the class of Homogeneous Polynomially Parameter-Dependent Quadratic Lyapunov Functions (HPD-QLFs) and showed that a polytope of matrices is stable if and only if there exists a HPD-QLF.

If the system is *time-variant*, i.e. for dynamic changes of the parameters, such an analysis falls short of proving stability: Stability of a structure-varying system, as given by the employed model of the Hybrid Neuroprosthesis, does *not* follow from stability of the edge matrices [22].

Time-Varying Uncertain Parameters

Stability of linear systems with time-varying parametric uncertainties has been investigated via Lyapunov functions for a long time (e.g. [253], [165]). If there are only two parameters p_1 and p_2, such that $\mathbf{A}_c$ in (4.48) is described by a convex combination of two matrices, necessary and sufficient condition for stability are computable [29, 87]. However, even for such a two-dimensional case, the necessary conditions are complex. Therefore, a popular method is to employ a simple positive-definite quadratic Lyapunov function candidate of the form

$$V = \boldsymbol{x}^T \mathbf{P} \boldsymbol{x}, \quad \mathbf{P} > 0, \tag{4.49}$$

which provides a sufficient stability criterion, denominated *quadratic stability*, for the entire matrix polytope [113].

Quadratic stability is not a necessary condition for asymptotic stability, i.e. there are stable systems which are not quadratically stable [36]. Therefore, a common quadratic Lyapunov function may lead to excessively conservative results. In consequence, less conservative classes of Lyapunov functions have been proposed, e.g. the popular piecewise quadratic Lyapunov functions. Piecewise Lyapunov functions have e.g. been used by Rantzer and colleagues [124] to assess the stability of hybrid systems with discrete switching. However, in order to use Rantzer's approach, explicit a priori knowledge of the switching time or condition is required. Xie and colleagues [283] investigated systems with time-varying perturbations, and they applied the so-called S-procedure [4] to derive necessary and sufficient conditions for the stability of polytopes that consist only of two matrices. Later, their ideas were extended by Almeida [9] and applied to polytopes including more than two matrices. Several other classes of Lyapunov functions have also been proposed, e.g. polyhedral Lyapunov functions [30, 208]. The main disadvantage of non-quadratic Lyapunov function candidates is their complexity, because they lead to non-convex optimization problems.

A major source of conservatism is the polytopic problem description (4.48) itself. Allowing arbitrary variation within the polytope neglects a potential dependency of parameters on system states or time. Such an assumption may lead to conservative results, because examples of stable structure-varying systems can be found for which stability cannot be

shown by a convex Lyapunov function [32], but only by taking the form of parametric variation explicitly into account. In other words, if stability cannot be shown by a polytopic description, more explicit analysis of the parameter variations might still reveal that the system is stable. For example, there exist approaches that consider bounded rates of variation of the parameters [49], which reduce conservatism if parameters vary slowly (e.g. provoked by the comparably slow process of muscle fatigue). However, for the given example, as for many other biomechanical applications, the time-course of most parameters is either hard to quantify (as it is the case for compliance between exoskeleton and bone) or at least requires substantially increased identification and modeling effort (as it is the case for torque-length and torque-velocity characteristics of the muscle).

In conclusion, a pragmatic strategy is to check whether stability can be shown via the sufficient condition of quadratic stability for a polytopic system description, and to resort to more explicit modeling and more complex Lyapunov function candidates only if the condition is violated.

4.4.2 Polytopic Problem Description

The parameter vector $\boldsymbol{p}(t)$ is assumed to be confined in a polytope with the center $\boldsymbol{p}_{i,\mathrm{nom}}$, which can be written in dependency of the N auxiliary vertices $\boldsymbol{v}_m$ as:

$$\boldsymbol{p}(t) = \boldsymbol{p}_{\mathrm{nom}} + \sum_{m=1}^{N} \lambda_m(t)\boldsymbol{v}_m \quad , \quad \sum_{m=1}^{N} \lambda_m(t) = 1\,. \tag{4.50}$$

Substituting this polytopic parameter description in (4.48) leads to

$$\mathbf{A}_c(t) = \mathbf{A}_0 + \sum_{i=1}^{n} p_{i,\mathrm{nom}}\mathbf{A}_i + \sum_{i=1}^{n}\left(\sum_{m=1}^{N} \lambda_m(t) v_{m,i}\right)\mathbf{A}_i. \tag{4.51}$$

Defining

$$\mathbf{A}_{\mathrm{nom}} := \mathbf{A}_0 + \sum_{i=1}^{n} p_{i,\mathrm{nom}}\mathbf{A}_i \tag{4.52}$$

and

$$\boldsymbol{\Delta}_m := \sum_{i=1}^{n} v_{m,i}\mathbf{A}_i, \quad m = 1, ..., N \tag{4.53}$$

the set Ω containing all possible system matrices $\mathbf{A}_c(t)$ is given by:

$$\mathbf{A}_c(t) = \mathbf{A}_{\mathrm{nom}} + \boldsymbol{\Delta}(t), \quad \boldsymbol{\Delta}(t) \in Co\{\boldsymbol{\Delta}_1, ...\boldsymbol{\Delta}_N\}, \tag{4.54}$$

whereby the notation $Co\{\boldsymbol{\Delta}_1, ..., \boldsymbol{\Delta}_N\}$ describes the convex hull of all possible matrix variations around the mean matrix $\mathbf{A}_{\mathrm{nom}}$. Equation (4.54) is termed a "Polytopic LDI", and the set Ω will from here on be called a *matrix polytope*.

In the special case that the n parameters are independent, the $2n$ extreme parameter values define, on the maximum, $N = 2^n$ vertices in matrix space.

To improve conditioning, the problem is scaled before the numerical stability analysis.

4.4.3 Conditions for Quadratic Stability

The time derivative of the common Lyapunov function of 4.49 is:

$$\dot{V} = \boldsymbol{x}^T [\mathbf{A}_c(t)^T \mathbf{P} + \mathbf{P}\mathbf{A}_c(t)]\, \boldsymbol{x}, \tag{4.55}$$

which can be rewritten using the matrix $\mathbf{Q}$ with

$$\mathbf{Q} = \mathbf{A}_c(t)^T \mathbf{P} + \mathbf{P}\mathbf{A}_c(t), \tag{4.56}$$

to yield:

$$\dot{V} = \boldsymbol{x}^T \mathbf{Q}\, \boldsymbol{x}. \tag{4.57}$$

If $\mathbf{Q}$ is negative definite for any matrix $\mathbf{A}_c(t)$ under consideration,

$$\mathbf{Q} < 0 \quad \forall\, \mathbf{A}_c(t) \in \Omega, \tag{4.58}$$

the redundant system is stable for any variation of the recruitment factor $r(t)$, and for any isolated or simultaneous variation of plant parameters, whether state-dependent or not, and even for discrete switching.

The challenge now lies in the definition of a suitable matrix $\mathbf{P}$.

4.4.4 Solution of the Problem using LMIs

It can be shown that in order to ensure (4.58), it suffices to check the vertices of the matrix polytope [36]. Ignoring the fact that some of the N matrices in (4.53) might actually be internal points instead of vertices (a simplification that leads only to computational overhead), this can be written as:

$$\mathbf{Q}_m < 0 \quad \forall \mathbf{A}_m = \mathbf{A}_{\text{nom}} + \boldsymbol{\Delta}_m, m = 1, ..., N \Rightarrow \mathbf{Q} < 0 \quad \forall \mathbf{A}_c \in \Omega \tag{4.59}$$

This leads to a set of $N + 1$ Linear Matrix Inequalities (LMIs), which is parameterized by the matrices $\mathbf{A}_m$:

$$\mathbf{A}_m^T \mathbf{P} + \mathbf{P}\mathbf{A}_m < 0,\ m = 1, ..., N \tag{4.60}$$

$$\mathbf{P} > 0. \tag{4.61}$$

These LMIs can efficiently be solved numerically, and if a solution in form of the matrix $\mathbf{P}$ can be found, the system is stable.

4.4.5 Alternative Solution Using Ideal Lyapunov Functions

It should be mentioned that there is also a different way of determining $\mathbf{P}$, which does not require solving a set of LMIs and thus allows easier, non-iterative computation. It is based on the so-called *Ideal Lyapunov Functions* developed by Itschner [121].

The task for the Ideal Lyapunov Functions is: Given the system matrix $\mathbf{A}_{\text{nom}}$, an optimal function $\mathbf{P}$ is to be found, which maximizes the range of possible variations of the matrix elements $a_{i,j}$ that do not compromise the positive definiteness of the resulting $\mathbf{Q}$ matrices. The matrix $\mathbf{P}$ is "ideal" in the sense that the range of acceptable variations (termed "potato" by Itschner) is as large as possible.

Without further discussion of the proof (this can be found in [121]), the solution is directly given:

$$\mathbf{P} = \mathbf{T}^{*-1}\mathbf{R}\mathbf{T}^{-1}, \tag{4.62}$$

with $\mathbf{T}$ being the matrix of eigenvectors of $\mathbf{A}_{\text{nom}}$, the asterisk denoting the conjugate transpose, and $\mathbf{R}$ being a diagonal weighting matrix with positive and real entries. It now suffices to check whether the matrix found fulfills the required matrix inequalities (4.60-4.61). This method offers the advantage of reduced calculation effort, as the solution is analytically described.

The drawback of this approach is that there is no systematic way yet to determine the entries of the weighting matrix $\mathbf{R}$ depending on how the parameters $a_{i,j}$ vary in the given problem, i.e. depending on the p_i and their ranges. Therefore, this approach will generally lead to more conservative results. Furthermore, the numerical solution of the above mentioned LMIs is not a computational challenge anymore today.

4.4.6 Sensitivity of System Stability to Parameter Uncertainties

The stability analysis that was presented in the preceding section can be used to ensure that the system is stable and to justify the application of a certain controller. However, the analysis does not illuminate the influence of each individual parameter uncertainty, which would be useful in order to know which model simplifications are most hazardous, and where more accurate modeling of nonlinearities is not necessary in terms of stability. For a more thorough investigation of these individual influences, a sensitivity analysis is now performed based on very similar ideas as the so-called *quadratic stability margin* [36].

The sensitivity analysis is now performed for the case that the individual parameter variations are independent. The uncertainty interval of each p_i around the nominal mean value is represented by a fractional deviation δ_i:

$$p_i(t) \in [p_{\text{nom},i}(1-\delta_i), p_{\text{nom},i}(1+\delta_i)]. \tag{4.63}$$

This representation bears the advantage that variations are interpretable as fractions of the nominal value, independently of absolute scaling.

As the parameters are independent, the vertices $\boldsymbol{v}_m$ of the auxiliary parameter polytope consist of all possible combinations of minimum and maximum deviations of the parameters. This can be coded more formally:

$$v_{m,i} = (-1)^{r_{m,i}}\delta_i p_{\text{nom},i}, \quad i = 1, ..., n, \quad m = 1, ..., N, \tag{4.64}$$

whereby the set of exponents $r_{m,1}, ..., r_{m,n}$ for the m-th vertex follows from

$$\sum_{i=1}^{n} 2^{i-1} r_{m,i} = m - 1 \tag{4.65}$$

$$\wedge \quad r_{m,i} \in \{0, 1\}. \tag{4.66}$$

The quadratic stability margin provides a measure of how much the polytope of variations around the nominal matrix $\mathbf{A}_{\text{nom}}$ can be expanded about this center with the LDI remaining quadratically stable. It is defined as the largest nonnegative α for which

$$\dot{\boldsymbol{x}} = (\mathbf{A}_{\text{nom}} + \alpha \boldsymbol{\Delta}(t))\boldsymbol{x} \tag{4.67}$$

is quadratically stable.

In parameter space, the vertices would thus simply be scaled with α. However, such a purely symmetric augmentation may become excessively conservative for $\alpha v_{m,i} < -p_{i,\text{nom}}$, or equivalently, $\alpha\delta_i > 1$, because then the parameter polytope (4.54) includes also negative parameter values. Biomechanical parameters are often constrained to positive values. For example, for the parameters under consideration here, it is assured that the stiffness generated by gravity and passive elastic joint moments, as well as stiffness of the exoskeleton coupling are nonnegative (which is assured by their passive nature), and that each muscle responds with a torque of unvarying direction to stimulation (which is assured by the mechanical principle of a muscle). Therefore, some conservatism can be removed by constraining the vertices of the augmented polytope to positive values, such that the modified vertices $\tilde{\boldsymbol{v}}_m$ are composed by the entries:

$$\tilde{v}_{m,i}(\alpha) = \max\{\alpha v_{m,i}, -p_{i,\text{nom}}\} \tag{4.68}$$

This conditionally asymmetric augmentation is illustrated in Fig. 4.7 for the special case that the parameters p_i vary independently, in which case the polytope is defined by all possible combinations of extreme values.

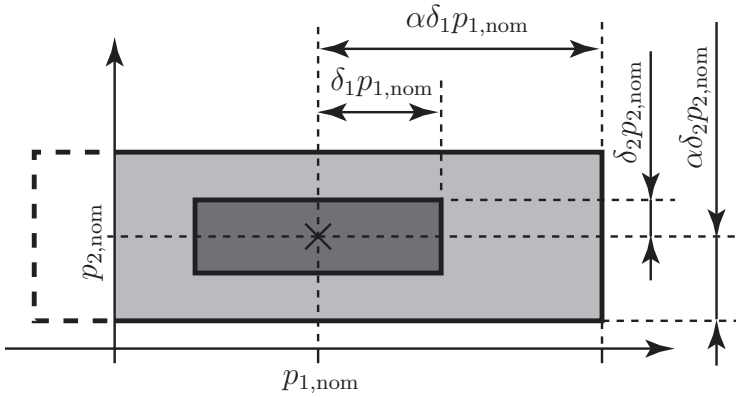

Figure 4.7: The uncertainty interval (dark gray) is augmented using the factor α in order to obtain the sensitivity to each individual parameter uncertainty. The augmented interval (light gray) is bounded by 0 in order to avoid excessive conservatism, because the biomechanical parameters are always positive.

A stability analysis following (4.59)- (4.61) now provides means to evaluate α for a given set of constant δ_i in the form of an optimization problem: With

$$\tilde{\mathbf{\Delta}}_m(\alpha) := \sum_{i=1}^{n} \tilde{v}_{m,i}(\alpha)\mathbf{A}_i, \quad m = 1, ..., N, \tag{4.69}$$

maximize α subject to

$$\mathbf{P} > 0, \alpha \geq 0, \mathbf{A}_{\text{nom}}^T\mathbf{P} + \mathbf{P}\mathbf{A}_{\text{nom}} + (\tilde{\mathbf{\Delta}}_m(\alpha)^T\mathbf{P} + \mathbf{P}\tilde{\mathbf{\Delta}}_m(\alpha)) < 0, m = 1, ..., N. \tag{4.70}$$

Numerical evaluation of this optimization problem for different uncertainty intervals and fixed nominal values $p_{\text{nom},i}$ allows to express the stability margin α as a function of the maximum parameter deviations δ_i:

$$\alpha = f(\delta_1, ..., \delta_n). \tag{4.71}$$

The variation of α as a function of the δ_i provides a useful measure of how much the individual uncertainty of each parameter influences stability. Especially if the function is of high dimensionality, such that a graphical representation becomes difficult, the numerical gradient with entries

$$\frac{\Delta\alpha}{\Delta\delta_i} \approx \frac{\partial\alpha}{\partial\delta_i} \tag{4.72}$$

can be used to evaluate sensitivity to each parameter uncertainty at the problem-specific point in the δ-space.

4.4.7 Application to the Hybrid Neuroprosthesis

Types of Variability

The formulation of the plant in dependence of uncertain time-varying parameters has already been prepared during modeling and control.

Both the leg and the coupling model include varying stiffness and damping. Nonlinear passive joint moments and nonlinearity of the gravitational torque are considered by varying leg stiffness c_{leg} and damping k_{leg}. The coupling between exoskeleton and leg is compliant with nonlinear stiffness c_{exo} and damping k_{exo}. During control design, rigid exoskeleton coupling has been assumed, which corresponds to infinite stiffness and damping. To analyze stability, the full model is used with non-rigid coupling. Both for leg and coupling, stiffness c and damping k are variable, yet they are highly correlated. Therefore, it would be too conservative to allow independent variation of c and k, which would include highly underdamped systems. To avoid this, the inter-dependency is taken into account. Using a first-order approximation, the damping values are varied linearly depending on the elasticity values, maintaining the ratio observed for nominal conditions (where damping equals about 10% of the stiffness value).

The muscle model includes variabilities of the first, second and third kind listed in Sec. 4.2.1, which have all been subsumed within the generalized functions $n_{\text{fes}}(t)$ and $k_{\text{sat}}(t)$, as described in Sec. 4.2.4.

The variation in control feedback gains has been considered in form of an interpolation between two matrices depending on the scalar recruitment factor $r(t)$ in (4.47). This more general factor also includes the saturation factor $k_{\mathrm{sat}}(t)$. No further assumptions are made in the following regarding the origin or form of the trajectory of $r(t)$ (e.g. whether it depends on the states), instead even arbitrary switching is allowed, in order to evaluate how robustly the controllers would react.

The vector of varying parameters thus contains 4 components:

$$\boldsymbol{p}^T = \begin{pmatrix} p_1 & p_2 & p_3 & p_4 \end{pmatrix} = \begin{pmatrix} c_{\mathrm{exo}} & c_{\mathrm{leg}} & n_{\mathrm{fes}} & r \end{pmatrix}. \tag{4.73}$$

The parameter variations are named equivalently:

$$\boldsymbol{\delta}^T = \begin{pmatrix} \delta_1 & \delta_2 & \delta_3 & \delta_4 \end{pmatrix} = \begin{pmatrix} \delta_{\mathrm{cexo}} & \delta_{\mathrm{cleg}} & \delta_{\mathrm{nfes}} & \delta_r \end{pmatrix}. \tag{4.74}$$

Model Reliability and Uncertainty Levels

Muscle recruitment uncertainty is threefold: The first one is due to insufficient fit of the Hammerstein model to the observed isometric muscle dynamics, as observed in Chap. 3. The second uncertainty is generated by inter-trial variability of the muscle torque generation due to disturbances (e.g. tissue displacement), which has also been quantified during the identification process. These effects may lead to an error of factor two compared to the prediction of the model. Thirdly, unmodeled force-length and force-velocity nonlinearities in the non-isometric case, as outlined in Sec. 4.2.4, can reduce the muscle torque to 0. Overall, an uncertainty δ_{nfes} of 100% around the nominal value of $n_{\mathrm{fes}} = 1$ is assumed, as already presented in (4.14). This includes both the case that the muscle does not react at all to stimulation, as well as the case that it produces twice the force as expected in any time instant.

In contrast to muscle identification, the nonlinear identification procedure for the leg dynamics described in App. E showed plausible results and robust convergence in all practical experiments [144,170]. A noticeable characteristic of the nonlinear dependency of (4.3) on the knee joint angle is that it is actually a superposition of two functions: The gravitational component of the shank depends on $\sin(\varphi_{\mathrm{leg}})$ and is thus represented by a convex function in the angle-torque diagram. The passive elastic joint moments, on the contrary, are represented by a concave function of φ_{leg} [69]. The superposition of these two functions leads to only small variations in slope over a wide range of angles, such that a linear system description captures the main features. This explains an identified variation δ_{cleg} of only about 3-4% for the two subjects.

For the orthosis, nominal stiffness c_{exo} and the respective uncertainty interval δ_{cexo} are quantified using the test setup described in 4.2.5. By comparing maximum and minimum measured stiffness, a very large uncertainty was identified: For torques that produce knee flexion, the stiff and direct connection between tibia and orthosis leads to a ten times higher stiffness compared to knee extension, where the soft tissue of the calf is coupled to the orthosis via elastic straps. The variation δ_{cexo} in coupling stiffness therefore reaches a level of 89% and 78% for subject 1 and 2, respectively.

4.5 Evaluation and Results

In this section, the evaluation procedure and results of the robustness analysis and control performance of the Hybrid Neuroprosthesis are presented. The four control approaches will be evaluated according to robustness, energy consumption of motor and muscles, as well as tracking performance. It is of special interest in how far the first three control approaches using observer-based closed-loop FES control are superior to the simple feed-forward approach in the presence of large modeling uncertainties in muscles and coupling stiffness.

4.5.1 Stability Analysis: Theoretical Results

The stability analysis is performed for all four different control strategies of Sec. 4.3.3. To illustrate the results, the limits of feasibility of the LMIs, i.e. the surfaces defined by $\alpha = 1$, are plotted in Fig. 4.8 in dependency of the δ_i. The maximum expected deviations in the system in percent, as quantified above, are indicated by a point in the δ-space. If this point is on the same side of the surface as the coordinate origin, the system is stable, whereby the closer this point comes to the surface, the smaller the stability margin gets. When the point is on the other side of the surface, system stability is not ensured anymore.

To allow a three-dimensional representation although there are 4 uncertain parameters, the variation of the recruitment factor r is not done gradually. Instead, the feasibility limits are evaluated for 3 nominal values of r (0, 0.5 and 1) with $\delta_r = 0$, as well as for arbitrary variation of r within the interval [0,1], i.e. $\delta_r = 1$. The first column thus shows stability margins for a system controlled by the motor only. The last column shows the worst case, given that (4.44) includes the saturation factor k_{sat} in r. This factor k_{sat} represents input saturation in FES, as defined in (4.12), and $k_{\text{sat}} \leq 1$. In the calculation of the stability margin, the interval of r is therefore not augmented anymore. In the first three cases, i.e. the first three columns, it is assumed that the desired torque produced by the muscles is never larger than the maximum possible muscle torque, such that the linearized system description is valid. Furthermore, no purposeful variations in muscle recruitment are considered either.

For the system at hand, limits of feasibility, i.e. $\alpha = 1$, are frequently not reached in certain parameter directions before the corresponding δ_i reach a value of 1. This means that also with 100% parameter variation (and thus including a parameter value of 0), the system stays stable. However, in order to be able to display the stability margins in the graph, for values of $\delta_i > 1$, an asymmetric augmentation of the interval in analogy to (4.68) and Fig. 4.7 around the nominal value of the parameters is performed. This augmentation is only of theoretic interest and is done to avoid ambiguity, because the mean of the augmented interval shifts away from the nominal value, and re-definition of the nominal value could always limit variations to below 100%.

For the same example, table 4.1 shows the values of α for each controller for both subjects at the indicated point in the δ-space, as well as the numerical gradient of (4.72).

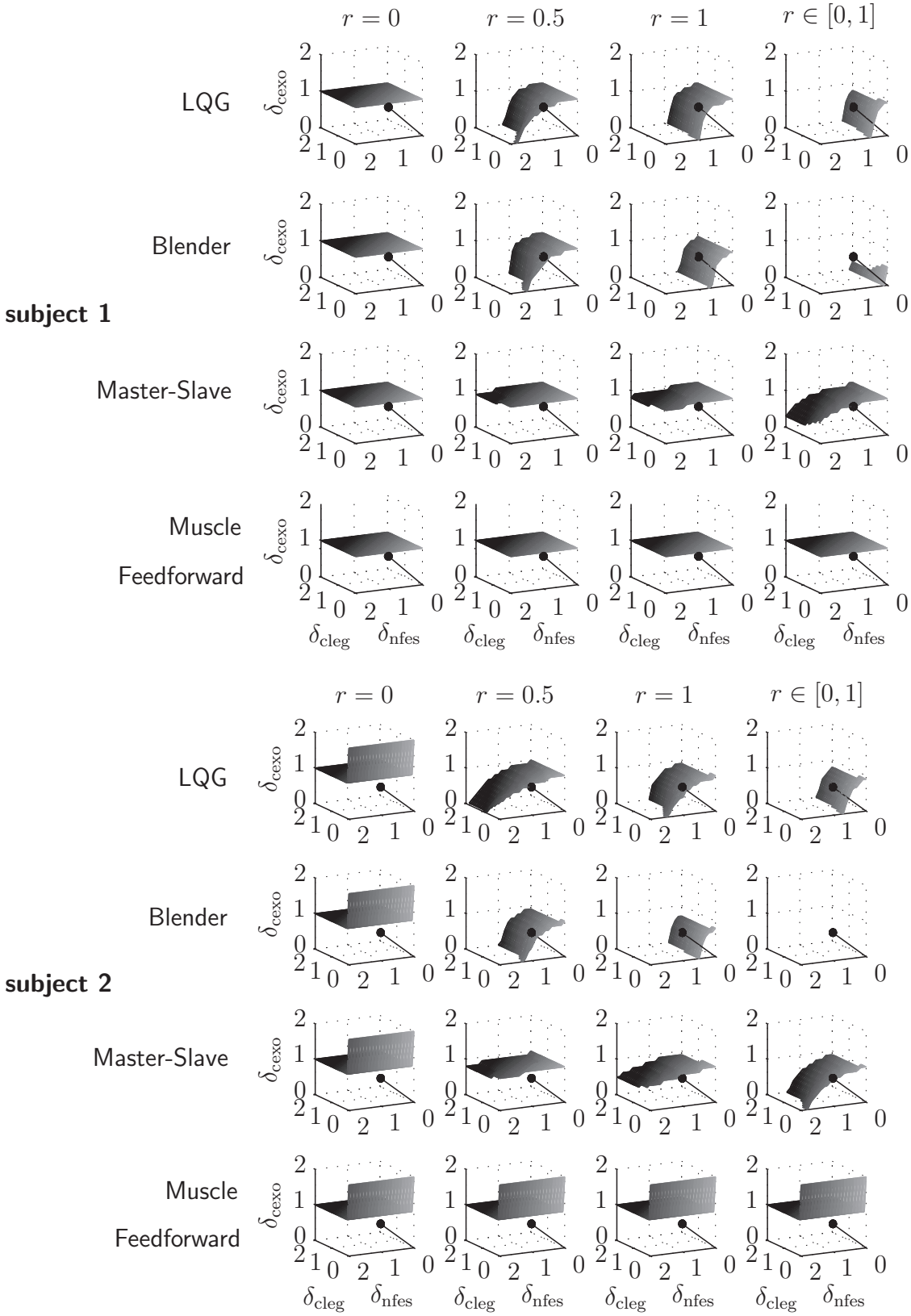

Figure 4.8: Limits of allowed parameter uncertainty intervals around the nominal value for all controllers, for constant and variable recruitment factors r, and for both subjects. The surfaces are defined by $\alpha = 1$ in (4.71), which amounts to marginal stability.

Controller	α	$\frac{\frac{\partial\alpha}{\partial\delta_{\text{cleg}}}}{\lvert\nabla_{\boldsymbol{\delta}}\alpha\rvert}$	$\frac{\frac{\partial\alpha}{\partial\delta_{\text{nfes}}}}{\lvert\nabla_{\boldsymbol{\delta}}\alpha\rvert}$	$\frac{\frac{\partial\alpha}{\partial\delta_{\text{cexo}}}}{\lvert\nabla_{\boldsymbol{\delta}}\alpha\rvert}$	α	$\frac{\frac{\partial\alpha}{\partial\delta_{\text{cleg}}}}{\lvert\nabla_{\boldsymbol{\delta}}\alpha\rvert}$	$\frac{\frac{\partial\alpha}{\partial\delta_{\text{nfes}}}}{\lvert\nabla_{\boldsymbol{\delta}}\alpha\rvert}$	$\frac{\frac{\partial\alpha}{\partial\delta_{\text{cexo}}}}{\lvert\nabla_{\boldsymbol{\delta}}\alpha\rvert}$
LQG								
$r = 0$ (motor only)	1.13	−0.00	0	−1.00	1.68	−0.98	0	−0.20
$r = 0.5$	0.95	−0.00	−0.45	−0.89	1.04	−0.00	−0.45	−0.89
$r = 1$	0.80	−0.00	−0.83	−0.55	0.88	−0.67	−0.33	−0.67
$r \in [0, 1]$	0.46	−0.26	−0.93	−0.26	0.50	−0.00	−0.89	−0.45
Actuator Blending								
$r = 0$ (motor only)	1.13	−0.00	0	−1.00	1.67	−0.98	0	−0.22
$r = 0.5$	0.90	−0.00	−0.71	−0.71	0.85	−0.00	−0.71	−0.71
$r = 1$ (muscles only)	0.66	−0.00	−0.95	−0.32	0.48	−0.00	−0.95	−0.32
$r \in [0, 1]$	≈ 0				≈ 0			
Master-Slave								
$r = 0$ (motor only)	1.13	−0.00	0	−1.00	1.67	−0.98	0	−0.22
$r = 0.5$	1.13	−0.00	−0.00	−1.00	1.26	−0.67	−0.33	−0.67
$r = 1$	1.13	−0.00	−0.00	−1.00	1.12	−0.00	−0.45	−0.89
$r \in [0, 1]$	1.01	−0.00	−0.00	−1.00	0.96	−0.00	−0.45	−0.89
Muscle Feedforward								
r arbitrary	1.13	−0.00	0	−1.00	1.67	−0.98	0	−0.22

Table 4.1: Stability Margins α and normalized partial derivatives in direction of parameter variations. Left: Subject 1, right: Subject 2. The stability margin is the factor by which the uncertainty intervals can safely be expanded while maintaining quadratic stability. For values of $\alpha < 1$, stability cannot be proven. Missing values are due to numerical issues.

4.5.2 Stability Analysis: Experimental Results

In practical experiments conducted with the neuroprosthetic setup, indeed instability occurred, though only for the blending controller: Exclusive muscle control ($r = 1$) could not be used at all due to instable behavior, blending control with $r = 0.8$ appeared more docile, but posterior analysis of the recorded data showed that the system was excited to oscillations with slowly increasing amplitude. For $r = 0.5$, such behavior was not observed anymore. The three other control schemes showed no instabilities during the practical experiments.

4.5.3 Stability Analysis: Discussion

Both Fig. 4.8 and Tab. 4.1 show a pronounced trend in sensitivity to parameter variations: Dominant stability risks are introduced when the elasticity of coupling or nonlinearities of muscle recruitment are neglected. This is an important result, because commonly, elasticity of the coupling in robotic exoskeletons is entirely neglected.

Nonlinear variation of intrinsic joint stiffness, on the contrary, can be neglected due to two reasons: a) the variations in percent themselves are small, as described earlier, and b) its influence on stability is small (indicated by the small sensitivity of α). This small influence on the system properties can be explained by the fact that in the system matrix of (4.28)

or (F.5), the joint impedance parameters c_{leg} and k_{leg} do not appear in an isolated manner, but only in sum with the (much larger) coupling impedance parameters c_{exo} and k_{exo}.

Interaction between the uncertainties is also evident in the figure: The more uncertainty is present in the coupling stiffness, the less uncertainty is allowed for the muscles, and vice versa. This interaction is more or less pronounced for the different controllers.

Of the different control designs, especially those controllers that rely on closed-loop FES control suffer from stability risks. The extreme is the blending controller, which takes the muscles as sole actuators for $r = 1$.

However, the performed stability analysis is conservative due to multiple overbounding. For example, when calculating the stability margin, the intervals are augmented in both directions. In consequence, for $\alpha\delta_{\text{cexo}} \geq 1$, not only very stiff systems, but also systems with zero stiffness and damping are included. Due to the assumption that damping varies linearly with stiffness, interpolated systems with low stiffness have strongly underdamped characteristics, which is a known hazard to stability. This is unrealistic, because tissue does not exhibit oscillations, such that it is at least critically damped.

4.5.4 Control Performance: Benchmark and Evaluation Criteria

The setup consists of the orthosis and a stimulator, which controls the hamstrings and quadriceps of a sitting subject with freely hanging shank, as displayed in Fig. 4.1. Both the electrical motor and the stimulator are controlled by the same real time process using Matlab/Simulink Real Time Workshop and Rtai Linux.

Of the four different control concepts in Fig. 4.6, 11 parameterizations are chosen. All are used with a constant nominal value r_{nom} of $r(t)$, i.e. no purposeful adaptive strategy is employed and $r(t)$ only varies unpredictably depending on input saturations, i.e. depending on $k_{\text{sat}}(t)$ of (4.12). Four concepts are taken without feedforward components, thus requiring no a priori knowledge of the task: The LQG with $r_{\text{nom}} = 1$, the Blender with $r_{\text{nom}} = 0.75$, $r_{\text{nom}} = 0.5$ and $r_{\text{nom}} = 0$ (the last one providing the special case of only motor with no muscle recruitment), and the Master-Slave with $r_{\text{nom}} = 1$. The special case of only muscle control ($r_{\text{nom}} = 1$ in the blending control) was attempted in preliminary experiments, but the linear quadratic muscle controller led to an unstable system, as mentioned before. Therefore, this case was not included.

Concerning feedforward elements, the necessity of an a priori division complicates a comparison of the controllers' performance, because differing divisions have to be realized depending on the control concept. However, an attempt was made to perform the torque division in correspondence with the respective controller: In the fourth concept, the motor always receives the full torque feedforward, as well as the muscles. The redundancy is resolved by the compensation based on the observed muscle torque. For the master-slave concept, the motor also receives the full torque, but the muscles receive no extra feedforward. In the blending controller, the same recruitment factor r_{nom} that is used for blending is also used to distribute the feedforward torque (as displayed in the figure), i.e. both factors s_{ff} equal 1. For the LQG controller, an assumption has to be made on how the controller will distribute the torque, and this has been estimated via prior simulations with

#	Control Scheme	Feedforward Muscles $s_{\mathrm{ff,fes}}$	Feedforward Motor $s_{\mathrm{ff,exo}}$	Recruitment Factor r_{nom}	Acronym
	Predictive				
1	LQG	0.75	0.25	1	FLQG
2	Actuator Blending	1	1	0.5	FBle5
3	Actuator Blending	1	1	0.75	FBle75
4	Master-Slave	0	1	1	FMaS
5	Muscle Feedforward	1	1	0.75	FMF75
6	Muscle Feedforward	1	1	1	FMF1
7	Motor (Blender)	0	1	0	FMot
	Not Pred.				
8	LQG	0	0	1	LQG
9	Actuator Blending	0	0	0.5	Ble5
10	Master-Slave	0	0	1	MaS
11	Motor (Blender)	0	0	0	Mot

Table 4.2: Controllers, acronyms, and selected parameters. For the control schemes in Fig. 4.6, 11 parameterizations are chosen: 4 do not require predictive knowledge, and 7 use flatness-based feedforward components that are calculated off-line. Control gains (not shown) are the result of LQ optimization.

a nominal value of $r_{\mathrm{nom}} = 1$. The observed aproximate division of the torque of 75 : 25 in favor of the muscles is then used also for the feedforward components. Six concepts are taken with feedforward components. Table 4.2 summarizes the controllers and the nominal value of r_{nom} and both s_{ff}.

The control task is equal for all controllers and consists of a reference angle for the leg to be tracked. This reference profile is a sine sweep with mirror symmetry, i.e. it starts with a constant signal, the frequency increases from 0.1 to 1 Hz and then decreases again, whereby the amplitude is held constant. The mean of this oscillation is not in the equilibrium position of the leg, but in a more extended position. This way, a constant torque offset due to gravitational load is demanded from the actuators.

To determine representative values under the heavy uncertainties and time-variabilities, the experimental protocol contains a large number of randomized repetitions: the benchmark signal is repeated 55 times in one trial, with no pause in between. Each time, a different controller is chosen randomly in a double-blind manner, with each controller occuring exactly five times. This way, subconscious preference of the tester or the subject shall be excluded as far as possible, because the two subjects were not naive to the purpose of the study. After one trial, a short pause follows. For one subject, 6 trials were recorded, resulting in a total of 30 measurements, for the second subjects, 4 trials were recorded, giving a total of 20 runs for each controller.

As evaluation criteria, tracking performance and energy consumption of the actuators is used. Motor torque and velocity are measurable, therefore energy consumption can be determined accurately. Positive and negative work introduced into the leg are determined by taking the integral of the positive and negative power, respectively. Muscle torque

and joint velocity, however, are not measured. Therefore, in order to be independent of possibly erroneous estimates, the measure for muscle activation is simply the integral of the squared commanded activation levels u^* in (4.10), whereby no division is possible into accelerating and decelerating components.

4.5.5 Control Performance: Experimental Results

Fig. 4.9 displays cost values of the considered controllers for the two subjects. One of

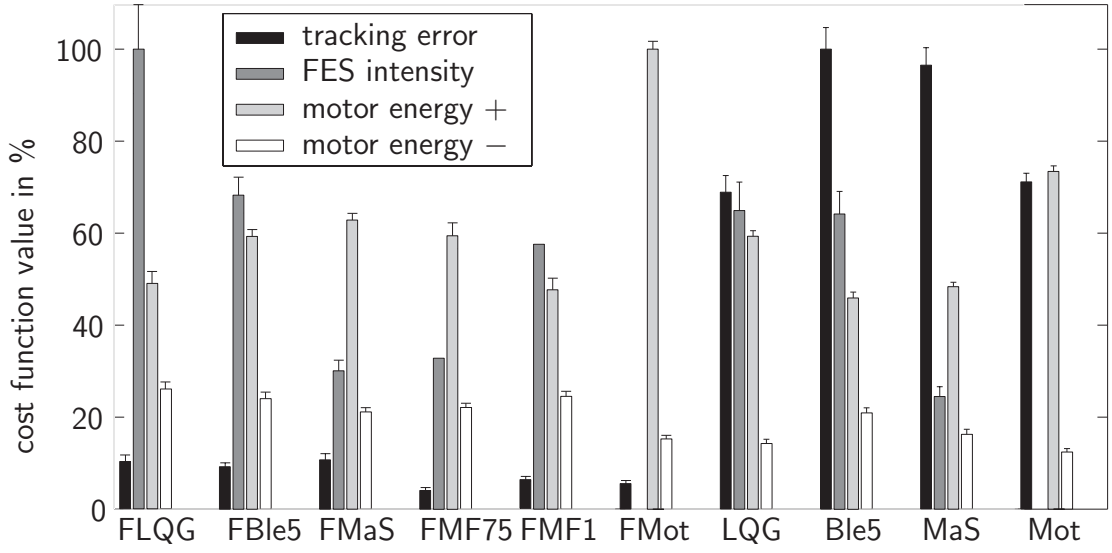

(a) Scaled Cost Function Values of Subject 1

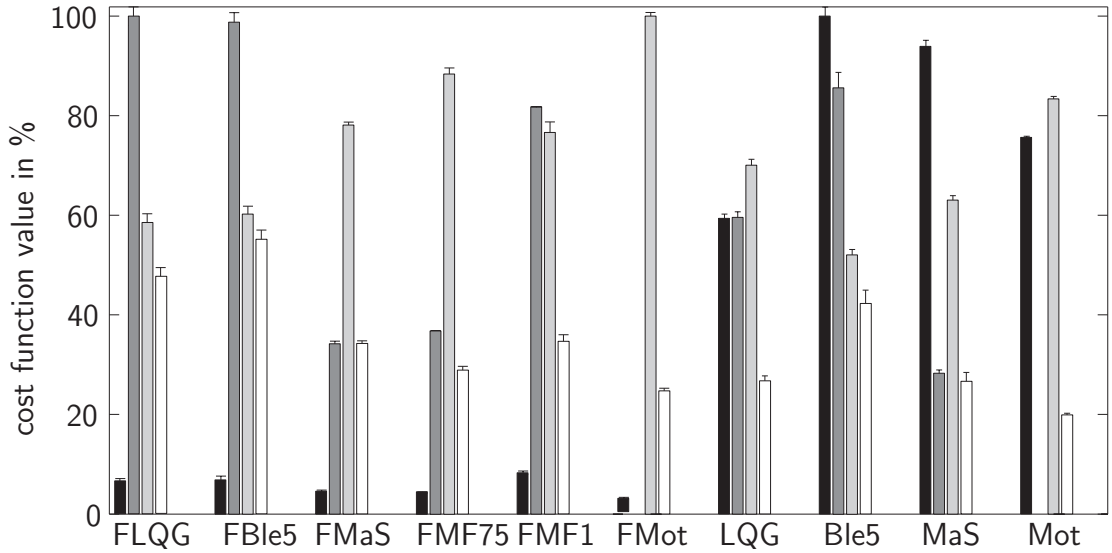

(b) Scaled Cost Function Values of Subject 2

Figure 4.9: Mean and standard error of cost function values for all controllers and both subjects. Displayed are the integrals of: Squared muscle activation, quadratic tracking error, positive and negative motor power. Energy, tracking error, and FES intensity are scaled to their maximum value.

the controllers, the blending controller with predominant muscle activity ($r = 0.8$) is not included in this analysis, because it led to oscillations with slowly increasing amplitude and was thus discarded as unstable. This went unnoticed in the trials, which consisted of oscillations anyways, and where each controller was active only for a short time, such that the following controller stabilized the system again.

The most prominent fact seen in the figure is the improved tracking performance when feedforward elements are used, i.e. the difference between the first 6 and the last 4 controllers. This effect is obvious in all controllers.

The next observation is the strong correlation between muscle activity and motor energy consumption. The more the muscles are recruited, the less positive energy is required by the motor. However, at the same time, the negative work introduced into the system by the motor, i.e. braking activity, increases.

In the last four cases, where no feedforward components are active, shifting the load distribution from the motor to the muscles is negatively correlated with tracking. However, in the first 6 controllers, where feedforward elements are available, this effect is not observable.

Substantial differences between subjects are evident, which make it impossible to derive more detailed consistent results from this very small sample.

In these 10 prototypical controllers, often more than one parameter had to be changed from one design to the other, such that the 10 controllers are not directly comparable. To allow a qualitative comparison, though, the factors that came out as most important are analyzed in the following multivariate analysis. The results of this analysis have to be read with extreme precaution though, because there is a large number of design parameters involved, and these factors have not been varied systematically nor independently. This would be almost impossible to realize in a practical setup, as it would require many more parameter combinations, and the experimental sessions already take more than two hours and are painful for the subjects.

Fig. 4.10 illustrates statistical results of a stepwise regression that investigates how the 4 individual cost function values depend on the individual controller parameters. Not all control parameters are included, but representative ones: The muscle angle tracking gain and motor angle tracking gain, muscle torque feedback gains for both actuators and feedforward components FF. These feedforward components are $FF_{\mathrm{fes}} = s_{\mathrm{ff,fes}} r_{\mathrm{nom}}$ for the muscles, and $FF_{\mathrm{drv}} = s_{\mathrm{ff,drv}}$ for the motor (except for the blender, there $FF_{\mathrm{drv}} = s_{\mathrm{ff,drv}}(1 - r_{\mathrm{nom}})$). The cost function values are log-transformed (based on an iterative analysis of residuals), and all input variables are scaled prior to regression, to allow dimensionless comparison. A dummy variable (0 for subject 1, 1 for subject 2) is used to investigate possible differences between subjects. Confidence intervals are shown, whereby α is set to 0.01 instead of 0.05, in order to avoid overfitting with a high number of factors. The p-value of the entire model, as well as the adjusted coefficient of determination R^2 are given (Adjustment is performed to account for the number of explanatory terms in the model). As the figure shows, the largest and also the only significant influence on tracking is the motor feedforward. FES energy consumption is explained mainly by the FES gains, the FES feedforward element, and the motor feedback gains. Positive Motor energy is explained by the parameters of motor control only, the muscle gains have no significant

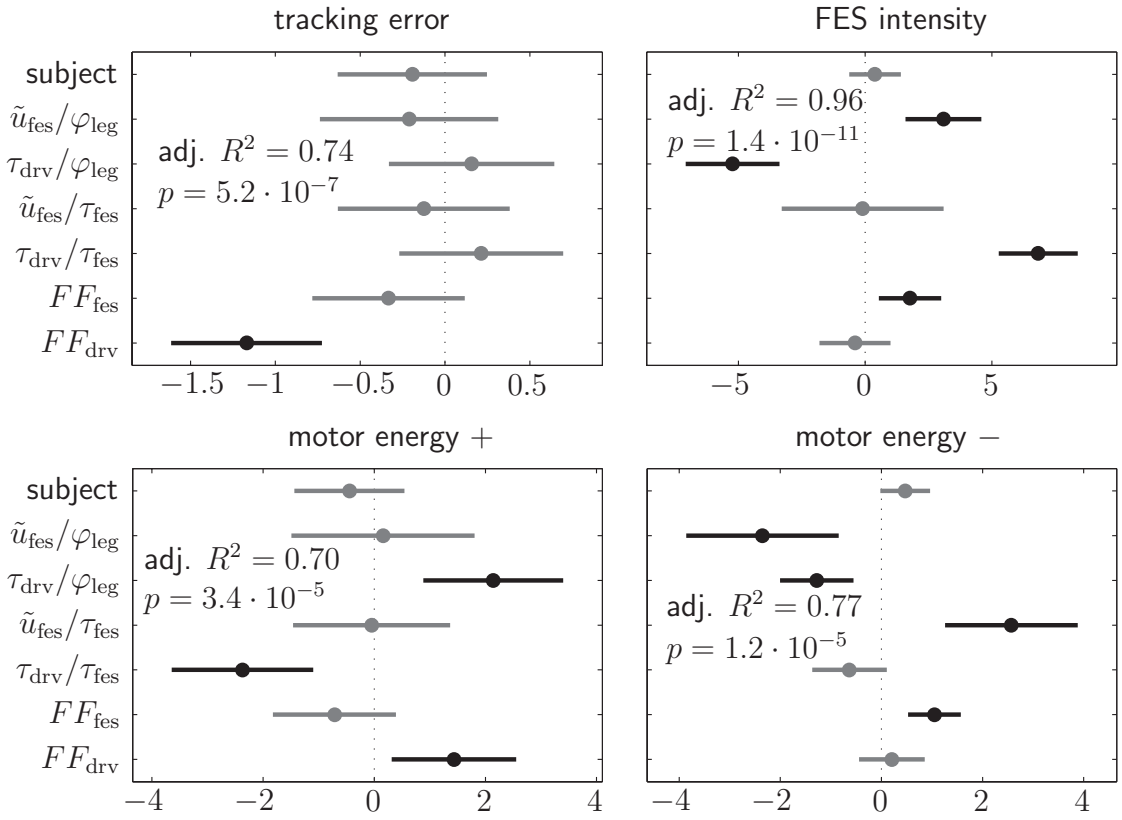

Figure 4.10: Cost value dependency on control parameters. Regression shows the influence of control gains and feedforward on tracking error and actuator load. Negative values: The cost function values decrease, positive values: The cost function values increase. A 99% confidence interval is drawn for the mean value. Insignificant factors (gray) are excluded.

influence. Negative energy, in contrast, is significantly influenced by the FES gains, the torque gain increases negative energy consumption, the angle feedback gain decreases it.

4.5.6 Control Performance: Discussion

A first remarkable fact is that the dummy variable "subject" does not have a significant influence, which means that both subjects react similarly. Furthermore, a prominent observation is that at least for the motor, the effect of feedforward elements on tracking is positive, which indicates a good fit of the leg and exoskeleton model.

Concerning the FES part of the system, the figure indicates that muscle control has no significant influence on tracking, and it does not significantly reduce required motor energy either. If FES is included, it seems advisable to use angle feedback and no torque feedback, because the only influence of the torque gain is to increase negative motor energy, which implies that this form of feedback does not lead to cooperative behavior of the actors. This means that FES does not contribute in a significantly positive manner to control performance of the Hybrid Neuroprosthesis, and that if it is included, a simple controller based on the leg angle suffices.

There might be several reasons for the unsatisfying performance of the FES component: Firstly, the muscle behavior is subject to heavy uncertainties, as outlined in the previous chapter. Furthermore, the controller completely neglects compliant coupling between leg and exoskeleton. Therefore, the observed states may not be reliable enough. Whereas the compliance does not seem to be a problem for the motor, it is for the muscles.

4.6 General Discussion

Adverse effects of compliant exoskeleton coupling have been reported before, although not in the context of FES. Without FES, unmodeled compliance becomes the main source of discrepancies between model and real world, as e.g. observed by [83]. It has also been reported to be a disturbing factor in an actuated orthosis by [8] and by [184]. When the latter group included a model of soft tissue (approximating tissue elasticity by a first-order filter between the CoM of the arm and bone motion), they found that the augmented model matched their data much better. They used a cast, which would be an ideal exoskeleton, and they looked at the arm, where there is less soft tissue in comparison to the leg. Therefore, it is reasonable to expect further increased influence in a simple orthosis for the lower extremities.

Still, most modeling approaches of human and robot motion are based on rigid-body models. The results obtained here justify this procedure, yet only for certain purposes: Identification of the leg is robustly possible with the assumption of rigid coupling, feedforward elements based on this simplified model lead to considerably improved performance, and robustly stable control of the exoskeleton can be achieved.

However, as soon as closed-loop control of FES is attempted, some problems arise: Both the theoretic stability analysis as well as practical experiments showed considerable risks introduced by the existence and/or negligence of the compliant coupling during controller design. The theoretically derived limits of the stability analysis seem too conservative, because higher gains are realizable in practical experiments. The difference can be explained by the considerable overbounding applied to simplify the analysis, as outlined earlier. Nevertheless, both theoretical and practical experiments show the same tendency: Closed-loop control of FES using sensors on the exoskeleton introduces stability risks. This is congruent with expectations drawn from the literature: The motor control is collocated, because the encoder measures the motor angle at the shaft. For the muscles, control is non-collocated, because the coupling dynamics cause differences between leg angle and motor angle. Such configurations with *non-collocated actuation and sensing* are known to potentially lead to unstable dynamics [126].

To solve this problem, one possibility would be to use the full model for control design of the muscles. However, it would be difficult to do such a model-based approach that accounts for the coupling, because the interaction between human motor apparatus and exoskeleton is heavily influenced by the direction-dependent elasticity of the orthosis-leg coupling, which is hard to quantify reliably. Therefore, the torque applied to the joint is difficult to observe. Complex sensing mechanisms have been proposed to measure this

torque redundantly, e.g. by [10], but for a practical clinical application, observer-based control will introduce severe additional uncertainties and thus stability hazards.

An alternative solution to include muscle activity without stability risks and without the actuators working against each other too much seems to be simple feedforward control of the muscles. Then, muscle activity can be triggered for therapeutic reasons, and adverse effects in terms of stability are avoided.

What is also noticeable is that varying passive elastic joint moments within the leg hardly have any influence on stability. This can be explained by the fact that the leg's stiffness parameters only appear in sum with the coupling stiffness parameters in the system matrix. Given that the coupling stiffness is much higher than the leg's stiffness, the influence of the leg's intrinsic stiffness on system behavior is small. Therefore, it can be justified to use simple linear models for the biomechanical properties of the leg.

4.7 Conclusion

This chapter presented a systematic assessment of a hybrid robotic/biomechanical systems. The example system is a Hybrid Neuroprosthesis, a combination of mechanical exoskeleton and Functional Electrical Stimulation (FES). Various sources of time-variability and nonlinearity are unified into an affine representation with uncertain, time-varying parameters. This allows simplified control design with nominal values, as well as stability analysis based on a polytopic system description. The model is parameterized based on identified values.

Four different prototypical control approaches were presented for a redundantly actuated system where both actuators have different capabilities: An LQG controller, a blending controller with variable load sharing, a Master-Slave concept where the motor is in charge of tracking, and a controller with exclusively feedforward recruitment of the muscles and feedback control of the motor. The four controllers are evaluated in a single-joint test setup regarding their performance and robustness.

The analysis of quadratic stability gives an impression of which variabilities are most hazardous for stability, and which controllers deal with the uncertainties most robustly. Indisputable drawbacks of using an interval description of nonlinearities are that only suboptimal controllers can be used, and that a certain conservatism is introduced in the later stability analysis. Despite this conservatism, tendencies that were found during the theoretical analysis were in congruence with results of practical experiments.

Concerning robustness, feedforward control of the muscles combined with feedback control of the motor shows considerable benefits compared to feedback control of both actuators. This is due to the dominant influence of unmodeled elasticity in the transmission, i.e. in the coupling between leg and exoskeleton. These additional dynamics are especially hazardous in the present setup, because muscles are controlled using the encoder position for feedback, which introduces non-collocated actuation and sensing. Concerning performance of muscle control, there were hardly any positive effects of closed-loop FES control either. This observation confirms that the uncertainty in muscle recruitment and in compliant

exoskeleton-leg coupling is so large that closed-loop control of the muscles has hardly any benefits.

Another main outcome of the experiments conducted is that feedforward, i.e. predictive elements for the motor are beneficial for performance. This is independent of whether the muscles are recruited or not. This implies that at least the reliability of the leg model is sufficient to make predictive elements beneficial.

A tentative answer can now be given to the introductory questions concerning which model complexity is necessary, or which simplifications are justifiable: When modeling the human in conjunction with an exoskeleton, it seems justifiable to use rather simple biomechanical models for identification and control design. In contrast to nonlinear elastic joint moments in the leg, which have only a small influence on the system behavior, coupling compliance needs to be addressed during stability analysis, and its negligence can generate considerable security hazards. In any case, it is desirable to keep undesired elasticity in the transmission as small as possible. This can be achieved by using contact points of high stiffness (ankle) and long moment arms (this increases the reflected joint stiffness quadratically). The latter strategy also lowers interaction forces between patient and exoskeleton. These recommendations are intuitive, and corresponding designs have already been realized by rehabilitation robots like LOPES [269] and Lokomat [56] and the robotic muscle trainer training device MotionMaker [154].

5 The Human in Command: Patient-Controlled Assistance

5.1 Introduction and State of the Art

For gait rehabilitation robots, an important question is how to ensure stable gait, while avoiding any interaction forces between robot and human in case the patient walks correctly. To achieve this, the definition of "correct" gait needs to adapted both to the individual patient and to the situation. In this chapter, a method for online trajectory generation is proposed and described on the example of hemiparetic patients. Desired states for one (disabled) leg are generated on-line based on the movements of the other (sound) leg. An instantaneous mapping between legs is performed by exploiting physiological inter-joint couplings. This way, the patient generates the reference motion for the affected leg autonomously. This *Complementary Limb Motion Estimation* (CLME) is implemented on the LOPES gait rehabilitation robot and evaluated with healthy subjects in two different experiments.

5.1.1 Reference Generation for Assistive Robots

To promote effective rehabilitation after brain injury, the key element is intensive training [140,141,227,245]. The strenuous labor of physiotherapists associated with conventional therapy can be alleviated by rehabilitation robots such as the commercial devices Lokomat [55], Gait Trainer 1 [105], or AutoAmbulator [228]. The first exemplars simply used position control along a fixed reference gait trajectory, which has been proven to be as effective in retraining as traditional manual therapy for severely affected patients [118, 183]. For only mildly impaired subjects, this does not hold, these patients profit more from manual therapy [114].

New results on motor learning and neural plasticity indicate that this is not the full potential of rehabilitation robots; instead it is believed that treatment outcome could be further optimized by increasing the active participation of the patient. This paradigm has been confirmed in various evaluation studies on rehabilitation strategies such as Constraint Induced Movement Therapy (CIMT) [243], Functional Electrical Therapy (FET) [192], or Assist-as-Needed (AAN) control [44, 82, 110, 138].

The patient's movements should thus not be just externally imposed, but rather assisted to match the correct pattern. One of the key questions, however, is what that "correct" reference should look like. It is possible to use trajectories of healthy subjects, to let the therapist manually teach the robot a gait pattern for the patient, or to generate trajectories for a given task that resemble very much the average pattern of a healthy subject, e.g. using

optimization [247]. However, this reference trajectory might not be perfectly tailored to the individual patient. Furthermore, any reference trajectory that is fixed in space and/or time constrains the natural variability of gait.

Generally, there are three approaches to solve this problem of reference generation, which are partly complementary: The first is to tolerate deviations from the (possibly not optimal) reference trajectory, e.g. by use of a compliant device [13, 269] or a compliant controller [205] instead of stiff position control. The allowed deviations do not have to be only of spatial nature, they can also be temporal. For example, the pneumatic assisting robot presented by [13] is compliant, and it uses a reference trajectory that is variable in time and always synchronized with the patient's gait. Another strategy that allows both spatial and temporal deviation is Path Control [254]. This controller tolerates all movements within a virtual "tunnel" of allowed joint angles. The second approach to solve the reference generation problem consists in adaptation of an initially suboptimal reference trajectory to the individual patient. Jezernik and colleagues suggested such a strategy, and they used interaction torques as the criterion to be minimized by the adaptation [123]. The third approach is not to use a fixed reference trajectory at all. For example, in [3] and in [166], gravity-compensating devices are presented. These devices relieve the patient from body weight support, thus lowering the threshold of muscle force needed to walk. An approach that offers more guidance is Virtual Model Control (VMC), which has been implemented on the compliant LOPES robot [71, 263]. VMC does not define any a priori reference trajectory either, instead it only assists pre-selected subtasks of walking for specific training foci (e.g. foot clearance).

Whether deviations are tolerated, the reference is adapted, or no reference is used at all, the listed control strategies all rely on voluntary, sufficiently coordinated activity in the impaired limbs. This implies that severely affected patients have little to no influence on the reference, and they are invariably led along the path of a fixed gait pattern.

5.1.2 Contribution and Outline of this Chapter

To enable self-dominated gait also for patients with severe unilateral impairment (e.g. resulting from stroke), an automated, generic method is proposed that generates reference motion on-line [257]. The starting point of the idea is a particularity of human motor control: During complex, learned motions such as grasping or walking, the individual Degrees of Freedom (DoFs) are strongly coupled [6, 231]; these linear correlations are also called *synergies*, and they are often quantified and analyzed using Principal Component Analysis (PCA). This observation indicates a reduced set of manipulated variables. Possibly, our brain has developed such refined control methodologies to deal with the redundancy or "abundance" [200] of human DoFs (A phenomenon first referred to as "motor equivalence" by Bernstein [25]). Although the coupling of joint variables can be quantified and analyzed, the driving control variables themselves and the way how the brain generates them remain speculative. One hypothesis is e.g. the existence of a so-called *Central Pattern Generator* (CPG) in the human spinal cord [68, 142], yet this theory is controversial. Another explanation is given by the principle of optimality [247], which suggest a so-called "minimal intervention principle". This strategy explains the observation of an *uncontrolled*

manifold: only task-relevant features (e.g. end-effector position) are controlled, and the others are left uncontrolled. This way, both control effort can be reduced and accuracy increased, because motor noise, which depends on muscle force, in the task-relevant direction is reduced.

Whatever the origin of couplings my be, the effect itself can be exploited for the simplified generation of motion patterns with a reduced subset of control variables [148], and it has been used for animation [159, 181] and robot gait [129, 242]. Extending the idea beyond the autonomous *generation* of full motion patterns, the method proposed here exploits joint couplings also for the *completion* of partially preserved human motor capabilities, as needed for rehabilitation and intelligent prostheses. This *Complementary Limb Motion Estimation* (CLME) uses statistical regression - either PCA, or Best Linear Unbiased Estimation (BLUE)- and couplings between limbs in healthy synergetic motion. Using these physiological couplings and a patient's sound limb motion, it estimates the corresponding motion of the patient's affected limbs. This inference does not cause any delay like *echo control* [94], where the reference is a time-shifted replay of the sound leg's motion; instead states are mapped instantaneously.

As CLME does not use a fixed template gait pattern, it can be categorized in the third group of controllers mentioned above. By defining "correct" walking only on the basis of interjoint couplings, CLME allows a much wider range of movements compared to a predefined reference trajectory. Other advantages are that sound limbs are not directly influenced, and that the reference for the affected leg is intrinsically synchronized.

The strong inter-limb coordination during human walking allows for a very accurate right leg-left leg inference using pre-recorded trajectories in simulations [257]. However, the suitability for control of gait rehabilitation robots can only be answered by practical experiments, where the human closes the loop. This evaluation proceeds along two questions: The first question is related to *functionality*, denoting the requirement that even in the case of no voluntary control in the paretic leg, the patient can walk, and without tripping nor falling. This is important for patients in an early state of therapy. The second question concerns whether in the case of coordinated voluntary activity in the assisted leg, the controller allows self-determined gait with minimum *interference* by the robot. The term "interference" here refers to the form and amount of actuator power introduced to the human body, and to the repercussions in terms of altered EMG activity and kinematic trajectories. This is important to see whether CLME can be used in a later stage of therapy, where the algorithm mainly supervises gait and applies only minor corrections.

Two studies have been conducted on the LOPES gait rehabilitation robot addressing these requirements. This robot consists of a treadmill in combination with a light-weight exoskeleton for the lower extremities. It actuates sideways and forward motion, hip abduction, hip flexion and knee flexion using the principle of Series Elastic Actuation and Bowden cable transmission. The mechanical design of LOPES is described in App. A, and the low-level impedance control design and performance is described in Chap. 2.

The first study addresses the question whether subjects with no control at all of one leg can walk with a robotic assistance of this leg based on CLME. Results of this first study have already been presented in [258]. Healthy subjects are recruited, and a one-sided impairment is simulated using the exoskeleton leg as a prosthesis. Subjects thus walk with

their own right leg and the robotic left leg, the motion of which is commanded by PCA-based CLME in dependence of the right leg. Each subject walks based on the extracted coupling and scaling of another person, whose gait pattern has previously been recorded. This first study aims to evaluate whether CLME generates *functional* reference motion.

The second study evaluates the performance of CLME regarding *interference* with self-determined gait of healthy subjects. Results of this study have been presented in [261]. The goal is to see whether CLME interferes significantly less with self-determined gait than control with a fixed trajectory. The study also compares the two alternative regression methods (PCA and BLUE). Criteria used to evaluate the requirement of minimum interference are: Interaction torques or introduced power, respectively, distortion of EMG patterns, and distortion of the kinematic gait pattern. The optimum would be to match the robot's behavior in zero-torque control, where desired interaction torques are zero, and this behavior is chosen as the baseline for comparison.

After a short explanation of the basic ideas of CLME, simulation results will be provided, and the two studies will be described in detail.

5.2 Complementary Limb Motion Estimation

The goal of Complementary Limb Motion Estimation (CLME) is to find a mapping function that outputs the states of impaired limbs (angles and velocities) in dependence of the states of sound limbs. To obtain this function, inter-joint coordination strategies are extracted from recorded healthy gait trajectories. Then, reference motion can be generated on-line for inoperable joints, using the current motion of the sound limbs. There are numerous approaches in statistical regression to tackle this problem. 2 simple ones among them have been investigated: One approach uses Principal Component Analysis (PCA) [125, 177], which is the most commonly used approach for analysis of joint synergies, as e.g. in [231], and one uses the conventional Best Linear Unbiased Estimator (BLUE) as the baseline approach to regression [5].

Assuming that the subject has only an impairment of the left leg, the states of the right leg are known variables, and they are subsumed in the vector $\boldsymbol{x}_r$:

$$\boldsymbol{x}_r^T = (\boldsymbol{\varphi}_r^T, \dot{\boldsymbol{\varphi}}_r^T) \ . \tag{5.1}$$

The states of the left leg,

$$\boldsymbol{x}_l^T = (\boldsymbol{\varphi}_l^T, \dot{\boldsymbol{\varphi}}_l^T) \ , \tag{5.2}$$

now need to be estimated. This is only an example; there could be other limbs involved, for example trunk motion as part of the known variables in $\boldsymbol{x}_r$. Moreover, the state vectors of sound and impaired limbs do not have to be of equal size. For example, hip flexion and knee flexion of the right leg could be used to estimate only the knee motion of the left leg, or they could be used to estimate its hip flexion, hip abduction and knee flexion.

Prior to regression analysis, biases of angles are removed, and all variables are normalized to a standard deviation of 1. In a first attempt [256, 257], Principal Component Analysis

is used to provide an estimate of $\boldsymbol{x}_l$ by minimizing the quadratic error function

$$\left|\left|\begin{pmatrix} \boldsymbol{x}_r \\ \boldsymbol{x}_l \end{pmatrix} - \begin{pmatrix} \boldsymbol{\Gamma}_1 \\ \boldsymbol{\Gamma}_2 \end{pmatrix} \boldsymbol{y}\right|\right|^2 \rightarrow min. \tag{5.3}$$

with unknown matrix $\boldsymbol{\Gamma} = [\boldsymbol{\Gamma}_1^T \boldsymbol{\Gamma}_2^T]^T \in \mathbb{R}^{d \times p}$, $p < d$, and orthogonal column vectors, such that the vector $\boldsymbol{y} \in \mathbb{R}^p$ is of lower dimensionality than $\boldsymbol{x} = [\boldsymbol{x}_r^T \boldsymbol{x}_l^T]^T \in \mathbb{R}^d$. The basis of this approach is the assumption that the command signals sent to the limbs stem from a common source in a lower-dimensional subspace, i.e. that there is a subset of control variables $\boldsymbol{y}$ that can be reconstructed and used to estimate the remaining joint variables.

For a simple representation of the solution of the optimization problem, the matrix $\mathbf{C}_{\text{PCA}}$ is defined, with

$$\mathbf{C}_{\text{PCA}} := \boldsymbol{\Gamma}_2 \boldsymbol{\Gamma}_1^{\#}, \tag{5.4}$$

and with the superscript $^{\#}$ denoting the left pseudoinverse. The estimator $\hat{\boldsymbol{x}}_{l,\text{PCA}}$ is given by

$$\hat{\boldsymbol{x}}_{l,\text{PCA}} = \boldsymbol{\Gamma}_2 \boldsymbol{\Gamma}_1^{\#} \boldsymbol{x}_r = \mathbf{C}_{\text{PCA}} \boldsymbol{x}_r \ . \tag{5.5}$$

The matrix $\boldsymbol{\Gamma}$ contains the first eigenvectors (the so-called principal components) of the covariance matrix $\mathbf{M}$ of $\boldsymbol{x}$.

The PCA-based approach to CLME is based on the hypothesis that the coupling between legs is caused by some kind of common control. Another approach is to exploit the statistical coupling between legs without using any additional knowledge at all, i.e. to find a solution to the general optimization problem

$$||\boldsymbol{x}_l - \mathbf{C}\boldsymbol{x}_r||^2 \rightarrow min, \tag{5.6}$$

with unknown matrix $\mathbf{C}$. The solution is the Best Linear Unbiased Estimator (BLUE). Using the respective covariance matrices, this estimator is given by:

$$\hat{\boldsymbol{x}}_{l,\text{BLUE}} = (\mathbf{M}_{rr}^{-1} \mathbf{M}_{rl})^T \boldsymbol{x}_r \ . \tag{5.7}$$

Again, this is rewritten in a simplified manner with the matrix $\mathbf{C}_{\text{BLUE}}$ defined as

$$\mathbf{C}_{\text{BLUE}} := (\mathbf{M}_{rr}^{-1} \mathbf{M}_{rl})^T, \tag{5.8}$$

such that

$$\hat{\boldsymbol{x}}_{l,\text{BLUE}} = \mathbf{C}_{\text{BLUE}} \boldsymbol{x}_r \ . \tag{5.9}$$

The difference between the two regression methods is that PCA-based CLME departs from the hypothesis of a "common controller" for both legs, and it reconstructs the common variables in an intermediate step; BLUE-based CLME, in contrast, simply exploits the phenomenological coupling between legs, and infers directly from right to left without consideration of underlying reasons.

The outputs of both regression approaches are augmented again by mean value and standard deviation, yielding reference angles and velocities for the impaired joints. The estimated angles and velocities are both subject to uncertainty. Thus, the estimated velocity can differ from the differentiated estimated position. To merge the two pieces of information, an additional Kalman filter is used, yielding the most plausible motion intention. The filter is designed for each joint separately based on the simple dynamic model of a double integrator. During filtering, each of the values is smoothed and corrected, so that angle and velocity become coherent. Under the assumption that the errors in the CLME-estimated variables $\hat{\varphi}$ and $\hat{\dot{\varphi}}$ can be modelled as Gaussian, uncorrelated noise (considering that the velocity is independently estimated, and not calculated via differentiation of the angle), better estimates $\hat{\varphi}_k$ and $\hat{\dot{\varphi}}_k$ are produced on-line. This design is displayed in Fig. 5.1[1]. The

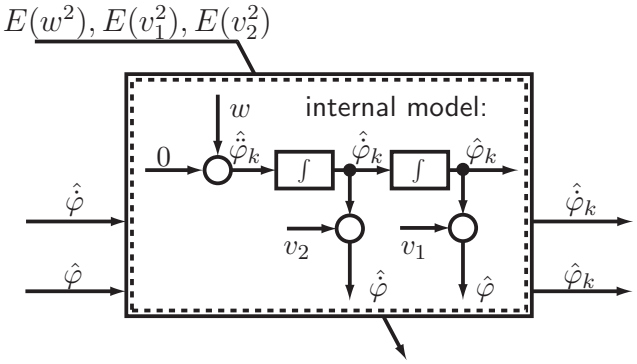

Figure 5.1: Design of the Kalman Filter. The estimated values $\hat{\varphi}$ and $\hat{\dot{\varphi}}$ are regarded as noisy outputs of a double integrator, and the filter produces improved values $\hat{\varphi}_k$ and $\hat{\dot{\varphi}}_k$ via stochastic optimization. The needed noise levels $E(v_1^2)$ and $E(v_2^2)$ are assessed by an error analysis of CLME-reconstructed trajectories, and $E(w^2) = E(\ddot{\varphi}^2)$.

"measurement noise" levels $E(v_1^2)$ and $E(v_2^2)$ are quantified by a simulated right leg/left leg inference in recorded healthy gait patterns, followed by an analysis of the errors between PCA-reconstructed angles and velocities and original angles and velocities. The "process noise" level $E(w^2)$ equals the original acceleration variance.

Preliminary attempts included not only the states, i.e. angles and velocities, but also accelerations of both legs as inputs and outputs of the regression, respectively. However, simulation results showed that the estimated accelerations hardly improve performance [257]. Providing accelerations on the input side would rely on additional sensors or noisy numerical derivatives of the sound leg's states. Therefore, only angles and velocities are used for both legs.

In summary, a recorded physiological gait pattern is reduced to the regression matrix, the Kalman gains, and mean values and standard deviations of the states. These parameters are then used to drive the on-line reference generation algorithm.

[1]Figures in this chapter are re-printed, with permission, from [256], ©[2006] IEEE / [258], ©[2007] IEEE / [261], ©[2008] IEEE.

5.3 Simulative Evaluation

Fist, simulation studies with motion capture data are presented, to evaluate the success of the proposed method in theory. These results have been shown already in [255]. 10 pre-recorded gait patterns of healthy male subjects are included in the analysis, whereby the data is obtained from the public Carnegie Mellon motion capture database[2]. The subject group was extremely heterogeneous, concerning height, age and weight. The recorded gait pattern of one subject is analyzed, yielding statistical characteristics for normalization (mean and variance of angles, and variance of the time derivatives) and the eigenvector matrix $\mathbf{\Gamma}$. Then, reconstruction performance is evaluated by a simulated impairment: The corresponding motion variables are eliminated from the trajectories and subsequently reconstructed from sound limb motion. The coupling matrix and statistical characteristics are extracted from the averaged gait of the nine other healthy subjects. Finally, the reconstructed motion is compared to the original motion. This procedure is repeated for each subject.

As a result, BLUE-based CLME shows higher accuracy in reconstruction than PCA. Fig. 5.2 shows the results of PCA-based CLME in this simulation for a representative subject. Results of these theoretical investigations, however, can not be a guarantee for a stable walking pattern. This is due to the fact that walking is a controlled motion, where the limbs of the body interact in the control task. By contrast, a simulation studies simply extracts a feedforward control input of the "sound" leg, which is taken from an intact controlled system. Questions that arose were: Can a person walk with unidirectional coupling? How will his own internal controller interfere? Can he maintain a normal walking pattern with one leg, if the other one is not walking normally (e.g. due to immperfect controller performance)? What happens to the overall functional performance of the coupled system, if he changes the behavior of the sound leg? Can a person adapt to the coupling of someone else?

To find answers to these question, two studies with healthy subjects are described in the following, each addressing one of the extremes: A completely inactive subject, and a completely unaffected subject, in order to evaluate both functionality and minimum interference.

5.4 Functionality Study: Experimental Design

5.4.1 Setup and Protocol

In the study, 8 healthy subjects took part (6 male, 4 female, aged between 18 and 28, weight between 68 and 82 kg). First, they walked for 3 minutes at 3 km/h in the LOPES in zero-torque mode in order to get used to the robot. Then, they were asked to "sit" left-sidedly on a small board mounted to the LOPES frame. Furthermore, a foot was attached

[2]The Carnegie Mellon motion capture database on `mocap.cs.cmu.edu` was created with funding from NSF EIA-0196217. To process the data, the *Mocap toolbox for MATLAB* was used, which was developed by N. D. Lawrence, University of Sheffield, UK.

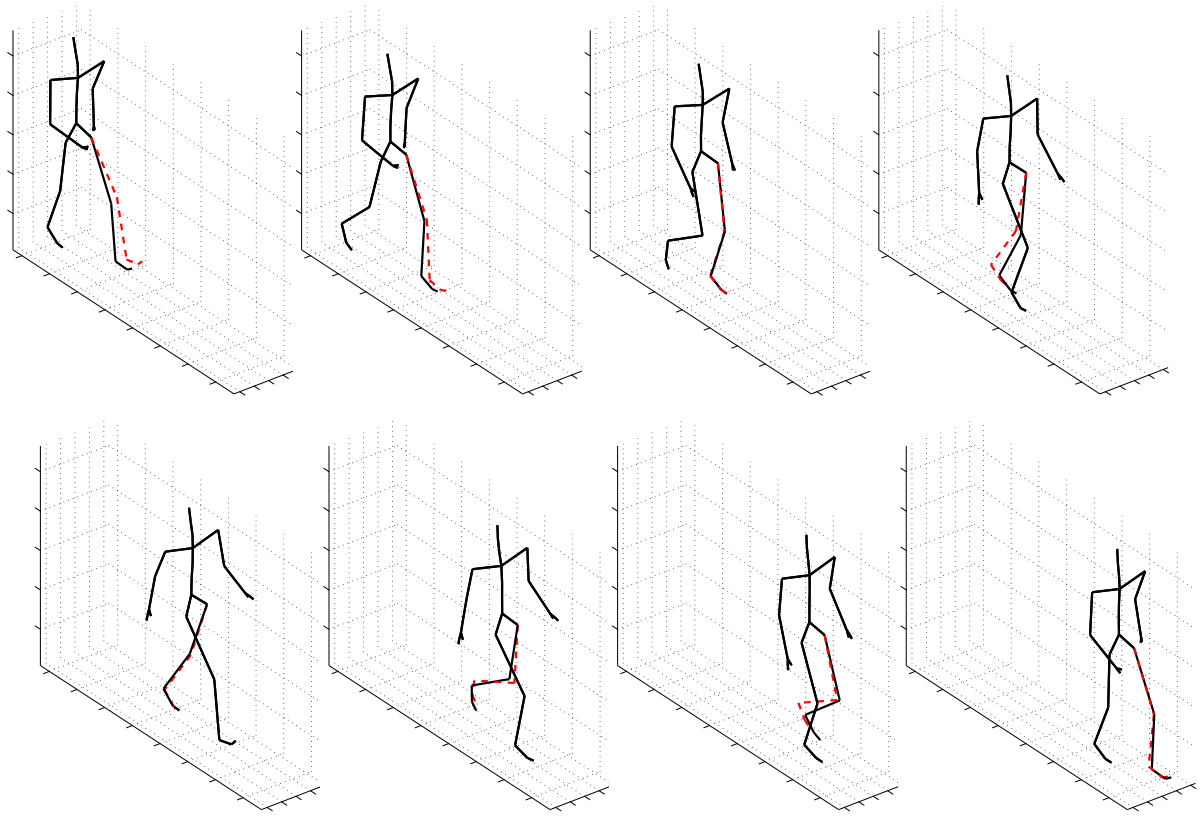

Figure 5.2: Comparison of the estimated motion (red dashed) of the left leg of the actual leg motion (solid black). The motion estimation is based on separate coupling analyses of stance and swing in the averaged gait patterns of 9 other healthy subjects.

to the exoskeleton leg on this side, such that the left LOPES leg became a prosthesis. Fig. 5.3 shows the setup in action.

Furthermore, a partial weight compensation system was used in order to lower the forces acting on the exoskeleton (which was being challenged far beyond its originally intended function as a joint torque source). This weight compensation was always adapted to lower the subject weight to residual 50 kg, thus the weight compensated was different for each subject.

Each subject then walked at 3 km/h with CLME based on the extracted coupling and scaling parameters of a physiologically comparable person (criteria were gender, hip height and weight), whose gait pattern had previously been recorded in zero-torque mode at 3 km/h. Each subject was assigned a different reference subject, whereby the original gait pattern of most subjects in this study also provided a reference for others. The matching was not ideal due to the limited number of available subjects. The most unfavourable compromise was taken for subject 6, whose hip height is approximately 8.5 cm lower than that of his reference subject. Subjects were allowed to hold on to the lateral bars of the LOPES frame in order to maintain balance. Prior to the experimental series, a workable input of DoFs of the right leg was tried out. First, hip abduction, hip flexion and knee flexion angles of the right leg plus the respective velocities were used to estimate the same variables for the left leg. Whereas the simulative forecast looked fine, this appeared not to be a workable

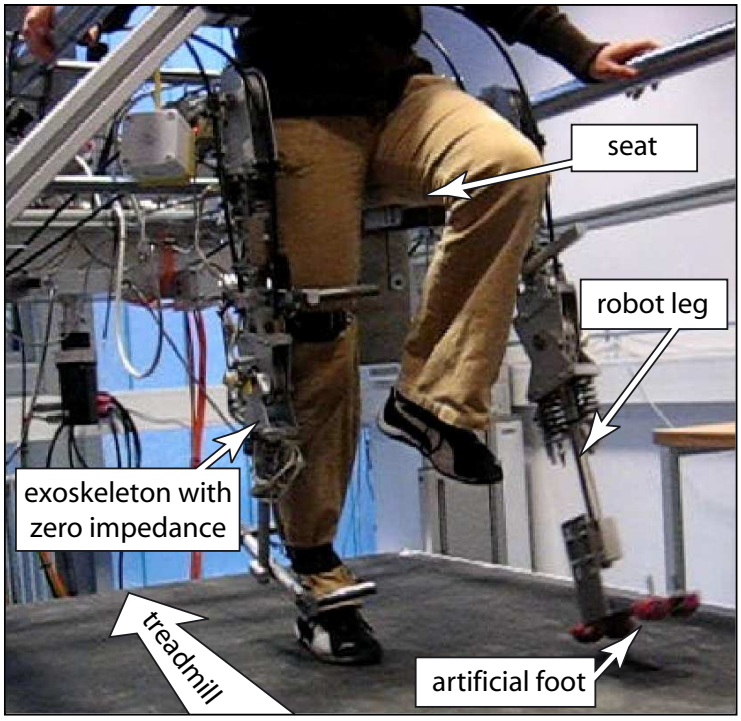

Figure 5.3: Experimental setup with the LOPES robot (without weight support). The subject rests his left buttock on a board, which is supported by the LOPES exoskeleton leg with a foot attached to it. The subject's right leg is free and its motion is used as input for CLME to give the reference motion for the robotic leg.

approach in practice. This is due to the fact that the reconstruction algorithm (working with normalized values) becomes very sensitive to small abduction movements, because the range of abduction is very small compared to hip and knee flexion. It was almost impossible for the subjects to dominate their abduction with sufficient exactitude. Therefore, walking with this configuration was neither robust nor intuitive and was replaced by another approach: Only hip flexion and knee flexion angles and velocities of the right side were taken to estimate the corresponding abduction, hip flexion and knee flexion of the left side. Although this showed slightly less precise results in simulation, walking now became feasible and robust.

5.4.2 Evaluation Criteria and Data Analysis

In a professional gait analysis [179], joint angles are generally measured via a motion tracking system, and ground reaction forces are recorded using force platforms or sensor insoles. However, the test setup for this experiment did not include measurements apart from joint angle information. Neither ground reaction forces nor events like heel-strike or toe-off were detected, because the primary goal of this study is to answer the binary question of feasibility. However, using only kinematic data (exoskeleton angles), still some important tendencies can be detected concerning control strategies of the right leg, spatio-temporal gait characteristics, and gait symmetry. To assess these gait characteristics, simple criteria are defined in this section.

Control Strategies of the Sound Leg

It is of particular interest in how far the subjects maintain or adapt the control strategies of their right leg when walking with the robotic left leg. This question is assessed by looking at the synergies present in the right leg only, i.e. a PCA is performed on right angles and velocites. Then, a correlation is sought between the original subject's coupling, the reference subject's coupling, and the coupling during CLME-controlled walking. Features of interest are the amount of variance explained by the first principal components, i.e. the strength of correlation, and the form of correlation itself. For the qualitative analysis of the trajectories of the first two principal components, step-to-step variance is eliminated by the application of a Fourier series fit with four harmonics: First, the fundamental frequency is extracted using Fast Fourier Transformation, then, a least-squares approach is used to identify the Fourier coefficients.

Spatio-Temporal Joint Motion

Temporal joint motion is assessed by a quantification of the walking cadence, i.e. the frequency, which has already been extracted during the Fourier series fit. Given a fixed velocity (commanded by the treadmill), the frequency is inversely proportional to the average step length. For a further quantification of spatial joint motion, the mean values $\bar{\varphi}$ and the standard deviation $S(\varphi)$ of the individual joint angles are calculated. The standard deviation of the hip angle provides an indicator for hip excursion, and thus the step length and the duration of stance. The hip angle is defined with respect to the vertical axis, because the subject's trunk inclination is not measured.

Gait Symmetry

For symmetry, a large amount of criteria and indices are available. In [213], a thorough survey on gait symmetry measures is given. Most compare the same gait parameter, e.g. step length or stance to swing ratio, between legs. A frequently used symmetry index SI, which compares left and right parameter values x_l and x_r, has been introduced by [211]. Later, it has been slightly modified such that its absolute value ranges between 0 % and 100 % for positive parameters [65]:

$$SI = \frac{x_r - x_l}{x_r + x_l} \cdot 100\% \ . \tag{5.10}$$

0% indicates perfect symmetry, such that the index could actually be considered a measure of asymmetry.

This index is used in this study, and the chosen parameter x is the standard deviation of the hip and knee angle (with the hip value representing an indirect measure of stance duration and step length).

5.5 Functionality Study: Results

All subjects were able to walk with the prosthetic robotic leg after a very short time of practice (15-30 sec). The observations made during these trials, as well as the quantitative measures will be described in this section.

5.5.1 Qualitative Observations

All subjects first exhibited exaggerated right hip flexion and too little extension. This was due to the fact that their left leg was "sitting", the hip continuously being flexed. Anatomical constraints such as elastic joint moments then obstruct the correct extension of the contralateral leg. The repercussions of this shifted hip motion (during the adaptation phase) on the robotic leg were the following (which accords with calculations): Excessive right hip flexion caused excessive extension of the left (robotic) hip, combined with excessive knee flexion. However, this caused much less functional problems than the lack of right hip extension, which produced a lack of left hip flexion on the other side, combined with insufficient knee extension. This led to deficient foot placement. All subjects quickly learned to control left foot placement by adjusting their right hip extension, but many maintained their functionally uncritical excessive hip flexion.

Apart from these difficulties, which were caused by the experimental setup, no major difficulties appeared. Several subjects hesitated to shift their weight onto the left leg, although the foot was properly placed. This increased the stance phase and the step length of the right side (due to the running treadmill). Others (expecially subjects 3,7, and 8) were more confident of their "prosthetic" foot and reached an almost normal-looking walking pattern.

5.5.2 Quantitative Analysis

This section describes the outcome of the criteria defined in 5.4.2.

Subject Control Strategies for the Right Leg

From the analysis, only a few observations are above the level of significance (here and in the following, $p = 0.05$): The cumulative fraction of variance explained by the first 2 principal components decreases slightly (from an average of 88.9% to 85.2%). This shows a decrease of the strength of correlations. The form of synergies changes as well, indicated by a slight variation of the first 2 eigenvectors. However, no clear correlation was found (e.g. that the new eigenvectors would resemble more those of the reference subjects). Instead, there was a large variance among subjects. To illustrate these individual differences, in figure 5.4, the trajectories of the first 2 principal components, approximated by their Fourier series equivalents, are depicted exemplarily for four subjects. Whereas subject 5 maintained the original couplings almost entirely, subject 8 adopted the couplings of the reference gait.

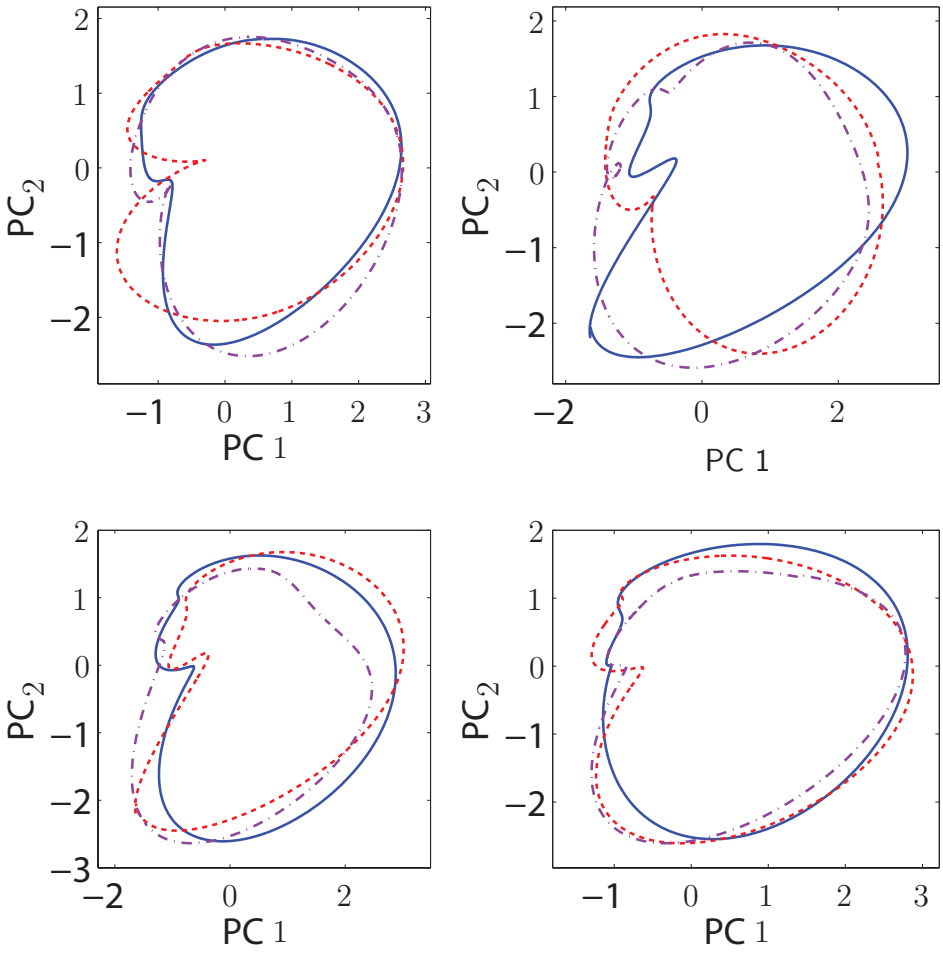

Figure 5.4: Fourier-series approximations with 4 harmonics of the first 2 PCs of the right leg for subjects 5-8. Solid blue line: Original gait of the subject, dotted red line: Gait pattern of the reference subject, dash-dotted magenta line: Gait trajectory during CLME walking. The reference gait for each subject is different.

However, no conclusions can be drawn from these contradictory results, especially given the small sample.

Spatio-Temporal Joint Motion

The step frequency decreases in all subjects (from an average of 89 to 65 steps per minute), which is equivalent to an increase in average step length. This is further affirmed by a significant increase in the standard deviation of the right hip flexion by 5.6°. There is also a slight increase in the standard deviation of the left hip, but below the level of significance.

Several correlations seem to exist between the change of statistical parameters of the subject and the statistical parameters of the reference person, but only one observation is above the level of statistical significance (considering the small number of subjects): The mean hip angle of the reference subject is correlated with the mean hip angle in

CLME-walking, although the mean of the original subject's hip angle is uncorrelated with both.

Gait Symmetry

To illustrate gait symmetry, the indices have been plotted in Fig. 5.5 for the eight subjects, showing both original values and values for CLME walking. Negative values show a prevalence of the left leg, positive values of the right leg.

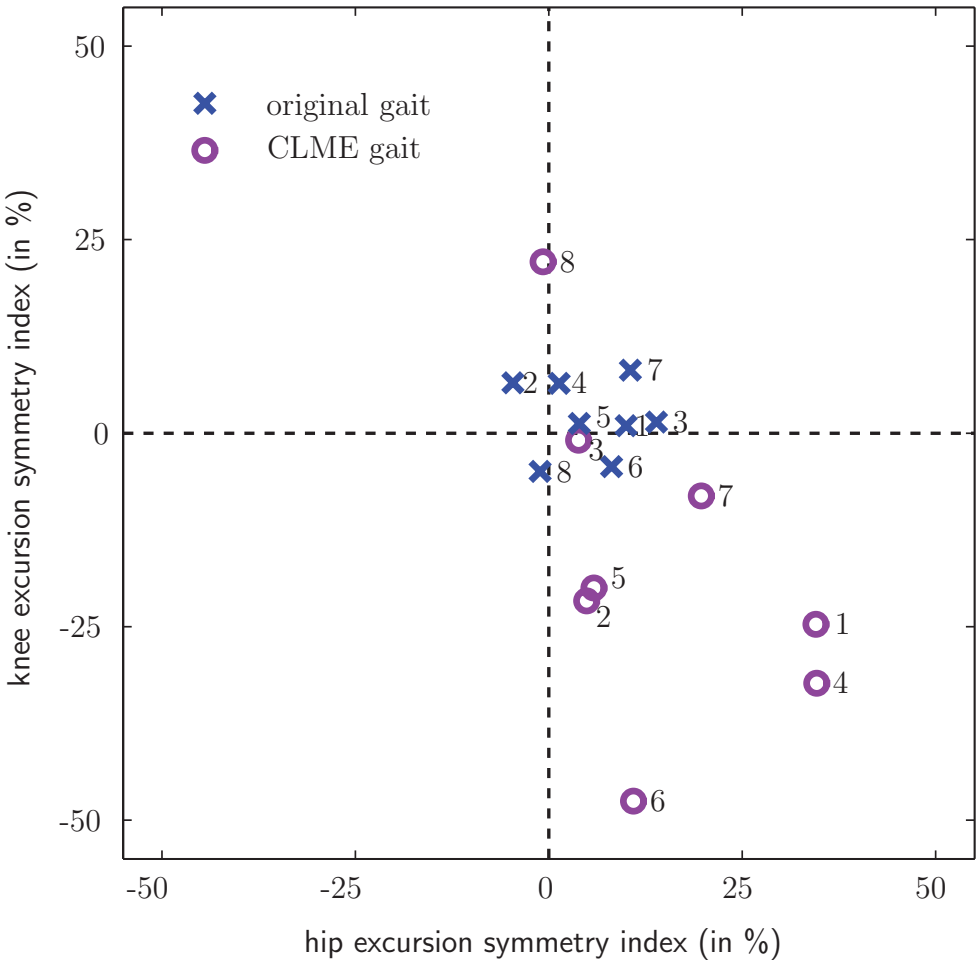

Figure 5.5: Symmetry indices SI for hip and knee flexion. 0 % indicates perfect symmetry; the labelling refers to subject numbers. Displayed are the SI for each subject's normal gait and gait with the robotic prosthesis replacing the left leg. Positive values indicate a prevalence of the right leg.

The changes in joint excursion symmetry are not consistent among subjects (some maintain a very high level of symmetry), but there is a tendency to increase the dominance of the right foot. This is indicated by a larger hip standard deviation on the right, and more knee

excursion on the left. This means, the right leg makes longer steps and thus has a longer stance phase and shorter swing than the left leg.

5.6 Functionality Study: Discussion

A prominent result is increased asymmetry, meaning that many subjects exhibited a longer stance phase on the right than on the left leg. This can be seen both by direct observation, as well as in the increased standard deviation of the right hip flexion, in the symmetry index, and in overall decreased step frequency. This behavior can be explained by lack of confidence in the robotic leg, given the short practice time of only 2 minutes.

The fact that inter-joint coordination in the right leg is less pronounced when walking with CLME might be an indication that less automated, or pre-programmed control strategies are used, instead more voluntary or conscious control of individual joints appears.

The correlation between the mean angle of the hip of the reference subject and the mean angle of the hip in CLME-walking is a small indication that subjects might adapt to the employed reference gait pattern during CLME walking, at least concerning certain features.

Longer practice times might have given both more confidence and more time for adaptation to all subjects, but due to the uncomfortable and exhausting posture and due to the high mechanical strain on the device, longer trials were not possible.

5.7 Interference Study: Experimental Design

To study interference with self-determined gait, healthy subjects walk in LOPES (on both their own legs) with CLME, with conventional fixed-reference impedance control of both legs, and with zero-torque control of both legs [261]. To rate the relative performance of CLME concerning undesired interaction compared to the two other control modes, evaluation criteria are formulated in terms of interaction torques, distortion of EMG patterns, and distortion of joint trajectories.

5.7.1 Setup and Protocol

9 healthy subjects took part (aged 19 to 37, weight 51 to 100 kg, 2 female, 7 male). Some subjects already had experience walking in the device with other controllers, and most had at least some knowledge on the purpose of the study. Each subject walked with four different controllers: Impedance control of both legs along a fixed reference trajectory, PCA-based CLME control (with the right leg in zero-torque mode), BLUE-based CLME control in the same configuration, zero-torque control of both legs. The block diagrams for these three controllers are displayed in Fig. 5.6. The impedance for both legs in fixed-reference mode, and of the left leg in CLME mode was identically set to the maximum achievable value of 155 Nm/rad (the maximum stiffness is limited, as described in Chap. 2). Sideways and forward Degrees of Freedom of the robot were controlled in Zero Torque, the

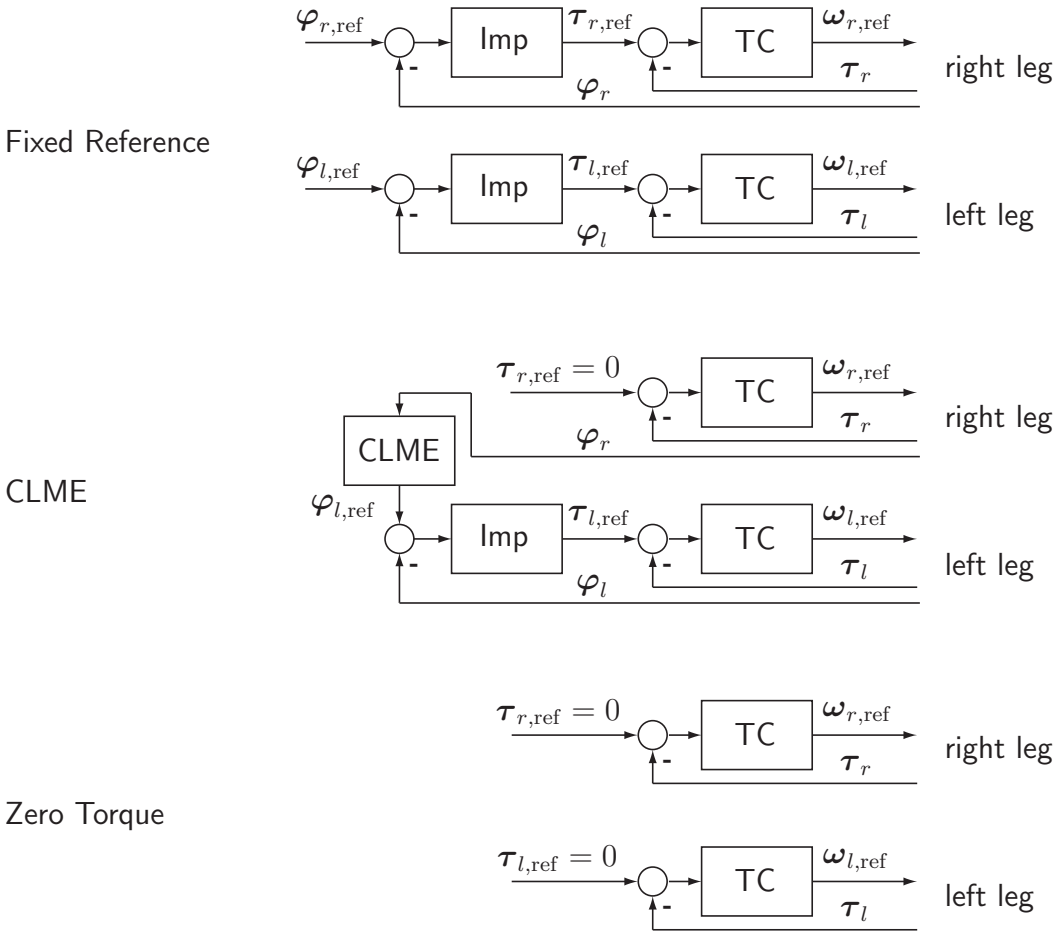

Figure 5.6: Block diagrams of the three controllers. The first guides right and left legs along fixed joint angles $\varphi_{r,\mathrm{ref}}$ and $\varphi_{l,\mathrm{ref}}$. CLME uses the joint coupling of the same reference gait, and it complements the right leg's motion on-line to generate the reference for the left leg. Control gains for joint impedance (IMP) and torque control (TC) are identical.

vertical DoF is passively weight compensated. The four control modes directly followed each other, whereby each controller was active for 2 minutes, with a gradual blending of 5 seconds between controllers. Subjects were not informed which controller was active, and they were instructed to walk actively the way they wanted to, yet to avoid walking out of phase with the robot (which was possible due to the limited stiffness). The reference gait pattern used for each subject stemmed from a randomly chosen preceding participant in zero-torque mode, who was not necessarily of comparable physique. This alien reference was used both for the fixed reference mode (by simple replay), and for the CLME controllers (by extraction of the mapping function). The experiment was repeated with the subject's own recorded gait pattern in zero-torque mode as reference, in order to assess also the potential benefit of an individually tailored reference.

Recorded signals were: Joint torques of the exoskeleton, EMG signals, and joint angle trajectories. The EMG signals were recorded from four major muscle groups of each leg: Rectus Femoris, Biceps Femoris, Tibialis Anterior, and Gastrocnemius. The EMG is first highpass-filtered ($n = 2$, $\omega_e = 5$ Hz), to extract movement artifacts and drift. It is rectified and then smoothed by spline approximation. Angle and displacement trajectories

were recorded using the integrated sensors in each degree of freedom of the robot, whereby in the later analysis, only hip flexion and knee flexion in the sagittal plane are analyzed. Subjective feedback of the subjects was documented as well.

5.7.2 Evaluation Criteria and Data Analysis

For the evaluation, the results of Zero Torque are defined as the baseline, i.e. the best achievable result, with the following reasoning behind: Both for the fixed reference and in CLME mode, a joint-space impedance controller calculates the desired interaction torques as a reference for the low-level force controller (see Fig. 5.6). If the reference joint trajectory matched the subject's actual motion flawlessly, the *desired* interaction torques would be zero, and the resulting behavior would be identical to zero-torque mode. This behavior does not imply zero *actual* interaction forces, because the underlying force controller cannot be ideal, and there is still some resistance generated (mainly due to uncompensated friction). Thus, zero-torque mode represents the best possible outcome given a perfectly matched reference trajectory.

A first and very direct criterion of interference is given by the robot's joint torques. In order to distinguish between torques that assist and those that resist, the torques are not compared directly, but instead the power delivered to the left leg is calculated by a multiplication with the joint velocity (The power introduced to the right leg does not provide any additional knowledge, because this leg is in zero-torque mode in both CLME controllers.). To obtain a single number for statistical analysis, accumulated power is calculated via integration. In order to exclude adaptation effects, only the last 60 seconds of each mode are used.

A second criterion is derived from muscle activity, as measured by the EMG. Highpass filters ($n = 2$, $\omega_e = 5$ Hz) are used to extract movement artifacts and drift. Afterward, the EMG is rectified and then smoothed by spline approximation. The criterion used is the distortion with respect to the "normal", minimally perturbed muscle activity pattern in zero-torque mode. In order to assess this distortion of muscle activity quantitatively in a systematic way, EMG of each muscle and each single step is compared to the respective subject's mean EMG activity in zero-torque mode. This comparison is performed using the algorithm of *spatio-temporal correspondence* developed by Giese and Poggio [90], which has already been used for various tasks in motion analysis, e.g. to assess cerebellar dysfunction [119]. This algorithm minimizes a quadratic cost functional by dynamically warping a (possibly multi-dimensional) template trajectory onto a trial trajectory. It is based on dynamic programming and outputs a temporal and spatial, non-uniform distortion of the template. Therefore, it can adaptively cope with varying combinations of spatial and temporal distortions. Fig. 5.7 shows the principle of the spatio-temporal correspondence. EMG signals are scaled to have a standard deviation of 1 in zero-torque mode. It also illustrates a weakness of the algorithm that has to be taken into account when applying it to periodic patterns: The outcome highly depends on the chosen begin and end of the trajectory, because any distortion there is interpreted as spatial distortion. This explains the incorrect matching observable here at beginning and end (heel strike). This problem is avoided in the further analysis by a varying definition of the gait cycle begin for each

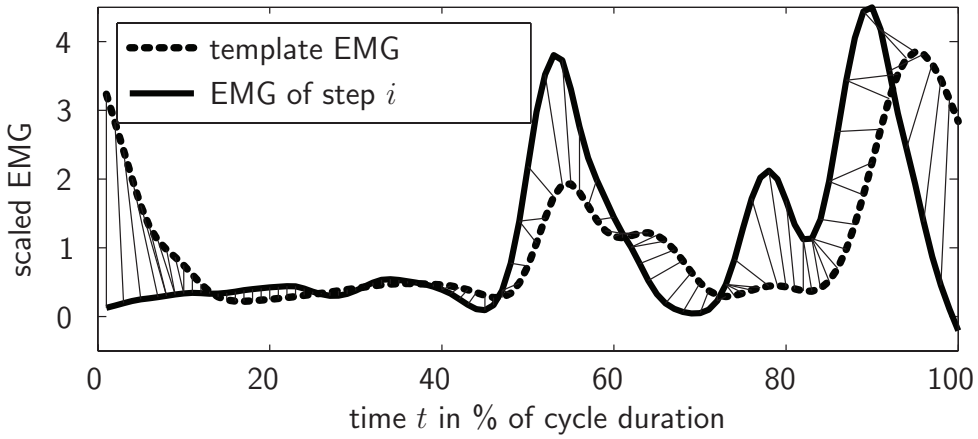

Figure 5.7: Spatio-Temporal Correspondence: EMG of the Rectus Femoris in step i is compared to the template, which is the average EMG in zero-torque mode. Dynamic optimization separates temporal and spatial distortion of each sample: Horizontal connection lines represent purely temporal distortion; vertical lines represent purely spatial distortion.

muscle: The start- and endpoint of each muscle's EMG trajectory is defined at a different constant offset from the heel strike, in such a way that the major burst of the muscle's Zero Torque EMG pattern is in the middle. The process is robustly automated for each subject and muscle using a sinusoidal approximation of the EMG. This way, distortion values of the same order of magnitude are achieved for all muscles. For one step, average absolute temporal and spatial distortions are calculated, as suggested by [119]. In order to exclude adaptation effects, only the last 30 steps with each controller are used to calculate a mean distortion value for each subject, muscle, and controller. Furthermore, all trajectories are scaled by the standard deviation of the zero-torque activity.

A third criterion is obtained by an analysis of kinematic trajectories. In order to asses distortions of hip and knee trajectory with respect to zero-torque gait quantitatively, the spatio-temporal algorithm is used again. Here, it is applied to compare the two-dimensional hip-knee trajectories of each of the last 30 steps in each condition to the zero-torque mean.

Statistical analysis of all three criteria is performed independently, but in a similar fashion. A two-factor ANOVA (factor 1: controller, factor 2: own or alien gait) is performed for both legs separately and for each of the criteria: Accumulated joint power, EMG distortion, and kinematic distortion. The chosen level of significance is $\alpha = 0.05$, and a Bonferroni adjustment compensates for multiple comparisons. This statistical analysis of all criteria, especially of EMG and kinematic distortions, can only be performed after a transformation of the data, because the distributions are skewed, and standard deviations differ heavily between conditions. Transformations are applied to obtain normally distributed data between steps for each condition (verified using Kolmogorov test) and to fulfill the requirement of sphericity between conditions. Accumulated power is transformed by offsetting and taking the square root. To EMG and kinematic distortions, the log-transform is applied twice. As a scalar parameter for the statistical analysis, the mean of the transformed EMG of all muscles is used.

5.8 Interference Study: Results

Due to technical problems, two subjects completed only one of the two conditions, one (#9) walked only with his own, the other (#5) with an alien gait. These unmatched trials are included in the plots (such that the number of subjects there is 8 in each case), but they are not included in the later multivariate statistical analysis (such that the number of observations there is 7).

5.8.1 Subjective Feedback and General Observations

All subjects noticed the transition between fixed-reference control of both legs and CLME, as well as between CLME and Zero Torque, although the latter often not at once. 4 of the subjects did not notice any difference between PCA and BLUE mode, 4 preferred the BLUE controller, 1 the PCA controller. For both CLME conditions, most reported that they needed to do more active foot clearance than usual or they mentioned a general impression of increased resistance in comparison to Zero Torque. One subject (#2) could not cope with PCA-based CLME and walked, although stably, in a strange manner.

5.8.2 Interaction Torques between Robot and Human

For a first look at robot-human interaction, Fig. 5.8 displays the cumulative power, i.e. energy introduced over time. Impedance control with a fixed reference exhibits consid-

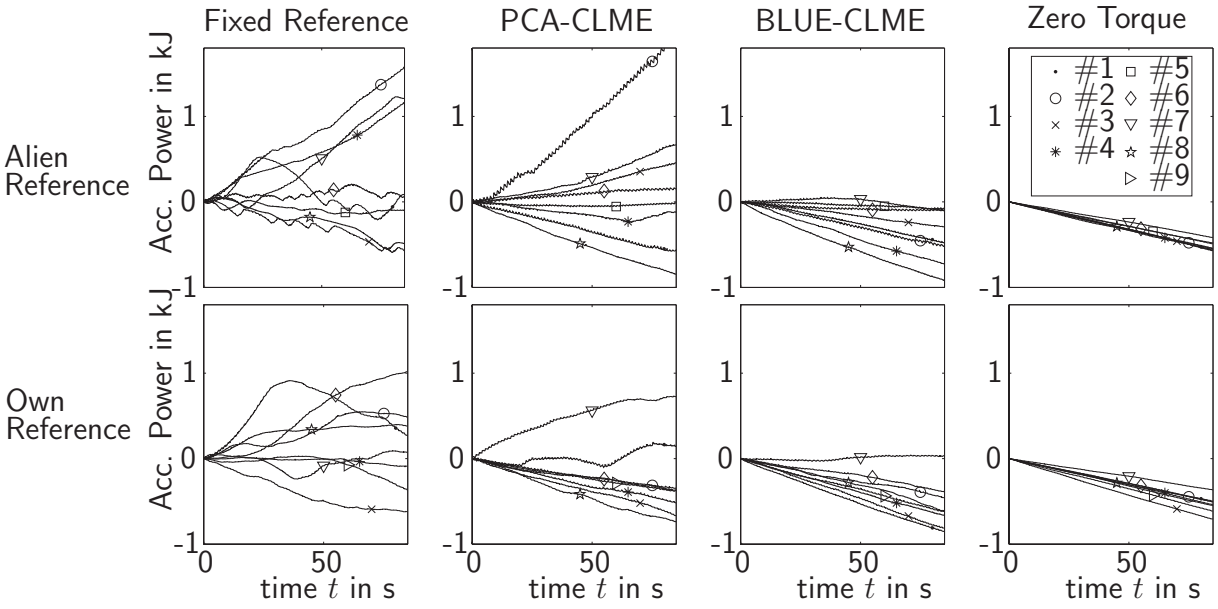

Figure 5.8: Introduced cumulative power to the left leg over time (excluding initial adaptation), when walking with an alien reference gait and the own gait pattern as reference for all three controllers, and zero-torque mode for comparison. Positive slopes indicate that the robot assists, negative mean that it resists the subject's motion.

erable inter- and intra-subject variances. For several subjects, the interaction oscillates. This phenomenon is especially strong and also visible in the figure when walking with an alien's gait (top). When walking with the own gait, the phenomenon also occurs, yet less pronounced. Apart from these oscillations, there are several abrupt changes in slope with the fixed reference. With the CLME controllers, the slope is rather constant.

Furthermore, introduced power tends to be higher in fixed-reference mode compared to BLUE. For PCA-based CLME, systematic differences to the other two controllers are less obvious. These observations hold both for the own and the alien reference gait.

The two-factor ANOVA for the left leg confirms the difference between BLUE and fixed-reference mode: BLUE does indeed introduce significantly less power than fixed-reference control, it does not even differ significantly from Zero Torque. PCA does not differ significantly from neither of the other conditions. The upper part of Fig. 5.9 shows confidence intervals for accumulated power with respect to factor 1, i.e. comparing the four controllers. A significant influence of the second factor (own or alien gait) cannot be shown, and the interaction between factors is not significant either.

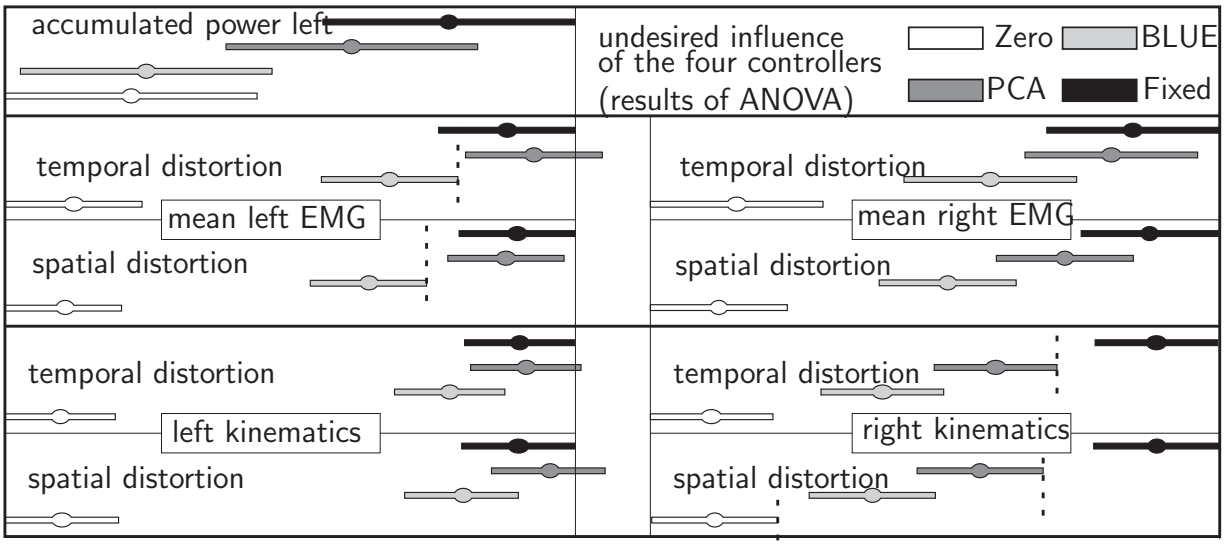

Figure 5.9: Multiple comparisons between controllers resulting from the two-factor ANOVA. Top: Accumulated power, middle: EMG distortions, bottom: Kinematic distortions. Non-overlapping intervals indicate significant differences of the means ($\alpha = .05$). All graphs are scaled to fixed reference and Zero Torque.

5.8.3 EMG signals

As an example, Fig. 5.10 shows the EMG of the Biceps Femoris for the last 30 steps. The median is taken instead of the mean in order to lower the effects of variation in timing of the EMG bursts present in fixed-reference mode, which lower the mean EMG amplitude there and give the other controllers an unfair advantage in visual impression. Fig. 5.11 shows the distribution of the transformed (double logarithmic, as stated earlier) mean EMG distortions among the 8 subjects. Between fixed reference mode and PCA, there is

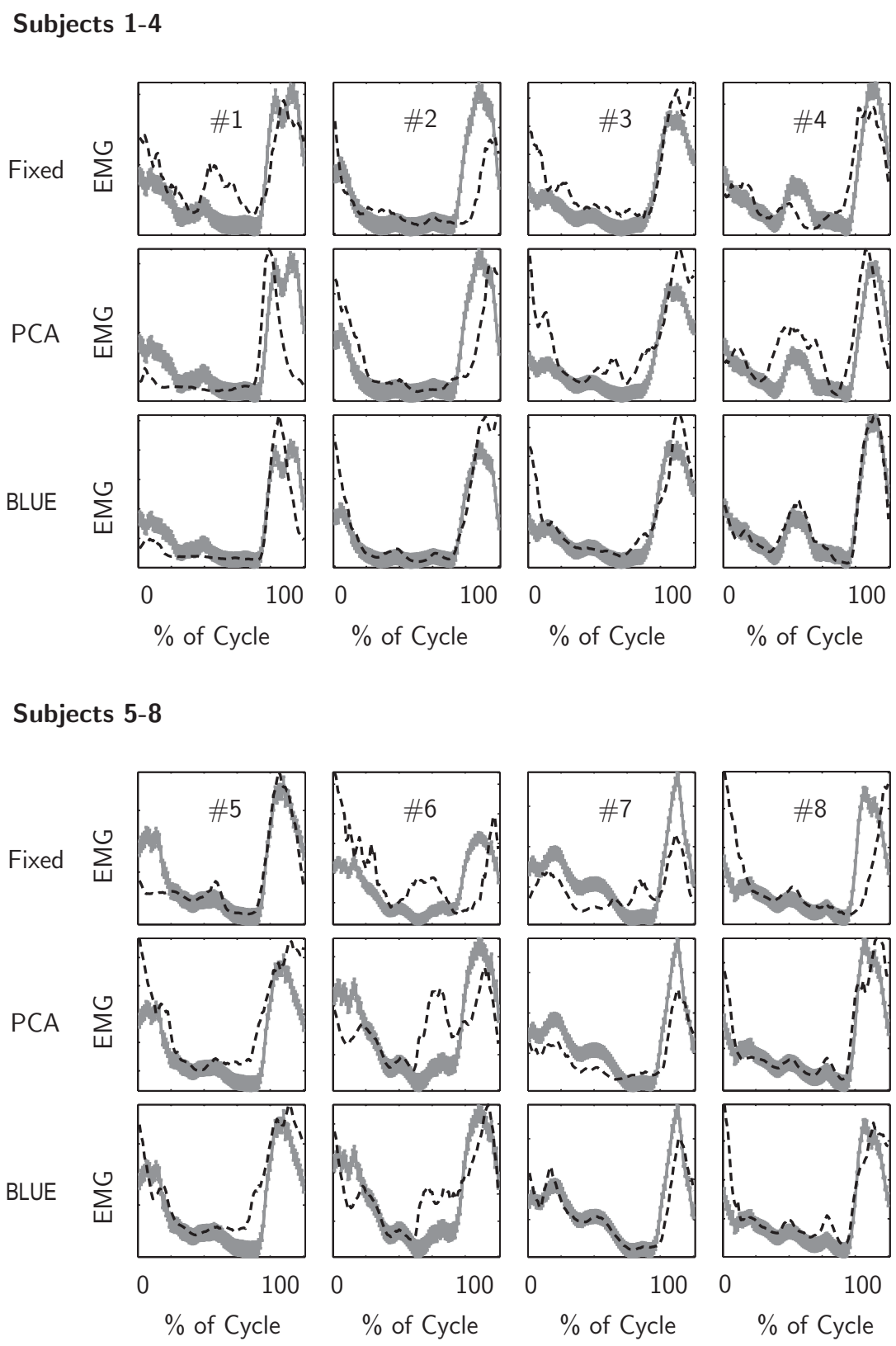

Figure 5.10: EMG of the Biceps Femoris of all subjects. Displayed are the median EMG of the last 30 steps with each controller (dashed black line), as well as the median EMG in zero-torque mode with standard error (gray shade), when walking with alien reference.

no clear tendency for one or the other. In contrast, BLUE seems to lower the distortion compared to a fixed reference. The two-factor ANOVA for spatial distortions shows no

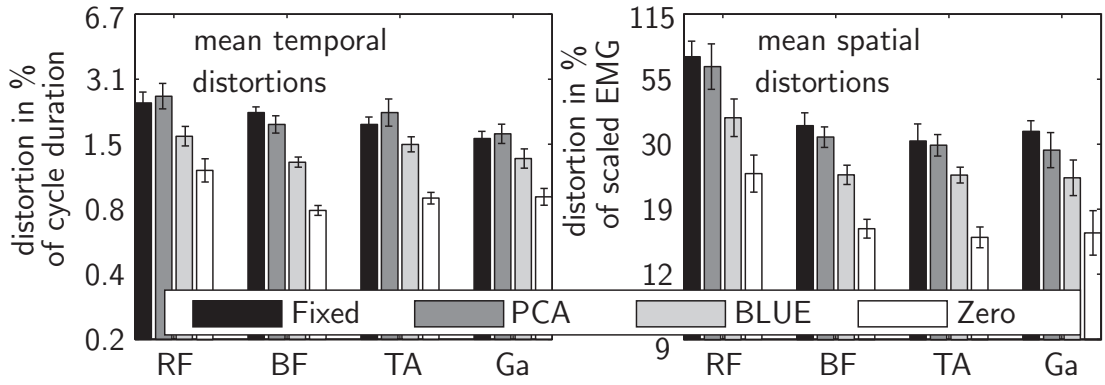

Figure 5.11: Mean absolute spatial and temporal distortions of the left leg's EMG with respect to Zero Torque and standard error among the 8 subjects when walking with an alien reference. Mean values are drawn from the last 30 steps for each controller. RF: Rectus Femoris, BF: Biceps Femoris, TA: Tibialis Anterior, Ga: Gastrocnemius.

significant differences between PCA-CLME and the fixed reference, but it confirms the difference between BLUE-CLME and fixed-reference mode for both legs. Only in the left leg, distortions with BLUE are also significantly lower than with PCA. For temporal distortions, neither BLUE nor PCA cause significantly less distortions than the fixed reference. The analysis also shows that all assistive controllers distort the EMG of left and right leg both temporally and spatially significantly more than explained by normal variation in Zero Torque. The second factor (own or alien gait) reaches a level of significance for the left leg's spatial EMG distortions only. The interaction of both factors is not significant. The middle part of Fig. 5.9 illustrates the significant differences in temporal and spatial EMG distortions between controllers.

5.8.4 Kinematics

To assess kinematics, knee and hip joint trajectories are analyzed. For a visual impression, Fig. 5.12 illustrates temporal and spatial distortions of the subject's median gait pattern for 30 successive steps at the end of each controller condition. The median is again chosen in order to obtain functional steps for fixed-reference mode. Statistical values are given in Fig. 5.13. The results of the two-factor ANOVA with respect to the first factor (controller) are displayed in the bottom part of Fig.5.9. For the left leg, CLME does not show clear advantages. The right leg's path, however, is disturbed significantly less by both CLME algorithms. For both sides and both criteria, all assistive controllers differ from Zero Torque, and PCA and BLUE do not differ significantly from each other. For the left leg, the second factor, i.e. whether own or alien reference is used, reaches significance only for spatial distortions. For the right leg, the factor is significant both in temporal and spatial distortions. For all controllers, distortions are lower when the subject's own gait pattern is used, interaction of both factors is not significant.

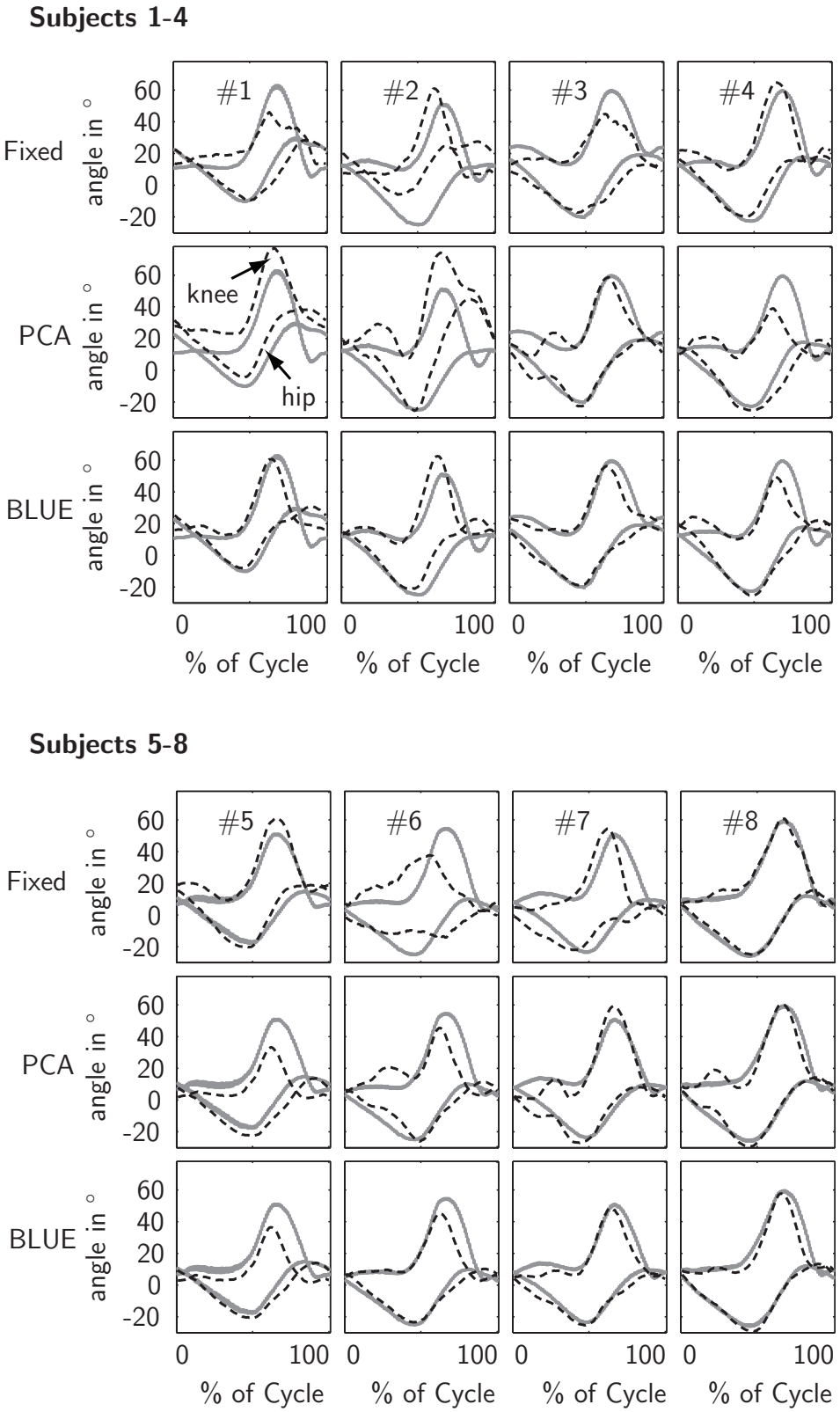

Figure 5.12: Median hip and knee trajectories (dashed black lines) of the 30 last steps for each controller and each subject when walking with an alien reference gait pattern, each compared to the mean zero-torque trajectory with standard error (gray).

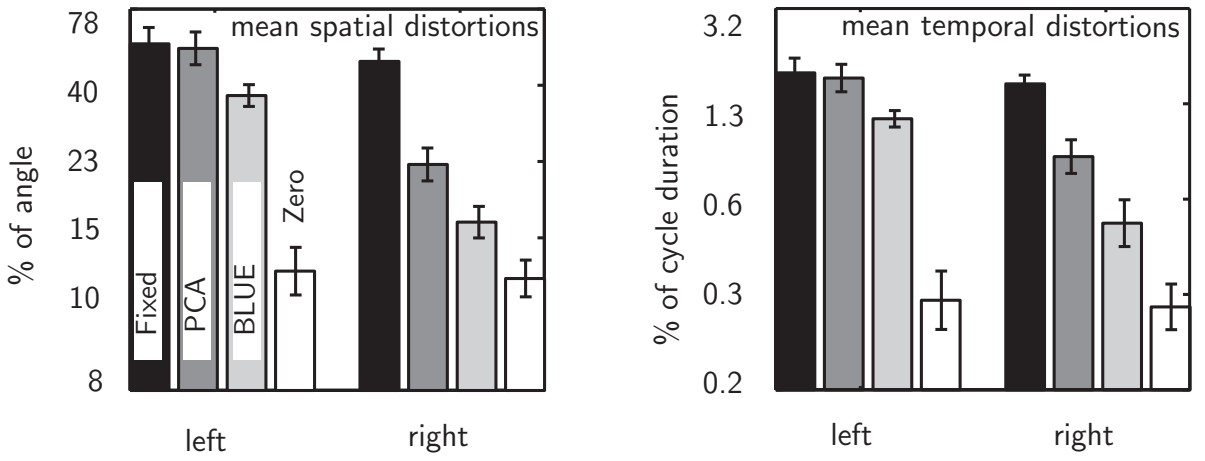

Figure 5.13: Mean and standard error among subjects of spatial and temporal distortions of the hip-knee trajectory for the left and for the right leg, analogous to EMG.

5.9 Interference Study: Discussion

The periodic fluctuations of the introduced power can be explained by the compliance of the device: Subjects can walk out of phase with respect to a fixed reference pattern. This leads to cyclic oscillations with a frequency of about 0.05 to 0.1 Hz, which has been observed and described as *beat phenomenon* by [13] for a pneumatic gait training robot. The controllers suggested here, the CLME controllers, inherently avoid out-of-phase walking, and thus no beat phenomenon occurs. However, the phenomenon could also be avoided by a temporally variable reference with a constant synchronization between reference pattern and subject gait, as suggested by [13].

The differences in introduced power suggest that fixed-reference control tends to assist the subjects, although they would be able to walk on their own. Concerning this criterion, BLUE-based CLME hardly differs from the results of zero-torque mode (the best achievable result with the robot), both moderately resist the subject's motions. Furthermore, the fixed reference provokes changes in slope, which might stem from adaptation of the subject. In BLUE mode, on the contrary, each subject is influenced almost invariably over time, leading to the deduction that there is hardly any adaptation needed to walk with this controller.

With respect to timing, the improvement of BLUE compared to a fixed reference is less pronounced than compared to spatial distortion, both for kinematic and for EMG data. This leads to the conclusion that deficient synchronization of reference patterns might not be the only cause of undesired interaction torques.

In Fig. 5.12, the distortion introduced by BLUE seems systematic and always concerns the late swing phase. This is in congruence with subject commentaries and with simulated reconstructions of one leg based on the other. An explanation is the weakness of the linear estimator used for BLUE, which cannot capture all details of the gait cycle and systematically under-estimates knee flexion amplitudes. It is probable that better results could be obtained by using a non-linear estimator. In contrast, PCA and fixed-reference

control show rather unsystematic distortions among subjects. Furthermore, their inter-subject variation is also higher.

It would be expected that subjects are less perturbed when their own gait pattern is used as a reference, because then the reference is tailored to them. This fact seems confirmed by Fig. 5.11. However, for the statistical analysis, this effect is too small compared to the controller type used, because significance of this second factor could not be shown for most variables (considering the small sample).

An interesting, yet not further analyzed observation is that BLUE and PCA both significantly influence the right leg in comparison to Zero Torque. This might be an indication that disturbances on one side show repercussions on the other due to mechanical coupling, but it could also be due to adaptation effects of the subject.

All observed effects are rather small, which is due to the high level of compliance of the robot: Even in the stiffest possible configuration, subjects are able to walk their normal pattern (depending somewhat on their physical strength), and they exhibit almost natural EMG activity.

5.10 Conclusion

This chapter presented Complementary Limb Motion Estimation (CLME) as a new control method to achieve patient-cooperative behavior of rehabilitation robots. The patient's intended motion for impaired limbs is deduced from residual body motion, using knowledge of physiological interjoint coupling. Two experimental studies with the with the gait rehabilitation robot LOPES addressed the extreme requirements that have to be fulfilled to let a patient participate actively: Functionality on the one hand, and minimum interference with independent subject activity on the other hand.

The first study investigated the capability of humans to control their leg via the other one, meaning how far a subject can cope with a unidirectional coupling scheme of sound and robotically moved DoFs. This study confirmed that CLME is capable of generating functional gait for subjects with no control of the assisted leg. Functional walking was reached after a very short time by all subjects. The level of gait symmetry varies widely among subjects, probably due to a varying level of confidence in the robotic prosthesis. It has also been shown that it is possible to use synergy information from other healthy reference subjects, and indications of adaptation to the reference pattern have been found. Thus, the question can be answered affirmatively: Inoperable limbs can be controlled on-line using motion information of sound limbs.

The second study aimed to evaluate interference with self-determined gait. Two regression algorithms for CLME (BLUE and PCA) are used to generate the reference for an impedance controller on-line, and they are compared to two extreme control strategies: One extreme is impedance control along a fixed gait pattern, which does not leave any freedom to the subject except for the robot's intrinsic compliance. The other extreme is zero-torque control, which gives maximum freedom to the subjects. Results indicate that interference of the robot is lower with BLUE-based CLME than with control along a fixed reference

trajectory, mainly in terms of lowered introduced power and more natural EMG activity. This implies that subjects can walk more naturally with CLME, and they are assisted less by the robot when it is not needed. Furthermore, the fixed reference trajectory causes out-of-phase walking in the compliant robot. This problem is inherently avoided by CLME. For all criteria, BLUE-based CLME outperforms the original PCA method, which does not show any significant improvement compared to a fixed reference, except for the solution of the synchronization problem. Subject reaction to all controllers varies strongly, like in the first experiment. Only for BLUE-based CLME, all subjects react more or less similar: They walk almost naturally, exhibiting only a small systematic distortion concerning a specific gait feature, which is foot clearance.

The predictable behavior of BLUE-based CLME makes further fine-tuning easier, e.g. using superposed Virtual Model Control, which is specialized for correction of specific features. This leads to a superposition of two controllers: CLME generates a trajectory for a severely impaired subject who cannot walk functionally without help, then VMC fine-tunes this trajectory. This superposition has been tested in preliminary experiments, and it showed very promising results. Furthermore, the fact that the specific method of regression has such a big influence on performance motivates further investigations in this direction, possibly by an extension into the nonlinear domain.

The described experiments with healthy subjects are not sufficient yet to prove the suitability of CLME for stroke patients, who might not dispose of one perfectly "sound" or "unaffected" leg to control their paretic leg. Optimistic expectations can be drawn from the fact that stroke patients mostly exhibit only mild impairments on the "unaffected" side (which seem to be due to cognitive deficiencies) [240] and fast recovery thereof, at least for right hemispheric stroke [239]. However, clinical studies with CLME have to show whether these expectations are justified.

6 Conclusions and Future Directions

6.1 Summary of Methodic Contributions

This thesis investigated several control aspects for assistive devices, with major foci on user-dominated control, and on stability of such coupled robotic/biomechanical systems.

Chap. 2 is concerned with control of Series Elastic Actuators (SEAs). A state-of-the-art cascaded control scheme is employed for impedance control, where a motor velocity loop is embedded in the force controller. Based on a passivity analysis of this control scheme, parameter limitations are found both for the inner force control loop and the outer impedance control loop. The passivity analysis for the impedance control loop leads to an important result: If passivity is desired, the rendered stiffness cannot exceed the stiffness of the mechanical element of the SEA. A second result is found during the analysis of the force control loop: A cascaded controller with internal velocity loop allows to use integrators without jeopardizing passivity. This is useful to treat static friction, and it contrasts earlier control schemes, where passivity analysis showed that no integrators should be used [194]. The good performance of the controller is demonstrated in practical experiments, which also confirm the theoretically predicted stability limitations.

Chap. 3 investigates an anti-causal identification method for nonlinear systems of Hammerstein type. Hammerstein models are commonly employed to describe muscle reaction to Functional Electrical Stimulation. The proposed concept is advantageous if the inverted model is easier to describe than the original causal system. This is the case for muscles, where the inverted recruitment curve can be approximated well by a simple third-order polynomial. Another advantage of the inverted identification is that the inverted nonlinearity is directly available for further control design steps like input-output linearization. For evaluation, the method is compared to linear and nonlinear forward identification methods. As all algorithms are based on analytical solutions of optimization problems, the global minimum is reliably found in all approaches. However, the complex identification algorithms do not perform much better than a simple linear model in the practical experiments, which leads to the conclusion that the Hammerstein model itself might not have many advantages in modeling muscle behavior in this context. One explanation are numerous unmodeled factors and parameter variations during artificial muscle recruitment.

Chap. 4 focuses on the trade-off between modeling accuracy and practical applicability of control strategies for hybrid robotic/biomechanical systems. The example system is a Hybrid Neuroprosthesis, where both human muscles and an external exoskeleton are used to actuate the human leg. In this context, rigid coupling between robot and human limbs is the common assumption. However, the results of a stability analysis heavily depend on the validity of such an assumption, and closed-loop control might become unstable. Here, a stability analysis is contributed that analyzes the effect of simplifications such as

negligence of input saturation, nonlinearities, and time-varying and uncertain parameters in hybrid robotic/biomechanical systems. All the mentioned adverse effects are described via an affine system representation. Using this representation, a sensitivity analysis is performed to detect time-varying parameters with destabilizing effects, and to identify the most robust control strategy. The results show the strongly negative effects of compliant coupling between human limbs and robot in terms of stability: The use of a simplified model with rigid coupling shows to be acceptable only in terms of exoskeleton control and efficiency of feedforward components. However, the simplified model causes risks during closed-loop FES control. The most robust controller in this case does not include feedback control of the muscles, but only feedforward stimulation. Control performance of this simple control concept does not deviate much from the other controllers. To deal with uncertain muscle behavior and uncertain coupling dynamics between human and robot, this analysis thus advocates the simple approach of open-loop FES control combined with closed-loop control only of the (almost precisely known) robotic part of the system.

Chap. 5 describes a new approach to user-dominated control of assistive systems: Complementary Limb Motion Estimation (CLME). The method can even be applied when the human user has absolutely no control of the limbs to be assisted. CLME is based on regression, and residual body motion is used as input for an instantaneous mapping of states to the impaired limbs. The example that is considered is a patient with unilateral paresis, and the impaired leg is estimated based on the sound leg's motion. CLME is tested in two experiments with extreme conditions: A subject with absolutely no control of one leg, and a fully active subjects with no impairment at all. In the first experiment, functionality of gait is confirmed. Results of the second experiment show that CLME lowers undesired interaction between robot and human significantly compared to impedance control along a fixed reference for both legs. Furthermore, muscle activity patterns are less altered with respect to undisturbed gait. This second experiment also compares two different regression approaches: One is based on Principal Component Analysis (PCA), the other on Best Linear Unbiased Estimation (BLUE). BLUE-based CLME clearly outperforms the original PCA method.

6.2 Implications for Control of Assistive Devices and Future Work

In light of the increasing proximity of robots and humans, there still remain many open questions concerning suitable control strategies. The methods described in this thesis might be extended in different directions in search for answers.

Modeling the human sensorimotor system has received enormous interest, and the obtained models are becoming more and more detailed. However, there is still a gap between the model complexity that is achieved in state-of-the-art sensorimotor models, and how much of this knowledge can be made available to improve control of robots that interact with the human. One reason is that the current models are subject to high structural uncertainty, because only assumptions can be made concerning the exact functioning of spinal cord and brain. Another reason is that parameterization and possibly even structural reconfiguration

of the models is necessary for each individual, especially for impaired subjects. Under laboratory conditions, isolated parts of the models can be targeted and identified. In contrast, under practical circumstances, a large number of unmodeled influencing factors remains. Moreover, there is limited and possibly noisy data available, especially when using only non-invasive methods. Under such circumstances, it is difficult to identify the high number of parameters in complex models. The shortcomings of such an approach have been demonstrated in Chap. 3, where a complex model's parameters are assigned contrary to their original meaning in the model, even if the global optimum is found. In this case, simple linear identification performs just as well. Considering these shortcomings in identification of complex models, the solution to biomechanical uncertainty and variability will probably not lie in an exhaustive calibration prior to the actual use of an assistive device. Instead, a feasible strategy is to control the device in a way that it needs minimal biomechanical information and can handle heavy parameter uncertainties.

Simple, generic concepts that allow global optimization and a macroscopic view are beneficial not only during identification, but also in control: Generic safety mechanisms can deal with growing complexity more reliably than heuristic supervision and fault detection. Compliant actuation has been a major step in this direction. Although still a young principle, it is more and more becoming the default approach in new designs. The investigations concerning passivity of compliant actuators, as presented in this thesis, are a small contribution to this field. Another piece of the puzzle towards generic safety concepts might be the described polytopic approach to analyze robustness of Hybrid Neuroprostheses and the resulting advocacy for simple control concepts. Both for SEA control, as well as for the Hybrid Neuroprosthesis, the theoretically predicted stability limitations are not far from the ones encountered in practical experiments. These results justify theoretical exploration of stability limitations even though a macroscopic view enforces conservative methods.

New developments in control of assistive devices increasingly aim at adaptive and learning behavior of the controllers. For example, *Assist-as-Needed* control attempts to continuously challenge a neurologically impaired subject during training, and it therefore reduces assistance when tracking errors are small [281]. Adaptive strategies could be combined with various methods presented in this thesis. For example, the passivity analysis of SEAs should be extended to investigate also implications and limitations of a variable impedance in the outer loop. Furthermore, adaptive strategies can be used to calibrate FES control in Hybrid Neuroprostheses, which would replace model parameterization via prior identification. FES control could instead be optimized by a rather simple cycle-to-cycle on-line adaptation during operation like in [162] or [86]. However, adaptive behavior of control gains can lead to new stability risks. Following indicative results of this thesis, these risks should not be underestimated, but they can be counteracted by avoiding unnecessary complexity in the structural description of the system.

A major issue for assistive devices will be to find better interfaces to enable humans to control robots like an extension of their own body. These interfaces have to be convenient to use, and the less invasive they can be, the better. An important prerequisite is that robot behavior should be predictable to allow efficient use by the human operator. This can be achieved either by making robots behave human-like, or by keeping their control very simple. The first possibility is still far away. The second is more in reach, and it has another fundamental advantage: The device can be optimized in a form that both

healthy and impaired humans can integrate all their functions and only use the robot as an extension for tasks that they cannot perform alone, avoiding needless duplication of capabilities. CLME can be seen as one step in this direction of simple robot behavior with an intuitive interface, but it is still far away from being called a symbiosis between robot and human. Future work to improve CLME might aim at a further generalization of the presented motion intention estimation. Considering the different results of the two regression methods BLUE and PCA, an interesting question is to find yet a better mapping, e.g. using nonlinear regression. This might reduce the systematic error introduced by BLUE concerning disturbed foot clearance. Another, though less elegant approach to solve this problem would be a gait phase-specific fine-tuning of the reference pattern. Preliminary experiments to combine CLME with Virtual Model Control, which can be used to selectively increase foot clearance [71, 263], indicated that a superposition of the two assistive control concepts can be effective. Future investigations should also aim at a clinical evaluation of CLME with hemiplegic patients, to show whether the cooperative behavior with healthy subjects transfers to the clinical domain and whether it eventually leads to improved therapeutic outcome.

CLME can be applied not only to exoskeletons, but also to above-knee prostheses. Preliminary experiments showed a highly accurate estimation of the knee angle, and one above-knee amputee has already successfully walked with a prosthesis controlled by BLUE-based CLME. However, for practical application, more motions (e.g. stair climbing) and also the transition between motion primitives must be addressed. The required motion segmentation could be performed by hand, but possibly also by dynamic clustering, using methodologies such as Generalized Principal Component Analysis [270] or Correlation Clustering [28].

Concerning interfaces, this thesis only focused on appropriate input devices for the human to convey his intention to the robot. However, multisensory feedback from the robot to the human is just as important, and future investigations should aim at an integrated solution of input and output devices.

A LOPES: A Low Weight Exoskeleton with Series Elastic Actuated Joints

The experiments described in Chap. 2 and 5 have been carried out using the LOPES gait rehabilitation robot [269], which was developed at the Laboratory of Biomechanical Engineering at the University of Twente. The hardware description given in [262] by the coauthoring developer Jan Veneman is reproduced here, slightly modified and shortened.

Main goal during the hardware design process was to provide a platform that can leave maximum freedom to the user, both concerning Degrees of Freedom (DoFs), as well as concerning low realizable impedance. In order to allow kinematically natural walking

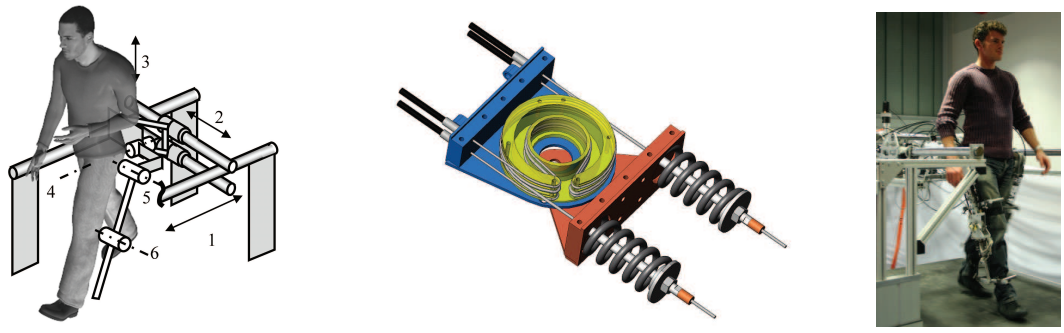

(a) (b) (c)

Figure A.1: Design of the LOPES robot: (a) Degrees of freedom of the pelvis and leg segments of the LOPES gait rehabilitation robot. (b) Design of the SEAs: Bowden cables connect the springs to EM motors, which are detached from the exoskeleton. (c) Photographic impression of LOPES in operation.

patterns, both horizontal pelvis translations are actuated (1 and 2 in Fig. A.1); the vertical motion of the pelvis is free with passive weight compensation (3). There are three rotational joints per leg: Hip abduction (4), hip flexion (5), and knee flexion (6). With these nine DoFs, LOPES allows more versatile motion than just forward stepping (as provided by commercial devices like the Lokomat [55]). Maintaining the fundamental instability of a standing or walking human, LOPES allows to train balance, which has been recognized as an important aspect of gait training [120,199]. Pelvis motion is also increasingly integrated into other new robotic devices such as ALEX [19] or KineAssist [180].

To achieve low impedance, it is crucial to minimize inertia of the actuated construction (the exoskeleton), because the means to reduce apparent mass by control are limited [54]. The strategy to reduce inertia is two-fold: Firstly, the exoskeleton is lightweight, and the heavy actuators are not mounted on it; instead, they are mounted on a frame behind the robot, and Bowden cables provide flexible torque transmission to the joints (see Fig A.1(a)). Secondly, Series Elastic Actuators (SEAs) actuate the joints, which detach actuator inertia

from the user via compliant elements (springs). SEAs are described and analyzed in Chap. 2. For the rotary joints, two compression springs are connected to the actuator disk with a cable so that a torsion spring is created between the actuator disc and the load side (see Fig. A.1(b)). Both springs are pre-tensioned with the maximum desired force, thus the cables are always under tension during operation. The concept, construction and functionality of the joints are described in [269]. The sideways pelvis translation is equipped with a translatory SEA. In contrast to the devices mentioned above, Lokomat, ALEX and KineAssist, which use stiff actuators, the SEAs make LOPES intrinsically compliant, similar to PAM and POGO presented in [13].

Table A.1 provides the geometric and inertial specifications of the exoskeleton part. For each segment of the exoskeleton, the length L, the centre of mass location with respect to the proximal joint L_{CoM}, the mass m, and the moment of inertia around the centre of mass J_{s1} and around the proximal joint J_{s2} are listed for an average configuration (the segment lengths are adaptable to the patient). Table A.2 gives the specifications of components used

	L	L_{CoM}	m	J_{s1}	J_{s2}
Upper limb	0.43 m	0.27 m	2.9 kg	0.088 kgm^2	0.30 kgm^2
Lower limb	0.37 m	0.17 m	2.25 kg	0.064 kgm^2	0.13 kgm^2
Pelvis B/F			35 kg		
Pelvis L/R			27 kg		

Table A.1: Dimensions and mass properties of the LOPES exoskeleton

in the actuation part. Motor and gear inertial properties and transmission ratio i determine the reflected inertia J_A or m_A of the drives in the exoskeleton coordinate system: For the sideways direction, the reflected mass m_A of the drive is 1.2 kg, much less than the mass of the pelvis segment, meaning all parts of the robot that move in lateral direction (27 kg). In contrast, the reflected moment of inertia J_A of the drives actuating the rotational joints is 0.13 kgm^2, which is in the same order of magnitude as the moment of inertia J_{s2} of the exoskeleton segments. However, as the motor mass is decoupled from the exoskeleton by the springs, the actuator mass is not felt by the subject, and the reflected mass of the device is reduced to the exoskeleton mass only. The disc radius r_d and the spring constant k_s in Table A.2 define the intrinsic rotational stiffness K of the SEA: For hip and knee, K is given by $2k_s r_d^2 = 155$ Nm/rad.

DoF	Power	Refl. inertia J_A, m_A	r_d	k_s
Flex/ext hip	567 W	0.13 kg m^2	0.047 m	35.1 kN/m
Flex/ext knee	567 W	0.13 kg m^2	0.047 m	35.1 kN/m
Ab/ad hip	567 W	0.13 kg m^2	0.047 m	57.2 kN/m
Left/right	690 W	1.2 kg	0.098 m	3.98 kN/m
Back/forward	250 W	2.3 kg		

Table A.2: Actuator specifications of the LOPES

B Limitations of a Series Elastic Actuated Robot in Cartesian Space

As illustrated in Chap. 2, both the bandwidth and the maximum stiffness are constrained in a Series Elastic Actuator. When a robotic manipulator, such as an exoskeleton, is actuated this way, the limitations map to limitations in Cartesian space. On the LOPES robot, one cooperative control scheme (besides Complementary Limb Motions Estimation, as described in Chap. 5) is Virtual Model Control (VMC) [71, 263]. VMC attempts to separately modify selected gait characteristics using virtual passive components such as springs and dampers. These elements are mainly implemented in Cartesian space, e.g. to separately modify step height and step length. Exoskeleton inertia generates undesired interaction forces that cannot be masked by the controller, due to the location of the force sensor between drives and exoskeleton. The influence of stiffness limitations in joint space and exoskeleton inertia on the achievable stiffness and bandwidth in Cartesian space has been analyzed in [262] by the coauthor Herman van der Kooij, and this analysis is reproduced here with minor modifications in nomenclature and conventions.

B.1 Performance Limitations due to Limited Stiffness

To meet passivity requirements, the maximal joint stiffness that can be realized by joint-space impedance control is limited by the spring stiffness of the series elastic element, as was shown in the previous section. This results in boundaries for the maximum displayed Cartesian stiffness, whereby the relation between the Cartesian stiffness matrix $\mathbf{K}_x$ and the joint stiffness matrix $\mathbf{K}_\varphi$ is defined by the Jacobian [57]:

$$\mathbf{K}_x = \mathbf{J}^{-T}\mathbf{K}_\varphi\mathbf{J}^{-1}. \tag{B.1}$$

The mapped Cartesian stiffness ellipse, with $\mathbf{K}_\varphi$ as the identity matrix and a joint stiffness of 1 Nm/rad at hip and knee is displayed in Fig. B.1. Its shape and orientation are determined by the eigenvalues and -vectors of $\mathbf{K}_x$, whereby it can be seen that the eigenvalues depend on the knee angle.

When the exoskeleton has 90° knee flexion, the smallest eigenvalue of $\mathbf{K}_x$ is 2.53, and it is 1.3 with 10° knee flexion. The worst case is when the knee is fully extended, and when the Cartesian stiffness ellipse is aligned with one of the virtual models. In this worst case scenario, the Cartesian stiffness is only 200 N/m given the maximal joint stiffness of the hip and knee of 155 Nm/rad, as given in Table A.1.

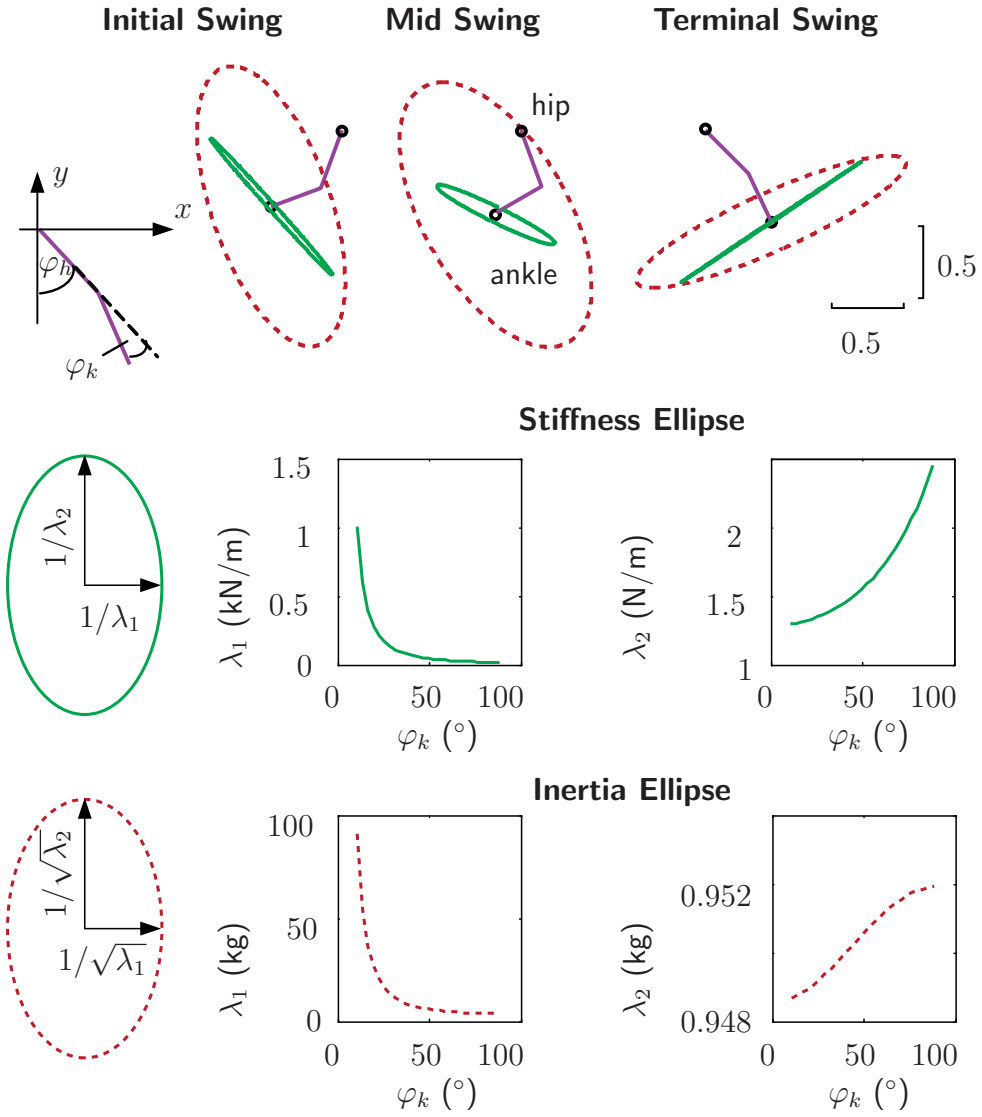

Figure B.1: Ellipses of reflected mass (red and dashed) and stiffness (green and solid) at the ankle. The larger the ellipses, the less mass or stiffness is reflected.

B.2 Performance Limitations due to Manipulator Dynamics

Without additional sensors, the controller cannot compensate for the open-loop impedance of the exoskeleton. As a consequence, in free space, the human operator will always feel the full inertia and friction of the manipulator [2], and thus not only the desired impedance.

The undesired additional interaction torques $\boldsymbol{\tau}$ in the swing phase are given by the equations of motion of the exoskeleton:

$$\boldsymbol{\tau} = \mathbf{M}_{\varphi}(\boldsymbol{\varphi})\ddot{\boldsymbol{\varphi}} + \boldsymbol{v}(\boldsymbol{\varphi}, \dot{\boldsymbol{\varphi}}) + \boldsymbol{g}(\boldsymbol{\varphi}), \tag{B.2}$$

where $\boldsymbol{\varphi}$ is the vector of joint angles, $\mathbf{M}_{\varphi}(\boldsymbol{\varphi})$ is the mass matrix in joint space, $\boldsymbol{v}(\boldsymbol{\varphi}, \dot{\boldsymbol{\varphi}})$ are Coriolis and centrifugal torques, and $\boldsymbol{g}(\boldsymbol{\varphi})$ are gravitational torques. To give an idea of the inertia of the device reflected at LOPES's ankle, these unwanted torques can be mapped to forces in Cartesian space with ankle position $\boldsymbol{x}$:

$$\boldsymbol{F} = \mathbf{M}_x(\boldsymbol{\varphi})\ddot{\boldsymbol{x}} + \boldsymbol{v}_x(\boldsymbol{\varphi}, \dot{\boldsymbol{\varphi}}) + \boldsymbol{g}_x(\boldsymbol{\varphi}), \tag{B.3}$$

whereby the relation between joint space and Cartesian space matrices can be derived using the Jacobian [57].

To compensate the components $\boldsymbol{v}_x(\boldsymbol{\varphi}, \dot{\boldsymbol{\varphi}})$ and $\boldsymbol{g}_x(\boldsymbol{\varphi})$, the impedance controller could be modified, since both terms only depend on joint angles and velocities. However, in our application, we compensate neither of these forces: Firstly, centrifugal and Coriolis forces in $\boldsymbol{v}_x$ are negligibly small. Secondly, subjects walking with compensated exoskeleton gravitational forces $\boldsymbol{g}_x$ reported that it felt unnatural, and compensating for $\boldsymbol{g}_x$ with constant $\mathbf{M}_x$ increases the natural frequency (As stated before, $\mathbf{M}_x$ can not be reduced by any causal controller).

Especially at high frequencies, the behavior of the device is dominated by the reflected mass $\mathbf{M}_x$ of the exoskeleton. With respect to the ankle, this reflected mass is related to the joint space mass matrix by:

$$\mathbf{M}_x = \mathbf{J}^{-T}\mathbf{M}_{\varphi}\mathbf{J}^{-1}. \tag{B.4}$$

Using the specifications given in Table A.1, this reflected mass is visualized by the inertia ellipse of Fig. B.1. Its shape and orientation are determined by the eigenvalues and -vectors of $\mathbf{M}_x$. The orientation of the ellipse is always perpendicular to the lower segment of the exoskeleton, which means that the reflected mass is minimal perpendicular to and maximal in the direction of the most distal segment of the exoskeleton. The eigenvalues of $\mathbf{M}_x$ only depend on the knee angle of the exoskeleton. The smallest eigenvalue remains fairly constant around 0.95 kg. The largest eigenvalue is minimal (3.9 kg) when the knee is 90° flexed, and increases when the knee is extended. Note that the reflected mass of the device would be much higher if the motors were not detached from the exoskeleton, and if the motor mass were not decoupled from the device by the series elastic element.

C Functional Electrical Stimulation

In physiological muscle recruitment, the nerves transmit motor commands to the muscles encoded in electrical pulses. Exploiting this mechanism, deficient motor control can be assisted using an external electrical field, which is called Functional Electrical Stimulation (FES). Muscle response to FES, however, is strongly nonlinear and time-variant. The torque depends on the spatial and temporal recruitment of muscle fibers, on the muscle length, and on the velocity of contraction. In the following, the physiological mechanisms will shortly be outlined, including intrinsic biomechanical properties as well as reflexes.

C.1 Signal Transport in the Nervous System

C.1.1 Physiological Nerve Function

The human Nervous System consists of the Central Nervous System (CNS), which incorporates Spinal Cord and brain, as well as peripheral nerve pathways. There are sensory nerve fibers, also called *afferent* and motor nerve fibers, also called *efferent*. The sensor pathways transmit information encoding external stimuli to the CNS, whereas the motor pathways transmit commands from brain and spinal cord to the muscles.

Signal transport in the nervous system is performed by the nerve cells or *neurons*. At rest, there is a difference of potential of about -80 mV at the neuron's cell membrane. This means that the cell is charged negatively with respect to the extracellular space. When external stimuli provoke a depolarization above a certain threshold (about -50 mV), internal positive feedback loops change the potential at the membrane abruptly, such that it reaches a value of about 30 mV. This value does not vary with the amount of external depolarization. The abrupt variation in potential is called *motor potential* or *action potential*.

A stimulus travels along the neuron, because an action potential at a local region of the membrane suffices to depolarize also neighboring membrane regions, initiating the positive feedback loops also there. As the amplitude of the action potentials is constant, they have binary character, and information is encoded in the frequency. For motor neurons, this frequency lies between 20 and 100 Hz. A detailed description of the physiological background can e.g. be found in standard works like [63].

C.1.2 External Nerve Stimulation

A lesion in the nervous system can disrupt the the generation of appropriate motor commands, or the signal transmission to the muscles, because possibilities for regeneration of

nerve cells are limited, in contrast to other cells of the human body. Depending on the type and level of a a lesion, it is possible to excite peripheral efferent neurons by external stimulation, and to cause muscle contractions this way. This is the basic principle of motor neuroprostheses, and it can be used both for functional restoration (mainly for spinal cord injury, SCI) and for therapy of the neurological deficits (e.g. after stroke). A depolarization of peripheral nerves can be achieved by pulsed magnetic or electric fields. The main advantage of *Repetitive Peripheral Magnetic Stimulation* (RPMS) is that it does not cause any pain in patients with intact sensory nerve pathways, whereas for mobile applications, the generation of stimuli by electric currents, so-called *Functional Electrical Stimulation* (FES), has the advantage of limited weight, size, and energy consumption of the devices.

According to the form the stimuli are supplied, three methods can be distinguished: Transcutaneous, percutaneous, and fully implanted electrodes. Transcutaneous electrodes are only attached to the skin, whereas percutaneous stimulation works via needle electrodes inserted into the muscle. A new development in implantable systems are so-called microstimulators [145], which dispose of a wireless connection to controller and energy supply outside the body. The advantages of implantable and percutaneous electrodes are improved selectivity, i.e. that the desired muscle can be targeted with much higher precision, and that also deeper muscle groups can be accessed. Furthermore, the required electric field strength can be substantially reduced compared to transcutaneous stimulation, where skin and fat tissue cause high impedances. An invasive method, however, always introduces the risk of infection. Fig. C.1 shows the transcutaneous stimulation setup used in this work: The eight-channel stimulator MOTIONSTIM8 of the company Krauth+Timmermann, Hamburg, is used to stimulate the quadriceps muscles and the hamstrings of the subjects.

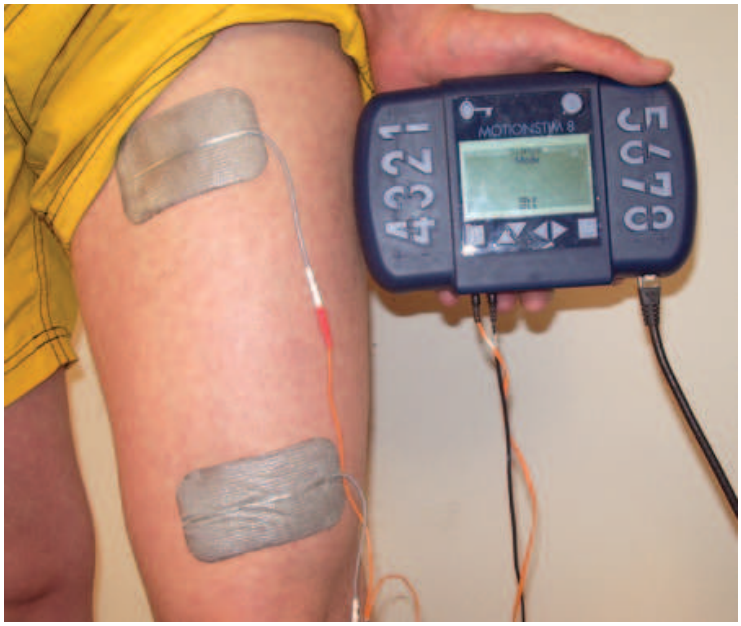

Figure C.1: The stimulator MOTIONSTIM8 from Krauth+Timmermann is used for transcutaneous stimulation of the quadriceps muscle group, which is responsible for knee extension, and hamstring muscles (on the back of the leg), which are responsible for knee flexion.

FES artificially causes action potentials in the neurons. To achieve this, pulses are generated, which depolarize the neurons. To avoid corrosive processes at the electrodes and

in the tissue by a cumulation of electric charge, the stimulators generate biphasic pulses: The depolarizing, mostly rectangular impulse is followed by a second, not depolarizing pulse in the opposite direction, which assures neutrality in the tissue. This second pulse is commonly not rectangular, but exponentially decreasing.

Generally, there are three different parameters, which all influence muscle behavior distinctly: The frequency, the pulse width, and the amplitude of the current impulses. The way how these parameters modulate muscle force will be outlined in the following.

C.2 Physiological and Artificial Muscle Recruitment

C.2.1 Modeling Muscle Response

Of the three types of muscles in the body, skeletal muscles, cardiac muscles, and smooth muscles, only the skeletal muscles will be considered here, which are responsible for the movement of limbs. The properties of the muscle are determined by its two main components: The *contractile elements*, and the tissue around them. The contractile elements consist of *filaments* (*actin* and *myosin*), which interact over cross bridges. The tissue around them is called *fascia*, and its dynamical properties can be approximated by springs and dampers.

In Sec. 3.1.1, several approaches have been summarized that aim to describe muscle response to FES mathematically. Here, the view is limited to the model of [268], which describes the muscle by a simplified nonlinear model in terms of the easily measurable quantities joint angle and velocity instead of muscle length and contraction velocity. This muscle model is illustrated in Fig. C.2: The pulse width PW of the stimulation signal is the input to a system with a static nonlinearity f_r (*recruitment curve*) in series with a linear dynamic model (*activation dynamics*), represented by the transfer function $G_a(s)$. The output of the nonlinearity is called *activation level* a. The output of the transfer function is multiplied with nonlinear terms depending on joint angle and angular velocity, and then yields the muscle torque τ_{fes} acting on the joint.

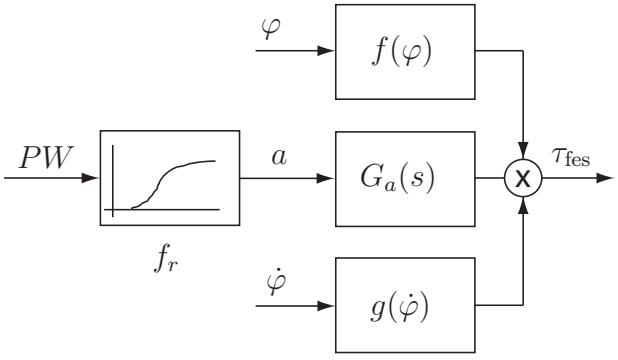

Figure C.2: Torque response τ_{fes} to FES is modeled with a nonlinear recruitment curve f_r that relates pulse width PW and activation level a, followed by a linear transfer function $G_a(s)$, and a multiplicative dependency on joint angle and angular velocity (modified from [185]).

In the following, a short description of characteristics and biological background of the model's components (activation dynamics, force-length and force-velocity feedback) will be given, which is mainly based on [279]. A more thorough description can be found there.

C.2.2 Activation Dynamics

The nonlinear activation dynamics are modeled by a succession of a static nonlinearity f_r and linear dynamics $G_a(s)$. The activation dynamics are determined by the behavior of the individual *motor units*, as well as the neural mechanisms that control their recruitment. The term motor unit subsumes three main elements of the command pathway to the muscle fiber: The *synaptic junction* in the spinal cord, the *motor axon*, and the *motor end plate* in the muscle fibers. One motor unit can control a varying number of fibers, whereby this number determines how finely the control task can be executed [81].

The motor units are recruited in an all-or-nothing event by means of the electrical pulses, the action potentials mentioned above. One action potential provokes a single muscle twitch. The action potentials have constant amplitude, whereby the larger the motor unit, the higher the action potential [155]. The force produced by the muscle can be increased by *temporal summation*, i.e. a higher frequency of action potentials, called firing rate, or by *spatial summation*, i.e. the recruitment of a higher number of motor units.

During physiological recruitment, both mechanisms are used in response to higher force requirements in a sort of hierarchical or overlapping manner: At low tension, first only one motor unit is recruited, and the exciting firing rate increases with tension. Before the firing rate reaches the maximum, the next motor unit is recruited. With growing tension, both firing rates further increase, and so on. The next motor unit is always recruited before the maximum firing rate of the preceding one is reached [77]. Spatial summation progresses according to the *size principle*: First, small motor units are recruited, which allow more fine control and are robust to fatigue. Later, larger motor units are recruited, which generate higher forces, but fatigue much more quickly.

Although normal and artificial action potentials are identical, there are several essential differences in muscle activation. An unfortunate difference is that artificial stimulation reverses the size principle: Amplitude and pulse width determine the strength of the generated electric field. The stronger the field, the more neurons are depolarized, leading to a spatial summation of action potentials and also increased muscle force. Larger motor units are recruited first during FES, smaller units later, because larger motor units also have commanding nerves with larger diameter, such that they are easier to depolarize by the electric field. Another difference to physiological recruitment is that all units are activated simultaneously. Both effects substantially increase fatigue. In response to a current impulse, the muscle reacts with a single twitch. To achieve a *tetanus*, i.e. a continuous contraction, the stimulation frequency must be at least 16-20 Hz. When the stimulation frequency further increases, a temporal summation of action potentials can be achieved, increasing muscle force. However, a side effect of increased frequency is increased fatigue. Therefore, stimulation is mostly done with the lowest possible frequency.

In response to external electrical stimulation, static and dynamic behavior are now modeled. Concerning the static response, so-called recruitment curves are recorded. These indicate how much force is obtained in response to stimulation at a certain constant intensity of stimulation at a constant frequency. Generally, stimulation frequency is held constant, and the electrical field is varied either by amplitude or pulse width, whereby the respective other parameter is held constant. The recruitment curves are generally characterized by S-shaped curves or ojives, which exhibit a threshold for low stimulation intensity, below which no force is produced, and a saturation of force at high intensities. These recruitment curves differ strongly between subjects or muscles. Exemplary curves can be found in [17].

The dynamic response of a single twitch can well be approximated by the impulse response of a critically damped second-order system [156]. The time constants differ widely among muscles, as well as among subjects, and they heavily depend on the experimental protocol. For example, [39] found that upper limb muscles tend to have a higher eigenfrequency, and that eigenfrequency decreases dramatically with decreasing temperature (more than factor 2 between 37°C and 23°C). For leg muscles, about 1 to 4 Hz can be expected.

An important property of muscle behavior is that muscles take longer to turn off than to turn on. This is one reason why a linear representation of the activation dynamics can only provide a very crude approximation [278]. For example, hysteresis effects have been observed [137, 143], and the concept of superposition does not hold for muscle recruitment [41, 233, 284]. According to [178], the largest deviations from the linear assumption are transient and appear at the onset of recruitment and derecruitment.

However, it is common practice (and, as stated above, it leads to acceptable results) to use the linear transfer function $G_a(s)$, which represents a critically damped second-order system, to model the dynamics of muscle recruitment and derecruitment together.

$$G_a(s) = \frac{\tau_{\text{fes}}(s)}{a(s)} = \frac{\omega_0^2}{s^2 + 2\omega_0 s + \omega_0^2}\, e^{-sT_t} \quad . \tag{C.1}$$

The additional dead time T_t in this model is due to signal transport in the nerve pathways. Its value is about 25 ms [185].

It should be mentioned that there is elastic tissue in series with the contractile element, mainly the *tendon*, which couples muscle to bone. This elasticity is e.g. described in [223] and [38]. However, the influence of this tissue on the dynamics is negligible for frequencies below 4 Hz [265].

C.2.3 Force-Length Dependency

The generated muscle force, or the joint torque, respectively, strongly depends on the instantaneous length of the muscle. A physiological explanation of this dependency can be given by two major effects.

The first effect is activation-dependent and mainly caused by the cross bridges in the contractile elements: At resting length, there is the maximum number of cross bridges. During

shortening or lengthening with respect to resting length, the filaments are either pulled apart, such that cross bridges reduce, or cross bridges overlap and interfere. Therefore, the muscle force is reduced in both directions. At full length, the force can drop to zero. Brown and Loeb [37] developed a more accurate model, and they showed additional length dependencies that scale with activation but are independent of filament overlap. They attributed this effect to the passive elastic element, the fascicles, where thick filaments are compressed during active contractions at short lengths. The superposition of these nonlinear dependencies is accounted for in the model of Fig. C.2 by the nonlinearity $f(\varphi)$.

The second effect is activation-independent and also caused by the properties of the passive elastic tissue. This tissue generates tension mainly depending on the muscle length or joint angle, respectively. Thereby, it exhibits nonlinear characteristics: The tissue is slack if the muscle is at resting length or less, and it is stretched at a length higher than resting length. As they are independent of muscle activity, these passive elastic joint torques can be included in the model of the leg, together with the elastic properties of other tissue in parallel to the muscles, such as *ligaments*.

C.2.4 Force-Velocity Dependency

In addition to a force-length characteristic, there is also a force-velocity dependency described by the nonlinear function $g(\dot{\varphi})$ in Fig. C.2. Muscle force generation during shortening (*concentric contraction*) can be explained by the hyperbolic Hill model [106], whereby the muscle force can drop to zero for high shortening velocity. The effects are attributed to break and re-formation of cross-bridges during shortening, as well as damping effects of viscous fluids in the muscle. The separation of these passive and active components is complicated. For lengthening (*eccentric contraction*), the generated force depends heavily on the experimental protocol, which could e.g. be *isotonic* (constant tension) or *isovelocity*. In the first case, the muscle force increases with lengthening velocity, in the second case, it may even decrease, although not to zero. With a value of 1 for *isometric* (constant length) conditions, g increases with lengthening velocity to a plateau at typical maximum values of 1.2 to 1.8 [14]. For concentric contractions, g decreases, and it approaches a minimum of 0 for shortening with ballistic velocities.

Recruitment dynamics (i.e. activation dynamics and recruitment curve) are frequently identified together in a nonlinear identification, but under isometric conditions (constant muscle length, i.e. $\dot{\varphi}_l(t) = 0\,\forall t$). Then, the muscle model of Fig. C.2 has the structure of a Hammerstein Model, as displayed in Fig. 3.1, because the nonlinear influence of muscle length and contraction velocity is eliminated.

C.3 Intrinsic versus Reflexive Feedback

The muscle model above explains the nonlinear viscoelastic characteristics by intrinsic properties of the muscle, yet it neglects the strong influence of reflexive feedback loops in intact limbs. In fact, the observed impedance in the limbs is dominated by such proprioceptive feedback [265]. The feedback loops are closed using the force sensors in the tendon,

the so-called *Golgi-tendon-organs*, as well as the muscle's length and velocity sensors, the *muscle spindles*. In [265], an augmented muscle model including these proprioceptive feedback loops is described. In [220], intrinsic and reflexive feedback are effectively separated and identified using the knowledge that reflexive feedback must exhibit a time delay in contrast to the intrinsic muscle properties. An important observation is that reflexive feedback is highly time-variant and that reflex gains are continuously "tuned" in a way that mechanical resistance to external force disturbances is maximized. Reflexes may still be active although high-level control of the muscles is lost, possibly leading to undesired effects such as spasticity. In the experiments with artificially recruited muscles presented in this thesis, subjects tried to suppress any control of the muscles and to relax, meaning that also the reflex gains were set low, however, it is hardly quantifiable (if not improbable) whether they succeeded. To some extent, the undesired, reflexive feedback can mathematically be regarded as an additional contribution to the functions f (position feedback) and g (velocity feedback) in Fig. C.2, which are simply modeled as arbitrarily time-varying, bounded functions of time t during control design in Chap. 4.

D Analytic Solution of Anti-Causal Hammerstein Identification

D.1 Convexity of Constraints

To justify the statements made in Chap. 3, and more specifically in Sec. 3.3, it is now shown that the set $\mathbf{X}$ defined by the constraints

$$\mathbf{X} = \{\boldsymbol{r} = \begin{pmatrix} r_0 & r_1 & r_2 & r_3 \end{pmatrix}^T \,|\, r_3 \geq 0 \quad \wedge \quad r_2^2 - 3r_3 r_1 \leq 0\}. \tag{D.1}$$

is convex.

Proof. Convexity of $\mathbf{X}$ is shown by checking the condition:

$$\boldsymbol{r}_A \in \mathbf{X} \,\wedge\, \boldsymbol{r}_B \in \mathbf{X} \wedge \lambda \in [0,1] \Rightarrow (\lambda \boldsymbol{r}_A + (1-\lambda)\boldsymbol{r}_B) \in \mathbf{X}. \tag{D.2}$$

The inequality constraints are rewritten using the conventions of [173]:

$$\boldsymbol{h} = \begin{pmatrix} h_1 \\ h_2 \end{pmatrix} = \begin{pmatrix} -r_3 \\ \boldsymbol{r}^T \mathbf{N} \boldsymbol{r} \end{pmatrix} \leq \mathbf{0} \tag{D.3}$$

with

$$\mathbf{N} = \begin{pmatrix} 0 & 0 & 0 & 0 \\ 0 & 0 & 0 & -\frac{3}{2} \\ 0 & 0 & 1 & 0 \\ 0 & -\frac{3}{2} & 0 & 0 \end{pmatrix}.$$

This representation implies that for $\lambda \in [0,1]$:

$$\begin{array}{c} \left.\begin{array}{rcrcl} r_{A,3} & \geq 0 & \wedge & r_{B,3} & \geq 0 \\ \wedge\, \boldsymbol{r}_A^T \mathbf{N} \boldsymbol{r}_A & \leq 0 & \wedge & \boldsymbol{r}_B^T \mathbf{N} \boldsymbol{r}_B & \leq 0 \end{array}\right\} \\ \Rightarrow \left\{\begin{array}{rl} \lambda r_{A,3} + (1-\lambda) r_{B,3} & \geq 0 \\ (\lambda \boldsymbol{r}_A + (1-\lambda)\boldsymbol{r}_B)^T \mathbf{N} (\lambda \boldsymbol{r}_A + (1-\lambda)\boldsymbol{r}_B) & \leq 0 \end{array}\right. \end{array} \tag{D.4}$$

Of the two inequalities to be shown, the first is trivial. For the second to be fulfilled, negativity of the term $\boldsymbol{r}_A^T \mathbf{N} \boldsymbol{r}_B$ has to be verified. This leads to

$$2 r_{A,2} r_{B,2} \overset{!}{\leq} 3(r_{A,1} r_{B,3} + r_{A,3} r_{B,1}). \tag{D.5}$$

The conditions in (D.1) are only fulfilled for nonnegative r_1. The right side of (D.5) is thus always positive. Now, there are two possible cases:

For $\text{sign}(r_{A,2}) \neq \text{sign}(r_{B,2})$, (D.5) is fulfilled.

For $\text{sign}(r_{A,2}) = \text{sign}(r_{B,2})$, a bound for the left side can be derived from (D.1):

$$2r_{A,2}r_{B,2} \leq 6\sqrt{r_{A,1}r_{B,3}r_{A,3}r_{B,1}}. \tag{D.6}$$

Because of

$$2\sqrt{pq} \leq p + q \quad \text{for} \quad p \geq 0 \wedge q \geq 0, \tag{D.7}$$

for real numbers p and q, condition (D.5) is fulfilled in this case, too.

Therefore, the set $\mathbf{X}$ is convex. □

D.2 Optimization

Using a matrix notation of (3.7) for N measured samples:

$$\hat{\mathbf{A}}(\boldsymbol{y}, \boldsymbol{\alpha}) = \begin{pmatrix} g_0(\hat{a}(t_1)) & \dots & g_{m-1}(\hat{a}(t_1)) \\ \dots & \dots & \dots \\ g_0(\hat{a}(t_N)) & \dots & g_{m-1}(\hat{a}(t_N)) \end{pmatrix}, \tag{D.8}$$

the inverse error function C is written as

$$C = \frac{1}{N}||\boldsymbol{u} - \hat{\mathbf{A}}\boldsymbol{r}||^2_{\mathbf{Q}} \tag{D.9}$$

with a positive definite, symmetric weighting matrix $\mathbf{Q}$.

Defining the Lagrange function

$$L = C + \boldsymbol{\mu}^T \boldsymbol{h} \tag{D.10}$$

with the Kuhn-Tucker multiplicators $\boldsymbol{\mu} = [\mu_1 \quad \mu_2]^T$, the first order necessary conditions for optimality of $(\boldsymbol{x}^*, \boldsymbol{\mu}^*)$ are given by

$$\nabla_{\boldsymbol{r}} L(\boldsymbol{x}^*, \boldsymbol{\mu}^*) = \nabla_{\boldsymbol{r}} C + (\nabla_{\boldsymbol{r}} h)^T \boldsymbol{\mu}^* = \mathbf{0}, \tag{D.11}$$

$$\boldsymbol{h}(\boldsymbol{x}^*) \leq \mathbf{0}, \boldsymbol{h}^T(\boldsymbol{x}^*)\boldsymbol{\mu}^* = \mathbf{0}, \boldsymbol{\mu}^* \geq \mathbf{0}. \tag{D.12}$$

The operator ∇ indicates the gradient of a function f in direction of a vector $\boldsymbol{x}$. For reasons of plausibility of the solution, the first inequality constraint will not be strictly active, because this would imply that a decreasing recruitment curve would match the data set better than an increasing one. In this case, the solution is not trustworthy and should be discarded. Therefore, the multiplicator μ_1 will be zero for a valid solution, which allows to write (D.11) as

$$2\hat{\mathbf{A}}^T\mathbf{Q}\hat{\mathbf{A}}\boldsymbol{r}^* - 2\hat{\mathbf{A}}^T\mathbf{Q}\boldsymbol{u} + (\mathbf{N} + \mathbf{N}^T)\boldsymbol{r}^*\mu_2^* = \mathbf{0}. \tag{D.13}$$

The solution of this equation is given for

$$\boldsymbol{r}^* = (\hat{\mathbf{A}}^T\mathbf{Q}\hat{\mathbf{A}} + \frac{1}{2}(\mathbf{N} + \mathbf{N}^T)\mu_2^*)^{-1}\hat{\mathbf{A}}^T\mathbf{Q}\boldsymbol{u}. \tag{D.14}$$

Substituting this in (D.3), the auxiliary equality

$$\boldsymbol{r}^{*T}(\mu_{2p})\mathbf{N}\boldsymbol{r}^{*}(\mu_{2p}) = 0 \tag{D.15}$$

yields a fraction in the preliminary variable μ_{2p} with a polynomial of second order in the numerator. The roots $\mu_{2p,1}, \mu_{2p,2}$ determine the optimal value of μ_2^*:

$$\mu_2^* = \begin{cases} \mu_{2p} & \text{for} \quad \max\{\mu_{2p,1}, \mu_{2p,2}\} > 0 \\ 0 & \text{for} \quad \max\{\mu_{2p,1}, \mu_{2p,2}\} \leq 0 \end{cases} . \tag{D.16}$$

With this value of the Kuhn-Tucker multiplicator and (D.14), the optimal parameter vector $\boldsymbol{r}^*$ of the nonlinearity is found. Calculation time can be saved by calculating the minimum of the unconstrained problem first from (D.14) with $\mu_2 = 0$, and to solve (D.15) for μ_2 only if the constraint is violated.

Because the optimization problem is convex in $\boldsymbol{r}$, the solution at $\boldsymbol{r}^*$ is the global minimum for a given $\boldsymbol{\alpha}$.

E Identification of Leg Biomechanics

E.1 State of the Art

Biomechanical properties differ between subjects, and parameterization for a specific patient is important for model-based control. Approximate values can be taken from the literature or calculated based on empirical formulae, e.g. mass and inertia of certain body segments can be calculated based on segment length and body mass [279]. Although the reliability of this data is acceptable for many purposes such as simulations, they introduce a high degree of uncertainty when used as a basis for controller design.

One possibility is to quantify all parameters in separate tests. The advantage is high robustness, as the number of error sources can be minimized in each test by holding certain factors constant. The biomechanical properties of the leg are often quantified in two separate experimental procedures, a *pull test* and a *pendulum test* [234]: In the *pull test*, passive elastic joint moments are measured: The limb is slowly moved throughout its range of motion. During this procedure, angles are measured with a goniometer, and torques are measured with a dynamometer. In the *pendulum test*, the limb is lifted against gravity and subsequently dropped, while again measuring angles and torques. However, as stated by Stein et al. [234], the pendulum test can only be used if subjects are able to stand on one leg for a few minutes and to relax completely under these conditions, which they reported to be difficult even for healthy control subjects. Therefore, this method is not generally applicable.

A severe disadvantage of separate calibration tests in separate setups is the time needed for each patient, prior to the actual therapy. Therefore, the realization is almost impossible in a practical clinical therapy environment. Therefore, it has been proposed to quantify all the properties in a single, multi-purpose measurement device, e.g. as suggested by Riener and Fuhr, who designed a Multi-Moment Chair [202]. This way, complex biomechanical models can be parameterized. However, although such a procedure allows best possible accuracy, the time this consumes is still considerable and makes its use in daily clinical application difficult.

Identification methods have been suggested for the biomechanical properties of the leg, mainly in the context of linearized models. Standard techniques used for the identification of robot segments can be used. For example, [23] suggested to identify inertial properties of a patient's legs in the specific training device, in this case the Lokomat. Such an approach usually assumes rigid coupling between human and robot. It is also possible to include nonlinearities in the leg, generated by elastic joint moments, in a nonlinear identification approach, e.g. using orthonormal bases [61,92]. The application of this method to estimate the leg's parameters is described in the following.

E.2 Nonlinear Identification

The parameters of the leg model of Sec. 4.2.3, i.e. inertia J_{leg}, gravitational components and elasticity (subsumed in c_{leg}), and damping k_{leg} are identified using the exoskeleton, as described in detail in Lindner's thesis at LSR [144]. Simplifying assumptions are rigid coupling between leg and exoskeleton, dependency of the nonlinear elasticity c_{leg} only on the leg angle φ_{leg}, as well as constant joint damping k_{leg}. A sine sweep position control is applied to the motor, and motor torque and angle are used as inputs for the identification algorithm. After identification of the coupled system leg-exoskeleton, the known drive inertia J_{drv} is subtracted from the identified value.

The leg dynamics are identified in the discrete time domain using state-of-the-art nonlinear identification methods, which are based on orthonormal bases [61, 92]. As this identification method is formulated in the discrete-time, transfer function domain, an alternative, discrete-time description of the leg model in (4.3) is used:

$$y_k = G(z)u_k - G(z)\mathcal{N}(y_k). \tag{E.1}$$

These variables have the following physical notions: $G(z)$ models the linearized mechanical properties of the human shank, and $\mathcal{N}(y_k)$ refers to residual nonlinearities. The input u is the joint torque τ_{leg}, the output y is the joint angle φ_{leg}. The linear discrete dynamics $G(z)$ are described as a weighted superposition of time responses, which are obtained from orthonormal basis functions:

$$G(z) = \sum_{l=0}^{p-1} b_l \mathcal{B}_l(z), \tag{E.2}$$

with p referring to the system order, and b_l being the unknown weighting parameters of the basis functions $\mathcal{B}_l(z)$.

The nonlinearity $\mathcal{N}(y_k)$ (with the output y_k being the discretized joint angle φ_{leg}) is also represented by a weighted sum:

$$\mathcal{N}(y_k) = \sum_{i=0}^{r} a_i g_i(y_k), \tag{E.3}$$

with $g_i(y_k)$ being nonlinear functions depending on y_k. The weightings a_i are unknown parameters.

An efficient methodology for underdamped systems like the leg is to chose the $\mathcal{B}_l(z)$ according to the 2-parameter-Kautz construction described by [92], and this procedure is therefore used here. A least squares estimate is then calculated for the parameter vector, as described in [92]. Choosing the $g_i(y_k)$ as powers of the output y_k with $r = 4$, such that $\mathcal{N}(y_k)$ is a fourth order polynomial, showed the best results. Back-transformation of the identified $G(z)$ into the continuous domain provides the desired representation of (4.3).

The anthropometric data provided by Winter [279] allows to estimate model parameters like the weight m_{leg} of the limb in relation to the entire body mass, as well as center of mass l_s and inertia J_{leg} of the segments. These values are used to estimate the plausibility of the identified results.

The algorithm has been compared to several other identification methods (Linear Prediction Error estimate, Least Squares identification in linear and nonlinear form) [170]. Both in simulations and practical experiments, the Kautz method was found superior concerning exactitude and robustness. Despite the high uncertainty in coupling stiffness, as outlined in Chap. 4, the simplified model of leg and exoskeleton with rigid coupling explains experimental data well: The coefficient of determination R^2 ranges around 0.82 in all data sets. The reliability of the simplified model for leg and orthosis is thus much higher than the reliability of the muscle model presented in Chap. 3.

F State-Space Model of the Hybrid Neuroprosthesis

The explicit matrices of the state space representation

$$\dot{\boldsymbol{x}} = \mathbf{A}(t)\boldsymbol{x} + \mathbf{B}(t)\boldsymbol{u} \tag{F.1}$$
$$y = \boldsymbol{c}^T\boldsymbol{x} \tag{F.2}$$

in Sec. 4.2.6 are:

$$\mathbf{A}(t) = \begin{pmatrix} \mathbf{A}_{\text{fes}} & \mathbf{0} & \mathbf{0} \\ \mathbf{0} & \mathbf{A}_{\text{exo}} & \mathbf{B}_{\text{exo}} \\ \boldsymbol{b}_{\text{leg}}\boldsymbol{c}_{\text{fes}}^T & \boldsymbol{b}_{\text{leg}}\boldsymbol{c}_{\text{exo}}^T & \mathbf{A}_{\text{leg}} + \boldsymbol{b}_{\text{leg}}\boldsymbol{d}_{\text{exo}}^T \end{pmatrix} \tag{F.3}$$

(F.4)

$$= \left(\begin{array}{cc|cc|cc} 0 & 1 & 0 & 0 & 0 & 0 \\ -\omega_0^2 & -2\omega_0 & 0 & 0 & 0 & 0 \\ \hline 0 & 0 & 0 & 1 & 0 & 0 \\ 0 & 0 & -\frac{c_{\text{exo}}}{J_{\text{drv}}} & -\frac{k_{\text{exo}}+v}{J_{\text{drv}}} & \frac{c_{\text{exo}}}{J_{\text{drv}}} & \frac{k_{\text{exo}}}{J_{\text{drv}}} \\ \hline 0 & 0 & 0 & 0 & 0 & 1 \\ \frac{n_{\text{fes}}}{J_{\text{leg}}} & 0 & \frac{c_{\text{exo}}}{J_{\text{leg}}} & \frac{k_{\text{exo}}}{J_{\text{leg}}} & -\frac{c_{\text{leg}}+c_{\text{exo}}}{J_{\text{leg}}} & -\frac{k_{\text{leg}}+k_{\text{exo}}}{J_{\text{leg}}} \end{array}\right) \tag{F.5}$$

(F.6)

$$\mathbf{B}(t) = \begin{pmatrix} \boldsymbol{b}_{\text{fes}} & \mathbf{0} \\ \mathbf{0} & \boldsymbol{b}_{\text{drv}} \\ \mathbf{0} & \mathbf{0} \end{pmatrix} = \begin{pmatrix} 0 & 0 \\ k_{\text{sat}}\omega_0^2 & 0 \\ \hline 0 & 0 \\ 0 & \frac{1}{J_{\text{drv}}} \\ \hline 0 & 0 \\ 0 & 0 \end{pmatrix}, \quad \boldsymbol{c}^T = \begin{pmatrix} 0 & 0 & 1 & 0 & 0 & 0 \end{pmatrix} \tag{F.7}$$

$$\boldsymbol{x} = \begin{pmatrix} \boldsymbol{x}_{\text{fes}} \\ \boldsymbol{x}_{\text{exo}} \\ \boldsymbol{x}_{\text{leg}} \end{pmatrix}, \quad y = \varphi_{\text{drv}}, \quad \boldsymbol{u} = \begin{pmatrix} \tilde{u}_{\text{fes}}(t - T_t) \\ \tau_{\text{drv}} \end{pmatrix}. \tag{F.8}$$

Bibliography

[1] D. K. E. Aarno. *Intention Recognition in Human Machine Collaborative Systems*. Ph.D. thesis, KTH School of Computer Science and Communication, 2007.

[2] R. W. Adams & B. Hannaford. Control Law Design for Haptic Interfaces to Virtual Reality. *IEEE Transactions on Control and Systems Technology*, 10(1):3–13, 2002.

[3] S. K. Agrawal, S. K. Banala, A. Fattah, V. Sangwan, V. Krishnamoorthy, J. R. Scholz & W. L. Hsu. Assessment of motion of a swing leg and gait rehabilitation with a gravity balancing exoskeleton. *IEEE Transactions on Neural Systems and Rehabilitation Engineering*, 15:410–420, 2007.

[4] M. A. Aiserman & F. R. Gantmacher. *Die absolute Stabilität von Regelsystemen*. Oldenbourg-Verlag, 1965.

[5] A. Aitken. On Least Squares and Linear Combinations of Observations. *Proceedings Royal Society of Edinburgh*, 55:42–48, 1935.

[6] A. Alexandrov, A. Frolov & J. Massion. Axial Synergies During Human Upper Trunk Bending. *Experimental Brain Research*, 118(2):210–220, 1998.

[7] R. P. Allred, M. A. Maldonado, J. E. Hsu And & T. A. Jones. Training the "less-affected" forelimb after unilateral cortical infarcts interferes with functional recovery of the impaired forelimb in rats. *Restorative Neurology and Neuroscience*, 23:297–302, 2005.

[8] J. H. Allum & L. R. Young. The relaxed oscillation technique for the determination of the moment of inertia of limb segments. *Journal of Biomechanics*, 9(1):21–25, 1976.

[9] H. Almeida, A. Bhaya, D. Falcao & E. Kaszkurewicz. A team algorithm for robust stability analysis and control design of uncertain time-varying linear systems using piecewise quadratics Lyapunov functions. *International Journal of Robust and Nonlinear Control*, 11:357–371, 2001.

[10] D. S. Andreasen, A. A. Aviles, S. K. Allen, K. B. Guthrie, B. R. Jennings & S. H. Sprigle. Exoskeleton for forearm pronation and supination rehabilitation. *Proceedings of the Annual International Conference of the IEEE EMBS*, 4:2714–2717, 2004.

[11] B. Andrews & R. Baxendale. Hybrid FES orthosis incorporating closed loop control and sensory feedback. *Journal of Biomedical Engineering*, 10:189–195, 1988.

[12] B. T. Angerer, D. Schröder & A. Struppler. Nonlinear System Identification of Muscle Contractions induced by Repetitive Peripheral Magnetic Stimulation. In *Proceedings of the Stuttgart Symposium on Nonlinear Control Systems (NOLCOS),*

Preprints Volume 2, pp. 696–674. IFAC, VDI/VDE, 2004.

[13] D. Aoyagi, W. E. Ichinose, S. J. Harkema, D. J. Reinkensmeyer & J. E. Bobrow. A robot and control algorithm that can synchronously assist in naturalistic motion during body-weight-supported gait training following neurologic injury. *IEEE Transactions on Neural Systems and Rehabilitation Engineering*, 15(3):387–400, 2007.

[14] M. L. Audu & D. T. Davy. The influence of muscle model complexity in musculoskeletal motion modeling. *Journal of Biomechanical Engineering*, 107(2):147–157, 1985.

[15] C. Azevedo & R. Héliot. Rehabilitation of Functional Posture and Walking: Coordination of Healthy and Impaired Limbs. *Journal of Automatic Control*, 15(Supplement):12–14, 2005.

[16] E. Bai. Decoupling the linear and nonlinear parts in Hammerstein model identification. *Automatica*, 40(4):671–676, 2004.

[17] T. J. Bajzek & R. J. Jaeger. Characterization and control of muscle response to electrical stimulation. *Annals of Biomedical Engineering*, 15(5):485–501, 1987.

[18] M. J. Balas. Active control of flexible systems. *Journal of Optimization Theory and Applications*, 25(3):415–436, 1978.

[19] S. Banala, S. Agrawal & J. Scholz. Active Leg Exoskeleton (ALEX) for Gait Rehabilitation of Motor-Impaired Patients. In *Proceedings of the IEEE International Conference on Rehabilitation Robotics (ICORR)*, pp. 401–407. 2007.

[20] R. Baratta, M. Solomonow, B. Zhou, D. Letson, R. Chuinard & R. D'Ambrosia. Muscular Coactivation. The Role of the Antagonist Musculature in Maintaining Knee Stability. *American Journal of Sports Medicine*, 16(2):113–122, 1988.

[21] B. Barmish. Kharitonov's theorem and its extensions and applications: An introduction. In *Proceedings of the IEEE Conference on Decision and Control (CDC)*, volume 26, pp. 2060–2061. 1987.

[22] B. R. Barmish, M. Fu & S. Saleh. Stability of a Polytope of Matrices: Counterexamples. *IEEE Transactions on Automatic Control*, 33:569–572, 1988.

[23] M. Bernhardt. *Entwicklung und Implementierung einer kraftunterstützenden Regelung für eine aktuierte Gangorthese*. Diplomarbeit, Lehrstuhl für Steuerungs- und Regelungstechnik, Technische Universität München, 2004.

[24] M. Bernhardt, B. Angerer, M. Buss & A. Struppler. Nonlinear System Identification in Stroke Rehabilitation. *at-Automatisierungstechnik*, 55(11):570–579, 2007.

[25] N. Bernstein. *The Coordination and Regulation of Movements*. Pergamon Press Ltd., London, 1967.

[26] L. Bevan, Y. Laouris, R. M. Reinking & D. G. Stuart. The effect of the stimulation pattern on the fatigue of single motor units in adult cats. *Journal of Physiology*, 449:85–108, 1992.

[27] P. Beyl, M. Van Damme, R. Van Ham, R. Versluys, B. Vanderborght & D. Lefeber. An exoskeleton for gait rehabilitation: Prototype design and control principle. In *Proceedings of the IEEE International Conference on Robotics and Automation (ICRA)*, pp. 2037–2042. 2008.

[28] C. Böhm, K. Kailing, P. Kröger & A. Zimek. Computing Clusters of Correlation Connected Objects. In *Proceedings of the ACM SIGMOD International Conference on Management of Data (COMAD)*. 2004.

[29] S. Bialas. A Necessary and Sufficient Condition for the Stability of Convex Combinations of Stable Polynomials or Matrices. *Bulletin of the Polish Academy of Sciences*, 33:473–480, 1985.

[30] F. Blanchini. Nonquadratic Lyapunov functions for robust control. *Automatica*, 31:451–461, 1995.

[31] F. Blanchini & S. Miani. Stabilization of LPV systems: state feedback, state estimation and duality. In *Proceedings of the IEEE Conference on Decision and Control (CDC)*, volume 2, pp. 1492–1497. 2003.

[32] F. Blanchini & C. Savorgnan. Stabilizability of switched linear systems does not imply the existence of convex Lyapunov functions. In *Proceedings of the IEEE Conference on Decision and Control (CDC)*, pp. 119–124. 2006.

[33] P. R. Bélanger. Estimation of Noise Covariance Matrices for a Linear Time-Varying Stochastic Process. *Automatica*, 10:267–275, 1974.

[34] P.-A. Bliman. Nonconservative LMI approach to robust stability for systems with uncertain scalar parameters. *Proceedings of the IEEE Conference on Decision and Control (CDC)*, 1:305–310, 2002.

[35] M. Bouri, Y. Stauffer, C. Schmitt, Y. Allemand, S. Gnemmi, R. Clavel, P. Metrailler & R. Brodard. The WalkTrainer: A Robotic System for Walking Rehabilitation. In *Proceedings of the IEEE International Conference on Robotics and Biomimetics (ROBIO)*, pp. 1616–1621. 2006.

[36] S. Boyd, L. E. Ghaoui, E. Feron & V. Balakrishnan. *Linear Matrix Inequalities in Systems and Control Theory*. Society for Industrial and Applied Mathematics (SIAM), 1994.

[37] I. E. Brown, E. J. Cheng & G. E. Loeb. Measured and modeled properties of mammalian skeletal muscle. II. The effects of stimulus frequency on force-length and force-velocity relationships. *Journal of Muscle Research and Cell Motility*, 20(7):627–643, 1999.

[38] I. E. Brown, S. H. Scott & G. E. Loeb. Mechanics of feline soleus: II. Design and validation of a mathematical model. *Journal of Muscle Research and Cell Motility*, 17(2):221–233, 1996.

[39] F. Buchthal & H. Schmalbruch. Contraction times and fibre types in intact human muscle. *Acta Physiologica Scandinavica*, 79(4):435–452, 1970.

[40] S. Buerger & N. Hogan. Complementary Stability and Loop Shaping for Improved Human-Robot Interaction. *IEEE Transactions on Robotics*, 23(2):232–244, 2007.

[41] R. E. Burke, P. Rudomin & F. E. Zajac. The effect of activation history on tension production by individual muscle units. *Brain Research*, 109(3):515–529, 1976.

[42] J. H. Burridge & M. Ladouceur. Clinical and Therapeutic Applications of Neuromuscular Stimulation: A Review of Current Use and Speculation into Future Developments. *Neuromodulation*, 4(4):147–154, 2001.

[43] K. Busch. *Laufbandtherapie per funktioneller Elektrostimulation für Schlaganfallpatienten: Benefits im Vergleich zur Physiotherapie nach Bobath.* Ph.D. thesis, Universität Witten / Herdecke, 2004.

[44] L. L. Cai, A. J. Fong, C. K. Otoshi, Y. Liang, J. W. Burdick, R. R. Roy & V. R. Edgerton. Implications of assist-as-needed robotic step training after a complete spinal cord injury on intrinsic strategies of motor learning. *Journal of Neuroscience*, 26(41):10564–8, 2006.

[45] C. Carignan & K. Cleary. Closed-loop force control for haptic simulation of virtual environments. *Haptics-e*, 1(2), 2000.

[46] M. Casadio, V. Sanguineti, P. G. Morasso & V. Arrichiello. Braccio di Ferro: A new haptic workstation for neuromotor rehabilitation. *Technology and Health Care*, 14:123–142, 2006.

[47] F. Chang, F. Chang & R. Luus. A noniterative method for identification using Hammerstein model. *IEEE Transactions on Automatic Control*, 16(5):464–468, 1971.

[48] G. Chesi, A. Garulli, A. Tesi & A. Vicino. Robust stability of polytopic systems via polynomially parameter-dependent Lyapunov functions. In *Proceedings of the IEEE Conference on Decision and Control (CDC)*, volume 5, pp. 4670–4675. 2003.

[49] G. Chesi, A. Garulli, A. Tesi & A. Vicino. Robust stability of time-varying polytopic systems via parameter-dependent homogeneous Lyapunov functions. *Automatica*, 43(2):309–316, 2007.

[50] C.-M. Chew, G.-S. Hong & W. Zhou. Series Damper Actuator: A Novel Force/Torque Control Actuator. In *Proceedings of the IEEE-RAS/RSJ International Conference on Humanoid Robots*. Los Angeles, CA, USA, 2004.

[51] D. S. Chou. *Efficacy of Hammerstein Models in Capturing the Dynamics of Isometric Muscle Stimulated at Various Frequencies*. Master's thesis, Massachusetts Institute of Technology, 2006.

[52] A. Chu, H. Kazerooni & A. Zoss. On the Biomimetic Design of the Berkeley Lower Extremity Exoskeleton (BLEEX). In *Proceedings of the IEEE International Conference on Robotics and Automation (ICRA)*, pp. 4356–4363. 2005.

[53] E. Colgate & N. Hogan. An analysis of contact instability in terms of passive physical equivalents. In *Proceedings of the IEEE International Conference on Robotics and Automation (ICRA)*, pp. 404–409. Scottsdale, AZ, USA, 1989.

[54] J. E. Colgate. *The Control of Dynamically Interacting Systems*. Ph.D. thesis, MIT Department of Mechanical Engineering, 1988.

[55] G. Colombo, M. Joerg, R. Schreier & V. Dietz. Treadmill training of paraplegic patients using a robotic orthosis. *Journal of Rehabilitation Research and Development*, 37(6):693–700, 2000.

[56] G. Colombo, M. Jörg & S. Jezernik. Automatisiertes Lokomotionstraining auf dem Laufband. *at-Automatisierungstechnik*, 50:287–295, 2002.

[57] J. Craig. *Introduction to Robotics: Mechanics and Control*. Addison-Wesley Publishing company Inc. USA, 2nd edition, 1989.

[58] L. Crawford, V. Iragavarapu & P. Menon. Numerical synthesis of nonlinear adaptive control systems for missiles. In *Proceedings of the American Control Conference (ACC)*. 2000.

[59] V. Darsalia, U. Heldmann, O. Lindvall & Z. Kokaia. Stroke-Induced Neurogenesis in Aged Brain. *Stroke*, 36(8):1790–1795, 2005.

[60] M. Davis & R. Vinter. *Stochastic Modelling and Control*. Chapman and Hall, London, 1985.

[61] T. J. de Hoog. *Rational orthonormal bases and related transforms in linear system modeling*. Ph.D. thesis, Technische Universiteit Delft, 2001.

[62] R. de Leon, J. Hodgson, R. Roy & V. Edgerton. Locomotor capacity attributable to step training versus spontaneous recovery after spinalization in adult cats. *Journal of Neurophysiology*, 79:1329–1340, 1998.

[63] P. Deetjen. *Physiologie*. Urban & Schwarzenberg, München, 2nd edition, 1994.

[64] E. Demeester, A. Huntemann, D. Vanhooydonck, G. Vanacker, A. Degeest, H. V. Brussel & M. Nuttin. Bayesian Estimation of Wheelchair Driver Intents: Modeling Intents as Geometric Paths Tracked by the Driver. In *Proceedings of the IEEE/RSJ International Conference on Intelligent Robots and Systems (IROS)*, pp. 5775–5780. 2006.

[65] J. B. Dingwell, B. L. Davis & D. M. Frazier. Use Of An Instrumented Treadmill For Real-Time Gait Symmetry Evaluation And Feedback In Normal And Below-Knee Amputee Subjects. *Prosthetics and Orthotics International*, 20:101–110, 1996.

[66] A. Dollar & H. Herr. Active Orthoses for the Lower-Limbs: Challenges and State of the Art. In *Proceedings of the IEEE International Conference on Rehabilitation Robotics (ICORR)*, pp. 968–977. 2007.

[67] A. Duschau-Wicke, J. Zitzewitz, M. Wellner, A. König, L. Lünenburger & R. Riener. Path Control - A Strategy for Patient-Cooperative Training of Gait Timing. In *Proceedings of the Automed Workshop, Fortschritt-Berichte VDI, Reihe 17, Nr. 267, 7*, pp. 1–2. 2007.

[68] J. Duysens & H. V. de Crommert. Neural Control of Locomotion: The Central Pattern Generator from Cats to Humans. *Gait & Posture*, 7(2):131–141, 1998.

[69] T. Edrich, R. Riener & J. Quintern. Analysis of Passive Elastic Joint Moments in Paraplegics. *IEEE Transactions on Biomedical Engineering*, 47(8):1058–1065, 2000.

[70] R. Ekkelenkamp, E. van Asseldonk, B. Koopman, P. H. Veltink, S. Stramigioli & H. van der Kooij. Swing Phase Adaptation during Walking by Virtual Model Control of a Powered Exoskeleton. *IEEE Transactions on Neural Systems and Rehabilitation Engineering*, 2008. Submitted for Special Issue on Lower Extremity Exoskeletons.

[71] R. Ekkelenkamp, J. Veneman & H. van der Kooij. LOPES: Selective control of gait functions during the gait rehabilitation of CVA patients. In *Proceedings of the IEEE International Conference on Rehabilitation Robotics (ICORR)*, pp. 361– 364. 2005.

[72] T. Elbert, H. Flor, N. Birbaumer, S. Knecht, S. Hampson, W. L. W & E. Taub. Extensive reorganization of the somatosensory cortex in adult humans after nervous system injury. *Neuroreport*, 5(18):2593–2597, 1994.

[73] T. Elbert, C. Pantev, C. Wienbruch, B. Rockstroh & E. Taub. Increased cortical representation of the fingers of the left hand in string players. *Science*, 270(5234):305–307, 1995.

[74] J. L. Emken, R. Benitez & D. J. Reinkensmeyer. Human-robot cooperative movement training: Learning a novel sensory motor transformation during walking with robotic assistance-as-needed. *Journal of NeuroEngineering and Rehabilitation*, 4(8), 2007.

[75] J. L. Emken & D. J. Reinkensmeyer. Robot-enhanced motor learning: accelerating internal model formation during locomotion by transient dynamic amplification. *IEEE Transactions on Neural Systems and Rehabilitation Engineering*, 13:33, 2005.

[76] S. D. Eppinger & W. P. Seering. Understanding bandwidth limitations in robot force control. In *Proceedings of the International Conference on Robotics and Automation (ICRA)*, pp. 904– 909. 1987.

[77] Z. Erim, C. J. D. Luca, K. Mineo & T. Aoki. Rank-ordered regulation of motor units. *Muscle & Nerve*, 19(5):563–573, 1996.

[78] H. Esen, A. Sachsenhauser, K. Yano & M. Buss. A Multi-User Virtual Training System Concept and Objective Assessment of Trainings. In *Proceedings of the IEEE International Symposium on Robot and Human Interactive Communication (RO-MAN)*, pp. 1084–1089. 2007.

[79] P. C. Eser, N. de N Donaldson, H. Knecht & E. Stüssi. Influence of different stimulation frequencies on power output and fatigue during FES-cycling in recently injured SCI people. *IEEE Transactions on Neural Systems and Rehabilitation Engineering*, 11(3):236–240, 2003.

[80] B. Everitt. *Cambridge Dictionary of Statistics*. CUP, 2nd edition, 2002.

[81] B. Feinstein, B. Lindegard, E. Nyman & G. Wohlfart. Morphologic studies of motor units in normal human muscles. *Acta anatomica (Basel)*, 23(2):127–142, 1955.

[82] M. Ferraro, J. J. Palazzolo, J. Krol, H. I. Krebs, N. Hogan & B. T. Volpe. Robot-aided sensorimotor arm training improves outcome in patients with chronic stroke. *Neurology*, 61(11):1604–7, 2003.

[83] C. Fleischer. *Controlling Exoskeletons with EMG signals and a Biomechanical Body Model*. Ph.D. thesis, Technische Universität Berlin, 2007.

[84] M. Fliess, J. L. Lévine, P. Martin & P. Rouchon. Flatness and defect of nonlinear systems: Introductory theory and examples. *International Journal of Control*, 61(6):1327–1361, 1995.

[85] H. Franken, A. van Harn, P. Veltink, M. Thomsen & H. Boom. The effect of a stimulation pattern on force and fatigue of paralyzed human quadriceps. In *Proceedings of the Annual International Conference of the IEEE Engineering in Medicine and Biology Society (EMBS)*, pp. 1184–1185. 1993.

[86] H. M. Franken, P. H. Veltink, G. Baardman, R. A. Redmeyer & H. B. Boom. Cycle-to-cycle control of swing phase of paraplegic gait induced by surface electrical stimulation. *Medical & Biological Engineering & Computing*, 33(3):440–451, 1995.

[87] M. Fu & B. R. Barmish. Stability of Convex and Linear Combinations of Polynomials and Matrices Arising in Robustness Problems. In *Proceedings of the Conference on Information Sciences and Systems (CISS)*. 1987.

[88] T. Fuhr. *Ein kooperatives, patientengeführtes Regelungssystem zur Bewegungsrestitution mit einer Neuroprothese*. Ph.D. thesis, Lehrstuhl für Steuerungs- und Regelungstechnik, Technische Universität München, 2004.

[89] T. Fuhr & J. Quintern. Stair Ascending and Descending with the Cooperative Neuroprosthesis WALK. *International Neuromodulation Society*, 6(1):57–67, 2003.

[90] M. A. Giese & T. Poggio. Morphable Models for the Analysis and Synthesis of Complex Motion Patterns. *International Journal of Computer Vision*, 38(1):59–73, 2000.

[91] P. Goldsmith, B. Francis & A. Goldenberg. Stability of Hybrid Position/force Control Applied to Manipulators With Flexible Joints. *International Journal of Robotics and Automation*, 14(4), 1999.

[92] J. C. Gomez & E. Baeyens. Identification of Nonlinear Systems Using Orthonormal Bases. In *Proceedings of the IASTED International Conference on Intelligent Systems and Control (ISC)*, pp. 126–131. Tampa, Florida, U.S.A, 2001.

[93] W. B. Griffin. *Shared Control for Dexterous Telemanipulation with Haptic Feedbak*. Ph.D. thesis, Dept of Mechanical Engineering, Stanford University, 2003.

[94] D. Grimes, W. C. Flowers & M. Donath. Feasibility of an active control scheme for A/K prostheses. *Journal of Biomedical Engineering*, 99:215–221, 1977.

[95] M. A. Guadagnoli & T. D. Lee. Challenge point: a framework for conceptualizing the effects of various practice conditions in motor learning. *Journal of Motor Behavior*, 36(2):212–224, 2004.

[96] R. V. Ham, B. Vanderborght, B. Verrelst, M. V. Damme & D. Lefeber. MACCEPA: the Mechanically Adjustable Compliance and Controllable Equilibrium Position Actuator used in the Controlled Passive Walking biped Veronica. In *Proceedings of the International Symposium on Measurement and Control in Robotics (ISMCR)*. 2005.

[97] W. S. Harwin. Robots with a gentle touch: advances in assistive robotics and prosthetics. *Technology and Health Care*, 7(6):411–417, 1999.

[98] M. Hashimoto & Y. Imamura. An Instrumented Compliant Wrist Using a Parallel Mechanism. In *Proceedings of the ASME Japan/USA Symposium on Flexible Automation (ISFA)*, pp. 741–744. 1992.

[99] H. Hatze. A complete set of control equations for the human musculo-skeletal system. *Journal of Biomechanics*, 10:799–805, 1977.

[100] T. Hayashi, T. Tanaka & M. Q. Feng. Smart Power Suit with Variable Stiffness Mechanism. In *Proceedings of the 2004 IEEE International Workshop on Robot and Human Interactive Communication*, pp. 20–22. Kurashiki, Okayama Japan, 2004.

[101] H. Herr, A. Wilkenfeld & J. Blaya. Patient-Adaptive Prosthetic and Orthotic Leg Systems. In *Proceedings of the 12th Nordic Baltic Conference on Biomedical Engineering and Medical Physics*, pp. 123–128. Reykjavik, Iceland, 2002.

[102] S. Hesse, H. Schmidt, C. Werner & A. Bardeleben. Upper and lower extremity robotic devices for rehabilitation and for studying motor control. *Current Opinion in Neurology*, 16:705–710, 2003.

[103] S. Hesse, G. Schulte-Tigges, M. Konrad, A. Bardeleben & C. Werner. Robot-assisted arm trainer for the passive and active practice of bilateral forearm and wrist movements in hemiparetic subjects. *Archives of Physical Medicine and Rehabilitation*, 84(6):915–920, 2003.

[104] S. Hesse & D. Uhlenbrock. A Mechanized Gait Trainer for Restoration of Gait. *Journal of Rehabilitation Research and Development*, 37(6):701–708, 2000.

[105] S. Hesse, D. Uhlenbrock & T. Sarkodie-Gyan. Gait pattern of severely disabled hemiparetic subjects on a new controlled gait trainer as compared to assisted treadmill walking with partial body weight support. *Clinical Rehabilitation*, 13:401–10., 1999.

[106] A. V. Hill. The heat of shortening and the dynamic constants of muscle. *Proceedings of the Royal Society of London Series B, Biological Sciences*, B126:136–195, 1938.

[107] S. Hirokawa, M. Grimm, T. Le, M. Solomonow, R. Baratta, H. Shoji & R. D'Ambrosia. Energy Consumption of Paraplegics Gait Using Five Different Walking Orthoses. In *Proceedings of the Annual International Conference of the IEEE Engineering in Medicine and Biology Society (EMBS)*, volume 3, pp. 1014 – 1015. Seattle, WA, 1989.

[108] N. Hogan. Impedance control: An approach to manipulation. Part I - Theory, Part II - Implementation, Part III - Applications. *ASME Journal of Dynamic Systems, Measurement, and Control*, 107:1–24, 1985.

[109] N. Hogan, H. Krebs, A. Sharon & J. Charnnarong. Interactive robotic therapist. US patent 5,466,213, 1995.

[110] N. Hogan, H. I. Krebs, B. Rohrer, J. J. Palazzolo, L. Dipietro, S. E. Fasoli, J. Stein, R. Hughes, W. R. Frontera, D. Lynch & B. T. Volpe. Motions or muscles?: Some behavioral factors underlying robotic assistance of motor recovery. *Journal of Reha-*

bilitation Research & Development, 43(5):605–18, 2006.

[111] K. Hollander, T. Sugar & D. Herring. Adjustable Robotic Tendon using a 'Jack Spring'. In *Proceedings of the IEEE International Conference on Rehabilitation Robotics (ICORR)*, pp. 113–118. 2005.

[112] J. M. Hollerbach, I. W. Hunter & J. Ballantyne. *The robotics review 2*, chapter A comparative analysis of actuator technologies for robotics, pp. 299–342. MIT Press, Cambridge, MA, USA, 1992.

[113] P. Horisberger, H.; Belanger. Regulators for linear, time invariant plants with uncertain parameters. *IEEE Transactions on Automatic Control*, 21(5):705 – 708, 1976.

[114] T. G. Hornby, D. D. Campbell, J. H. Kahn, T. Demott, J. L. Moore & H. R. Roth. Enhanced gait-related improvements after therapist- versus robotic-assisted locomotor training in subjects with chronic stroke: a randomized controlled study. *Stroke*, 39(6):1786–1792, 2008.

[115] K. J. Hunt, M. Munih, N. Donaldson & F. M. D. Barr. Optimal Control of Ankle Joint Moment: Toward Unsupported Standing in Paraplegia. *IEEE Transactions on Automatic Control*, 43(6):819–832, 1998.

[116] K. J. Hunt, M. Munih, N. N. Donaldson & F. M. Barr. Investigation of the Hammerstein hypothesis in the modeling of electrically stimulated muscle. *IEEE Transactions on Biomedical Engineering*, 45(8):998–1009, 1998.

[117] K. J. Hunt, B. Stone, N.-O. Negård, T. Schauer, M. H. Fraser, A. J. Cathcart, C. Ferrario, S. A. Ward & S. Grant. Control Strategies for Integration of Electric Motor Assist and Functional Electrical Stimulation in Paraplegic Cycling: Utility for Exercise Testing and Mobile Cycling. *IEEE Transactions on Neural Systems and Rehabilitation Engineering*, 12(1):89–101, 2004.

[118] B. Husemann, F. Müller, C. Krewer, S. Heller & E. Koenig. Effects of locomotion training with assistance of a robot-driven gait orthosis in hemiparetic patients after stroke: a randomized controlled pilot study. *Stroke*, 38(2):349–354, 2007.

[119] W. Ilg, H. Golla, P. Thier & M. A.Giese. Specific influences of cerebellar dysfunctions on gait. *Brain*, 130:786–798, 2007.

[120] J. F. Israel, D. D. Campbell, J. H. Kahn & T. G. Hornby. Metabolic costs and muscle activity patterns during robotic- and therapist-assisted treadmill walking in individuals with incomplete spinal cord injury. *Physical Therapy*, 86(11):1466–1478, 2006.

[121] B. Itschner. Einführung Idealer Ljapunov-Funktionen. *Regelungstechnik*, 7:216–222, 1977.

[122] S. Jezernik, G. Colombo, T. Keller, H. Frueh & M. Morari. Robotic orthosis Lokomat: A research and rehabilitation tool. *Neuromodulation*, 6 (2):108–115, 2003.

[123] S. Jezernik, G. Colombo & M. Morari. Automatic Gait-Pattern Adaptation Algorithms for Rehabilitation With a 4-DOF Robotic Orthosis. *IEEE Transactions on Robotics and Automation*, 20(3):574–582, 2004.

[124] M. Johansson & A. Rantzer. Computation of piecewise quadratic Lyapunov functions for hybrid systems. *IEEE Transactions on Automatic Control*, 43(4):555–559, 1998.

[125] I. T. Jolliffe. *Principal Component Analysis*. Springer- Verlag, New York, 2nd edition, 2002.

[126] R. H. C. Jr & D. E. Rosenthal. Experiments in Control of Flexible Structures with Noncolocated Sensors and Actuators. *Journal of Guidance*, 7(5):546–553, 1984.

[127] M. Kachourbos. Relief at Last. *TeamRehab Report*, 8:31–351, 1997.

[128] Z. Z. Karu, W. K. Durfee & A. M. Barzilai. Reducing muscle fatigue in FES applications by stimulating with N-let pulse trains. *IEEE Transactions on Biomedical Engineering*, 42(8):809–817, 1995.

[129] D. Katic & M. Vukobratovic. Survey of Intelligent Control Techniques for Humanoid Robots. *Journal of Intelligent and Robotic Systems*, 37:117–141, 2003.

[130] H. Kawamoto & S. Kanbe. Power Assist Method for HAL3, Estimating Operator Intention Based on Motion Information. In *Proceedings of the IEEE International Workshop on Robot and Human Interactive Communication*, pp. 67–72. 2003.

[131] H. Kazerooni, J.-L. Racine, L. Huang & R. Steger. On the Control of the Berkeley Lower Extremity Exoskeleton (BLEEX). In *Proceedings of the IEEE International Conference on Robotics and Automation (ICRA)*, pp. 4364–4371. 2005.

[132] T. Keller. *Surface Functional Electrical Stimulation (FES) Neuroprostheses for Grasping*. Ph.D. thesis, ETH Zürich, 2001.

[133] V. L. Kharitonov. [Asymptotic stability of an equilibrium position of a family of systems of differential equations]. *Differentsialnye uravneniya*, 14:2086–2088, 1978. (Russian).

[134] M. Kim, J. Weber & S. Cha. A Design of a Modular Force Sensing Robot Arm for Self-Assembling Robots in a System. In *Proceedings of Robotics and Applications*. Honolulu, Hawaii USA, 2006.

[135] D. Kleinman. Optimal control of linear systems with time-delay and observation noise. *IEEE Transactions on Automatic Control*, 14(5):524–527, 1969.

[136] K. Kong & D. Jeon. Design and control of an exoskeleton for the elderly and patients. *IEEE/ASME Transactions on Mechatronics*, 11(4):428–432, 2006.

[137] A. I. Kostiukov. [The nonlinear properties of changes in length of an active muscle]. *Neirofiziologiia*, 20(6):736–743, 1988.

[138] H. I. Krebs, J. J. Palazzolo, L. Dipietro, B. T. Volpe & N. Hogan. Rehabilitation robotics: Performance-based progressive robot-assisted therapy. *Autonomous Robots*, 15:7–20, 2003.

[139] A. E. Kritter. Myoelectric prostheses. *The Journal of Bone and Joint Surgery (American Volume)*, 67(4):654–657, 1985.

[140] G. Kwakkel, R. van Peppen, R. C. Wagenaar, S. Wood Dauphinee, C. Richards, A. Ashburn, K. Miller, N. Lincoln, C. Partridge, I. Wellwood & P. Langhorne. Effects of augmented exercise therapy time after stroke: a meta-analysis. *Stroke*, 35:2529–39, 2004.

[141] G. Kwakkel, R. C. Wagenaar, T. W. Koelman, G. J. Lankhorst & J. C. Koetsier. Effects of intensity of rehabilitation after stroke. A research synthesis. *Stroke*, 28(8):1550–6, 1997.

[142] F. Lacquaniti, R. Grasso & M. Zago. Motor Patterns in Walking. *News Physiol Sci*, 14:168–174, 1999.

[143] M. Levy, J. Mizrahi & Z. Susak. Recruitment, force and fatigue characteristics of quadriceps muscles of paraplegics isometrically activated by surface functional electrical stimulation. *Journal of Biomedical Engineering*, 12(2):150–156, 1990.

[144] A. Lindner. Identifikation biomechanischer Parameter der unteren Extremitäten. Studienarbeit, Lehrstuhl für Steuerungs- und Regelungstechnik, Technische Universität München, 2006.

[145] G. E. Loeb, R. A. Peck, W. H. Moore & K. Hood. BION system for distributed neural prosthetic interfaces. *Medical Engineering & Physics*, 23(1):9–18, 2001.

[146] A. Lyapunov. *The General Problem of the Stability of Motion*. Taylor and Francis, 1992. English translation of the original 1892 Russian version.

[147] G. M. Lyons, T. Sinkjaer, J. H. Burridge & D. J. Wilcox. A review of portable FES-based neural orthoses for the correction of drop foot. *IEEE Transactions on Neural Systems and Rehabilitation Engineering*, 10(4):260–279, 2002.

[148] C. D. Mah, M. Hulliger, R. G. Lee & I. S. O'Callaghan. Quantitative Analysis of Human Movement Synergies: Constructive Pattern Analysis for Gait. *J Mot Behav*, 26(2):83–102., 1994.

[149] P. Mai & C. Hillermeier. Least-Squares-basierte Ableitungsschätzung: Theorie und Einstellregeln für den praktischen Einsatz. *at-Automatisierungstechnik*, 56(10):530–538, 2008.

[150] G. E. Mann, J. H. Burridge, L. Malone & P. Strike. A pilot study to investigate the effects of electrical stimulation on recovery of hand function and sensation in subacute stroke patients. *Neuromodulation*, 8(3):193 – 202, 2005).

[151] V. Z. Marmarelis & X. Zhao. Volterra models and three-layer perceptrons. *IEEE Transactions on Neural Networks*, 8(6):1421–1433, 1997.

[152] N. Mazzaro, E. Spaich, O. Andersen, M. Grey, D. Popović & T. Sinkjær. Electrical stimulation augmented rehabilitation of hemiparetic gait. In *Proceedings of the IEEE EMBS Annual International Conference*. New York, 2006.

[153] P. K. Menon & V. R. Iragavarapu. Adaptive Techniques for Multiple Actuator Blending. In *Proceedings of the American Control Conference (ACC)*. Chicago, Illinois, 2000.

[154] P. Metrailler, V. Blanchard, I. Perrin, R. Brodard, R. Frischknecht, C. Schmitt, J. Fournier, M. Bouri & R. Clavel. Improvement of rehabilitation possibilities with the MotionMaker. In *Proceedings of the IEEE/RAS-EMBS International Conference on Biomedical Robotics and Biomechatronics (BioRob)*, pp. 359–364. 2006.

[155] H. S. Milner-Brown & R. B. Stein. The relation between the surface electromyogram and muscular force. *Journal of Physiology*, 246(3):549–569, 1975.

[156] H. S. Milner-Brown, R. B. Stein & R. Yemm. The contractile properties of human motor units during voluntary isometric contractions. *Journal of Physiology*, 228(2):285–306, 1973.

[157] J. Misuraca & C. Mavroidis. Lower Limb Human Muscle Enhancer. In *Proceedings of the International Mechanical Engineering Conference and Exposition (IMECE)*, pp. 1–7. New York, 2001.

[158] S. Mohammed, P. Poignet, P. Fraisse & D. Guiraud. *Rehabilitation Robotics*, chapter Rehabilitation of the Paralyzed Lower Limbs Using Functional Electrical Stimulation: Robust Closed Loop Control, pp. 387–358. Itech Education and Publishing, Vienna, Austria, 2007.

[159] F. Multon, L. France, M.-P. Cani & G. Debunne. Computer Animation of Human Walking: a Survey. *Journal of Visualization and Computer Animation (JVCA)*, 10:39–54, 1999.

[160] M. Munih, K. Hunt & N. Donaldson. Variation of recruitment nonlinearity and dynamic response of ankle plantarflexors. *Medical Engineering & Physics*, 22(2):97–107, 2000.

[161] K. Nagai, S. Iwasa, Y. Nakagawa & K. Ohno. Development of a redundant macro-micro manipulator for compliantmotion. In *Proceedings of the International Conference on Advanced Robotics*. 1997.

[162] H. Nahrstaedt, T. Schauer, S. Hesse & J. Raisch. Iterativ Lernende Regelung einer Gang-Neuroprothese. *at-Automatisierungstechnik*, 56(9):494–501, 2008.

[163] K. Narendra & A. Annaswamy. *Stable adaptive control*. Prentice Hall, 1989.

[164] K. Narendra, K. Narendra & P. Gallman. An iterative method for the identification of nonlinear systems using a Hammerstein model. *IEEE Transactions on Automatic Control*, 11(3):546–550, 1966.

[165] K. Narendra & J. Taylor. *Frequency domain criteria for absolute stability*. Academic Press Inc, New York, 1973.

[166] T. Nef, D. Brennan, I. Black & J. Hidler. Patient-tracking for an Over-ground Gait Training System. In *Submitted for the IEEE International Conference on Robotics and Automation (ICRA)*. 2009.

[167] T. Nef, M. Mihelj & R. Riener. ARMin: a robot for patient-cooperative arm therapy. *Medical & Biological Engineering & Computing*, 45(9):887–900, 2007.

[168] G. Nelles. Cortical reorganization–effects of intensive therapy. *Restorative Neurology and Neuroscience*, 22:239–44, 2004.

[169] P. Neuhaus, M. O'Sullivan, D. Eaton, J. Carff & J. Pratt. Concept designs for underwater swimming exoskeletons. In *Proceedings of the IEEE International Conference on Robotics and Automation (ICRA)*, volume 5, pp. 4893–4898. 2004.

[170] M. Neumaier. *Vergleich verschiedener Regelungsstrategien einer hybriden Neuroprothese*. Master's thesis, Lehrstuhl für Steuerungs- und Regelungstechnik, Technische Universität München, 2007.

[171] J. Nikitczuk, B. Weinberg & C. Mavroidis. RehAbilitative Knee Orthosis Driven by Electro-Rheological Fluid Based Actuators. In *Proceedings of the IEEE International Conference on Robotics and Automation (ICRA)*, pp. 2283–2289. 2005.

[172] N. I. of Neurological Disorders & Stroke. NINDS Stroke Information Page. http://www.ninds.nih.gov/disorders/stroke/stroke.htm, 2007.

[173] M. Papageorgiou. *Optimierung. Statische, dynamische, stochastische Verfahren für die Anwendung*. Oldenbourg-Verlag, 1991.

[174] J. Park. *Control Strategies for Robots in Contact*. Ph.D. thesis, Stanford University, 2006.

[175] F. Parmiggiani & R. B. Stein. Nonlinear summation of contractions in cat muscles. II. Later facilitation and stiffness changes. *Journal of General Physiology*, 78(3):295–311, 1981.

[176] J. L. Patton, M. E. Stoykov, M. Kovic & F. A. Mussa-Ivaldi. Evaluation of robotic training forces that either enhance or reduce error in chronic hemiparetic stroke survivors. *Experimental Brain Research*, 168(3):368–383, 2006.

[177] K. Pearson. On Lines and Planes of Closest Fit to Systems of Points in Space. *Philosophical Magazine*, 2(6):559–572., 1901.

[178] E. J. Perreault, S. J. Day, M. Hulliger, C. J. Heckman & T. G. Sandercock. Summation of forces from multiple motor units in the cat soleus muscle. *Journal of Neurophysiology*, 89(2):738–744, 2003.

[179] J. Perry. *Gait Analysis: Normal and Pathological Function*. Slack, Inc., 1992.

[180] M. Peshkin, D. A. Brown, J. J. Santos-Munné, A. Makhlin, E. Lewis, J. E. Colgate, J. Patton & D. Schwandt. KineAssist: A robotic overground gait and balance training device. In *Proceedings of the IEEE International Conference on Rehabilitation Robotics (ICORR)*, pp. 241–246. Chicago, 2005.

[181] P.Glardon, R. Boulic & D. Thalmann. PCA-Based Walking Engine Using Motion Capture Data. In *Proceedings of Computer Graphics International 2004*, pp. 292–298. 2004.

[182] R. Pintelon & J. Schoukens. *System identification: a frequency domain approach*. John Wiley and Sons, 2001.

[183] M. Pohl, C. Werner, M. Holzgraefe, G. Kroczek, J. Mehrholz, I. Wingendorf, G. Hoolig, R. Koch & S. Hesse. Repetitive locomotor training and physiotherapy improve walking and basic activities of daily living after stroke: a single-blind, randomized multicentre trial (DEutsche GAngtrainerStudie, DEGAS). *Clinical Rehabilitation*, 21:17–27, 2007.

[184] F. Popescu, J. M. Hidler & W. Z. Rymer. Elbow impedance during goal-directed movements. *Experimental Brain Research*, 152(1):17–28, 2003.

[185] D. Popović. A Customized Model For Control Of Movement With Neuroprostheses. In *On-line Proceedings of the 6th Internet World Congress on Biomedical Sciences*, p. http://www.uclm.es/inabis2000/symposia/files/063/session.htm. Castilla La Mancha University, Spain, 2000.

[186] D. Popović & T. Sinkjær. *Control of Movement for the Physically Disabled*. Springer, 2000.

[187] D. Popović, R. Stein & R. Tomović. *Nonanalytical Methods for Motor Control*. World Scientific Pub, 1995.

[188] D. Popović, R. Tomović & L. Schwirtlich. Hybrid assistive system–the motor neuroprosthesis. *IEEE Transactions on Biomedical Engineering*, 36(7):729–737, 1989.

[189] D. Popović, R. Tomović & D. Tepavac. Control aspects of active above-knee prosthesis. *Int J Man-Machine Studies*, 35(6):751–767, 1991.

[190] D. B. Popović & M. B. Popović. Hybrid Assistive Systems for Rehabilitation : Lessons Learned from Functional Electrical Therapy in Hemiplegics. In *Proceedings of the Annual International Conference of the IEEE Engineering in Medicine and Biology Society (EMBS)*. New York, USA, 2006.

[191] D. B. Popović, M. B. Popović, T. Sinkjaer, A. Stefanovic & L. Schwirtlich. Therapy of paretic arm in hemiplegic subjects augmented with a neural prosthesis: a cross-over study. *Canadian Journal of Physiology and Pharmacology*, 82(8-9):749–756, 2004.

[192] M. B. Popović, D. B. Popović, T. Sinkjær, A. Stefanović & L. Schwirtlich. Clinical evaluation of functional electrical therapy in acute hemiplegic subjects. *Journal of Rehabilitation Research and Development*, 40(5):443–454, 2003.

[193] A. Popović-Bijelić, G. Bijelić, N. Jorgovanović, D. Bojanić, M. B. Popović & D. B. Popović. Multi-field surface electrode for selective electrical stimulation. *Artif Organs*, 29(6):448–452, 2005.

[194] G. A. Pratt, M. M. Williamson, P. Dillworth, J. Pratt, K. Ulland & A. Wright. Stiffness Isn't Everything. In *International Symposium on Experimental Robotics (ISER)*. 1995.

[195] G. A. Pratt, P. Willisson, C. Bolton & A. Hofman. Late Motor Processing in Low-Impedance Robots: Impedance Control of Series-Elastic Actuators. In *Proceedings of the 2004 ACC*, pp. 3245–3251. 2004.

[196] J. Pratt, B. Krupp, C. Morse & S. Collins. The RoboKnee: An exoskeleton for enhancing strength and endurance during walking. In *Proceedings of the IEEE International Conference on Robotics and Automation (ICRA)*, pp. 2430–2435. 2004.

[197] M. Rank. Identifikation von Muskeldynamiken und Prädiktive Regelung Funktioneller Elektrischer Stimulation. Projektpraktikum, Lehrstuhl für Steuerungs- und Regelungstechnik, Technische Universität München, 2006.

[198] M. Rank. Modellbasierte Regelung von FES unter Berücksichtigung von Eigenaktivität und Muskelermüdung des Patienten. Bachelor Thesis, LSR, Technische Universität München, 2006.

[199] D. J. Reinkensmeyer, D. Aoyagi, J. L. Emken, J. A. Galvez, W. Ichinose, G. Kerdanyan, S. Maneekobkunwong, K. Minakata, J. A. Nessler, R. Weber, R. R. Roy, R. de Leon, J. E. Bobrow, S. J. Harkema & V. R. Edgerton. Tools for understanding and optimizing robotic gait training. *Journal of Rehabilitation Research & Development*, 43(5):657–70, 2006.

[200] D. S. Reisman & J. P. Scholz. Aspects of Joint Coordination are Preserved During Pointing in Persons with Post-Stroke Hemiparesis. *Brain*, 126(11):2510–2527, 2003.

[201] M. C. Ridding & J. C. Rothwell. Afferent input and cortical organisation: a study with magnetic stimulation. *Experimental Brain Research*, 126(4):536–544, 1999.

[202] R. Riener, M. Angeli, T. Fuhr, N. Donaldson & D. Wood. A New Design of a Multi-Moment-Chair System. In *6th Conference of the International Functional Electrical Stimulation Society (IFESS)*, pp. 288–290. Cleveland, OH, USA, 2001.

[203] R. Riener, M. Frey, T. Pröll, F. Regenfelder & R. Burgkart. Phantom-based multimodal interactions for medical education and training: the Munich Knee Joint Simulator. *IEEE Trans Inf Technol Biomed*, 8(2):208–216, 2004.

[204] R. Riener & T. Fuhr. Patient-Driven Control of FES-Supported Standing Up: A Simulation Study. *IEEE Transactions on Rehabilitation Engineering*, 6:113–124, 1998.

[205] R. Riener, L. Lunenburger, S. Jezernik, M. Anderschitz, G. Colombo & V. Dietz. Patient-cooperative strategies for robot-aided treadmill training: first experimental results. *IEEE Transactions on Neural Systems and Rehabilitation Engineering*, 13:380–394, 2005.

[206] J. Riess & J. J. Abbas. Adaptive Neural Network Control of Cyclic Movements Using Functional Neuromuscular Stimulation. *IEEE Trans on Rehabilitation Engineering*, 8(1):42–52, 2000.

[207] J. Riess & J. J. Abbas. Adaptive control of cyclic movements as muscles fatigue using functional neuromuscular stimulation. *IEEE Transactions on Neural Systems and Rehabilitation Engineering*, 9(3):326–330, 2001.

[208] C. H. T. Robert K Brayton. Stability of dynamical systems: A constructive approach. *IEEE Transactions on Circuits and Systems*, 26(4):224–234, 1979.

[209] D. W. Robinson. *Design and analysis of series elasticity in closed-loop actuator force control*. Ph.D. thesis, Department of Mechanical Engineering, Massachusetts Institute of Technology, 2000.

[210] D. W. Robinson, J. E. Pratt, D. J. Paluska & G. A. Pratt. Series Elastic Actuator Development for a Biomimetic Walking Robot. In *1999 IEEE/ASME International Conference on Advanced Intelligent Mechatronics*. 1999.

[211] R. Robinson, W. Herzog & B. Nigg. Use of force platform variables to quantify the effects of chiropractic manipulation on gait symmetry. *J Manipulative Physiol Ther*, 10:172–6, 1987.

[212] L. Rosenberg. *Virtual fixtures: Perceptual overlays enhance operator performance in telepresence tasks*. Ph.D. thesis, Stanford University, CA, 1994.

[213] H. Sadeghi, P. Allard, F. Prince & H. Labelle. Symmetry and limb dominance in able-bodied gait: a review. *Gait & Posture*, 12:34–45, 2000.

[214] I. Sardellitti, J. Park, D. Shin & O. Khatib. Air Muscle Controller Design in the Distributed Macro-Mini (DM2) Actuation Approach. In *Proceedings of the IEEE/RSJ International Conference on Intelligent Robots and Systems (IROS)*. San Diego, CA, 2007.

[215] T. Schauer, K. J. Hunt, A. Ronchi, M. H. Fraser & W. Stewart. ROBUST CONTROL OF KNEE-JOINT MOTION. In *Proceedings of the 6th Annual Conference of the International Functional Electrical Stimulation Society (IFESS 2001)*, pp. 232–234. - 6th Annual Conference of the International Functional Electrical Stimulation Society (IFESS 2001).

[216] T. Schauer, N.-O. Negård, F. Previdi, K. J. Hunt, M. H. Fraser, E. Ferchland & J. Raisch. Online identification and nonlinear control of the electrically stimulated quadriceps muscle. *Control engineering practice*, 13(1207-1219):9, 2005.

[217] T. Schauer, R. Salbert, N.-O.Negård & J. Raisch. Detection and Filtering of EMG for Assessing Voluntary Muscle Activity During FES. In *Proceedings of the 9th Annual Conference of the International FES Society*. Bournemouth, UK, 2004.

[218] R. A. Scheidt, J. B. Dingwell & F. A. Mussa-Ivaldi. Learning to move amid uncertainty. *Journal of Neurophysiology*, 86:971–85, 2001.

[219] H. Schmidt, S. Hesse, R. Bernhardt & J. Krüger. HapticWalker - a novel haptic foot device. *ACM Transactions on Applied Perception*, 2(2):166–180, 2005.

[220] A. C. Schouten, E. de Vlugt, J. J. B. van Hilten & F. C. T. van der Helm. Quantifying proprioceptive reflexes during position control of the human arm. *IEEE Transactions on Biomedical Engineering*, 55(1):311–321, 2008.

[221] D. Schröder. *Intelligent Observer and Control Design for Nonlinear Systems*. Springer, Heidelberg, 2000.

[222] L. Sciavicco & B. Siciliano. *Modelling and Control of Robot Manipulators*. Springer, 2nd edition, 2005.

[223] S. H. Scott & G. E. Loeb. Mechanical properties of aponeurosis and tendon of the cat soleus muscle during whole-muscle isometric contractions. *J Morphol*, 224(1):73–86, 1995.

[224] J. Sensinger & R. Weir. Design and analysis of a non-backdrivable series elastic actuator. In *Proceedings of the IEEE International Conference on Rehabilitation Robotics (ICORR)*, pp. 390– 393. 2005.

[225] J. Sensinger & R. Weir. Unconstrained Impedance Control Using a Compact Series Elastic Actuator. In *Proceedings of the 2nd IEEE/ASME International Conference on Mechatronic and Embedded Systems and Applications*, pp. 1 – 6. 2006.

[226] J. W. Sensinger & R. Weir. Improvements to Series Elastic Actuators. In *Proceedings of the 2nd IEEE/ASME International Conference on Mechatronic and Embedded Systems and Applications*, pp. 1–7. 2006.

[227] T. Sinkjær & D. B. Popović. Trends in the Rehabilitation of Hemiplegic Subjects. *Journal of Automatic Control*, 15:1–10, 2005.

[228] K. J. Siranosian. AutoAmbulator Improves Functionality For HealthSouth's Rehab Patients. Special Hospital Feature, www.braintreerehabhospital.com.

[229] M. Sobotka. *Hybrid Dynamical System Methods for Legged Robot Locomotion with Variable Ground Contact*. Ph.D. thesis, Institute of Automatic Control Engineering, Technische Universität München, 2007.

[230] M. Solomonow, E. Eldred, J. Lyman & J. Foster. Fatigue considerations of muscle contractile force during high-frequency stimulation. *Am J Phys Med*, 62(3):117–122, 1983.

[231] N. St-Onge & A. G. Feldman. Interjoint Coordination in Lower Limbs During Different Movements in Humans. *Experimental Brain Research*, 148(2):139–149, 2003.

[232] A. Stefanovska, L. Vodovnik, N. Gros, S. Rebersek & R. Acimović-Janezic. FES and spasticity. *IEEE Transactions on Biomedical Engineering*, 36(7):738–745, 1989.

[233] R. B. Stein & F. Parmiggiani. Nonlinear summation of contractions in cat muscles. I. Early depression. *Journal of General Physiology*, 78(3):277–293, 1981.

[234] R. B. Stein, E. P. Zehr, M. K. Lebiedowska, D. B. Popović, A. Scheiner & H. J. Chizeck. Estimating mechanical parameters of leg segments in individuals with and without physical disabilities. *IEEE Transactions on Rehabilitation Engineering*, 4(3):201–211, 1996.

[235] A. H. A. Stienen, E. E. G. Hekman, F. C. T. Van der Helm, G. B. Prange, M. J. A. Jannink, A. M. M. Aalsma & H. Van der Kooij. Dampace: dynamic force-coordination trainer for the upper extremities. In *Proceedings of the IEEE International Conference on Rehabilitation Robotics (ICORR)*, pp. 820–826. Noordwijk, the Netherlands, 2007.

[236] S. W. Su, S. Huang, L. Wang, B. G. Celler, A. V. Savkin, Y. Guo & T. Cheng. Nonparametric Hammerstein model based model predictive control for heart rate regulation. *Proceedings of the Annual International Conference of the IEEE Engi-*

neering in Medicine and Biology Society (EMBS), 2007:2984–2987, 2007.

[237] T. G. Sugar. A novel selective compliant actuator. *Mechatronics*, 12(9):1157–1171, 2002.

[238] T. G. Sugar & V. Kumar. Design and Control of a Compliant Parallel Manipulator. *Journal of Mechanical Design*, 124(4):676–683, 2002.

[239] A. Sunderland. Recovery of ipsilateral dexterity after stroke. *Stroke*, 31(2):430–433, 2000.

[240] A. Sunderland, M. P. Bowers, S. M. Sluman, D. J. Wilcock & M. E. Ardron. Impaired dexterity of the ipsilateral hand after stroke and the relationship to cognitive deficit. *Stroke*, 30(5):949–955, 1999.

[241] J. Szecsi, M. Fiegel, S. Krafczyk, A. Straube, J. Quintern & T. Brandt. Querschnittgelähmte Patienten mit dem Fahrrad unterwegs. *MMW Fortschritte der Medizin*, 146(26):37–8, 40–1, 2004.

[242] K. Tatani & Y. Nakamura. Dimensionality Reduction and Reproduction with Hierarchical NLPCA Neural Networks - Extracting Common Space of Multiple Humanoid Motion Patterns. In *Proceedings of the 2003 IEEE International Conference on Robotics & Automation*, pp. 1927–1932. Taipei, Taiwan, 2003.

[243] E. Taub, G. Uswatte & R. Pidikiti. Constraint-induced movement therapy: a new family of techniques with broad application to physical rehabilitation: a clinical review. *Journal of Rehabilitation Research & Development*, 36(3):237–51, 1999.

[244] R. Taylor, P. Jensen, L. Whitcomb, A. Barnes, R. Kumar, D. Stoianovici, P. Gupta, Z. Wang, E. Dejuan & L. Kavoussi. A steady-hand robotic system for microsurgical augmentation. *The International Journal of Robotics Research*, 18(12):1201–1210, 1999.

[245] R. Teasell, J. Bitensky, K. Salter & N. A. Bayona. The role of timing and intensity of rehabilitation therapies. *Topics in Stroke Rehabilitation*, 12(3):46–57, 2005.

[246] K. A. Thoroughman & R. Shadmehr. Learning of action through adaptive combination of motor primitives. *Nature*, 407(6805):742–747, 2000.

[247] E. Todorov. Optimality principles in sensorimotor control. *Nature Neuroscience*, 7(9):907–915, 2004.

[248] R. Tomović, M. Vukobrativic & L. Vodovnik. *Advances in External Control of Human Extremities IV*, chapter Hybrid actuators for orthotic systems: hybrid assistive systems, pp. 231–238. Yugoslav Committee for ETAN, Belgrade, 1973.

[249] E. Torres-Jara & J. Banks. A simple and scalable force actuator. In *Proceedings of the International Symposium on Robotics*. Paris, France, 2004.

[250] A. Trnkoczy. Variability of electrically evoked muscle contractions with special regard to closed-loop controlled orthosis. *Annals of Biomedical Engineering*, 2(2):226–238, 1974.

[251] B. S. und O. Khatib (editor) *Handbook of Robotics*. Springer, 2008.

[252] U. Unterhinninghofen, F. Freyberger & M. Buss. *Haptics: Perception, Devices and Scenarios*, chapter Study on Computer Assistance for Telepresent Reaching Movements, pp. 745–754. LNCS, Springer, 2008.

[253] D. Šiljak. *Nonlinear Systems: Parametric Analysis and Design*. Wiley, New York, 1969.

[254] J. v. Zitzewitz, A. Duschau-Wicke, M. Wellner, L. Lünenburger & R. Riener. Path control: a new approach in patient-cooperative gait training with the rehabilitation robot Lokomat. In *Tagungsband der BMT 3-Länder-Tagung*. Zürich, 2006.

[255] H. Vallery & M. Buss. Bewegungsintentionserkennung mit Principal Components Analysis. In *Tagungsband Automed*. Rostock, Germany, 2006.

[256] H. Vallery & M. Buss. Complementary Limb Motion Estimation based on Interjoint Coordination using Principal Components Analysis. In *Proceedings of the IEEE International Conference on Control Applications (CCA)*. Munich, 2006.

[257] H. Vallery & M. Buss. Bewegungsintentionsschätzung auf Basis von Gelenkkoordination. *at-Automatisierungstechnik*, 55(10):503–510, 2007.

[258] H. Vallery, R. Ekkelenkamp, H. van der Kooij & M. Buss. Complementary Limb Motion Estimation based on Interjoint Coordination: Experimental Evaluation. In *Proceedings of the IEEE International Conference on Rehabilitation Robotics (ICORR)*, pp. 798–803. 2007.

[259] H. Vallery, R. Ekkelenkamp, H. van der Kooij & M. Buss. Passive and Accurate Torque Control of Series Elastic Actuators. In *Proceedings of the IEEE International Conference on Intelligent Robots and Systems (IROS)*, pp. 3534–3538. San Diego, USA, 2007.

[260] H. Vallery, M. Neumaier & M. Buss. Anti-Causal Identification of Hammerstein Models. In *European Control Conference (ECC)*. 2009.

[261] H. Vallery, E. van Asseldonk, M. Buss & H. van der Kooij. Reference Trajectory Generation for Rehabilitation Robots: Complementary Limb Motion Estimation. *IEEE Transactions on Neural Systems and Rehabilitation Engineering*, 17(1):23–30, 2009.

[262] H. Vallery, J. Veneman, E. van Asseldonk, R. Ekkelenkamp, M. Buss & H. van der Kooij. Compliant Actuation of Rehabilitation Robots - Benefits and Limitations of Series Elastic Actuators. *IEEE Robotics and Automation Magazine (RAM)*, 15(3):60–69, 2008.

[263] E. H. F. Van Asseldonk, R. Ekkelenkamp, J. F. Veneman, F. C. T. van der Helm & H. van der Kooij. Selective control of a subtask of walking in a robotic gait trainer (LOPES). In *Proceedings of the IEEE International Conference on Rehabilitation Robotics (ICORR)*, pp. 841–848. 2007.

[264] E. H. F. van Asseldonk, M. Wessels, A. H. A. Stienen, F. C. T. van der Helm & H. van der Kooij. Influence of haptic guidance in learning a novel visuomotor task.

Journal of Physiology - Paris, in press, 2009.

[265] L. A. van der Helm, F. C. T. Rozendaal. *Neural control of posture and movement*, chapter Musculoskeletal systems with intrinsic and proprioceptive feedback, pp. 164–174. Springer Verlag, 2000.

[266] G. van Overeem Hansen. EMG-controlled functional electrical stimulation of the paretic hand. *Scandinavian Journal of Rehabilitation Medicine*, 11(4):189–193, 1979.

[267] A. Veg, D. B. Popović & S. Došen. Customizing to User Functional Electrical Stimulation of Walking: Optimal Control. *FME Transactions*, 35:135–140, 2007.

[268] P. H. Veltink, H. J. Chizeck, P. E. Crago & A. el Bialy. Nonlinear joint angle control for artificially stimulated muscle. *IEEE Transactions on Biomedical Engineering*, 39(4):368–380, 1992.

[269] J. F. Veneman, R. Ekkelenkamp, R. Kruidhof, F. van der Helm & H. van der Kooij. A Series Elastic- and Bowden-Cable-Based Actuation System for Use as Torque Actuator in Exoskeleton-Type Robots. *International Journal of Robotic Research*, 25(3):261–281, 2006.

[270] R. Vidal, Y. Ma & S. Sastry. Generalized Principal Component Analysis (GPCA). *IEEE Transactions on Pattern Analysis and Machine Intelligence*, 27(12):1945–1959, 2005.

[271] L. Vodovnik, W. J. Crochetiere & J. B. Reswick. Control of a skeletal joint by electrical stimulation of antagonists. *Medical & Biological Engineering & Computing*, 5(2):97–109, 1967.

[272] L. Vodovnik, C. Long, J. B. Reswick, A. Lippay & D. Starbuck. Myo-electric control of paralyzed muscles. *IEEE Transactions on Biomedical Engineering*, 12(3):169–172, 1965.

[273] D. E. Voss, M. M. Ionta & B. J. Meyers. *Proprioceptive Neurofacilitation: Patterns & Techniques*. Harper & Rowe, 1985.

[274] M. Vukobratovic, D. Hristic & Z. Stojiljkovic. Development of active anthropomorphic exoskeletons. *Medical & Biological Engineering & Computing*, 12(1):66–80, 1974.

[275] D. J. Weber, R. B. Stein, K. M. Chan, G. Loeb, F. Richmond, R. Rolf, K. James & S. L. Chong. BIONic WalkAide for correcting foot drop. *IEEE Transactions on Neural Systems and Rehabilitation Engineering*, 13(2):242–246, 2005.

[276] A. Weiss, T. Suzuki, J. Bean & R. A. Fielding. High intensity strength training improves strength and functional performance after stroke. *American Journal of Physical Medicine & Rehabilitation*, 79(4):369–76, 2000.

[277] C. Werner, S. Von Frankenberg, T. Treig, M. Konrad & S. Hesse. Treadmill training with partial body weight support and an electromechanical gait trainer for restoration of gait in subacute stroke patients: a randomized crossover study. *Stroke*, 33:2895–901, 2002.

[278] G. F. Wilhere, P. E. Crago & H. J. Chizeck. Design and evaluation of a digital closed-loop controller for the regulation of muscle force by recruitment modulation. *IEEE Transactions on Biomedical Engineering*, 32(9):668–676, 1985.

[279] D. A. Winter. *Biomechanics and Motor Control of Human Movement*. Wiley-Interscience, New York, 3rd edition, 2004.

[280] J. M. Winters & L. Stark. Muscle models: what is gained and what is lost by varying model complexity. *Biological Cybernetics*, 55(6):403–420, 1987.

[281] E. Wolbrecht, V. Chan, V. Le, S. Cramer, D. Reinkensmeyer & J. Bobrow. Real-time computer modeling of weakness following stroke optimizes robotic assistance for movement therapy. In *Proceedings of the IEEE/EMBS International Conference on Neural Engineering (CNE)*, pp. 152–158. 2007.

[282] G. Wyeth. Control Issues for Velocity Sourced Series Elastic Actuators. In *Proceedings of the Australasian Conference on Robotics and Automation*. 2006.

[283] L. Xie, S. Shishkin & M. Fu. Piecewise Lyapunov functions for robust stability of linear time-varying systems. *Systems & Control Letters*, 31:165–171, 1997.

[284] F. E. Zajac & J. L. Young. Properties of stimulus trains producing maximum tension-time area per pulse from single motor units in medial gastrocnemiu muscle of the cat. *Journal of Neurophysiology*, 43(5):1206–1220, 1980.

[285] J. Zheng, G. Guo & Y. Wang. Feedforward decoupling control design for dual-actuator system in hard disk drives. *IEEE Transactions on Magnetics*, 40(4):2080–2082, 2004.

[286] M. Zinn, O. Khatib, B. Roth & J. Salisbury. Actuation Methods For Human-Centered Robotics and Associated Control Challenges. In *Second Joint CSS/RAS International Workshop on Control Problems in Robotics and Automation*. Las Vegas, NV, 2002.